

Investigating the Homeostatic Regulation of Kenyon Cells in
Drosophila

The University of Sheffield

Faculty of Science

School of Biosciences

By Katie Greenin-Whitehead

December 2022

Contents

Acknowledgements.....	5
Preface.....	6
Summary.....	7
List of Abbreviations.....	9
1 General Introduction.....	11
1.1 Homeostasis.....	11
1.1.1 The importance of homeostasis.....	11
1.1.2 There are multiple types of homeostasis.....	13
1.1.2.1 Synaptic homeostasis.....	13
1.1.2.2 Intrinsic homeostasis.....	15
1.1.3 Cells can use multiple types of homeostasis together.....	18
1.2 Neuronal excitability and regulation.....	20
1.3 Ion channels.....	21
1.3.1 Sodium channels.....	22
1.3.2 NaChBac.....	23
1.3.3 Endogenous sodium channel para.....	26
1.4 Distal axon initial segment.....	27
1.5 Nicotinic receptors.....	29
1.6 Potassium channels.....	30
1.6.1 Shaker.....	33
1.6.2 Shab.....	34
1.6.3 Shaw.....	35
1.6.4 Shal.....	36
1.7 <i>Drosophila</i> as a model organism.....	37
1.8 <i>Drosophila</i> olfaction and olfactory memory.....	39
1.9 Kenyon cells use sparse coding to create and store odour associative memories.....	43
1.10 Comparing Olfaction in <i>Drosophila</i> and Vertebrates.....	47
1.11 Two-photon calcium imaging.....	49
1.12 Computational theories about homeostasis in KCs.....	52
1.13 Focus of this thesis.....	53
2 Materials and Methods.....	55
2.1 Materials.....	55
2.1.1 Fly rearing.....	55
2.1.2 Fly lines.....	55
Fly lines used in Chapter 3.....	55
Fly lines used in Chapter 4.....	57
2.1.3 Equipment.....	58
2.1.4 Solutions.....	59

External solution	59
2.1.5 Other reagents	60
2.1.6 Filters used for two-photon microscopy	61
2.2 Methods	62
2.2.1 <i>Ex vivo</i> technique for two-photon microscopy	62
2.2.2 Calcium imaging	62
Two-photon imaging	62
Odour scripts	64
2.2.3 Molecular Biology	65
Gel electrophoresis	65
2.3 Analysis	66
2.3.1 Analysis of imaging data	66
2.3.2 3D-Skeletonisation of FlpTag Data	66
2.3.3 Statistical analysis	67
3 NaChBac expression in Kenyon cells reduces their odour responses	68
3.1 Introduction	68
3.1.1 Past literature demonstrates NaChBac expression increases neuronal excitation	68
3.1.2 Chapter direction	70
3.2 Results	71
3.2.1 Constitutive expression of NaChBac reduces odour responses in Kenyon cells	71
3.2.2 Acute 2-day NaChBac expression in adult flies weakens odour responses, but KCs can recover after 4-days of acute adult NaChBac expression	75
3.2.3 Acute expression of NaChBac in pupal development weakens odour responses	82
3.2.4 Summary of NaChBac expression in Kenyon cells	85
3.2.5 Constitutive expression of NaChBac reduces expression of Para sodium channels in KC distal axon initial segments	86
3.2.6 Changing the length of the distal axon initial segment may slightly weaken odour responses of KCs	89
3.2.7 The expression of paraRNAi reduces the odour responses in KCs but paraFlpStop increases the odour responses in the calyx	91
3.2.8 Preliminary results show that constitutive NaChBac expression in KCs increases the expression levels of Shaker potassium channels	94
3.2.9 No changes were observed in the expression levels of $\alpha 6$ and $\alpha 7$ subunit-containing nicotinic receptors with constitutive NaChBac expression	100
3.2.10 Constitutive NaChBac expression weakens peak odour responses of projection neurons	101
3.3 Discussion	103
3.3.1 NaChBac has a paradoxical effect in KCs	103
3.3.2 NaChBac weakens Para expression in KC distal axon initial segments and alters potassium channels	106
3.2.3 NaChBac expression doesn't alter the expression levels of acetylcholine receptors	108
3.2.4 Future work	109

4 Decreasing endogenous potassium channel expression levels reduces odour responses in Kenyon cells	111
4.1 Introduction.....	111
4.2 Results	114
4.2.1 Weakening the expression levels or expressing non-functional potassium channels weaken odour responses of KCs.....	114
4.2.2 Increasing Shaw channel expression weakens odour responses in KCs.....	124
4.2.3 Summary of Chapter 4 results in Kenyon cells	126
4.3 Discussion	127
4.3.1 Potassium channel disruption weakens the excitation of KCs	127
4.3.2 Future work	131
Chapter 5: General Discussion	132
5.1 Summary of findings.....	132
5.2 Contributions to neuronal excitability and homeostasis	133
5.3 Improving the experimental approach	137
5.3.1 Calcium imaging for neuronal activity.....	137
5.3.2 Altering ion channel levels through gene expression	139
5.4 Insights into the role of Kenyon cells in the mushroom body based on my results.....	141
5.5 Comparisons to other systems	141
6 References	143

Acknowledgements

I have nothing but gratitude to all the people who have helped me these last 4 years.

To Andrew - thank you for your guidance, support, and inspiration. I am lucky to have had such a great supervisor and mentor.

To Jem, my true other half - thank you for your understanding, patience, and moral support.

To my parents – thank you for your unconditional encouragement, belief, and positivity.

To my friends back home - I am officially the smartest of us all. Deal with that the best you can. Thank you for all the intelligent and unintelligent conversations we have had that have kept me grounded. Everyone deserves cheerleaders like you guys.

To all my Sheffield friends, especially Keivan, James, and Emma – Thank you for being such good friends. I don't know how I would have got through a PhD, a pandemic, and a wedding without you guys.

To my lab mates – thank you for creating such an encouraging and terrific workspace.

Above all, I thank Henry. You are the calming influence every PhD student deserves. You make each day happy, funny, and bright. Your positive attitude, mind-set and work ethic are an inspiration to me every day.

Preface

This dissertation is the result of my own work.

It has not been submitted previously to this or any other university.

Some portions of this work were taken from my first-year report.

Summary

How do Kenyon cells behave consistently with such a high variation of inputs?

In *Drosophila*, stimulus-specificity of associative memories requires sparse coding in the neurons that are storing the memory. Effective sparse coding requires that the neurons have approximately equal probabilities of firing across all stimuli. Otherwise, some cells will be disproportionately active or silent, and thereby be less informative about stimulus identity. I study the problem of how distributed sparse coding is maintained in Kenyon cells (KCs), which are the third-order olfactory neurons. I hypothesised that KCs homeostatically adjust their intrinsic properties to ensure even activity across the population of KCs. I investigated this hypothesis using a combination of two-photon imaging and genetic manipulation of ion channel expression.

Sodium and potassium channels are responsible for the depolarisation and repolarisation of the membrane, respectively. I conducted experiments to investigate the impact of artificially manipulating the expression of sodium and potassium channels on KCs' activity. Additionally, I examined whether this manipulation could potentially regulate the expression of other sodium and potassium channels through homeostatic mechanisms.

My results indicate that constitutively overexpressing NaChBac, an exogenous voltage-gated sodium channel, in KCs paradoxically decreases their activity. The neurons' activity was measured by amplitude of odour responses with calcium imaging. The developmental expression and two days of acute NaChBac expression in adults produced a significant decrease in odour responses. However, 4 days of acute expression in adults increased the odour responses of specific KCs. When NaChBac was expressed in adults for 8 days, odour responses were not significantly different from control. Thus, only specific acute expression of NaChBac causes an increase in excitability. When investigating whether the KCs had homeostatic mechanisms that counteracted NaChBac's effect, I found that the levels of other ion channels had adjusted. Constitutively expressing NaChBac decreased expression of para, the endogenous voltage-gated sodium channel responsible for generating action potentials. It may be that NaChBac expression decreases Para levels to prevent overexcitation. Furthermore, NaChBac expression also increases endogenous levels of the potassium

channel, Shaker. As NaChBac causes abnormally long action potentials due to its slow kinetics, while Shaker is normally responsible for membrane repolarisation at the end of an action potential, it may be that the increased Shaker is an attempt to compensate for the prolonged depolarisation caused by NaChBac. In contrast, knocking down or disrupting a multitude of endogenous potassium channels in KCs appeared to have very little effect on KC activity. This finding is unlike what it is typically found in most past literature that focuses on disrupting potassium channels.

The project revealed a paradoxical response of KCs when they were artificially excited by expressing NaChBac and disrupting their potassium channels. Additionally, the project discovered that KCs can modulate their ion channel expression levels in response to NaChBac expression.

List of Abbreviations

AL	Antennal lobe
AP	Action potential
APL	Anterior paired lateral
Ca ²⁺	Calcium
CDK5	Cyclin-dependent kinase 5
CDK5DN	Cyclin-dependent kinase 5 dominant negative
δD	Delta Decalactone
DAN	Dopaminergic neuron
DAIS	Distal axon initial segment
DN	Dominant negative
dNTP	Deoxynucleotide triphosphate
Eag	Ether-a-go-go potassium channel
EPSPs	Excitatory post synaptic potentials
EPSCs	Excitatory post synaptic currents
GABA	γ-aminobutyric acid
IA	Isoamyl Acetate
Ih	Hyperpolarisation-activated cation current
K ⁺	Potassium
KC	Kenyon cell
KCL	Potassium chloride
LH	Lateral horn
LHN	Lateral horn neurons
MB	Mushroom body
MBON	Mushroom body output neuron
MCH	4-methylcyclohexanol
MgCl ²	Magnesium chloride
MgSO ⁴	Magnesium sulphate
Na ⁺	Sodium
NaChBac	Bacterial sodium channel
nAChR	Nicotinic acetylcholine receptor
NaCl	Sodium chloride
NaH ² PO ⁴	Monosodium phosphate

OCT	3-octanol
ORNs	Olfactory receptor neurons
PN	Projection neuron
RNAi	Ribonucleic acid interference
Sh	Shaker potassium channel
ShakerDN	Shaker dominant negative
ShalDN	Shal dominant negative
ShalporeDN	Shal pore dominant negative
ShawWt	Wild type Shaw potassium channel
TES	N-tris(hydroxymethyl)methyl-2-aminoethanesulfonic acid

1 General Introduction

1.1 Homeostasis

1.1.1 The importance of homeostasis

Brain development, learning, memory, and sensory information processing all depend on a combination of homeostasis and plasticity. Homeostasis refers to the dynamic equilibrium that enables a system to sustain a stable internal state, which is essential for living organisms. Plasticity, particularly neuronal plasticity, refers to the brain's ability to change and adapt in response to experiences. In neuroscience, it is important to understand how homeostasis and plasticity interact to create functional networks.

Neurons are long-lived and have highly specialised electrical signalling properties which rely on short-lived ion channels and proteins and so there is a delicate balance between homeostasis and neuronal plasticity. An example of neuronal plasticity is Hebbian plasticity, which is based on the principle that “cells that fire together wire together” (Fernandes and Carvalho, 2016; Keck et al., 2017a; Keck et al., 2017b). The theory is that when two connected neurons are repeatedly activated simultaneously, the connection between them is strengthened, a process known as synaptic plasticity or long-term potentiation (LTP). Hebbian strengthening mechanisms enhance communication between neurons, facilitating learning, memory formation and cognitive processes. However, Hebbian strengthening can create a positive feedback loop: frequent coincident activity strengthens synapses among a group of neurons, promoting further coincident activity and triggering a self-reinforcing increase in overall activity. In the absence of regulation or control, this process can spiral into a cycle that drives networks to a state of hyperexcitability, which is associated with pathological conditions. Conversely, long-term depression (LTD) is also susceptible to positive feedback loops. LTD refers to the persistent weakening of synapses. If it develops into an unregulated positive feedback loop, it can lead to a cycle that propels brain activity into a state of reduced excitability. Therefore, homeostasis is required for maintaining balance and regulating these processes.

Homeostasis is the compensatory mechanisms that maintain overall stability and balance in neural circuits. They can counterbalance mechanisms like Hebbian strengthening, for example, by adjusting synaptic strength in response to changes in global neuronal activity levels. Homeostatic plasticity ensures that the neural network remains stable and functional despite ongoing synaptic modifications. In a healthy, correctly functioning nervous system, homeostasis and plasticity are in constant exchange with each other.

In intact systems, neurons are subject to continual perturbations from other networks, developmental changes, and environmental fluctuations. For example, in epilepsy, faulty stability mechanisms within a cell population can lead to increased neuronal excitability, resulting in seizures (reviewed in Stafstrom and Carmant, 2015). To ensure the proper functioning of networks, it is crucial to study homeostasis both from a global perspective and at the cellular level.

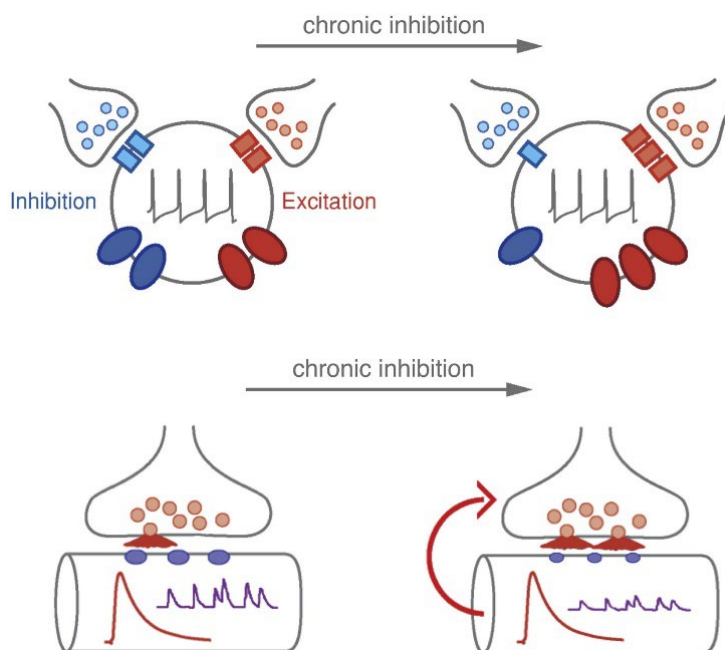


Figure 1 Diagram of an example of homeostatic control of excitation within cells.

Top: example of how firing properties of neurons can be determined by the balance between synaptic excitation (red ovals demonstrate ion channels, red circles represent vesicles and red rectangles show receptors), synaptic inhibition (blue ovals demonstrate ion channels, blue circles represent vesicles and blue rectangles show receptors). When there is chronic inhibition, the cells can alter the relative abundance of ion channels and receptors in the cell membrane. Thus, leading to the cell re-establishing a specific range of activity.

Bottom: when chronic inhibition is at the neuromuscular junction, receptor sensitivity or receptor abundance leads to a compensatory increase in presynaptic neurotransmitter release. This then can counteract the change in receptor function thus re-setting back to synaptic depolarisation at the junction.

(Image from Davis, (2013), evidence from Davis et al., (2006))

Homeostasis occurs in both the central and peripheral nervous systems (Figure 1; reviewed in Davis, 2006; Marder, 2011; Turrigiano, 2011) and it is evident that neurons must monitor their own intrinsic activity in order to function as an individual as well as within a network. While the exact mechanisms remain uncertain, it is evident that these homeostatic systems operate based on fundamental principles of feedback. Their purpose is to ensure that each neuron maintains specific levels of activity within an inherently unstable environment. In each system where a neuron uses homeostasis they must have (1) sensors to monitor activity, (2) a set range to remain within, (3) error signals to trigger the system and (4) a regulatory feedback mechanism for the system to return to the set range. While discussing these components may seem straightforward, there are many factors involved. It is unknown how neurons determine their range of activity or how they can sense that there has been a change in the cell. Questioning these variables is a major contributor to the project's aim. In this project I will be concentrating on homeostasis and how neurons can maintain stable activity levels.

1.1.2 There are multiple types of homeostasis

In neurons, there are multiple homeostatic mechanisms that have been proposed. These include but are not limited to: synaptic scaling, ratio of ion channel expression, activity-dependent gene expression, and posttranslational modification of ion channel conductance. Research on homeostasis helps us understand the mechanisms that regulate various physiological processes, and this knowledge can help us to understand how organisms adapt to changing environments.

1.1.2.1 Synaptic homeostasis

Mentioned earlier, homeostatic regulation can happen at synapses, where communication between neurons occurs. Thus, synapses must be precisely regulated to ensure accurate communication between neurons. Homeostatic mechanisms, such as synaptic scaling, help to regulate the strength of synapses and maintain proper

communication between neurons. Synaptic scaling can decrease the strength of synapses in response to increases in neural activity, ensuring that the overall balance of excitation and inhibition is maintained (Figure 1; Davis et al., 2006; Turrigiano et al., 1998; Kazama and Wilson, 2008).

Cultured cells can be used to investigate the global firing activity and how it can recover from disruption through homeostasis. When global firing activity was blocked by treatment with tetrodotoxin, a sodium channel blocker, for 48 hours, there was a pronounced increase in the amplitudes of miniature excitatory postsynaptic currents (mEPSCs) in pyramidal neurons (Turrigiano et al., 1998), showing that excitatory synapses were strengthened, presumably to compensate for the lack of activity. Conversely, when activity was increased by blocking GABA_A receptors with bicuculline for 48 hours, mEPSC amplitudes became much smaller, showing that the cells have methods of overcoming the blocker's effect to increase activity (Turrigiano et al., 1998). In this situation, there would be a change in excitation range to maintain neuronal stability as the blocker would not be surmounted. Thus, in this case, both increasing and decreasing activity can trigger synaptic homeostasis.

Neuronal homeostasis can be found throughout many types of organisms. Neuronal slices obtained from rodents can represent a valuable experimental model as they can provide more complex systems. For example, inducing overexcitation in pyramidal neurons of the hippocampus via optogenetic manipulation using channelrhodopsin-2, a light-gated cation channel, resulted in compensatory postsynaptic weakening (Goold and Nicoll, 2010). This effect was attributed to a reduction in AMPA and NMDA receptor responses, highlighting how changes in intrinsic firing rate can affect the sensitivity of synaptic receptors. Furthermore, experiments done on transgenic mice which have their Kv4.2 gene silenced during development had almost complete elimination of A-type potassium currents in the dendrites of the CA1 pyramidal cells (Andrásfalvy et al., 2008). Despite the absence or reduction of a key contributor to the potassium current in the cell, the level of cell excitability remained largely unchanged. It was found that the loss of the Kv4.2 gene triggered increases in GABAergic inhibition at the synapse (Andrásfalvy et al., 2008).

Past literature has shown that synaptic homeostatic effects can be sensitive to developmental timings. In early development stages, before synapse formation,

transfecting a single cell (in a cultured network) with Kir2.1, an inwardly rectifying potassium channel, produced no homeostatic response (Burrone et al., 2002). Instead, the presence of Kir2.1 caused neural silencing from a decrease in synapse formation as well as a decrease of mEPSCs frequency and evoked EPSC amplitude (Burrone et al., 2002). However, when Kir2.1 was transfected after synapse formation, there was a significant increase in the mEPSCs amplitude, synapse density and size. Therefore, the cells were able to over-come the effects of Kir2.1 and the cells were able to return to wild type levels of firing rates (Burrone et al., 2002). This work suggests that certain types of homeostasis can only be triggered at specific times within development. This could be because they haven't developed the right mechanisms to cope with the changes or they may need to establish certain structures, such as synaptic sites. In *Drosophila* they have multiple critical periods during development. A critical period refers to a specific time window during development when *Drosophila* are particularly susceptible to stimuli which can trigger long-lasting effects on their physiology or behaviour. For example, manipulating activity through changes in nitric oxide during a 2 hour window in late embryogenesis (17–19 hours after egg laying), is enough to permanently alter the developmental course of the synapses in the locomotor network (Giachello et al., 2021).

Through synaptic homeostasis, synapses efficiently adjust their strength to uphold the balance between excitation and inhibition, essential for optimal neuronal function.

1.1.2.2 Intrinsic homeostasis

Another mechanism for homeostatic regulation is by modulating a neuron's intrinsic excitability, for example by altering the expression or function of ion channels. This mechanism works because neuronal excitability is regulated by a specific balance of ions, such as sodium, potassium, and calcium, to generate and propagate action potentials for neural communication. Disruptions to this balance can result in hyperexcitability, which can cause miscommunication within a system or even cell death. Homeostatic mechanisms using ion pumps or channels can help to regulate the intracellular ion balance and maintain the resting potential of neurons.

One of the first major pieces of work that contributed to the initial ideas about intrinsic homeostasis, particularly regarding ion channel expression, was using lobster cell culture. Lobster stomatogastric ganglion neurons were isolated and due to the change

in environment, the culture had lost many cues required to maintain intrinsic electrical properties. However, over time the isolated neurons were able to rebalance back to the intrinsic firing properties they had *in vivo* (Turrigiano et al., 1994). This led to further experiments investigating homeostasis within cultured cells. For example, networks made up of excitatory pyramidal neurons and inhibitory interneurons displayed spontaneous activity after a few days of development *in vitro*. The activity of the neurons could be pharmacologically modulated for defined periods of time with presentation of toxins (Turrigiano and Nelson, 2004).

The explanation for how ion channels contribute to homeostatic mechanisms is not simple. However, using both computational and *in-vivo* experimentation, the homeostatic mechanisms in the stomatogastric ganglion of lobster have been well established (Prinz, Bucher and Marder, 2004; Marder, 2011; Figure 2). Over 20 million computational models of three-cell networks were tested, varied by intrinsic properties. It was found that ~400,000 models emulated stomatogastric ganglion activity (Prinz et al., 2004; Marder, 2011; Figure 2). Surprisingly, these models demonstrated that neurons can possess different ion channel combinations while maintaining consistent firing properties, indicating the flexibility of ion channel regulation (Figure 2). It was concluded that there are various combinations of ion channel levels that will result in same cell performance and underscores neurons' capacity to modulate their excitation via ion channel adjustments (Prinz et al., 2004; Marder, 2011). Furthermore, it has been shown that even within the same cell type (pyloric dilator neurons, lateral posterior gastric neurons, lateral gastric, gastric mill, lateral pyloric and inferior cardiac) and taken from the same location within the same animal, individual neurons exhibit highly variable levels of ion channel conductance and expression levels (Schulz et al., 2006). Past literature has shown how disrupting genes of ion channels and their associated proteins can invoke compensatory changes in the expression of other ion channels. This has been seen in both invertebrate and mammalian systems (Discussed later; MacLean et al., 2003; Swensen and Bean, 2005; Andrásfalvy et al., 2008).

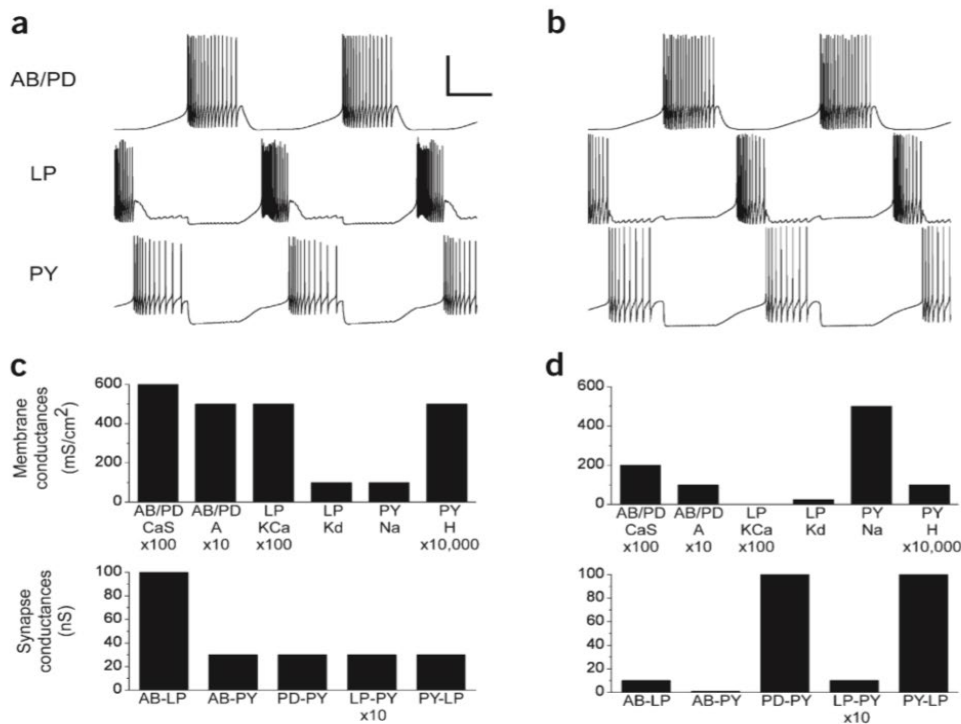


Figure 2 Results from Prinz et al., 2004 demonstrates how two networks with similar voltage traces can have very different ion channel expression levels.

(A-B) Example voltage traces from 2 pyloric computational networks. Scale bars, 0.5 s and 50 mV. (C) The top panel shows membrane conductance's and the bottom panel show synaptic conductance's of A. (D) The top panel shows membrane conductance's and the bottom panel show synaptic conductance's of B. Networks A and B have very similar activity despite having different cellular and synaptic properties.

AB = anterior burster neuron, PD = pyloric dilator neuron, LP = lateral pyloric neuron, PY = Pyloric neuron, CaS = slow transient calcium current, A = transient potassium current, KCa = calcium dependent potassium current, Kd = delayed rectifier potassium current, Na = sodium current, H = hyperpolarisation-activated inward current, x10- x10,000 = maximal conductance densities.

Furthermore, studies have introduced an activity-dependent mechanism for regulating ion channels via mRNA. Artificially elevating activity levels leads to a substantial decrease in Para (sodium channel) mRNA abundance, acting as a countermeasure against membrane excitation (Mee et al., 2004). Other factors can trigger regulation of the ion channels, such as pumilio, which is present in both flies and mice. Pumilio is required to alter sodium channels after chronic synaptic activity (Driscoll et al., 2013). Therefore, the regulation of ion channel levels in neurons to ensure homeostasis involves multiple factors. Consequently, while a particular system or pathway may suffice for one cell, it may not be applicable as a solution for another.

Overall, investigating homeostasis is important for advancing our understanding of basic physiological processes which can be applied to other systems or for developing

treatments for a range of health problems. This project will concentrate on homeostatic regulation using ion channels to maintain neuronal excitability.

1.1.3 Cells can use multiple types of homeostasis together

A cell can use multiple types of homeostasis simultaneously to maintain stability and regulate its functions. Homeostatic mechanisms are usually studied in isolation; consequently, our understanding of how these mechanisms may interact remains limited. For instance, when there is a loss of stability, do multiple homeostatic mechanisms activate within a single cell? And if they do, do they all exhibit the same threshold for changes in activity? For example, a neuron may use synaptic homeostasis to regulate the strength of its connections with other neurons, while also using intrinsic homeostasis to adjust its inherent properties, such as ion channel expression, to maintain stable firing rates.

Previous research has shown that different types of visual deprivation can trigger distinct homeostatic mechanisms. Both forms of visual deprivation led to an increase in the spontaneous firing. Chemical blocking by tetrodotoxin, increased the ratio of synaptic excitation to inhibition in layer 2/3 of the visual cortex, whereas eyelid suture increased the intrinsic excitability of layer 2/3 of the visual cortex (Maffei and Turrigiano, 2008). Thus, although both forms of visual deprivation led to an increase in the spontaneous firing, they did so through different homeostatic mechanisms.

Since many studies focus on isolated forms of homeostasis, compiling results from multiple sources has produced inferences into how multiple homeostatic compensations can work together. For example, combined evidence shows associative learning induces homeostasis in both the intrinsic and synaptic excitability of medial prefrontal cortex neurons to modulate conditioned fear and seeking behaviour (Porter and Sepulveda-Orengo, 2020). Furthermore, computational models support the notion that more than one form of homeostasis can happen simultaneously (Cannon and Miller, 2016). Simulations reveal that a dual homeostatic system, consisting of both synaptic and intrinsic mechanisms, effectively regulates both firing rate and variance. This parallel mechanism naturally adjusts a neuron's output to align with the dynamic range of its input (Cannon and Miller, 2016).

Additionally, intrinsic responses can happen in response to synaptic changes. Overexcitation can induce changes in the expression of ion channels that are not directly involved in synaptic transmission. For example, in *Drosophila* cultured neurons, blocking synaptic activity with curare, a reversible antagonist of nicotinic acetylcholine receptors, increased the expression of the nicotinic receptor nAChR α 7 (D α 7), which in turn triggered transcriptional and translational upregulation of the potassium channel Shal. This increase in Shal expression effectively stabilised the synaptic potentials in response to the enhanced excitatory input (Ping and Tsunoda, 2012).

Furthermore, previous research conducted in the Lin lab revealed that when an inhibitory neuron (anterior paired lateral neuron; APL) was artificially overactivated, but then the overactivation was removed, the responses of Kenyon cells (KCs) to odours increased, indicating that KCs had compensated for excess inhibition (Apostolopoulou and Lin., 2020). Five possible explanations were proposed: 1. KCs received more synaptic excitation. 2. KCs became intrinsically more excitable. 3. The over inhibition weakened the excitation between the KCs to the APL. 4. The APL became intrinsically less excitable. 5. KCs became less sensitive to the inhibition from the APL. Apostolopoulou and Lin (2020) showed that in some subtypes of KCs, the homeostatic adaptation was explained by only 3 and/or 4, while in other subtypes, the adaptation occurred through a combination of 3 and/or 4, together with 1 and/or 2. Having multiple forms of homeostatic plasticity likely serves to ensure that network compensation is possible in the face of various sensory disruptions.

This project is specifically interested in neuronal homeostasis which uses ion channels to stabilise activity. The aim of the project is to investigate the homeostatic mechanisms of Kenyon cells in *Drosophila melanogaster*. These cells contribute to odour associative memory production and storage. Discussed below are the parameters that I aim to investigate and how they could contribute to Kenyon cell (KC) homeostatic regulation of excitability. Particularly, KCs have a high variability in the number of inputs they receive but as they use sparse coding to encode information they must remain as excitable as one another to function correctly. Thus, do KCs use homeostatic regulation to perform consistently?

1.2 Neuronal excitability and regulation

Homeostasis in excitable cells is closely linked to their activity levels. Neurons, muscle cells and even some endocrine cells are all excitable cells. They can transmit information in the form of electrical signals because they have voltage-sensitive ion channels in their membranes. All cells, not just excitable cells, have a resting membrane potential (RMP). The RMP of a cell is the continuous electrical charge across the plasma membrane. In excitable cells, like neurons, their interiors are typically around -70 millivolts. The resting membrane potential of an excitable cell arises from the sodium/potassium pump that pushes 2 potassium ions (K^+) into the cell and 3 sodium ions (Na^+) out of the cell resulting in a net loss of positive charge from the cell due to their electrochemical gradient (Skou, 1998). An electrochemical gradient is a combined force that results from the concentration gradient and the electrical gradient across a membrane. It combines the difference in the concentration of ions on either side of a membrane and the difference in their electrical charge. The concentration gradient is a difference in the concentration of ions on either side of a membrane. It causes ions to move from an area of high concentration to an area of low concentration until that ions' equilibrium is reached. The electrical gradient is a difference in the electrical charge across a membrane. The charge difference results from the uneven distribution of ions across the membrane. For example, a membrane may have more negatively charged ions on one side and more positively charged ions on the other side, creating an electrical potential difference. Together, the concentration gradient and the electrical gradient create an electrochemical gradient that influences the movement of ions across the membrane, which is critical for various biological processes such as nerve and muscle function, as well as the transport of molecules across cellular membranes. Furthermore, there are K^+ channels that leak K^+ (Goldman, 1943) to push the potential to negative voltages. Excitable cells can be activated by external stimuli that depolarise the plasma membrane. For example, mechanical stimuli, such as in the auditory system, can activate mechanically-gated sodium channels like the mechanoelectrical transduction (MET) channels in hair cells of cochlear (Hodgkin, and Katz, 1949) which depolarise the cell. Alternatively, chemical stimuli such as neurotransmitters bind to receptors. For example, acetylcholine is a neurotransmitter that is used in the *Drosophila* olfactory system (Su and Dowd, 2003) that binds to ligand-gated cation channels, triggering them to open which leads to excitatory postsynaptic potentials

(EPSPs). In neurons, if enough EPSPs are generated, then the cell reaches a voltage threshold which opens voltage-gated sodium channels in the membrane close to the EPSP depolarisation (Ovchinnikov, 1981). During the millisecond that the channel remains open several thousand Na^+ rush into the cell to depolarise the membrane. This causes sodium channels in the adjacent sections of the membrane to open, creating a wave of depolarisation that sweeps along the cell, creating an action potential (AP). In the Kenyon cells (the cells used in this project) an action potential is formed in the distal axon initial segment. Sodium channels contribute to the depolarisation of the cells (there is a high concentration of sodium channels in the distal axon initial segment) whereas potassium channels and some chloride channels contribute to repolarising the cell. Opening the potassium channels creates an efflux of positive potassium ions, as the membrane is now permeable to potassium, returning the cell membrane back to a negative potential. This shifts the weights on the Goldman equation more towards the Nernst potential of potassium. Having a comprehensive understanding of these processes enables us to explore the consequences of any alterations made to the systems and thus their homeostatic mechanisms. This is especially true for ion channels, as they have been extensively studied, thus facilitating a clearer understanding of the potential impacts associated with their modifications.

1.3 Ion channels

Ion channels play a critical role in maintaining neuronal homeostasis by regulating excitability. Ion channels regulate the movement of ions into and out of neurons, which is essential for maintaining the proper electrical and chemical balance of the cell. For example, voltage-gated ion channels open in response to changes in the membrane potential, allowing ions to flow across the cell membrane and change the electrical potential necessary for neuronal signalling. Any disruption in the activity of ion channels can have significant consequences for cellular homeostasis and neural function. For example, mutations in ion channels can lead to channelopathies (Spillane et al., 2016), which are disorders characterised by abnormal ion channel activity and disrupted neural signalling. These conditions can have a range of symptoms, including muscle weakness (Jurkat-Rott et al., 1994), seizures (Claes et al., 2001), and cognitive impairment (Ophoff et al., 1996). Therefore, investigating ion channels in neurons is critical for

understanding how the brain maintains cellular homeostasis and processes information. By studying the role of ion channels, we can gain insights into various neurological disorders and conditions. This could then lead to the development of new treatments and therapies to restore cellular homeostasis and improve neural function.

1.3.1 Sodium channels

Sodium channels are responsible for the depolarisation of the membrane in excitable cells via an influx of positive sodium ions. In mammals, there are two major classes of sodium channels: voltage-gated sodium channels which are expressed throughout various excitable cell types (including neurons) and epithelium sodium channels, which are located primarily in the kidney and skin in mammals. Epithelial sodium channels are found in *Drosophila* (Zelle et al., 2013) but in this project I will be concentrating on voltage-gated sodium channels.

Voltage-gated sodium channels have numerous roles, but they are most often discussed in terms of their role in action potentials. Voltage-gated sodium channels are large and multimeric, which means they are composed of an α subunit and one or more β subunits (Strong, Chandy, and Gutman 1993; Figure 3). Structurally, the α subunit of voltage-gated sodium channels consists of four homologous domains, each composed of 6 α helices, S1-S6, and a central pore region made from S5-S6 (Charalambous and Wallace, 2011; Figure 3). The pore determines the ion selectivity of the channel and is typically just one or two atoms wide at its narrowest point. The channels are typically selective for sodium ions. However, some channels may be permeable to more than one type of ion and this usually occurs when those ions share a common charge. The β subunits are auxiliary and modify the kinetics and voltage-dependence of the channel, and they include the binding sites for many of the organically available toxins, for example, tetrodotoxin or saxitoxin (Gilchrist et al., 2014). The variability in the subunits distinguishes different isoforms of ion channels. This variability also contributes to the specialised functional roles of each isoform. The typical functioning of voltage-gate sodium channels is that depolarisation of the membrane opens the channel. Then, within milliseconds of opening the channels transition into a nonconducting inactive state, stopping the positive influx of sodium ions. Differences in voltage-gated sodium channels activation/inactivation vary with function and localisation. When fast

inactivation is incomplete, such as with mutations and defects of the channel, it can create persistent sodium currents. This leads to the cell having a more positive potential than it normal. This can cause a loss of information as the cells may be firing too much and action potentials are being triggered too easily.

In humans, when voltage-gated sodium channels malfunction, severe pathologies can arise due to over activation of excitable cells. For example, cardiac cells rely heavily on sodium channels to activate them; however, when the cells become too active they can cause cardiac arrhythmias such as tachycardia (Remme and Bezzina, 2010). Additionally, when neurons in the brain are overactive, this can cause epilepsy (Kaplan et al., 2016). Therefore, sodium channel expression levels must be kept within a set range for the system to function correctly.

For this project, I hypothesised that increasing the number of sodium channels would increase the influx of positive sodium ions into the KCs, thus depolarising the cells faster and making them more active and excitable. Thus, to assess KC homeostasis, increasing the excitability via artificially increasing sodium channels should trigger processes to maintain sparse coding in KCs.

1.3.2 NaChBac

One method of increasing the number of sodium channels in neurons can be achieved through regulation of gene expression. Ren *et al.*, (2001) identified the first prokaryotic voltage-gated sodium channel, named NaChBac, from *Bacillus halodurans*. Subsequently, this led to the detection of many homologous voltage-gated sodium channels in other prokaryotes (Ito et al., 2004; Koishi et al., 2004; Irie et al., 2010). In eukaryotes, voltage-gated sodium channels are found ubiquitously as they have multiple roles in various physiological functions. In contrast, voltage-gated channels are not ubiquitous in all prokaryotes and have not developed to play as vital role in the physiology of prokaryotes. However, in some bacteria, voltage-gated sodium channels have roles in motility and chemotaxis (Ren et al., 2001; Ito et al., 2004; Irie et al., 2010). *B. halodurans* live in very high salt conditions and thus they have a high influx of sodium through their channels. As sodium is the driving force of the flagellar motor in the *B.*

halodurans, a function not needed in all prokaryotic cells, it is likely that NaChBac has a role in the control of flagella activity (Ren et al., 2001).

NaChBac has four subunits that have identical amino acid sequences (Figure 3; Charaloambours and Wallace, 2011). This arrangement is unlike eukaryotic voltage-gated sodium channels which have different functions for each domain (Powl *et al.*, 2010; Nurani *et al.*, 2008). Furthermore, the C-terminus of NaChBac is significantly shorter than eukaryotic voltage-gated sodium channels and lacks a “ball and chain” structure usually seen in eukaryotic voltage-gated sodium channels. The “ball and chain” structure is the inactivation gate and contributes to the flow of sodium ions through the channel. The “ball” is a small protein domain, typically formed by the amino acid sequence known as the N-terminal domain. The “chain” refers to the linker segment connecting the inactivation ball to the rest of the sodium channel. In the inactivation state of eukaryotic voltage-gated sodium channels, the “ball” swings into the channel's central pore, blocking ion flow. Thus, NaChBac cannot ‘plug’ the pore in the inactivation state of the channel (Richardson et al. 2006; West et al. 1992; Stühmer, 1989). This also means that NaChBac has an inactivation rate 10-100 fold slower than the range of inactivation in eukaryotes (Ren et al., 2001; Koishi et al., 2004). NaChBac's sodium selectivity is determined by the P-loop in its subdomain (Charaloambours and Wallace, 2011, Figure 3).

NaChBac is 274 residues long and the sequence of NaChBac is similar to eukaryotic voltage-gated channels: 17-23% sodium channels, 18-23% to calcium channels and 12-17% potassium channels. Furthermore, they are 22-69% similar to prokaryotic voltage sensing sodium channels (Koishi et al., 2004; Ito et al., 2004; Irie et al., 2010; Charalambous and Wallace, 2011).

Although NaChBac is more similar to lower eukaryotic sodium channels it does have sections which are similar to sodium channels of higher eukaryotes such as electric eel, zebrafish and even humans (Charalambous and Wallace, 2011). Particularly, many of the critical functional residues are conserved throughout eukaryotes and prokaryotes, like NaChBac's glycine hinge and repeating sections in its S4, where their voltage sensor is (Figure 3; Chahine *et al.*, 2004). Unusually, NaChBac has a similar pore structure to the prokaryotic potassium channel KvAP (Richardson et al., 2006) and NaChBac has a similar structure to the Shaker potassium channel (discussed later) as

they have a similar spatial relationship between the pore and voltage sensor subdomains (Shimomura et al., 2011). Therefore, NaChBac's three-dimensional structure is conserved throughout eukaryotic and prokaryotic voltage-gated channels.

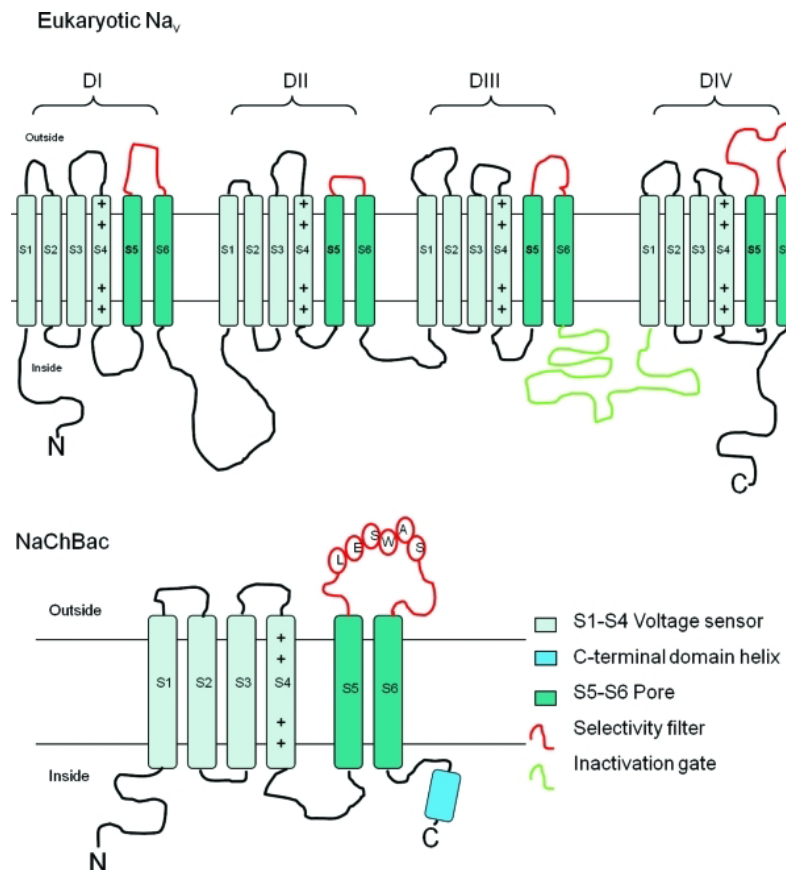


Figure 3 Schematic diagram comparing voltage-gated sodium channels from eukaryotes (top panel) and NaChBac (bottom panel).

Eukaryotic sodium channels have four homologous domains DI-DIV. The voltage sensor subdomains (S1-S4) are light green, S5 and S6 helices form the pore subdomains and are dark green. The selectivity filter regions are red. N = N-termini and C = C-termini (Charloambours and Wallace, 2011).

NaChBac has proven to be a good tool for examining voltage-dependent sodium channel function because of its ability to be expressed in a functional form in various experimental models. For example, even though *Escherichia coli* does not usually have sodium channels, NaChBac has been successfully expressed in the bacteria (Richardson et al., 2006; Nurani et al., 2008). In *Escherichia coli*, ligand and flux assays confirm the proper folding and sodium selectivity of NaChBac expressed, as well as the correct binding of typical channel blockers (Nurani et al 2008). Furthermore, NaChBac has been expressed in multiple mammalian systems, from monkey to human kidney cells (Ren et al., 2001; Chahine et al., 2004; Kuzmenkin et al., 2004).

Pharmacologically, NaChBac doesn't share all of its properties with eukaryotic voltage gated sodium channels as they have binding sites that NaChBac does not have (Guardiani et al., 2017). NaChBac is insensitive to tetrodotoxin, which is a well-known toxin for eukaryotic voltage-gated sodium channels. Zhu et al., (2020) tested 16 local anaesthetic compounds that are known to bind to the pore of Nav1.7 (eukaryote) and found that 11 of those compounds robustly blocked NaChBac. Additionally, NaChBac can be blocked by calcium channel blockers such as nifedipine and nimodipine (Ren et al., 2001). Thus, NaChBac has characteristics similar to eukaryotic channels.

To summarise, investigators commonly use NaChBac to research sodium currents due to the channel being well characterised with a simple structure and biophysical properties that are similar to mammalian sodium channels. By studying NaChBac, we can gain insights into the fundamental mechanisms of sodium channel functions and the effects it has on the cell that it is expressed in. These results can improve our understanding of how sodium channels contribute to neural activity and how they are involved in homeostatic regulation.

1.3.3 Endogenous sodium channel para

A disadvantage of NaChBac expression in Kenyon cells (the cells used in this project) is that it is an exogenous channel of *Drosophila*. Therefore, investigating other channels that are endogenous to *Drosophila* is more likely to reveal how homeostasis innately occurs. *Drosophila* only have one endogenous voltage-gated sodium channel gene, *paralytic* (DmNav/para; Feng et al., 1995; Miyazaki et al., 1996; Mee et al., 2004), that contributes to neuronal functioning. *Drosophilae* have another voltage gated sodium channel called Na channel protein 60E (NaCP60E). NaCP60E channels are primarily localised in the sensory neurons of external organs. However, as NaCP60E null animals are still viable with no loss of inward sodium currents these channels are not thought to be vital for neuronal firing (Hong and Ganetzky, 1994). While *Drosophila* possess only one essential voltage-gated sodium channel, Para, in contrast to mammals that have nine, it exhibits multiple functions due to gene splicing that alters its properties for different cellular roles (Catterall, 2000; Goldin et al., 2000; Yu and Catterall, 2003; Huang et al., 2017). Splicing results in para have predicted that there are ~60 isoforms which have different developmental expressions (Olson et al., 2008; Lin et al., 2009; Lin

et al., 2012). For example, Lin et al., 2012 found that a pair of mutually exclusive, membrane-spanning exons (K and L) that markedly affect the magnitude of the persistent current that occurs from incomplete inactivation of Para. Thus, the splice isoform expressed can determine the magnitude para's current (Lin et al., 2009). For example, artificially increasing synaptic excitation, alters para gene splicing to increase the fraction of transcripts with exon L, resulting in larger Para channel currents. This incomplete inactivation leads to increased action potential firing (Lin et al., 2012).

Para is expressed throughout development from embryo to adult (Amichot et al., 1993; Hong and Ganetzky, 1994), but it has a higher expression in adults than in larvae. The correlation between para localisation in active zones, the expression of activity-regulated genes and mature markers suggests that Para is expressed in active populations of neurons (Ravenscroft et al., 2020). In the neurons that express para, the channel is localised to the axonal segments distal to the soma, the distal axon initial segment (DAIS; Trunova et al., 2011). Electrophysiological recordings show that the DAIS is similar to the mammalian axon initial segment as voltage-gated sodium channel dependent action potentials initiate there (Ravenscroft et al., 2020). Although, Para is concentrated in the DAIS, there are low levels of expression distributed along the axons to propagate an action potential. Para expression in the axons is seen more in the long neurons of *Drosophila*, such as the motor neurons or cells that cross over the hemispheres of the brain (Ravenscroft et al., 2020).

While both Para and NaChBac channels are useful models for investigating sodium channel function, the well-characterisation and natural occurrence of para channels, makes them an attractive model for studying the innate relationships between neural activity and homeostasis.

1.4 Distal axon initial segment

As mentioned earlier, KCs have a distal axon initial segment (DAIS) where action potentials are generated when a large depolarisation current has travelled from the dendrites to the segment. There is a high concentration of Para in the DAIS, which is why action potentials form there, suggesting a potential correlation between the electrical characteristics of KCs and the size or location of the DAIS. Research into the

functional significance of the neuronal axon initial segment has revealed that its position and length can vary significantly across different cells (Hamada et al., 2016; Höfflin et al., 2017) and can be regulated by neuronal activity (Jamann et al., 2018).

Various factors have been shown to trigger the movement of axon initial segment positioning such as: changes in input resistance (Grubb and Burrone, 2010; Wefelmeyer et al., 2015; Hatch et al., 2017; Lezmy et al., 2017), phosphorylation of voltage-gated sodium channels (Evans et al., 2015), redistribution of voltage-gated potassium channels (Kuba et al., 2015) or changes in cell capacitance (Kuba et al., 2014).

Trunova, Baek and Giniger (2011) were able to successfully identify and label the distal axon initial segment in KCs. By genetically manipulating the system, they provided evidence that the integrity and membrane protein anchoring within the DAIS rely on the intact actin cytoskeleton. Thus, labelling with actin-GFP showed that the DAIS had a unique actin structural organisation, and it accumulates a specific ankyrin isoform, Ankyrin1. Furthermore, using this technique they were able to show that Cdk5/p35 kinase regulates the formation and maintenance of the DAIS. Increasing Cdk5 activity in γ KCs can extend the DAIS by as much as 100%, in contrast, abolishing Cdk5 activity causes the domain to shrink proximally or disappear altogether. Therefore, manipulations in proteins can move the DAIS which may affect the electrical parameters of the neuron. Past research has shown that triggering a distal shift of the axon initial segment is accompanied with a reduction of excitability (Grubb and Burrone, 2010). Furthermore, theoretical evidence supports these ideas and suggests that distal shift of the axon initial segment can produce small decreases in excitability (Lezmy et al., 2017; Goethals and Brette, 2020). Contrary to these ideas, other research has found that in L5 pyramidal neurons, the distal displacement of the axon initial segment increases excitability (Fékété et al., 2021).

Considering these factors, the DAIS represents an additional parameter that can influence the excitability of KCs by artificially manipulating its length or placement. Therefore, exploring alterations in the DAIS provides an additional method for investigating the homeostatic regulations of KCs in response to such changes.

1.5 Nicotinic receptors

Changing the electrical parameters of an action potential is not the only method of affecting neuronal excitability. Nicotinic acetylcholine receptors (nAChRs) are ionotropic receptors for acetylcholine and are expressed only in the central nervous system in *Drosophila*. nAChRs mediate fast, excitatory transmission between neurons at the postsynaptic density (Salvaterra and McCaman, 1985; Restifo and White, 1990; Yasuyama et al., 1995; Lee and O'Dowd, 1999). This is unlike mammals which also express nAChR in their peripheral nervous system such as the neuromuscular junction (Albuquerque et al., 2009). Within the *Drosophila* there are ten possible subunit genes of nAChR (7 α subunits and 3 β subunits; Dupuis et al., 2012). This means that there is a large diversity in the structure and function of nAChRs.

The structure of *Drosophila* nAChRs is similar to that found in other species. The receptors have an N-terminal extracellular domain, four transmembrane passes and a small extracellular C-terminal segment (Dupuis et al., 2012). In mammalian systems, the α subunit of the receptors are where the acetylcholine (ACh) binds. However, past literature have contrasting ideas about where the ligands bind in *Drosophila* nAChRs, but as the channels consist of either only α -subunits or α - and β -subunits we can assume that the ligand binding sites are located between two α -subunits or between α - and β -subunits (Rosenthal and Yuan, 2021). Activation of these channels can cause a rapid and reversible increase in intracellular calcium and sodium ions directly through the channel, as well activate voltage-gated calcium channels, to induce excitation within the cell (Campusano et al., 2007).

Both projection neurons and Kenyon cells are cholinergic (Barnstedt et al., 2016). Thus, KCs both receive cholinergic inputs as well as utilise acetylcholine for their outputs. KCs express both ionotropic (nicotinic) and metabotropic (muscarinic) acetylcholine receptors. The nAChRs mediate fast excitatory post synaptic potentials of KCs (Dowd, 2003). Blocking sodium dependent and independent activity in Kenyon cells revealed that nicotinic acetylcholine receptors facilitate most of the excitatory drive (Gu and O'Dowd, 2006). The cholinergic input to KCs comes from the projection neurons (Oleskevich, 1999; Yasuyama et al., 2002; Perez-Orive et al., 2002), which can fire spontaneously in the absence of applied odours, contributing to spontaneous cholinergic input (Wilson et al., 2004). Therefore, changes in nAChR levels can impact

the electrical properties of Kenyon cells via input excitation and by studying these receptors, we can gain a deeper understanding of homeostasis and its underlying mechanisms.

1.6 Potassium channels

Potassium channels play a crucial role alongside sodium channels in determining the excitability of neurons. These channels have been found in almost every cell type across all living organisms. Acting as membrane proteins, they regulate the movement of potassium ions (K^+) between the inside and outside of cells. Due to their involvement in numerous physiological processes potassium channels are widely distributed in organisms and cells. Potassium channels serve a multitude of vital functions such as homeostasis (Hille, 2001). The initial identification of potassium channels originated from the discovery of the Shaker phenotype in *Drosophila* (see Section 1.6.1 below). This finding sparked further research into the proteins responsible for facilitating the rapid movement of potassium ions across cellular membranes (Kaplan and Trout, 1969; Salkoff and Wyman, 1981; Tanouye et al., 1981; Wu et al., 1983; Kamb et al., 1987; Pongs et al., 1988; Tempel et al., 1987).

The discovery of K^+ channels led to the investigation of their structure (Jiang et al., 2002; Jiang et al., 2003). Potassium channels have transmembrane helices (TMs) that span the width of the cell membrane. Based on the structure and function of the channel they can be categorised into three major families: (1) six transmembrane domains (6TM) which can be either voltage gated and/or calcium dependent, (2) inward-rectifier K^+ channels that have 2 TMs and (3) tandem pore domain that have four TMs (Hille, 2001; Reviewed by Kuang et al., 2015). There are other potassium channels that do not fit into these major families such as 2/5 TMs ligand-gated channels. Regardless of the class it belongs to, potassium channels have two major components: the pore forming domain and the regulatory domain (Kuang et al., 2015; Figure 4). The pore-forming domain is similar in all types of K^+ channels and is responsible for the transportation of the K^+ ions. A simple explanation of the organisation of K^+ channels is a tetramer with each monomer containing one pore-forming domain (Figure 4; Reviewed in MacKinnon, 2003; Kuang et al., 2015).

The regulatory domains surrounding potassium channels are responsible for sensing stimuli, and these regions vary across different classes of channels. Additionally, in many cell types, K⁺ channels are regulated by their unique auxiliary subunits, resulting in diverse functional roles within the cell.

K⁺ channels must respond rapidly on sensing changes in the environment. Some of the K⁺ channels within neurons have a voltage sensor domain which is positioned at the periphery of the channel and consists of 4 subunits (S1-S4; Jiang et al., 2002). Other types of K⁺ channels are not voltage-dependent, such as "leak channels" which are the simplest type of ion channel and are always open to counterbalance the effects of other ion channels. For voltage dependent potassium channels the voltage sensing domain detects when there is a change in the membrane potential. The detection leads to a conformational change in the pore which either closes or opens the channel (Hodgkin and Huxley, 1952).

K⁺ selectivity is highly conserved in potassium channels and is located in the pore, which is the narrowest part of the channel (~3 Å; Doyle et al., 1998). The selectivity filter is lined with oxygen atoms which provide four binding sites for K⁺ ions. This mimics the arrangement of water molecules surrounding the K⁺ ions and when a K⁺ approaches the channel there is a configuration change that allows potassium ions to enter. Sodium ions have a different arrangement of water surrounding them and so they cannot enter the K⁺ channels as easily, but, under certain circumstances Na⁺ and Ca²⁺ can enter (Carrillo et al., 2015).

When potassium channels open, the potassium ions usually travel down their electrochemical gradient, thus, out of the cell. Potassium channels help repolarise the membrane after it has been depolarised by the sodium and/or calcium channels. Repolarising the membrane is necessary for returning to a negative membrane potential to terminate the action potential signal (Goldman, 1943; Hodgkin and Huxley, 1945; Hodgkin and Katz, 1949). The 6TM family of potassium channels are activated upon membrane depolarisation, termed "delayed rectifier," these channels exhibit a delay in altering membrane conductance following a depolarising voltage step as they are slowly activating. Primarily localised in axons, delayed rectifier channels, also known as K_v currents, represent the predominant potassium currents in most neurons. As the voltage

reaches a threshold, the conductance of these channels increases while their inactivation occurs slowly.

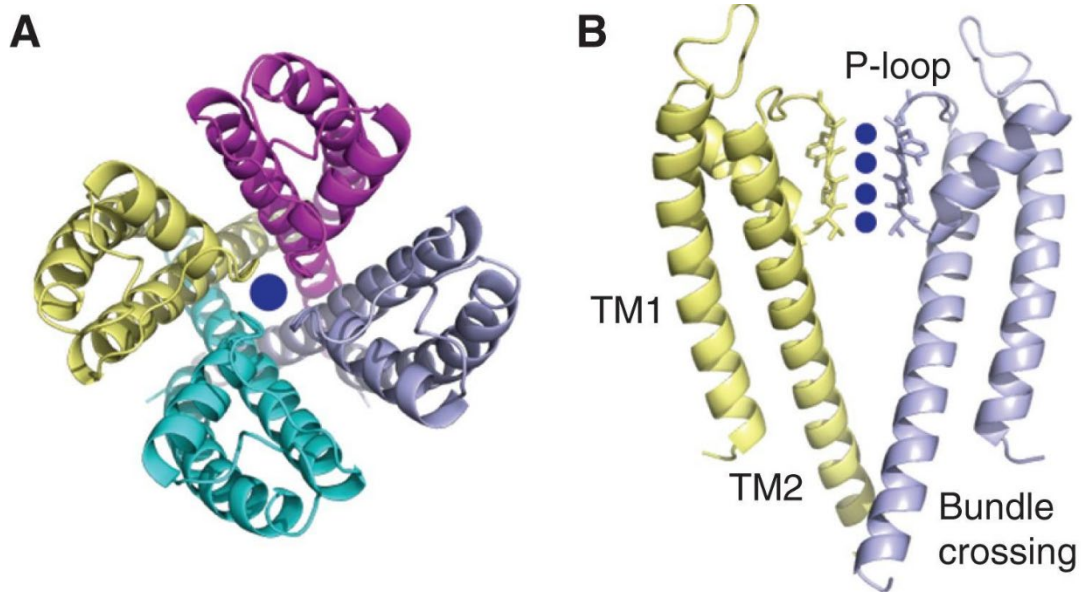


Figure 4 Schematics of potassium channel configuration taken from (Kim and Nimigean, 2016). (A) Potassium channel tetramer viewed from the top of the membrane. The subunits are each coloured uniquely, and the pore is shown with a K⁺ ion (blue sphere). (B) Side view of the potassium channel (2 subunits removed for simplicity). The P-loop forms the selectivity filter and four potassium ions connected.

Potassium channels are the most diverse ion channel family and *Drosophila* have over 30 potassium channels (Littleton and Ganetzky, 2000; Vähäsöyrinki et al., 2006). The presence of numerous distinct types of potassium channels can be attributed to the varying requirements of cells based on their specific functions. It is likely that different cells require different concentrations of channels because of their varying functions. For example, it is predicted that neurons that have high firing frequencies have high levels of Kv3 channel expression because they activate and deactivate extremely quickly, allowing fast repolarisation (Wicher et al., 2001; Wulff and Wisden, 2005). Given the contribution of potassium channels to neuronal function, I wanted to determine their involvement in regulating excitability specifically in KCs. In the following sections, I will discuss a few of the many endogenous potassium channels found in KCs and examine their impact on neuronal firing, modulation of membrane potential, and their significance to research.

1.6.1 Shaker

As mentioned earlier, the first potassium channel was discovered through a *Drosophila* mutant. The mutation caused uncontrollable leg shaking under anaesthetic and so the channel was labelled Shaker (Sh; Kaplan and Trout, 1969; Salkoff and Wyman, 1981; Tanouye et al., 1981; Wu et al., 1983; Kamb et al., 1987; Tempel et al., 1987; Pongs et al., 1988) Shaker channels pass fast transient A-type current (I_A). They are activated by membrane depolarisation and inactivate rapidly (Salkoff and Wyman, 1981; Wu et al., 1983; Pongs et al., 1988; Haugland and Wu, 1990). Shaker mutants lack I_A in their presynaptic terminals and so repolarisation of the cell is delayed. This causes a build-up of neurotransmitter to the neurons in control of leg movements and so they become overactive creating an uncontrollable shake (Salkoff and Wyman, 1981). In *Drosophila* neurons, the expression of the Shaker channels is restricted to axons and nerve terminals (Rogero et al., 1997) and their roles include; synaptic transmission, plasticity, information processing in the visual system, mating behaviour, sleep, learning and memory (Wu et al., 1983; Davis, 1993; Hall, 1994; Cirelli et al., 2005; Ueda and Wu, 2006; Guan et al., 2011).

Since the Shaker potassium channel is well characterised, both genomically and electrophysiologically, it makes them a good candidate for dominant-negative suppression to understand how Shaker's absence contributes to cell excitability. Mosca et al. (2005) produced a Shaker dominant negative (SDN) transgene as a tool for targeted increase in electrical excitability. SDN effectively suppressed type A current and increased spontaneous synaptic release events when expressed in larval muscle cell neurons (Mosca et al. 2005). Changes to Shaker expression not only affects the electrical properties of neurons but can change the gross morphology. When *Drosophila* motor neurons expressed ShakerDN, electrophysiological recordings showed a change in their intrinsic excitability and there was a significant increase in dendritic outgrowth and elongation of motor neuron dendrites (Duch et al., 2008).

Research has shown that Shaker expression levels can change in homeostatic response to changes in other ion channel expression levels (Peng and Wu, 2007). When the calcium channel α subunit (*cac*) is genetically disrupted in cultured *Drosophila* neurons, this leads to a decrease in calcium-gated potassium currents (*shab*; (Peng and Wu, 2007). To compensate for the loss of calcium-gated potassium current, voltage-

gated potassium channels (particularly Shaker) are upregulated (Peng and Wu, 2007). However, this relationship was not reciprocal as cac levels did not alter in response to various potassium channel mutations (Peng and Wu, 2007). Therefore, Shaker has possible involvements with homeostatic regulation to maintain stability.

While it is possible to chemically block Shaker channels, such as with 4-aminopyridine (4-AP) (Stocker et al., 1990), this project uses methods to block channels throughout development via genetic means, i.e. dominant negative strategies and RNAi. This is because the aim was to investigate homeostatic processes which are unlikely to occur within the limited timeframe of imaging. Considering Shaker's effects on neuronal excitability, I hypothesised it to be a good candidate tool for disrupting the channel's function and increase the excitability of KCs.

1.6.2 Shab

Following the identification of Shaker mutants, when Shaker was knocked down the flies still contained K⁺ currents like those produced by Shaker. To investigate this, Shaker-complementary DNA probes and low-stringency hybridisation were used to find three more genes: Shab, Shaw and Shal.

In mammals, Shab channels (K_v2.2.) are involved in maintaining the membrane potential, controlling the excitability of neurons, duration of action potentials and tonic spiking (Murakoshi and Trimmer, 1999; Baranauskas et al., 1999; Malin and Nerbonne, 2002; Misonou et al., 2004; Park et al., 2006). In *Drosophila*, Shab channels (K_v2) are involved in the sustaining K⁺ currents in neurons and muscles (Tsunoda and Salkoff, 1995b; Singh and Singh, 1999) and are localise to the axons (Werner et al., 2020). Furthermore, in *Drosophila*, Shab channels contribute to the regulation of action potentials, synaptic transmission, photoreceptor performance and larval locomotor behaviour (Ueda and Wu, 2006). Shab channels have been shown to regulate the membrane repolarisation and disruption of Shab in cultured *Drosophila* neurons produced a significant damping on repolarisation of the membrane (Peng and Wu, 2007). Furthermore, it has been shown that a reduction of Shab conductance in photoreceptors induces homeostasis. When Shab was reduced but not completely eliminated, there was a proportional decrease in input resistance of the photoreceptors

(Vähäsöyrinki et al., 2006). The decrease in input resistance, stimulated by increasing the leak conductance, was thought to act as a mechanism for maintaining neuronal functioning. Therefore, exploring Shaw inhibition is another potential method to increase KC excitability and investigate their involvement in homeostatic regulation.

1.6.3 Shaw

Another potassium channel found in *Drosophila* is Shaw. Two genes within this family have been found: Shaw (Kv3) and Shawl. In this project I will be concentrating on Shaw (Butler et al., 1989; Covarrubias et al., 1991; Hodge et al., 2005). Shaw potassium channels are slow-activating and conduct non-inactivating K⁺ current (Tsunoda and Salkoff, 1995a). Shaw channels are expressed throughout the nervous system and during rest Shaw potassium channels stay open, driving the potential towards negative voltages to potassium's equilibrium potential (Wei et al., 1990; Salkoff et al., 1992; S. Tsunoda and Salkoff, 1995a; Hodge et al., 2005; Parisky et al., 2008). Shaw channels also have physiological roles in other processes such as the circadian clock in *Drosophila* (Hodge et al., 2005; Smith et al., 2019).

Mutations in Shaw can increase neuronal excitation. Shaw is primarily neuronal and localised to axon terminals. In *Drosophila*, truncated versions of Shaw to increase somatic excitability by decreasing endogenous potassium currents (Hodge et al, 2005). Furthermore, broad expression of the dominant negative Shaw channel in *Drosophila* caused hyperexcitability phenotypes such as shaking or wing expansion (Hodge et al., 2005). Additionally, in the clock neurons of *Drosophila*, Shaw dominant negative (which weakens Shaw's ability to pass potassium currents) and Shaw-RNAi, increase neuronal excitation (Hodge and Stanewsky, 2008). Given the crucial role of Shaw channels in maintaining the resting membrane potential, I hypothesised that disrupting Shaw channels in KCs would result in heightened excitation, as the cells would be closer to the spiking threshold. This prediction stems from the understanding that Shaw channels play a pivotal role in regulating the membrane potential, and manipulating their function is expected to impact neuronal excitability in KCs.

1.6.4 Shal

The last potassium channel I will be discussing is called Shal (Kv4). Shal is the only other channel that conducts A-type K⁺ current in neurons and there are three members of the Shal family (Butler et al., 1989; Covarrubias et al., 1991; Singh et al., 2006) Shal is the most highly conserved K⁺ potassium channel between *Drosophila* and mice (Pak et al., 1991). The rapid inactivation of Shal currents has been noted to directly affect the membrane potential and play a critical role in post-synaptic potentials and neuronal firing. There is only one Shal potassium channel gene and it is present in virtually all neurons in *Drosophila* (Tsunoda and Salkoff, 1995a). Interestingly, although there is only Shal channel in *Drosophila*, it can swap to between either a 'fast' or 'slow' gating mode (Tsunoda and Salkoff, 1995a). However, the mechanisms of how the gating is changed are primarily unknown (Kise et al., 2021).

Shal channels are found in both cell bodies and dendrites of neurons in *Drosophila* (Diao et al., 2010). They act as the main determinants of dendritic excitability (Diao et al., 2010). Shal channels activate at significantly more negative voltages than other potassium channels and their inactivation is mostly independent of voltage. They activate at these voltages to control frequency of firing as well as locomotion in *Drosophila* (Ping et al., 2011).

In cultured *Drosophila* neurons, a dominant negative subunit in the Shal channel can eliminate the I_A without affecting other potassium or sodium currents (Ping et al., 2011). Research with the dominant negative Shal channel found that I_A from Shal is required for repetitive firing, as I_A contributes to membrane repolarisation which is needed before the next action potential can fire. This repetitive firing was then found to be critical in larval crawling, and adult climbing and grooming as the *Drosophila* become defective when a dominant negative version of Shal was expressed (Ping et al., 2011). Past research using electrophysiology, showed that when overexpressing Shal channels there was a decrease in excitability of α/β_c KCs. (Groschner et al., 2018). Furthermore, expressing ShalDN reduced the *Drosophila's* ability to distinguish between similar odours which is a behaviour consistent with an increase in KC excitability (Groschner et al., 2018). Therefore, despite the work from Ping et al., (2011), in this project I hypothesised that disrupting Shal currents should lead to an increase in excitability in

KCs. By employing this approach, I then aimed to investigate the underlying homeostatic mechanisms that would respond to the increased neuronal excitability.

1.7 *Drosophila* as a model organism

In this project I will be using *Drosophila melanogaster* to investigate the homeostatic effects of ion channel levels changing. *Drosophila melanogaster* are commonly used for biomedical research due to the benefits of low maintenance cost and a rapid generation time. *Drosophila* only have four chromosomes and have been studied extensively (Adams et al., 2000; Bier, 2005; Matthews et al., 2005). Compared to other model organisms, *Drosophila* genetics can be manipulated relatively easily, thanks to the many genetic tools developed over the last century (Bier, 2005; Hughes et al., 2012). More than 70% of disease-related human genes have orthologous genes with *Drosophila* (Reiter et al., 2001; Cavaliere and Hodge, 2011) and the two species share many cellular signalling pathways (Tickoo, 2002; Mattila et al., 2009). Therefore, studying mechanisms in *Drosophila* and systems within *Drosophila* may provide insights into human cell studies. However, there are some drawbacks to using *Drosophila* as a model system to study human mechanisms and disease. For example, *Drosophila* have a significantly different anatomy and organ system compared to humans. Some organs found in humans, such as the lungs, are absent in flies. Therefore, studying organ-specific diseases or mechanisms that rely on human-specific structures may be challenging. Furthermore, flies have a simpler immune system and drug metabolism, and so their responses may differ from humans.

Drosophila genetics benefits from balancer chromosomes (Muller, 1927) and genetic/phenotypic markers. Balancer chromosomes are used to maintain a fly line. They are able to keep homozygous lethal or sterile mutations from being dropped from a fly line and they prevent meiotic recombination separating multiple alleles on the same chromosome. The balancers can have recessive lethal mutations, dominant markers, and multiple chromosomal translocations and inversions that prevent recombination with the homologous chromosome. Balancers have mutations that cause phenotypes (physical markers) such as curly wings or divergent eye shapes, which reveal whether the balancer is present in a fly. This helps track the presence of transgenes on the

homologous chromosome to the balancer. In contrast, mice do not have naturally occurring balancer chromosomes or inversions that can be readily used for the same purpose. Human genetic research primarily relies on other tools, such as genetic mapping, gene-editing techniques (e.g., CRISPR/Cas9 (Jinek et al., 2012)), and the study of naturally occurring genetic variations (e.g., single nucleotide polymorphisms (Gray, 2000)).

The development of the GAL4/UAS system (Brand and Perrimon, 1993) has been revolutionary. It is used to express genes in specific cell types and structures within *Drosophila*. GAL4 is a transcriptional activator that binds to the Upstream Activating Sequence (UAS) promoter sequence (Figure 5). Once bound, this combination recruits RNA polymerase and initiates the transcription of the downstream sequence. The targeted integrated genes are only expressed when GAL4 is expressed (Figure 5).

GAL4 expression is restricted to particular cells either through placing engineered promoter/enhancers around the GAL4 transgene (usually upstream), or through inserting GAL4 with a bare promoter randomly in the genome and hoping that surrounding genomic enhancers will cause expression in an interesting population of cells. In the latter case, large libraries of GAL4 lines have been screened to pick out lines that label particular neurons (Tanaka et al., 2008).

The power of the GAL4/UAS system lies in the fact that any GAL4 line (expressing GAL4 in a restricted cell population) can be combined with any UAS line (expressing a gene of interest) to express any arbitrary sequence in (almost) any cell population. The discovery of the GAL4/UAS system led onto the invention of two alternative systems, the LexA/LexAop system (Lai and Lee, 2006) and the QF/QUAS system (Potter and Luo, 2011). These systems differ from GAL4/UAS as LexA is derived from *Escherichia coli*, and QF is derived from *Euprymna scolopes*. Each protein has different DNA binding specificities, leading to variations in the control of gene expression and potential applications.

Further control can be attained using the GAL80 gene. GAL80 represses GAL4 activity and GAL80^{ts} is a temperature-sensitive version that becomes non-functional at high temperatures (>29°C). GAL80^{ts} allows temporally controlled expression through the GAL4/UAS system by placing flies at a low temperature (no GAL4 activity, thus no

expression) or a high temperature (repression of GAL4 is relieved, thus allowing expression of the UAS transgene; McGuire, Mao and Davis, 2004; Pilauri et al., 2005; Figure 5). In addition, other techniques include Split-GAL4 lines, which restrict GAL4 expression to the intersection of two GAL4 lines' expression domains (Luan et al., 2006) and the MARCM system, which allows genetic manipulation of single neurons (Lee et al., 1999). More recently, new genetic schemes have been made that can regulate cell specific labelling, such as FlpTag (Fendl, Vieira and Borst, 2020; Figure 21). FlpTag can be used with green fluorescent protein (GFP) to selectively label cells or proteins, specifically when the target cell exhibits Flp expression. This is useful when investigating the expression levels of specific channels or proteins within a cell type. All these provide powerful genetic tools for investigating the upregulation, downregulation or insertion of ion channels in *Drosophila*. Some of these techniques that have been described will be used in the current project.

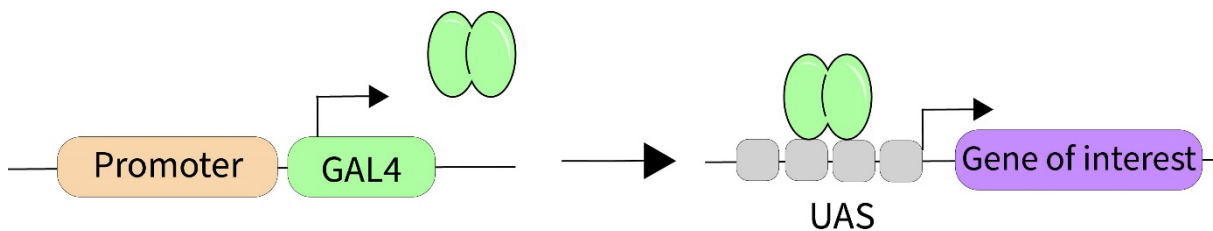


Figure 5 Schematic diagram of GAL4.

The promoter drives the expression of GAL4. The GAL4 protein binds to UAS which is located upstream of a gene of interest. When GAL4 binds to UAS, it initiates the transcription of the downstream gene which results in the increased expression of the target gene.

1.8 *Drosophila* olfaction and olfactory memory

The olfactory system is just one of many sensory systems within organisms that gather information from the surroundings. The ability of *Drosophila* to develop memories and learn adds another layer of significance to their olfactory system. Sense of smell is imperative to *Drosophila* as they rely heavily on it to seek out food (Beshel and Zhong, 2013), avoid danger (Suh et al., 2004) and find a partner to mate with (Kurtovic et al., 2007). The ability to discriminate between highly similar odours and recall their associations is critical for *Drosophila*, as it enables them to make decisions based on classified and organised stimuli (Keene and Waddell, 2007). *Drosophila* can learn to

associate specific odours with positive or negative experiences, forming memories that influence their future behaviour. Learning begins with the presentation of a conditioned stimulus, which is a distinct odour. This odour is then paired with either a positive or negative stimuli. For example, a negative stimulus could include exposure to an electric shock. As the fly repeatedly encounters the odour and reinforcement stimuli together, it forms an association between the odour and the experience. This association is stored as a memory, which can be either short-term or long-term, depending on the training conditions. When the fly encounters the learned odour again, the memory influences its behaviour: the fly will approach previously rewarded odours and avoid previously punished odours. Memory formation and retrieval of olfactory associative learning happens within the mushroom bodies of *Drosophila*.

Olfaction in *Drosophila melanogaster* starts with an odour (volatile chemical) activating olfactory receptor neurons (ORNs, Figure 6), which reside in the sensilla on the 3rd antennal segments and the maxillary palps (Vosshall and Stocker, 2007). *Drosophila* have ~1200-1500 ORNs which express a combination of ~60 odorant receptor genes (Clyne et al., 1999; Stocker, 2001; Robertson et al., 2003). However, each ORN typically expresses only one olfactory receptor gene (Vosshall et al., 1999). This is important as this gives the ORN odour specificity, as each receptor responds to a specific profile of odorants. Thus, when an odour is presented, an odour-specific set of ORNs will respond. ORNs project their axons into glomeruli of the antennal lobe (AL), and all 10-100 ORNs expressing the same OR terminate in the same AL glomerulus (Vosshall et al., 1999). There, ORNs synapse onto projection neurons (PNs; Jefferis et al., 2004; Jefferis et al., 2007; Figure 6). Each PN innervates a single glomerulus and thus receives input from the 10-100 ORNs expressing the same olfactory receptor (Vosshall et al., 1999), thus preserving the odour specificity of ORNs at the second layer of the olfactory system. PNs encode odours broadly as many PNs respond to most odour stimuli and many odours elicit responses in most PNs. This has been seen in both locusts and *Drosophila* (Moreaux and Laurent, 2007; Bhandawat et al., 2007). Furthermore, using local excitatory (Shang et al., 2007) and inhibitory (Python and Stocker, 2002; Wilson and Laurent, 2005) interactions, the antennal lobe broadens the tuning profiles of PNs relative to those of their similar ORNs, making better use of the coding space (Bhandawat et al., 2007). However, because PNs are broadly tuned,

odour encoding becomes densely combinatorial, which is inefficient for storing odour-specific memories.

PNs project to the lateral horn (LH) while creating en passant synapses onto the dendrites of the Kenyon cells (KCs) in the calyx of the mushroom bodies (Figure 6 and 7). The circuitry of the LH is stereotyped between individuals and is considered to mediate innate behaviours of the *Drosophila* (Wang et al., 2003; Min et al., 2013). Innate behaviours are defined as being genetically encoded and are hardwired into the brain, such as feeding or courtship behaviours. In contrast to the lateral horn, the Kenyon cells of the mushroom bodies (MB) are critical for the formation and storage of olfactory associative memories (Connolly et al., 1996; Dubnau et al., 2001).

Kenyon cells project their axons throughout the MB and terminate in specific lobes (Figure 8). Within each mushroom body there are ~2000 KCs. Their cell bodies are on the periphery of the calyx and their axons are split into 5 subsets: alpha (α) lobe, alpha prime (α') lobe, beta (β) lobe, beta prime (β') lobe and gamma (γ) lobe (Figure 8; Aso et al., 2014). $\alpha\beta$ KCs are the same neuron that has its axon split vertically and horizontally. This is the same structure for the $\alpha'\beta'$ KCs. KCs can be further classified into 7 types of KCs. There are two types of Kenyon cells that divide the γ lobe, the main and dorsal types; two types divide the α'/β' lobe into the middle (m) and anterior–posterior (ap) types; and three KC types divide the α/β lobe into the posterior, core (c), and surface layers (s; Aso et al., 2014). However, only 5 types receive olfactory information: γ_{main} , $\alpha'/\beta'_{\text{ap}}$, $\alpha'/\beta'_{\text{m}}$, α/β_{c} , and α/β_{s} (Aso et al., 2014). In these lobes, KCs synapse with mushroom body output neurons and dopaminergic neurons (Figure 6 and 8). There are 21 types of mushroom body output neurons (MBONs) and 20 types of dopaminergic neurons (DANs) innervating the MB (Aso et al., 2014). Dendrites of MBONs and axonal terminals of dopaminergic neurons intersect the longitudinal axis of the KC axons (Tanaka, Tanimoto and Ito, 2008; Figure 6). This system is analogous to other MBs in locusts and honey bees (Oleskevich, 1999; Perez-Orive et al., 2002). MBONs that use the same neurotransmitter extend dendrites to adjacent regions of the lobes; cholinergic MBONs in the vertical lobes, glutamatergic MBONs in the medial lobes, and GABAergic MBONs in an area of the lobes at the intersection between these two regions. Different populations of DANs are activated by unconditioned stimuli of different valence (e.g. reward like sugar or punishments like electric shock) and are the source of learning cues (Aso et al., 2014). MBONs are thought to encode learned valence of odours and can

lead to either avoidance or approach behaviour when artificially activated (Aso et al., 2014).

Olfactory associative memories form when DAN activity (signalling reward/punishment) coincides with KC activity (signalling an odour): the simultaneous activation of DANs with an odour-specific set of KCs depresses the synapses from the odour-activated KCs to MBONs leading to the “wrong” behaviour (Figure 8). For example, when an odour is associated with a punishment, like an electric shock, punishment-responsive DANs depress the synapses onto “approach” MBONs from the KCs that responded to the punished odour (Aso et al., 2014; Cohn et al., 2015; Handler et al., 2019; Figure 6). Therefore, the next time the learned odour is presented the relatively stronger behavioural output is triggered (in this case avoidance).

Entwined within each MB is an anterior paired lateral (APL) neuron. The APL neuron is a non-spiking γ -aminobutyric acid (GABA)-synthesising (GABAergic) neuron and is a crucial component of *Drosophila* odour associative memory as it provides feedback inhibition onto KCs (Pitman et al., 2011, Papadopoulou et al., 2011, Tanaka et al., 2008). When KCs are active, they activate APL which in turn inhibits KCs so they are not so overly activated by other odours. Furthermore, it has been shown that memory formation can induce plasticity in the APL neuron (Lin et al. 2014; Liu and Davis 2009; Zhou et al. 2019) to maintain proper functioning of odour associative memory.

A benefit of studying olfaction in *Drosophila* is that their olfactory processing can be investigated *in vivo*. For example, a single fly’s neuronal responses can be investigated with the animal still alive with calcium imaging. Another benefit is that behavioural tests can be used to determine a fly’s actions to an odour. Behavioural tests don’t have to be limited to one animal per trial as there are methods of investigating how populations of flies behave when confronted with olfactory choices in a controlled environment. The odour preference can be calculated by the amount of time the fly will spend in a certain area of a chamber designed to have odours in specific areas (Claridge-Chang et al., 2009). In contrast to these experiments, this project investigates *in vivo* neuronal signalling within a single fly. I am interested in understanding how Kenyon cells behave, on a cellular level, to a presented odour. In addition, given the critical role of the odour system in *Drosophila*, my research aimed to explore whether the Kenyon cells, a key component of this network, use homeostasis to sustain its functionality.

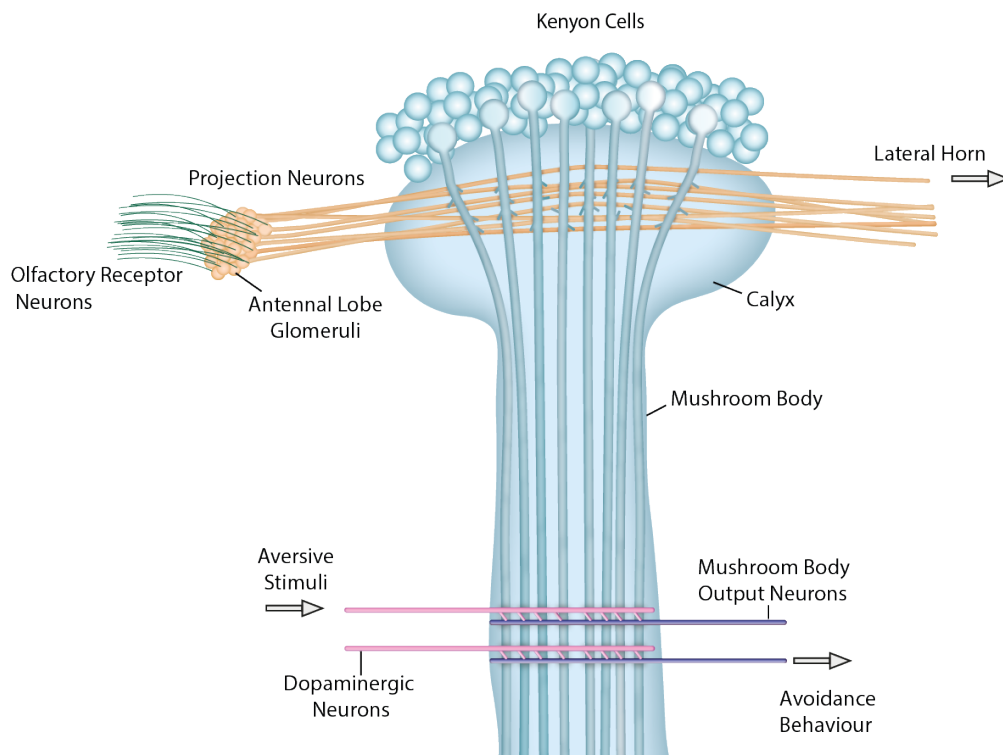


Figure 6 Schematic of the adult fly olfaction circuitry.

Axons from the olfactory receptor neurons project to antennal lobe glomeruli, which then connect to projection neurons. Projection neurons then form en passant synapses with Kenyon cell dendrites in the mushroom body calyx and terminate in the lateral horn. Some projection neurons bypass the mushroom body calyx and project only to the lateral horn. Kenyon cells project their axons throughout the mushroom body. Dopaminergic neurons and mushroom body output neurons synapse onto the Kenyon cells. When both the dopaminergic and Kenyon cell are activated simultaneously, their synapses weaken, and their accompanying behaviour is reduced.

1.9 Kenyon cells use sparse coding to create and store odour associative memories

The process described in the previous section produces odour-specific associative memories because only KCs activated by the odour paired with reward/punishment (as opposed to KCs activated by other, unreinforced odours) have their output synapses modified during learning. How does the mushroom body ensure that each KC doesn't respond to too many odours (which would decrease the specificity of olfactory memories)?

Neural coding is the pattern of activation of the neuronal population corresponding to an input. An important aspect of neural coding is the fraction of neurons that are strongly

active at any one time. A population with a low density code is sparsely coded, like the KCs, as they have strong activation in a relatively small set of neurons (Lin et al. 2014). As Kenyon cells use sparse coding, it means that they are required to be excitable as one another and that only 5-10% of them to respond to one odour (Wang, 2004; Turner et al., 2008). An increase of sparseness decreases the total energy consumption making it cost effective. Early studies investigating memory models showed that sparse coding is the most effective for storing patterns and associative memories (Kanerva, 1988). Sparse coding maximises memory capacity due to less cross over of activated neurons. The study of individual KCs shows very low spontaneous activity, along with stimulus selectivity and weak olfactory responses characterised by limited or absent action potentials in response to a stimulus (Turner, Bazhenov and Laurent, 2008; Demmer and Kloppenburg, 2009). KCs are unlike projection neurons, which have a broad spectrum of odours that activate them. Perez-Orive *et al.*, (2002) investigated the likelihood of odour activating PNs and KCs in locusts. They found that for all PNs and odours measured, the probability of an excitatory response was $p = 0.64$. In contrast, the probability for KCs under similar conditions was $p = 0.11$. They recorded spikes and found that PNs fired between 5 and 30 spikes, whereas KCs only fired one or two spikes (Perez-Orive *et al.*, 2002). The reduction in response in KCs was due to various underlying mechanisms causing KCs to be effective coincidence detectors leading to what is termed sparse coding.

When using a computational framework for the mushroom body under conditions of sparse coding, the effectiveness of associative memory diminishes due to realistic experimental fluctuations observed in maintaining neuronal excitability (spiking threshold and the number/strength of excitatory inputs) (Abdelrahman, Vasilaki and Lin, 2021). These shortages stem from uneven average activity levels exhibited by KCs. Nevertheless, memory performance can be rectified by introducing variability in one parameter to counterbalance the variability observed in other parameters. This equalises the average activity levels among the KCs, thereby restoring memory performance (Abdelrahman, Vasilaki and Lin, 2021). Thus, suggesting that sparse coding is generated through evenly spreading the activity across the KCs.

How can this even spread of activity across KCs be achieved? Answering this question requires understanding the basics of KC excitability. When presented with an odour, Kenyon cells get excitatory inputs from their dendrites in the calyx. The KC dendritic

claws, which form synapses with the axonal boutons of the PNs, become depolarised and the depolarisation travels to the peduncle (Figure 7). In the peduncle (cell axons) is the distal axon initial segment (DAIS) where an action potential (AP) is triggered if there is enough depolarisation from the EPSPs. The AP then travels down the axon into the lobe areas.

A single KC extends a small number of dendritic “claws”. Each claw typically receives information from one PN bouton. However, a single bouton can connect to multiple KC claws to form a discrete microglomerulus (Butcher et al., 2012; Figure 6 and 7). Anatomical and physiological studies have shown that, on average, a KC receives 6.4 inputs from a combination of PNs, and the identity of inputs into each KC is not stereotyped between flies (Murthy et al., 2008; Caron et al., 2013; Gruntman and Turner, 2013). However, KCs can have between 2 and 11 claws connected to projection neurons (Caron et al., 2013). Additionally, Turner, Bazhenov and Laurent (2008) show a variety of strength between PN-KC synapses and KC spiking threshold. Kenyon cells exhibit a distinctive input pattern that strikes a balance between randomness and selectivity. Kenyon cell inputs are mostly random which allows all the KC inputs to sample different parts of the projection neuron coding space. However, they’re not completely random this predisposes certain Kenyon cells to exhibit heightened responsiveness to specific categories of odours. This preference is attributed to the convergence of inputs from multiple glomeruli that share a common sensitivity to food-related odours. The randomness means that there is a high variety between each KC’s input as well as between each animal.

Kenyon cells generally require multiple simultaneous inputs to surpass their spiking threshold, a crucial mechanism for their selectivity (Gruntman and Turner., 2013). Reliable somatic action potentials typically demand the activation of multiple claws. While many odours activate just one or two claws, the presence of an accompanying somatic response is infrequent. However, when odours engage several claws, somatic responses are more common. This is a key cellular mechanism that allows KCs to be selective.

The APL neuron (mentioned previously) provides inhibitory feedback to the Kenyon cells, suppressing the activity of Kenyon cells (Lin et al., 2014). As a result, when the Kenyon cells become too active in response to an odour, the APL neuron can suppress

the Kenyon cell firing. This lateral inhibition enforced by the APL neuron enhances the contrast between active and inactive KCs. In the context of sparse coding, it ensures that only a small subset of KCs respond robustly to a particular odour, while others are inhibited. This helps in creating a distinct and efficient representation of different odours.

Caron *et al.*, 2013, analysed 665 connections to search for a defined structure between glomeruli and KCs. They concluded that the identity of a glomerulus connected to a KC provides no predictive information as to the identity of the remaining glomerular inputs onto that neuron. In contrast, Zheng *et al.* (2022) used EM-based mapping of PN-to-KC and the recently published connectome to reveal that there are actually non-random network structures. Typically, food-responsive PN types converged at above-chance levels on downstream KCs. Furthermore, convergent PN axons inclined to arborise near one another in the calyx, thus making the local KC dendrites more likely to receive input from those types of PNs.

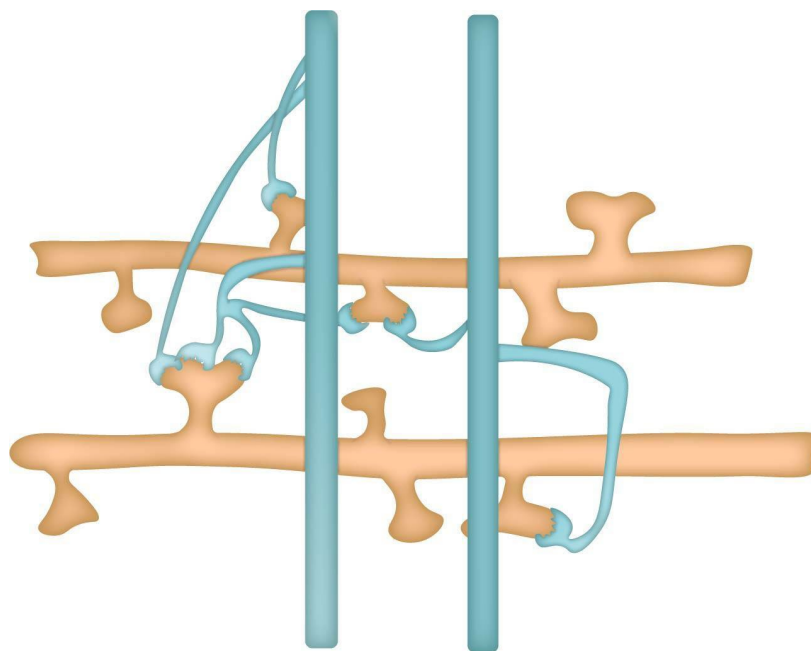


Figure 7 Schematic diagram of PNs and KCs connections. Kenyon cells (blue) have claws which synapse onto the boutons of the PNs (orange).

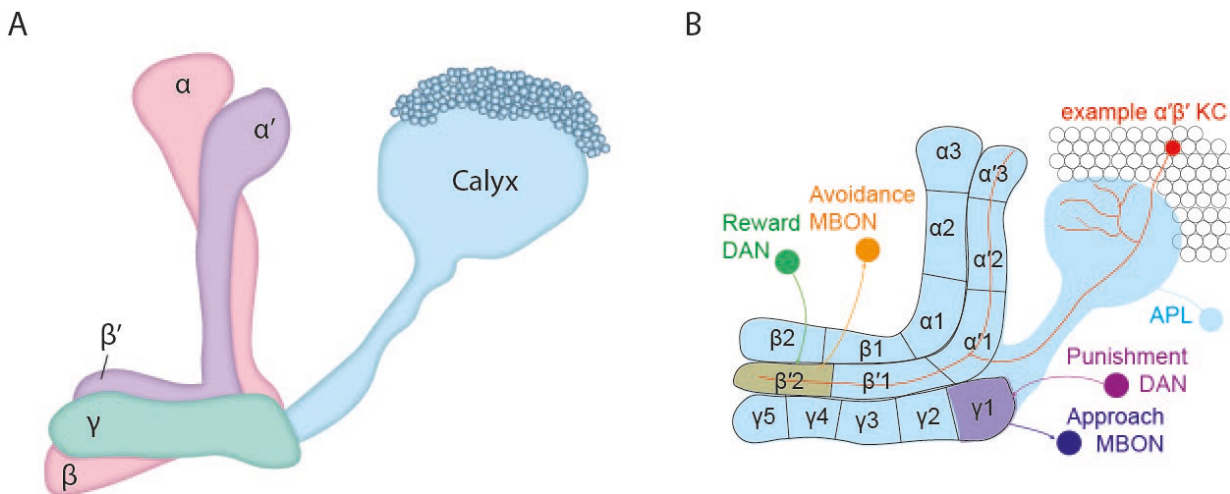


Figure 8 Subsets of KCs occupy different areas of the mushroom body. A. The schematic diagrams of the mushroom bodies show where the α , β , α' , β' and γ Kenyon cell axons occupy. B. The schematic shows the compartmentalisation of the KCs and for each lobe. DAN = Dopaminergic neurons, APL = Anterior paired lateral neuron, MBON = Mushroom body output neuron, KC = Kenyon cell.

All of the components discussed above mean that KCs are an exciting model to investigate homeostasis, as the KCs must remain stable in their activity to maintain only 5% population activity. A lack of sparseness predicts that the flies would be unable to differentiate between similar odours for odour association. This is because if an odour activates too many KCs the behavioural information for specific odours would be lost due to overlap of activity. Projection neurons are more broadly tuned to odours, and thus, KCs must rely on their own mechanisms to ensure that their population is equally excitable. To further this, if a Kenyon cell was active for multiple odours, it could lead to a learnt behaviour even in the absence of targeted training for that specific odour. I wanted to investigate whether they had robust homeostatic mechanisms which are triggered when their activity levels are artificially increased.

1.10 Comparing Olfaction in *Drosophila* and Vertebrates

After exploring the *Drosophila* olfactory system above, what can this teach us about sensory processing and learning in systems like our own? Like other insects and mammals, *Drosophila* have a wide array of motor, social and experience-based behaviours. This suggests that the *Drosophila* nervous system can carry out processes

that can be compared to those found in more complex animals, such as rodents. The *Drosophila*'s simpler system is valuable as it can lend itself to specific targets without becoming overly complex, for example, the anatomical separation of innate and learned odour association. This allows for the study of individual processes but also how those individual processes can be integrated with other systems to shape *Drosophila* behaviour.

To learn from *Drosophila*, we need to understand the comparisons to mammalian systems. A model commonly used for studying olfaction are rodents. Rodents have an olfactory anatomy close to our own. Their olfactory sensing neurons (OSNs) project across the cribriform plate and terminate in the olfactory bulb. Rodents maintain odour identity similar to *Drosophila* as their OSNs express specific odour receptors (ORs) and those with the same ORs project to distinct glomeruli in the olfactory bulb (Mombaerts et al., 1996). In the olfactory bulb the OSNs make synapses onto a variety of postsynaptic neurons including principal neurons and local interneurons. The principal neurons of the rodent's olfactory bulb drive learned and innate olfactory behaviours. This can be related to the PNs as they have a role in relaying olfactory information to higher brain regions, i.e. the mushroom body and lateral horn. Additionally, similar to what has been described earlier about KCs, odours evoke a sparse, unique ensemble of neurons in the piriform cortex (Stettler and Axel, 2009; Poo and Isaacson, 2009). Furthermore, inhibitory interneurons maintain this coding in the piriform cortex, which could be compared to the inhibitory APL neurons' effect on the KCs (Lin et al., 2014; Inada et al., 2017).

The olfactory system of the rodent is not the only vertebrate structure that has similarities to the mushroom body. Granule cell dendrites, within the cerebellum, also have claw-like ends which connect to the mossy fibre afferents and similarly to KCs, granule cells receive numerous multimodal inputs (Farris, 2011; Xiao and Scheiffele, 2018) which must be encoded and conveyed to the Purkinje cells, which they heavily converge upon. This can be related to how the parallel axons of KCs heavily converge upon the MBONs. Furthermore, like KCs, the cerebellum learns by long-term depression between granule cells and Purkinje cells (Steuber et al., 2007). By understanding the fundamental functionality of circuits, we can expand our knowledge to encompass other circuits that share similar structures, regardless of whether they are associated with olfaction or not.

Both insects and mammals have only two synapses separating the olfactory sensory neurons to the higher brain areas required for memory formation and responsive behaviour. Therefore, it is imperative to appreciate how these types of systems can operate in simpler (*Drosophila*) and in more complex (vertebrate) terms. To understand simpler systems is a way to begin to understand more complex structures. Therefore, using the *Drosophila* mushroom body to understand neuronal homeostasis for sparse coding will contribute to the knowledge of how vertebrate cells that use sparse coding may also use these mechanisms.

1.11 Two-photon calcium imaging

Two-photon calcium imaging is an excellent way to view neuronal activity and investigate odour responses of KCs in an intact *Drosophila* brain (Russell, 2011). Calcium ions generate versatile intracellular signals that are present in virtually all cell types in biology. Calcium ions can control many functions from heart muscle cell contractions to cell proliferation and cell death (Orrenius et al., 2003; Dulhunty, 2006). Within neurons, calcium ions have a variety of roles. In presynaptic terminals, calcium influxes initiate exocytosis of synaptic vesicles which contain neurotransmitters (see review Neher and Sakaba, 2008), whereas, postsynaptically, calcium is vital in activity dependent synaptic plasticity of dendritic spines (Zucker, 1999). Furthermore, in the nucleus, calcium is essential in regulating gene transcription (Lyons and West, 2011).

What is particularly useful for neurobiologists is that intracellular calcium levels rise in neurons when they are activated and fire action potentials. At rest, neurons have an intracellular concentration of ~20-100nM that can transiently rise during electrical activity 10-100 fold higher (Berridge et al., 2000). Only free calcium ions are biologically active and there are an array of mechanisms that underlie calcium influx, including but are not limited to: voltage gated calcium channels, ionotropic glutamate receptors, nicotinic acetylcholine receptors, and release from intracellular stores (Higley and Sabatini, 2008). Thus, intracellular calcium concentrations are a reasonable (though imperfect) proxy for neuronal activity levels, so several decades of effort have gone into developing methods to image intracellular calcium concentration in neurons.

The development of calcium imaging involved the innovation and refinement of calcium sensors along with the development of suitable technologies for capturing neuronal activity. Amongst the earliest calcium sensors to emerge was bioluminescent calcium-binding photoproteins (Ashley and Ridgway, 1968). There were many advancements throughout development, but a notable breakthrough happened with the introduction of fura-2 which was more sensitive and versatile (Neher, 1995). However, they still had drawbacks such as weak signals and high working concentrations. The next important development was the creation of protein-based genetically encoded calcium indicators (GECIs; Miyawaki *et al.*, 1997). These originally had limitations in their kinetics as they were slow to respond and had low signal-to-noise ratios.

Parallel to the development of calcium sensors was the production of new imaging technologies, ranging from video imaging to high-speed confocal microscopy (Smith and Augustine, 1988; Eilers *et al.*, 1995). The combination of these two technological and biological advancements enables the remarkable capability to capture real-time fluorescent changes at the single-cell level.

In this project I used two-photon imaging to investigate changes in calcium levels in the KCs. I use GCaMP which is a single-fluorophore genetically encoded calcium indicator. These types of indicators are especially useful for *in vivo* experiments because no external chemicals need to be added to the cell and they can be expressed specifically in particular neurons using genetic tools. GCaMP consists of an enhanced green fluorescent protein (EGFP) which is flanked by calmodulin (a calcium-binding protein) and M13 (a calmodulin-binding protein; Nakai *et al.*, 2001). When GCaMP is in the presence of calcium, the calmodulin-M13 component interacts with calcium which causes a conformational change in the fluorophore leading to an increase of emitted fluorescence (Nakai *et al.*, 2001). There have been many improvements upon the GCaMP family to increase dynamic range, response kinetics and signal to noise ratio. The development of GCaMP6f (f for fast) has been revolutionary for calcium imaging studies.

Chen *et al.*, (2013) show that GCaMP6f reliably detects fast calcium level changes triggered by action potentials and has a higher sensitivity than other calcium dyes. GCaMP6f can be used on a large group of neurons as well as on more specific subsets of neurons. An advantage of calcium imaging is that it allows real time analysis of

neurons and combined with two-photon imaging, investigating neurons located up to 500 μm below the cortical surface has become possible (Stosiek et al., 2003).

The development of the two-photon microscope was crucial as it allows for high-resolution and high-sensitivity fluorescence microscopy. This technique is particularly useful in imaging highly scattering brain tissue *in vivo* (Denk et al., 1990). In two-photon microscopy, two low-energy near-IR photons cooperate to excite a fluorescent molecule from its ground state. Using two-photon imaging reduces bleaching and out-of-focus excitation compared to other microscopy technologies because excitation only happens at the focal point. Two-photon imaging allows imaging deeper in tissue compared to regular confocal microscopy because it uses longer wavelengths of light for excitation (which penetrate biological tissue more easily) and because all emitted photons can be collected, even scattered photons, as no pinhole is needed to exclude out-of-focus excitation (as there is no out-of-focus excitation).

Drosophila are excellent models for investigating olfaction using two-photon calcium imaging. Their olfactory system is located close to the surface of the brain, eliminating the need for deep penetration and making it an ideal depth for two-photon imaging (Wang et al., 2003). Their genetic tools allow GCaMP to be expressed in specific neuronal populations. KC depolarisation triggers an increase in calcium concentration which can be detected by two-photon imaging. Since calcium is associated with cell excitation, an increase in GCaMP fluorescence generally corresponds to increased activity.

However, there are challenges when using *in-vivo* two-photon imaging. Brain movements can create artefacts that need to be corrected for using image registration. The signal-to-noise ratio might be poor if the GCaMP is too dim or too deep in the brain. However, an advantage of using *in vivo* calcium imaging for this project is that it allows the investigation of KC activity levels without the need for invasive techniques such as patch-clamp electrophysiology, and it allows us to record from many neurons simultaneously (whereas patch-clamp only allows recording from one cell at a time). A disadvantage is that two-photon calcium imaging does not show action potentials in a neuron as the kinetics are too slow. Nonetheless, the combination of two-photon calcium imaging and the genetic tools mentioned earlier enables effective investigation of KC activity levels.

1.12 Computational theories about homeostasis in KCs

The present study investigates the homeostatic responses of neurons to counteract artificial overexcitation. The project uses Kenyon cells in the olfactory system of *Drosophila melanogaster* as they must maintain a fragile balance of excitation and inhibition to remain at a stable activity state. As discussed earlier, the KC population receives a large input of olfactory information, but only ~5-10% of KCs respond. The KCs that do respond only fire a few spikes and therefore, they use sparse coding to interpret and store olfactory associative memories (Perez-Orive et al., 2002; Ito et al., 2008; Turner et al., 2008; Honegger et al., 2011). It is fundamental that the Kenyon cells are equally as excitable as one another, so that a subpopulation isn't being over activated. Thus, variability within the population would cause problems for the sparse coding and eventually behavioural output.

Past literature in the lab, from Abdelrahman, Vasilaki and Lin (2021), produced a computational model showing that KCs may use compensatory variability to enhance memory performance. They tested whether interneuronal variability would improve or weaken odour associative memory in KCs. For example, altering the number of PN inputs per KC, the strength of the synapses between PNs and KCs, or even KC spiking thresholds.

Adding experimentally realistic variability in neuronal excitation to the model reduced its memory performance. Variability was introduced step by step. First, they tested the performance of the model by holding three chosen parameters constant across all types of KC: the number of PN inputs per KC, the strength of each PN–KC synapse and the spiking threshold of the KCs. They would then vary only one of the parameters, continuing to two, and then lastly changing all three parameters. Therefore, there was a total of eight models. The increase in the inter-KC variability significantly impaired the model's performance during the testing of 100 input odours (Abdelrahman, Vasilaki and Lin., 2021).

Interestingly, the model with all the parameters fixed (not biologically realistic) outperformed the model with all the parameters variable (more biologically realistic). However, the biologically realistic model performance could be rescued when one

parameter's variability was compensated for another, thus cancelling out the variability to equalise the average activity among KCs. This meant that they still maintained their sparse coding, as shown by their ability to still respond uniquely to an odour. The study modelled two types of compensation. One type was using direct correlations between neuronal parameters, thus activity independent. This meant the modelled KCs adjusted their input synaptic weights to compensate for the variability in spiking threshold and number of PN inputs. Thus, a KC with a low spiking threshold or high number of PN inputs would have low synaptic input weight. The other model used activity-dependent homeostasis where the KC tuned its own input excitatory and inhibitory weight, or spiking threshold dependent on its activity levels. Both methods of compensation improved memory performance while still having the same amount of variability as the uncompensated model (Abdelrahman, Vasilaki and Lin., 2021). Activity-dependent homeostasis is likely to be more biological relevant, i.e. through tuning their synaptic weights or changing the levels of ion channel expression. However, they make the point that KCs are not infinitely flexible (as shown in their paper Apostolopoulou and Lin, 2020), thus, this type of activity dependent homeostasis may only contribute to how KCs are able to control their excitability. The results of this computational model show that, theoretically, KCs should have homeostatic regulations that maintain a stable excitability across their population, even in the presence of a high input variation.

1.13 Focus of this thesis

It is essential for KCs to have similar levels of excitability to prevent the formation of erroneous and overlapping odour associative memories. However, we still have a limited understanding of how KC activity is affected by various genetic manipulations of ion channels and what molecular mechanisms might be used to compensate for perturbations in activity. Therefore, this project aimed to investigate whether KCs employ homeostatic mechanisms to maintain their excitability and how neurons maintain consistent behaviours in encoding information despite inter-neuronal variability. Using calcium imaging, genetic manipulations and cell-specific GFP tagging the study sought to answer the following questions.

Firstly, how do KCs respond to an increase of sodium channels with NaChBac overexpression? Upregulating NaChBac expression in neurons is a widely used method

for boosting neuronal excitability. I asked whether expressing NaChBac would increase KC odour responses (as measured using calcium imaging) or whether homeostatic compensatory mechanisms might counteract the effect of NaChBac expression. To test what molecular mechanisms might account for NaChBac-induced changes in KC activity, I used GFP tagging to investigate how NaChBac expression changes the expression levels of ion channels that are associated with the excitability of KCs (specifically, the sodium channel Para, the potassium channel Shaker, hyperpolarisation-activated cation channels, and specific nicotinic acetylcholine receptors).

Secondly, to enhance neuronal excitability, alternative approaches exist beyond just increasing the expression of sodium channels. One effective method involves decreasing the levels or functionality of potassium channels, which prevents neuronal hyperpolarisation and sustains neurons in a depolarised state, increasing the likelihood of firing an action potential. Therefore, I decreased the levels or function of endogenous potassium channels in KCs with RNAis and dominant negative disruptions. I asked whether these manipulations would increase KC activity levels (measured by calcium imaging) and/or whether homeostatic compensation would cancel out these effects.

2 Materials and Methods

2.1 Materials

2.1.1 Fly rearing

Fly stocks and crosses were kept at 25°C or 18°C (for long-term stock maintenance or experimental reasons) on a 12hr light/12hr dark cycle in vials containing food mix with the measurements in Table 1.

Table 1 Fly food ingredients and measurements given to all flies.

Ingredient	Measurement
H ₂ O	1L
Medium Cornmeal	80g
Dried Yeast	18g
Soya Flour	10g
Malt Extract	80g
Molasses	40g
Agar	8g
10% Nipagin in Absolute Ethanol	25 ml
Propionic Acid	4ml

2.1.2 Fly lines

Fly lines used in Chapter 3

Fly lines used for investigating the effects of NaChBac in Kenyon Cells and projection neurons as well as the fly lines used to extend or shorten the distal axon initial segment in Chapter 3 are displayed in Table 2.

Table 2 Fly lines used to investigate the Kenyon cells and projection neurons with the expression of NaChBac with comments and citations of use.

Fly Line	Comment	Citation/Availability
lexAop-Gal80,UAS-GCaMP6F/R44E04-LexA;mb247-GAL4	Labels γ KCs	Bielopolski et al. 2019
UAS-GCaMP6f (attP40)	Fluorescent calcium sensors FLYB: FBst0042747	Chen et al 2013
R13F02- GAL4	Labels all KCs and inserts NaChBac in all KCs	Jenett et al. 2012
Gal80ts	Temperature controlled regulation of GAL4	McGuire et al. 2003
UAS-NaChBac	Bacterial sodium channel, BL 9468	Nitabach et al 2006
w[*];P{w[+mC]=UAS-NaChBac-EGFP}1/TM3, Sb[1]	NaChBac tagged GFP, BL 9466	Bloomington <i>Drosophila</i> Stock Center, (2006.3.19), FBrf0191601
Para ^{FlpTag}	Conditionally (cell specific) GFP-tagged Para sodium channel	Fendl, Vieira, and Borst 2020
UAS-Flp	Drives expression of FLP recombinase	Gifted by David Strutt
ParaRNAi	Stops the translation of the sodium channel para, BL 33923	Perkins et al. 2015
ShFlpTag	GFP tagged Shaker	Gifted by Borst Lab

lhFlpTag	GFP tagged lh channels	Gifted by Borst Lab
EagFlpTag	GFP tagged Eag potassium channels	Gifted by Borst Lab
nAChR α 6.EGFP	GFP tagged α 6 subunit, using CRISPR	Pribbenow et al. 2021
nAChR α 7.EGFP	GFP tagged α 7 subunit, using CRISPR	Pribbenow et al. 2021
GH146- GAL4	Expression in projection neurons	Stocker et al. 1997
UAS-CDK5 ^{DN}	The dominant negative version of CDK5 causes the DAIS to become shorter	From Ed Giniger
UAS-p35	Over expression of p35 causes the DAIS to become longer	From Ed Giniger

Fly lines used in Chapter 4

Table 3 shows the cell lines used in Chapter 4 to investigate the effects of potassium channel disruption on Kenyon cell odour responses.

Table 3 presents the fly lines used in the experiments, along with their descriptions, for investigating the effects of altering the expression levels of potassium channels and potassium channel disruptors. The table includes relevant citations and information regarding their availability.

Fly Line	Comment	Citation/Availability
UAS-Shaw-Truncated	Expresses a non-functional, truncated version of the Shaw channel, BL55748	Hodge et al., 2005

UAS-Shaw-RNAi	Stops the translation of the Shaw channel	Hodge and Stanewsky 2008
UAS-Shal poreDN	Expresses a non-functional, non-conducting version of the Shal channel	Smith et al., 2019
UAS-ShabRNAi	Stops the translation of the Shab channel, BL 55682	Smith et al., 2019
UAS-Shaker-RNAi	Stops the translation of the Shaker channel, KK104474	Smith et al., 2019
UAS-Shaker-DN	Expresses a non-functional version of Shaker	Mosca et al., 2005
UAS- ShawWT	Expresses the wild type Shaw channel	Hodge et al., 2005

2.1.3 Equipment

Equipment used for all experiments are described with vendor in Table 6.

Table 6 Table of equipment used for experiments with vendor.

Equipment	Vendor
Leica S8 APO stereomicroscope	Leica, London, UK
Narishige PC-10	Narishige Group, Tokyo, Japan
DSP controller LC.400 (1-Channel)	Npoint, Middleton, Wisconsin, USA
Pockels amplifier 350-80LA	Conoptics, Danbury, Connecticut, USA
Microscope movement controller MPC200	Sutter Instrument, Novato, California, USA
PXIe-1073	National Instruments, Austin, Texas, USA

Sutter Resonant scan box MDR-R	Sutter Instrument, Novato, California, USA
Sutter Moveable Objective Microscope	Sutter Instrument, Novato, California, USA
Shutter controller SC10	Thorlabs, Newton, New Jersey, USA
GO-5000M-USB camera	Jai, Hovedstaden, Denmark
Mai Tai eHP DeepSee Ti:S laser	Spectra-Physics, Mountain View, California, USA
Thermorack 401	Solid State Cooling Systems, Wappingers Falls, New York, USA
2-Channel PicoSpritzer III 0-30PSI	Parker Hannifin Corporation, Hollis, New Hampshire, USA
Micro Forge MF-900	Narishige Group, Tokyo, Japan

2.1.4 Solutions

External solution

The external solution should mimic the external conditions of Kenyon Cells so as to not disrupt the osmosis of the cell. The recipe used in this project has been used in past literature for functional imaging and electrophysiology in (Murthy and Turner., 2013; Groschner et al. 2018). The composition of this saline solution was determined by attempting to replicate, in dissected fly brains, the amplitude and shape of the electroretinogram observed in intact flies (Murthy and Turner., 2013). Table 8 shows the concentrations of the external solution. It has a pH of 7.3 and was used in all live imaging experiments with the two-photon microscope.

Table 8 Ingredients and their measurements, issue number and vendor for the external solution.

Ingredient	mM	g or ml for 500ml	Issue Number	Vendor
TES	5	0.573125 mg	T5691-100G	Sigma, Burlington, Massachusetts, United States
NaCl	103	3.00966 mg	S7653-1KG	Sigma, Burlington, Massachusetts, United States
KCl	3	1.5 ml	10735874	Fisher Scientific, Waltham, Massachusetts, United States
CaCl ₂	1.5	0.75 ml	21115-100ML	Sigma, Burlington, Massachusetts, United States
MgCl ₂	4	2 ml	M1028-100ML	Sigma, Burlington, Massachusetts, United States
NaHCO ₃	26	1.09213 mg	S6014-1KG	Sigma, Burlington, Massachusetts, United States
NaH ₂ PO ₄	1	0.05999 mg	S5011-100G	Sigma, Burlington, Massachusetts, United States
Trehalose	8	1.51332 mg	T9531-100G	Sigma, Burlington, Massachusetts, United States
Glucose	10	0.9008 mg	G8270-1KG	Sigma, Burlington, Massachusetts, United States

2.1.5 Other reagents

The odour delivery system requires zero grade compressed air to deliver the odours. Carbogen gas was used to bubble oxygen through the external solution. These were used for live imaging preparations (Table 9).

Table 9 Table of other reagents used with vendors and reference numbers.

Material	Model/Reference	Vendor
Carbogen gas tank	131-J	BOC, Sheffield, UK
Zero grade compressed air	270028-L	BOC, Sheffield, UK

2.1.6 Filters used for two-photon microscopy

Two-photon:

Zeiss filter holder (91015 ZEISS AXIO 2-5 Cube)

Green filter 525/50 from Semrock / Laser2000

Dichroic 565dcxr CO-O551400 25.6 x 36 x 1 mm (Chroma)

Red Filter 525/50 from Semrock / Laser2000

GFP filter cube

49002 from Chroma

excitation: 470/40

dichroic: long-pass 495

emission: 525/50

dsRed filter cube

49004 from Chroma

excitation: 545/25

dichroic: long-pass 565

emission: 605/70

2.2 Methods

2.2.1 *Ex vivo* technique for two-photon microscopy

The *Drosophila* were placed on ice for approximately 3 minutes until they were immobile. An individual fly was first submerged in a small petri dish filled with PBS and then another dish with 100% ethanol. The fly was then transferred to external solution (Table 8) and using fine forceps, the brain was dissected from the head.

If the brain required fixing, it was placed in 4% paraformaldehyde (PBT) for 20 minutes. The brain was then washed in PBT for 20 minutes 3 times. Two hole-reinforcement stickers (Catalog number: Avery 5722) were placed on a glass slide. The brain was pipetted up with the surrounding solution and placed in the centre of the sticker. The solution was then replaced with Vectashield. The cover slide was placed on top and then sealed with nail polish.

For imaging the ParaFlpTag flies, the brains were placed between two pieces of electrical tape within the hole reinforcement stickers so that the brain was standing in the superior position.

2.2.2 Calcium imaging

Two-photon imaging

The *Drosophila* were placed in an empty vial and then put on ice for approximately 5 minutes. Once immobile, the fly was placed on a holder with a hole about half the size of the fly. The fly was pinned down, in the supine position, using wax, the wings and legs were attached to the holder with its head and upper thorax protruding through the hole. Thus, the back of the head was accessible on the other side of the holder. Using wax and dental floss the head and proboscis was held down to stop movement. Once the *Drosophila* was fully secured, the holder was flipped over and external solution is pipetted into the ducts of the holder so that the exposed parts of the *Drosophila* are covered in external solution. With fine forceps, the cuticle on the back of the head is removed to create a 'window' into the brain. The fat cells, air ducts and glial sheath surrounding the KCs were removed to expose only the brain tissue. The prep was then

placed under the two-photon microscope and carbogen (95% oxygen/5% CO₂; Figure 9) is continuously bubbled through the external solution via a perfusion pump to recirculate external solution through the holder.

A tube which delivers odour was placed directly in front of the fly's head, around 5mm. The Kenyon cells were found via the light wide microscope (Moveable Objective Microscope, Sutter and xenon-arc lamp LAMBDA LS, Sutter). The microscope was then switched to the 2-photon. The set up for the 2-photon used Ti-Sapphire laser (Mai Tai eHP DS, 70 fs pulses, Spectra-Physics) set to 910 nm (unless specified in figure legends). The laser was then attenuated with a Pockels cell controller by a voltage amplifier (model 350-80LA, Conoptics). The amplifier was also connected to a galvo-resonant scanner (model MDR-R, Sutter). The laser was focused with a 1.0 NA 20X objective (Olympus) and the emitted light from the sample was detected and captured with GaAsP photomultiplier tubes (model PS-2LV, Hamamatsu Photonics). Then amplified with TIA-60 (Thorlabs). A piezo objective stage (nPFocus400, nPoint) and ScanImage 5 software was used to obtain volume imaging. Labview was used to deliver odours whilst recording the activity of the Kenyon cells (Table 10 and Table 11).

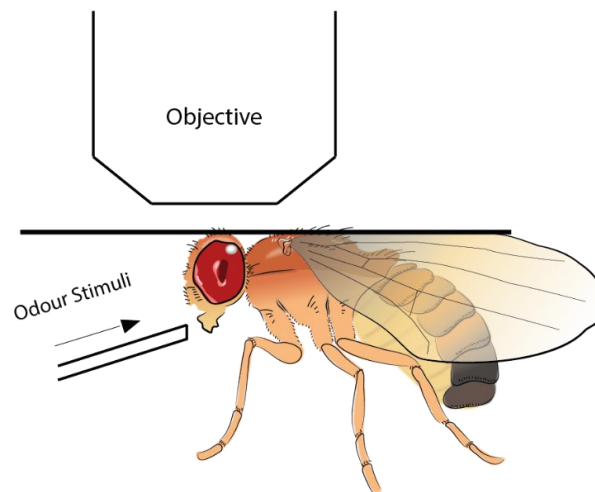


Figure 9 Diagram of calcium imaging setup. The *Drosophila* was pinned down with wax and dental floss. The brain was then exposed, and the objective was lowered to the brain.

For a discussion about the use of calcium imaging, please go to section 5.3.1.

Odour scripts

Labview 2015 (national Instruments) software was used to control the odour delivery system. The software allows for manipulation of odour sequence via scripts. Scripts used for experiments are outlined in Table 10 and Table 11. A vacuum tube was positioned behind the fly to eliminate any remaining odour.

Table 10 shows the odour script for experiments which presented Isoamyl acetate and Delta Decalactone.

Time (ms)	Isoamyl Acetate then Delta Decalactone
5	Image starts
10	Empty vial
15	off
25	Isoamyl acetate
30	Off
50	Delta Decalactone
55	Off

Table 11 shows the odour script for experiments which presented 4-methylcyclohexanol and 3-octanol.

Time (ms)	MCH and OCT
5	Image starts
10	Empty vial
15	Off
25	4-methylcyclohexanol
30	Off
50	3-octanol

55	Off
----	-----

2.2.3 Molecular Biology

Gel electrophoresis

Single fly genotyping was used to confirm insertion of genes and gene recombination.

For preparing DNA the following was used for a Squishing Buffer: 10 mM Tris-HCl pH8, 1 mM EDTA and 25 mM NaCl. The whole fly was added to the buffer as well as 200 µg/ml Proteinase K.

The solution was then incubated at 37°C for 30 min to allow the proteinase K to digest the proteins. Then, it was heated to 95°C for 3 min to inactivate the proteinase K.

Using the following recipe, PCR was performed: 5 µl 10x CoralLoad buffer, 1 µl dNTPs, 1 µl primer 1, 1 µl primer 2, 3 µl genomic DNA, 0.25 µl Taq and 38.75 µl H₂O (Table 12).

The following steps were used for the PCR program: (1) 15' 95°C (2) 15" 95°C, (3) 30" annealing temperature (50-65°C – depends on the primers), (4) X' 72°C (the amount of time for extension depends on your product size. This was ~1 min per kb), (5) Steps 2-4 cycled 35 times, (5) 10' 72°C (extra extension time for any 'loose ends').

1% agarose gel was used for gel electrophoresis and Sybr Safe was used, 5 µl per 50 ml of agarose. Electrophoreses was then run at 100 V for around 20-30 minutes.

Table 12 Reagents used in single fly genotyping protocol.

Reagents	Model/Reference No.	Vendor
Proteinase K	P2308-10MG	Sigma, Burlington, Massachusetts, United States
Taq DNA Polymerase Kit	201205	Qiagen, Manchester, UK

dNTPs	15393189	Fisher Scientific, Waltham, Massachusetts, United States
-------	----------	--

2.3 Analysis

2.3.1 Analysis of imaging data

After the images were captured, they were analysed in ImageJ:

$\Delta F/F$ calculation in ImageJ:

$$F(t) = F_{ROI}(t) - F_{Bkgnd}(t)$$

$F_0(t) = F_{mean}(t)$ over the user-defined pre-stimulus window

$$\Delta F/F = [F(t) - F_0(t)]/F_0(t)$$

$F(t)$ is the fluorescence signal at the time (t). It is the difference between the fluorescence signal in the ROIs (F_{ROI}) and fluorescence signal from the background ($F_{Bkgnd}(t)$); both defined by the user.

The baseline fluorescence, $F_0(t)$, is the mean fluorescence signal in the ROIs, $F_{mean}(t)$.

ROIs were drawn by hand around the mushroom body lobes from montages of the z-slices. Background fluorescence was taken from empty sections in the deepest slice. The raw $\Delta F/F$ was created in ImageJ and then transferred to Igor Pro (Wavemeterics).

2.3.2 3D-Skeletonisation of FlpTag Data

MATLAB code created by Andrew Lin and Hoger Amin was used to analyse the FlpTag data. The code generates a 3D visualisation of the mushroom body. The code enables a movie to be converted into an 'activityMap'. The code then stores a variety of data relevant to the movie such as pixel calibration, number of dimensions, dimension

lengths and frame rate. There is another class 'activityMapParams', which holds all the parameters required to create an activityMap object.

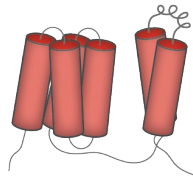
Once the movie has been selected, it is viewed as a montage. A mask is then created when the user draws ROIs around the parts of the mushroom body that is required. The user creates an ROI of the background. The ROIs are calculated, and a mask is displayed. The user then manually sets points along the mask to create a connecting series of points which equate to a branch. There are two branches when creating a skeleton of the whole mushroom body due to the vertical lobes. The user then defines a zero point from which a skeleton of the whole structure is generated. The code can then either create equally proportioned segments or absolute segments along the mask. The skeletons were normalised together, and the data was analysed in Prism.

2.3.3 Statistical analysis

Graphs and statistical analysis were carried out using GraphPad Prism 9. Statistical tests used and their values for each graph can be found at the end of each results chapter (see Appendices A and B). Significance is denoted by asterisks where * $p < 0.05$, ** $p < 0.01$, *** $p < 0.001$ and **** $p < 0.0001$. Odour responses were analysed using two-way ANOVAs and corrected with Šidák's or Tukey's multiple comparisons tests. All tests were two-tailed. To check the normality of the data I conducted normality tests via GraphPad Prism's feature to plot quantile-quantile (QQ) plots. Two-way ANOVA's were used for majority of the data analysis as they are considered "robust" to violations of normality and only require approximately normally distributed data (GraphPad, 2023). The Results text highlights experiments where low sample size means that firm conclusions cannot be drawn from the data. Peak odour response significance is shown on odour response trace figures and the average odour response is shown on the associated bar graph figures. The 'peak values' refers to the maximum value between two set points, i.e. 5 seconds of odour presentation. The 'average values' take the mean between two set points, i.e. the start and finish of the odour presentation.

3 NaChBac expression in Kenyon cells reduces their odour responses

3.1 Introduction



To investigate the potential homeostatic effects of Kenyon cells (KCs), I initially aimed to increase their excitability by overexpressing the exogenous sodium channel, NaChBac. As discussed in Chapter 1, NaChBac is a voltage-sensitive sodium channel that was discovered in the bacterium *Bacillus halodurans*. NaChBac expression has been shown to increase the excitability of various cell types, including mammalian and *Drosophila* neurons.

3.1.1 Past literature demonstrates NaChBac expression increases neuronal excitation

Several studies have demonstrated that NaChBac expression can induce excitation in various mammalian neuronal cell types. For example, in mammalian cells, Sim *et al.*, (2013) showed that the addition of NaChBac increased the excitability of adult dentate gyrus (DG) neurons. This caused the inputs to the cells to change and adapt to reduce the likelihood of the DG neurons firing. Furthermore, NaChBac expression in granule cells increased the excitability of the cells (Lin *et al.* 2010) and triggered depolarisations approximately 600 ms long (Kelsch *et al.*, 2009).

Research with NaChBac has not been limited to mammalian cells. Studies using *Drosophila* have demonstrated that the expression of NaChBac can also enhance the excitability of their neurons. Nitabach *et al.*, (2006) found that the expression of NaChBac in the lateral ventral neurons (circadian pacemaker cells) cancels out the inhibitory effect of Kir2.1 suggesting that NaChBac increases excitation. To verify the electrical properties and that NaChBac has increased the excitation of the lateral ventral neurons, whole-cell current-clamp recordings within the lateral ventral neurons were obtained and the data was verified by showing that there were strong sodium currents (Sheeba *et al.*, 2008). NaChBac expression has been shown to produce big, long action

potentials due to its slow kinetics (Ren et al., 2001; Giachello et al., 2022). In the lateral ventral neurons (l-LNv), NaChBac activates at -65 mV, and triggers massive increases in action potential amplitude and duration due to the channel staying open for 100s of ms (Ren et al., 2001; Sheeba et al., 2008; Giachello et al., 2022). Thus, the increase in the NaChBac sodium channel had increased the cell's excitation. Furthermore, NaChBac expression had caused spontaneous action potentials and a lower resting membrane potential than wild type cells (Sheeba et al., 2008). Research demonstrated that NaChBac expression in lateral ventral neurons did not alter their gross morphology but did affect their electrical parameters (Sheeba et al., 2008). Furthermore, when l-LNv neurons expressing NaChBac were selectively targeted, the flies were more active at night (when they are normally asleep). This effect can be attributed to the heightened excitation caused by the overactivation of l-LNv neurons, which promotes wakefulness. This finding provides an example of NaChBac expression increasing cellular activity (Sheeba et al., 2008).

Using NaChBac to change behaviour, Donlea et al. (2011) proposed that NaChBac increases excitation in their target neurons (ExF12 cells) due to the change in sleep patterns. NaChBac expression produced similar sleep patterns to *Drosophila* that had their ExF12 cells overexcited with TRPA (a well characterised channel that triggers the influx of calcium ions into cells; Hamada et al., 2008). Thus, they suggest that NaChBac excites cells in a similar manner as TRPA. Thus, NaChBac excitation can lead to changes in behaviour.

In addition to NaChBac expression, modified versions of the protein, such as GFP-tagged NaChBac, have been found to enhance excitability in *Drosophila*. Electroretinograms of NaChBac expressing photoreceptors exhibit large, slowly activating and inactivating depolarisations (shown in Ren et al. (2001)) which were absent in control flies (Luan et al., 2006). Furthermore, acute adult expression of NaChBac with GAL80^{ts} in glutamatergic neurons in *Drosophila* increases neuronal activity, which is the opposite effect of temperature sensitive Shibire (Shibire^{ts}) and EKO, which lowers activity (overactive Shaker) (Zimmerman et al., 2017). Shibire^{ts} is a temperature-sensitive mutation that encodes a dynamin orthologue that blocks vesicle endocytosis and thus synaptic transmission. Therefore, because NaChBac's expression produces the opposite effect of Shibire^{ts} and EKO (i.e. NaChBac increases

neuronal activity), the results suggest NaChBac increases excitation. Thus, even short expression of NaChBac is still enough to produce hyperexcitability in neurons.

Occasionally, the observed behaviour deviates from the expected outcome of hyperexcitation. Luan et al., (2006) found that increasing the electrical activity of a subset of *Drosophila* neurons that expresses crustacean cardioactive peptide by expressing NaChBac blocks tanning and wing expansion. This was the opposite effect of what they had expected from increasing the excitability of these cells. This suggests that excitation by NaChBac may not produce the predicted effect.

Based on this previous research, in the current project the overexpression of NaChBac was chosen as a method to increase sodium influx and consequently enhance the excitability of Kenyon cells. This method was expected to facilitate investigations into the compensatory mechanisms of Kenyon cells in response to overexcitation induced by NaChBac, providing valuable insights into the strategies employed by these cells to counteract the increase in excitation. While NaChBac has been commonly utilised to increase neuronal excitability, its potential to investigate homeostatic processes and its involvement with other ion channels in cellular responses remains largely unexplored.

3.1.2 Chapter direction

Typically, neuronal networks exhibit a low tolerance towards overactivity. Hence, biological systems have evolved with sophisticated homeostatic mechanisms to maintain critical functions (Marder and Prinz, 2002; Davis, 2006; Turrigiano, 2008). As described in Chapter 1, Kenyon cells exhibit a highly specific coding system that likely requires the presence of homeostatic mechanisms to maintain proper functioning and stability. In past research of homeostasis, it is common to change a single element within the system to examine the resulting corrective response of the system. Thus, the objective of this chapter is to overexpress sodium channels, hypothesising that this will elevate the excitability of Kenyon cells, based on the theory outlined above. The project therefore utilises a range of techniques including GFP tagging, overexpression of proteins, and knockdowns of channels in KCs to reveal their homeostatic mechanisms. Calcium imaging was used to evaluate the odour responses of KCs and to establish whether overexpression of the NaChBac led to an increase in their activity.

3.2 Results

3.2.1 Constitutive expression of NaChBac reduces odour responses in Kenyon cells

Firstly, NaChBac was expressed in γ KCs using R44E04-LexA, mb247-GAL4>LexAop-GAL80, GCaMP6f. The γ KCs are a specific subtype of KC, with their axons terminating in the γ lobe of the mushroom body (shown in Figure 8). To selectively enhance excitation without affecting all the KCs, I opted to express NaChBac specifically in one subtype. Figure 11 shows examples of raw fluorescent images before, during and after odour presentation.

The odour scripts are described in Section 2.2.2. For the experiments that tested Isoamyl acetate and delta Decalactone, an empty bottle is always presented first as a control response. Ten seconds later the first odour, Isoamyl acetate (IA), is presented for 5 seconds. Twenty seconds later the second odour, δ -Decalactone (δ D) is presented for 5 seconds. This order is kept the same for all experiments using IA and δ D. The peak response was taken as the maximum $\Delta F/F$ value during the odour pulse, while the average response was the average $\Delta F/F$ value across the 5 seconds of the odour pulse. A fly is exposed to the odour script only once, preventing habituation from taking place. Due to the short duration of the odour script and the precise excitation of 2-photon imaging, minimal bleaching occurs during the imaging session.

Surprisingly, in γ KCs expressing NaChBac constitutively throughout development and adulthood, the peak and average odour responses were significantly weaker in the calyx when presented with IA and δ D (Figure 10). Additionally, in response to IA, the lobes exhibited a weaker average response, suggesting that NaChBac expression in γ KCs weakens their excitability. The paradoxical outcome prompted me to investigate whether the decrease in odour responses was due to a reduction in activity caused by NaChBac, or if it was a result of increased baseline activity. An increase in baseline activity could potentially raise the baseline fluorescence level and make the odour responses appear smaller. To test this possibility, measurements of the average fluorescence were taken of the lobes and calyx of the γ KCs expressing NaChBac. The results show that there was a lower baseline fluorescence with NaChBac expression (Figure 10). It is unclear whether this reflects lower baseline calcium levels or decreased

levels of GCaMP6f protein. Regardless, these results suggest it is unlikely that the lower odour responses in the γ KCs are caused by higher baseline calcium levels.

I next wanted to look at the constitutive expression of NaChBac in all KC subtypes (using R13F02GAL4) to see if they had the same effect with NaChBac expression as the γ KCs. Because different KC subtypes send their axons to different lobes, the subtypes can be selectively targeted with region of interest (ROI) analysis (shown in Figure 11). NaChBac expression in all KCs produced overall significantly weaker peak odour responses to both IA and δ D (see Appendix A). Peak odour responses were significantly weaker in the β' and β lobes when presented with IA (Figure 11). Furthermore, the main effect of genotype showed significantly lower average odour responses to IA and δ D (Figure 20 and see Appendix A). The β' , β and γ lobes also had weaker average odour responses to IA (Figure 11). In responses to δ D, the γ lobe also had a much weaker average odour response (Figure 11). Therefore, NaChBac expression in all KC subtypes weakens their odour responses and thus likely reduces their excitability.

I then wanted to investigate whether NaChBac was expressed throughout the KCs and across the KC subtypes. To verify whether NaChBac had localised to the Kenyon cell membrane (as opposed to, e.g., being misfolded and stuck in the endoplasmic reticulum), I expressed GFP-tagged NaChBac with the driver R13F02GAL4 to determine its localisation. Figure 11 shows that GFP tagged NaChBac is distributed throughout the mushroom body and is not localised to a specific area.

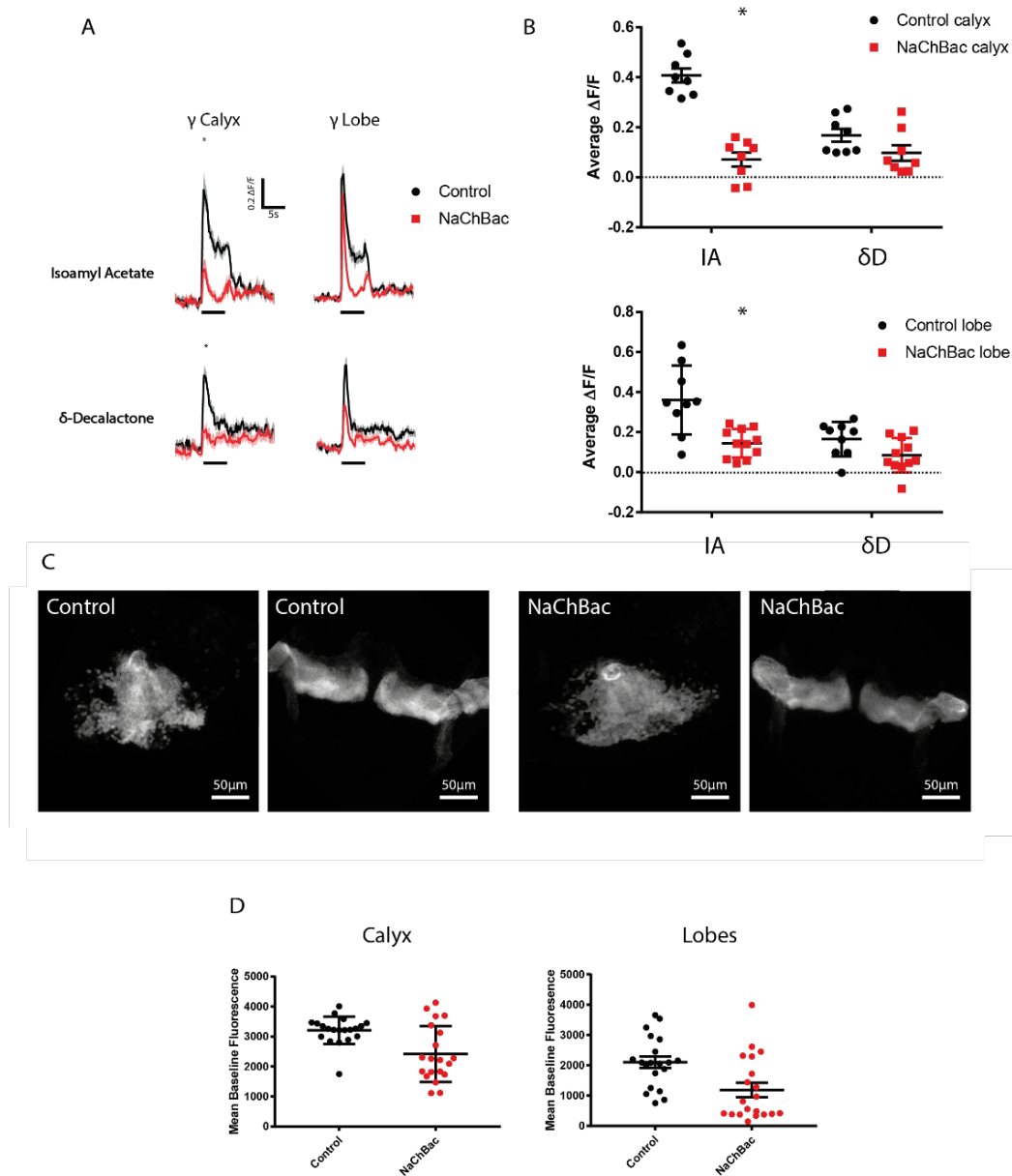


Figure 10 NaChBac expression in γ KCs significantly reduces odour responses.

Fly genotypes: Control = R44E04-LexA, mb247-GAL4>LexAop-GAL80,GCaMP6f. NaChBac = R44E04-LexA, mb247-GAL4>LexAop-GAL80,GCaMP6f,NaChBac.

(A) The odour response traces of γ Kenyon cells expressing NaChBac compared to their controls and segmented into calyx and lobe regions. * = peak odour response is $p < 0.05$, two-way ANOVA with Šidák multiple comparisons test. (B) The average odour response of γ KCs expressing NaChBac compared to their controls and divided into calyx and lobe regions. * = average odour response is $p < 0.05$, two-way ANOVA with Šidák multiple comparisons test (C) Baseline fluorescence images were obtained from both Control and NaChBac expressing γ KCs using a 2-photon microscope. (D) Quantification of panel C. $p > 0.05$, unpaired t-test. (A-D) Black = Control. Red = NaChBac expression. Black bars under odour response traces = 5 second odour presentation. Age past eclosion = 4 days.

For detailed statistics, please see the table in Appendix A.

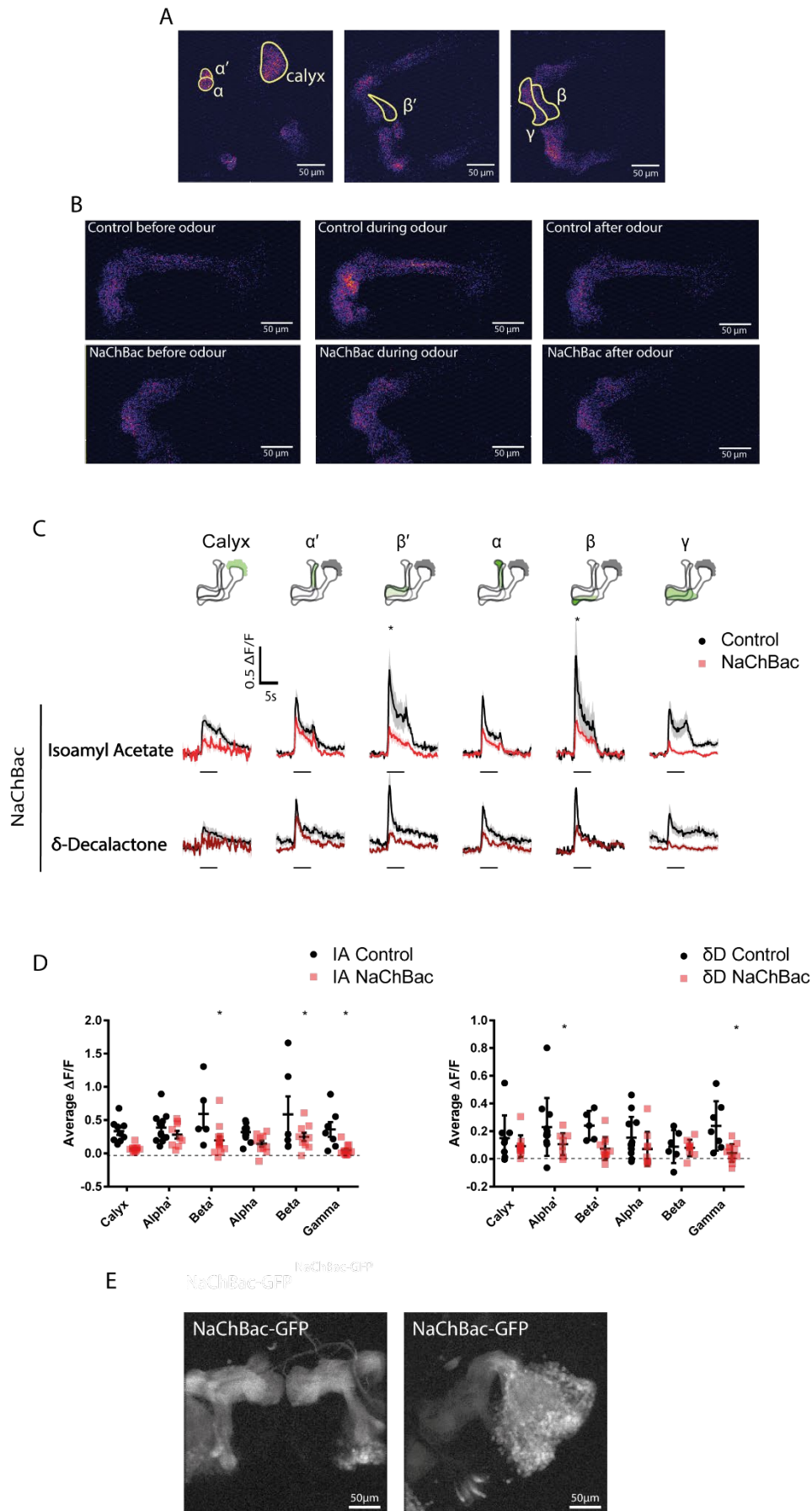


Figure 11 NaChBac expression in all Kenyon cell subsets weakens odour responses.

Fly genotypes: Control = R13F02GAL4>GCaMP6f. NaChBac = R13F02GAL4>GCaMP6f, NaChBac.

(A) Raw fluorescence images show the regions of interest for the calyx, α , β , α' , β' and γ lobes. (B) Raw fluorescence images show an example time lapse of before, during and after isoamyl acetate presentation. (C) A diagram of the subtypes of KCs. Odour response traces of KCs expressing NaChBac compared to control. The top panel are odour responses to isoamyl acetate. The bottom panel are odour responses to δ -Decalactone. * = peak odour response is $p < 0.05$, two-way ANOVA with Šidák multiple comparisons test. Black bars = 5 second odour presentation. (D) Quantification of the average fluorescent difference of the odour traces in panel C. * = average odour response is $p < 0.05$, two-way ANOVA with Šidák multiple comparisons test. (E) Z stack images of R13F02GAL4>GFP tagged NaChBac obtained on the 2-photon microscope. (C-D) Black= Control. Red= NaChBac. Age past eclosion = 4 days.

For detailed statistics, please see the table in Appendix A.

3.2.2 Acute 2-day NaChBac expression in adult flies weakens odour responses, but KCs can recover after 4-days of acute adult NaChBac expression

As the previous experiments used constitutive expression of NaChBac, I next asked whether NaChBac exerts the same effects during adulthood or development. The results of these experiments would then show if the development of the flies would influence how the KCs respond to the expression of NaChBac.

To investigate the developmental effects of NaChBac we sought to express NaChBac in a temporally restricted way. Acute expression of transgenes in *Drosophila* can be controlled by GAL80^{ts}. GAL80^{ts} will stop the production of a gene of interest (driven by GAL4) when the *Drosophila* is kept at 18°C (Figure 12). Subsequently, when the *Drosophila* are housed in temperatures above 29°C the GAL80^{ts} is inactivated, allowing the gene of interest to be expressed. Thus, how long a gene of interest is expressed is controlled by the temperature that the *Drosophila* are housed at.

Expressing NaChBac for 2 days after eclosion significantly reduced overall peak odour responses to IA and δ D. More specifically, the peak odour responses were significantly reduced in the β' , β and γ lobes with NaChBac expression (Figure 13; see also Figure 20 to compare to the effect of constitutive expression). Additionally, the average odour responses were significantly reduced overall and specifically in the β' and β lobes (Figure 14 and see Appendix A). In contrast, expressing NaChBac for 4 days after eclosion significantly increased peak and average odour responses, shown in their main effect of genotype (see Appendix A). Four days of acute expression in adults significantly increased peak and average odour responses in the β' Kenyon cells (Figure

13 and 14 and see Appendix A). Lastly, compared to all other manipulations, expressing NaChBac for 8 days after eclosion had no significant effect on odour responses (Figure 13, 14, 20 and see Appendix A). In summary, 2-day acute NaChBac expression in adult flies lowers odour responses but after 4 days of NaChBac expression the odour responses were significantly increased. These results suggest that KCs have lower excitation with short adult NaChBac expression which they can then recover from after 4 days.

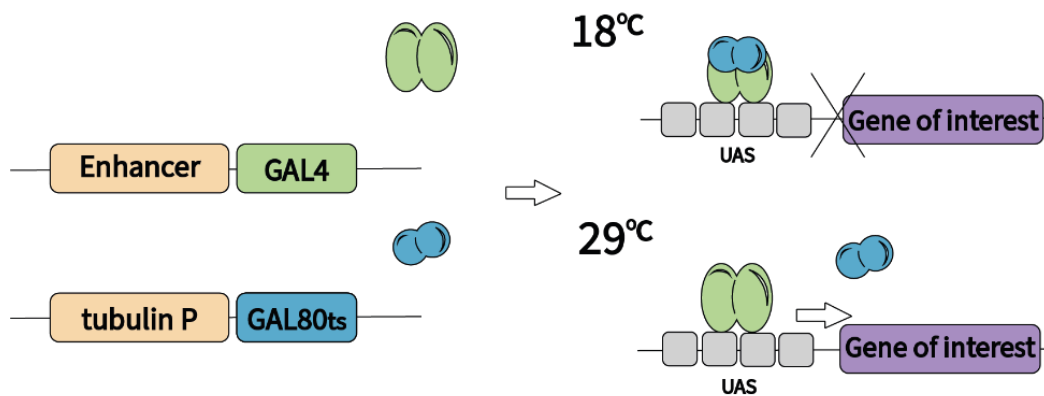


Figure 12 Diagram of how GAL80ts works.

An enhancer will transcribe a GAL4 gene (green). At 18°C, GAL80^{ts} (blue) will bind to the GAL4 protein and stop the function of the GAL4 protein. Therefore, GAL80^{ts} stops the production of the gene of interest (purple) as UAS has been blocked. At temperatures above 29°C the GAL80ts will not attach itself to the GAL4 and the gene of interest will be transcribed.

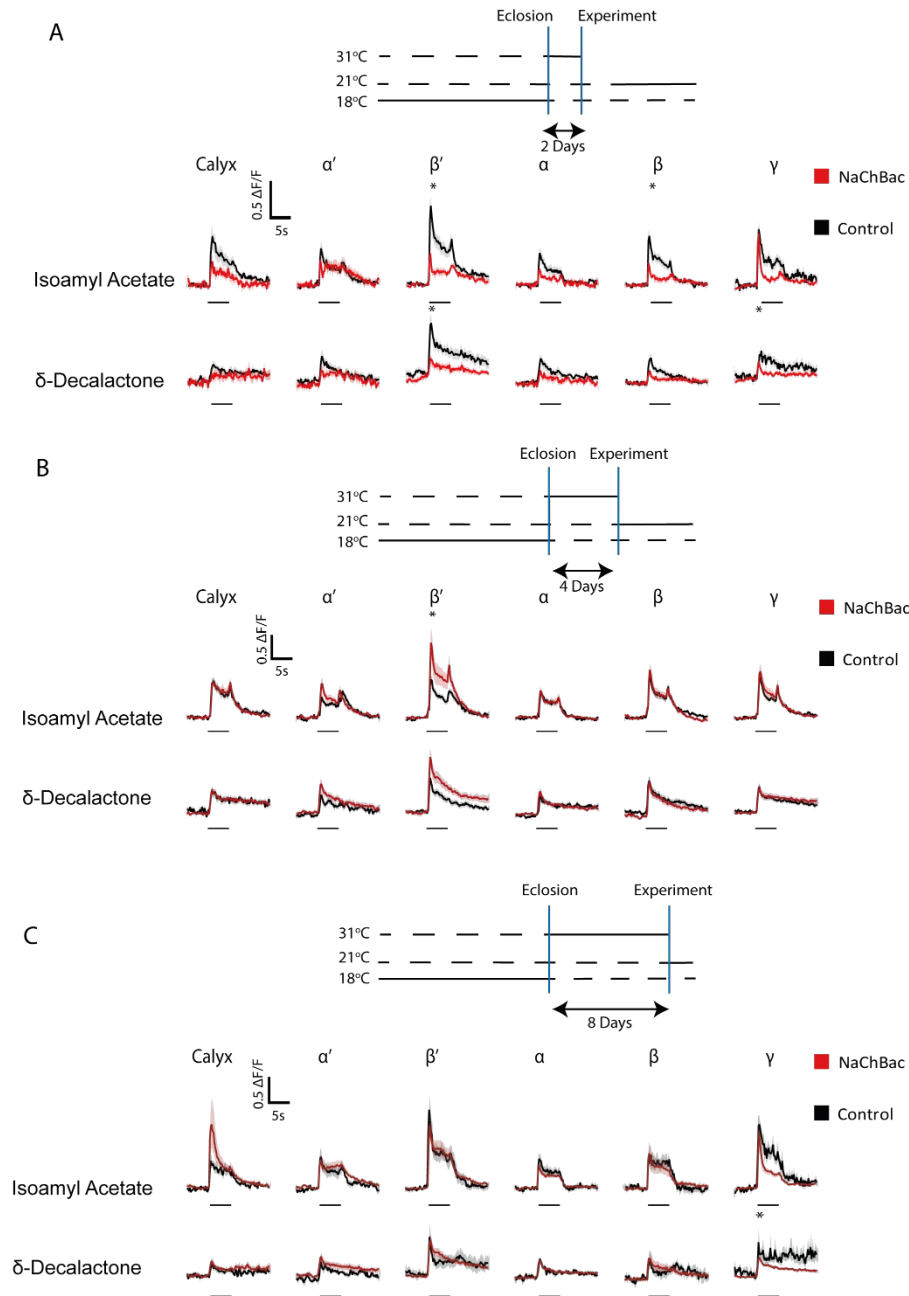


Figure 13 Adult KCs can return to normal activity when NaChBac is acutely expressed for ≥ 4 days.

Fly genotypes: Control = R13F02GAL4>GCaMP6f, GAL80^{ts}. NaChBac = R13F02GAL4>GCaMP6f, NaChBac, GAL80^{ts}.

(A) A diagram of the temperature the *Drosophila* were housed at and for how long (to activate the GAL80ts). The bottom panel shows the odour response traces of 2 day NaChBac expression in all subtypes of KCs compared to control flies. Age past eclosion = 2 days. (B) Diagram of the temperature the *Drosophila* were housed at and for how long. Odour response traces of 4 days NaChBac expression in all subtypes of KCs compared to control flies. Age past eclosion = 4 days. (C) A diagram of the temperature the *Drosophila* were housed at and for how long. Odour response traces of 8 days of NaChBac expression in all subtypes of KCs compared to control flies. Age past eclosion = 8 days. (A-C) Black = Control. Red = NaChBac. * = peak odour response is $p < 0.05$, two-way ANOVA with Šidák multiple comparisons test. Black bars = 5 seconds of odour presentation.

Average odour responses can be found in Figure 14. For detailed statistics, please see the table in Appendix A.

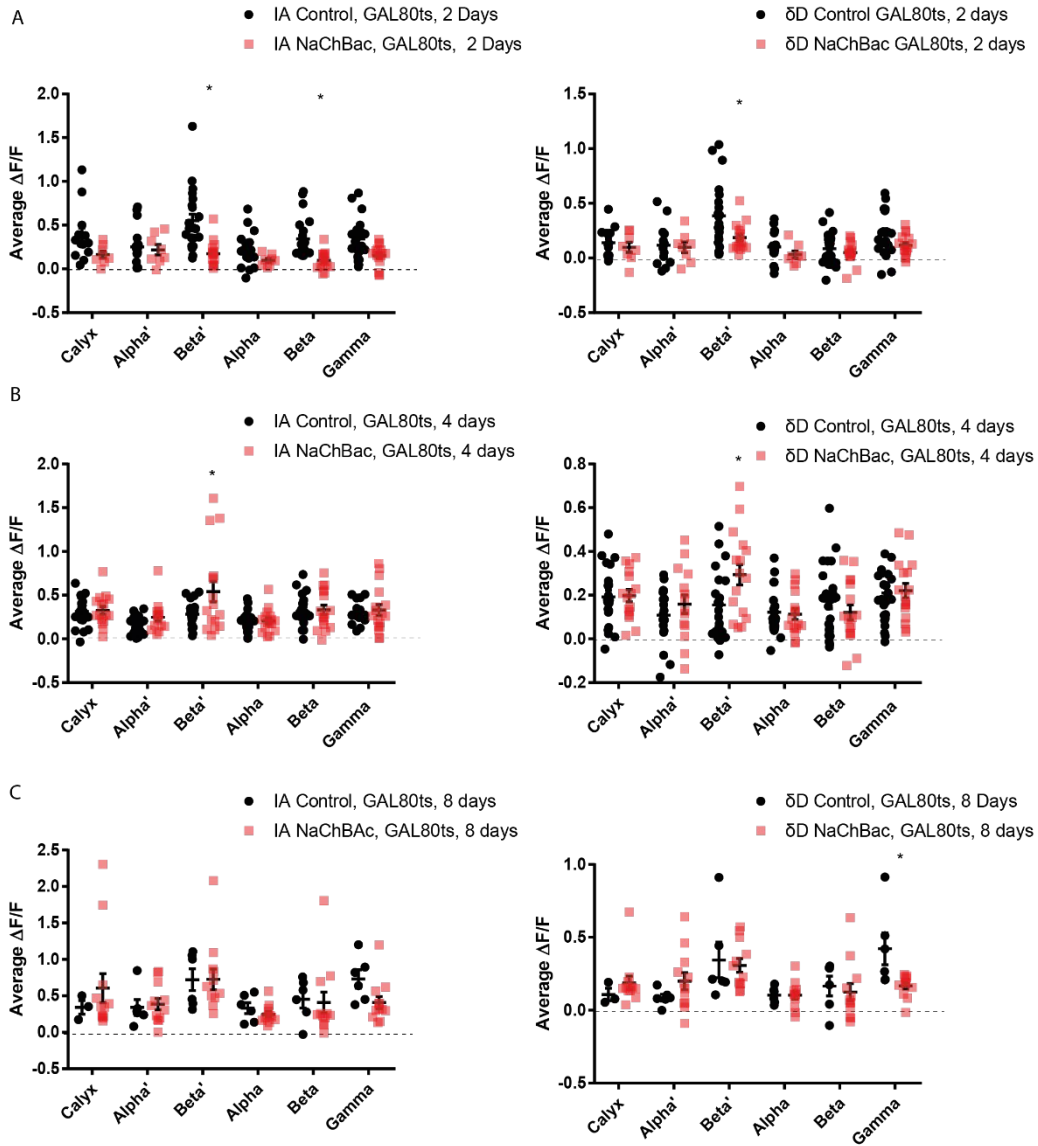


Figure 14 Quantification of average odour responses from Figure 13.

Fly genotypes: Control = R13F02GAL4>GCaMP6f, GAL80^{ts}. NaChBac = R13F02GAL4>GCaMP6f, NaChBac, GAL80^{ts}.

(A) Left side: Average odour responses to IA with 2 days adult NaChBac expression. Right side: Average odour responses to δ D with 2 days adult NaChBac expression. Age past eclosion = 2 days. (B) Left side: Average odour responses to IA with 4 days adult NaChBac expression. Right side: Average odour responses to δ D with 4 days adult NaChBac expression. Age past eclosion = 4 days. (C) Left side: Average odour responses to IA with 8 days adult NaChBac expression. Right side: Average odour responses to δ D with 8 days adult NaChBac expression. Age past eclosion = 8 days. (A-C) * = average odour response is $p < 0.05$, two-way ANOVA with Šidák multiple comparisons test. Black = Control. Red = NaChBac.

For detailed statistics, please see the table in Appendix A.

To test whether the temperature of the *Drosophila* used in the GAL80^{ts} experiments modified the effects of NaChBac, I used *Drosophila* expressing NaChBac but without GAL80^{ts} and housed them at 18°C until they eclosed. They were then moved to 31°C for 4 days and then their odour responses were recorded. This was to mimic the same housing procedure used for acutely expressing NaChBac in adult *Drosophila* for 4 days, i.e. Figure 13.

As shown in Figure 15, 20 and see Appendix A, NaChBac expression still significantly reduced peak and average odour responses when constitutively expressed in KCs but housed at 18°C until eclosion and then at 31°C for 4 days. Therefore, the temperature of the procedure does not affect the role of NaChBac in Kenyon cells.

Another control experiment was done to test if the recovery seen from 4 days of NaChBac expression was due to the *Drosophila* being an adult for 4 days, regardless of when NaChBac was being expressed. To investigate this, GAL80^{ts} was used to express NaChBac for 2 days, 2 days after eclosion (explanatory diagram shown in Figure 16). The results show that the peak odour responses were significantly weaker in the KCs to IA and δ D and the average odour responses were significantly weaker to IA (Figure 16 and see Appendix A). The peak and average odour responses significantly weaker in the β' and calyx (Figure 16). This suggests that the recovery in the KCs was due to the expression of NaChBac for 4 days and not just because they are adults for 4 days. It further shows that lower odour responses caused by 2 day adult expression of NaChBac is independent of when those 2 days occur after eclosion.

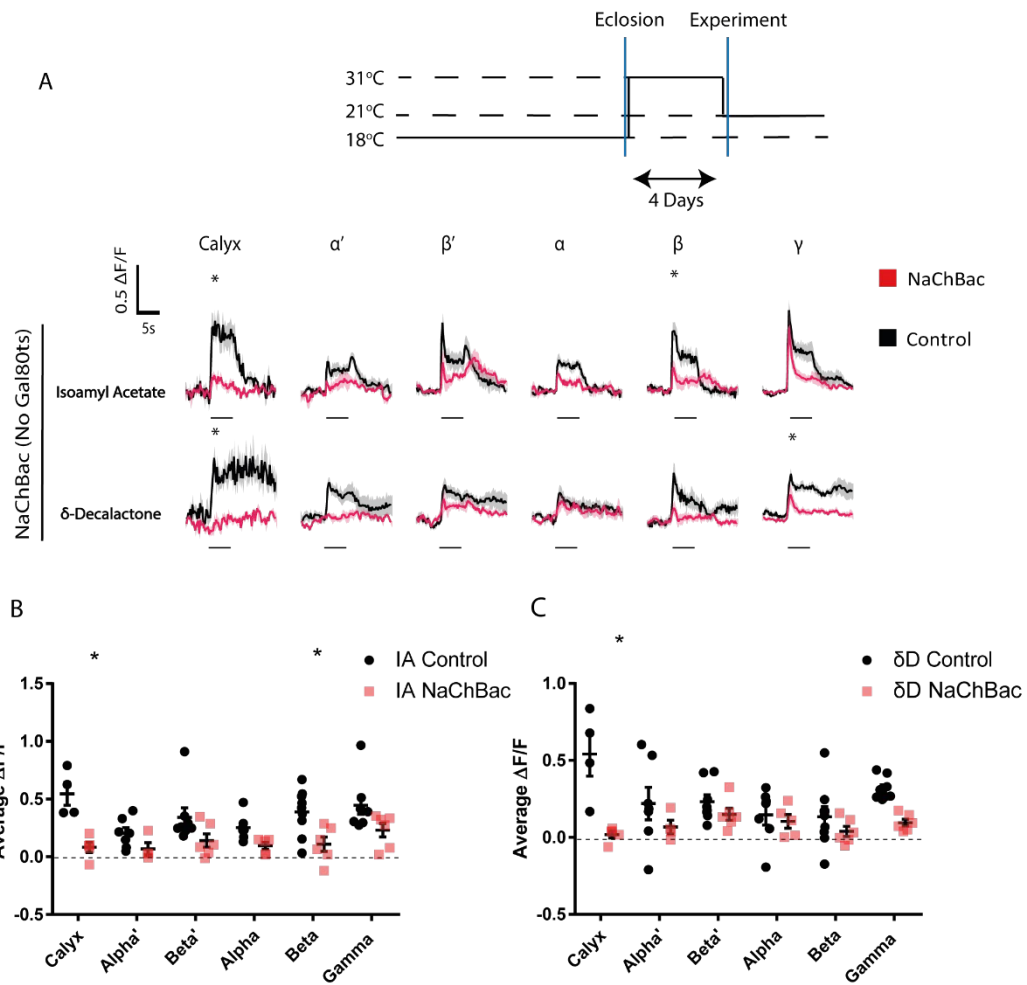


Figure 15 KCs expressing NaChBac with no GAL80^{ts} and housed at 31 degrees for 4 days after eclosion showed lower odour responses.

Fly genotypes: Control = R13F02GAL4>GCaMP6f. NaChBac = R13F02GAL4>GCaMP6f, NaChBac.

(A) A diagram of the temperature the *Drosophila* were housed at and for how long. Odour response traces of constitutive NaChBac expression compared to control. Black bars = 5 seconds of odour presentation. * = peak odour response is $p < 0.05$, two-way ANOVA with Šidák multiple comparisons test. (B-C) Quantification of the average odour responses of panel A. * = average odour response is $p < 0.05$, two-way ANOVA with Šidák multiple comparisons test. (A-C) Black = Control. Red = NaChBac. Age past eclosion = 4 days.

For detailed statistics, please see the table in Appendix A.

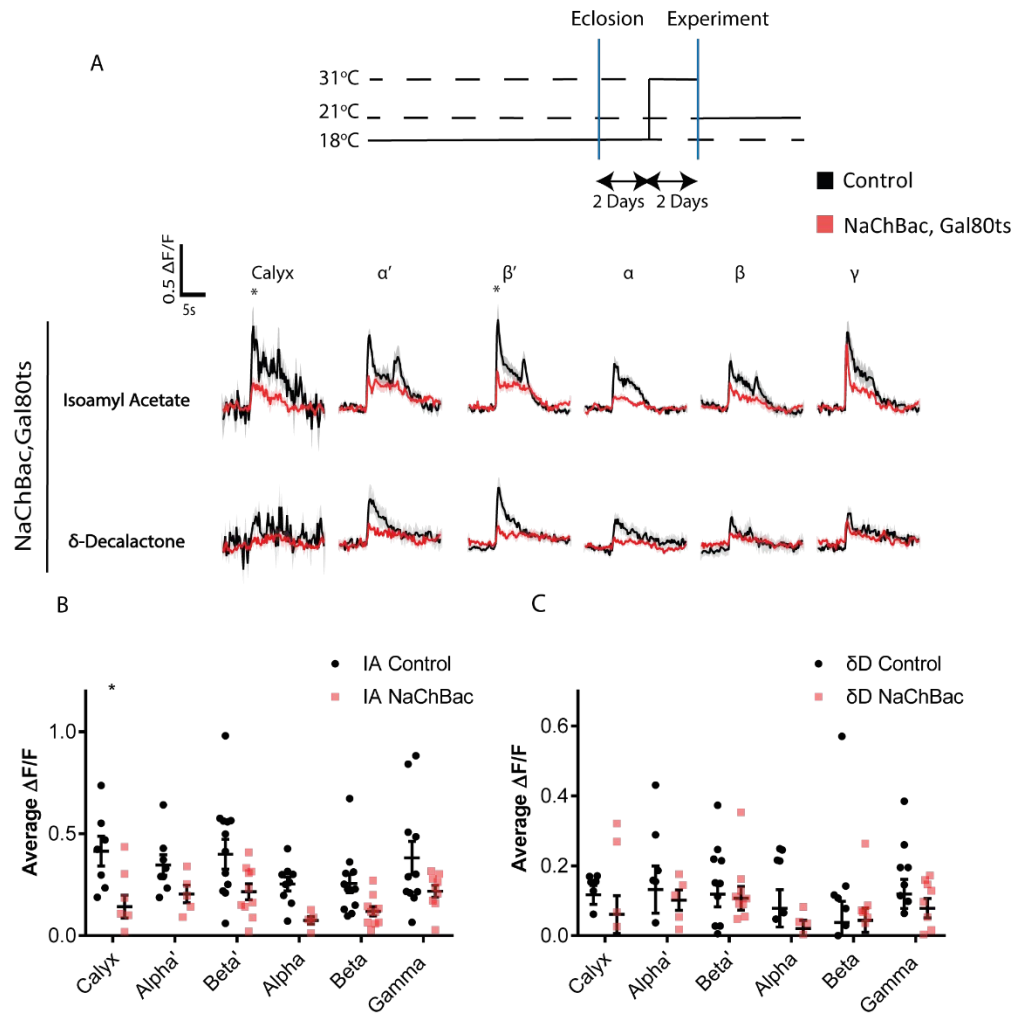


Figure 16 KCs expressing NaChBac and GAL80^{ts} but housed at 31°C for 2 days, 2 days after eclosion, showed lower odour responses.

Fly genotypes: Control = R13F02GAL4>GCaMP6f, GAL80^{ts}. NaChBac = R13F02GAL4>GCaMP6f, GAL80^{ts}, NaChBac.

(A) Diagram of the temperature the *Drosophila* were housed at and for how long. Odour response traces of *Drosophila* that expressed NaChBac, GAL80^{ts} that were housed at 31°C for 2 days, 2 days after eclosion, in all subtypes of KCs. Black bars = 5 seconds of odour presentation. * = peak odour response is p < 0.05, two-way ANOVA with Šidák multiple comparisons test. (B-C) Quantification of the average odour responses of panel A * = average odour response is p < 0.05, two-way ANOVA with Šidák multiple comparisons test. (A-C) Black = Control. Red = NaChBac. Age past eclosion = 4 days.

For detailed statistics, please see the table in Appendix A.

3.2.3 Acute expression of NaChBac in pupal development weakens odour responses

To further investigate the effects of NaChBac expression at different development stages on Kenyon cell odour responses, GAL80^{ts} was used to express NaChBac in pupae for varying durations (Figure 17). The mushroom body neurons start to form during embryogenesis and continue to be born throughout the larval and pupal stages (Lee et al., 1999). Figure 17 illustrates the three experimental procedures for investigating acute expression in pupae, with calcium imaging conducted 4 days after eclosion in each condition. The results show that acute NaChBac expression in developing flies lowers the activity levels of Kenyon cells which they can't recover from. Expressing NaChBac in the beginning stages of pupal development resulted in lower odour responses in the α' and γ lobes (Figure 18 and 19). Similarly, expressing NaChBac in later pupae stages resulted in significantly lower odour responses in the β' and α lobes (Figure 18 and 19). These results contribute to a potential theory that developmental expression of NaChBac may “lock in” the KCs to a state where they cannot recover their odour responses, whereas acute NaChBac expression in adults can be recovered from when they are over 4 days. However, the low n numbers in these experiments prevent definitive conclusions being drawn.

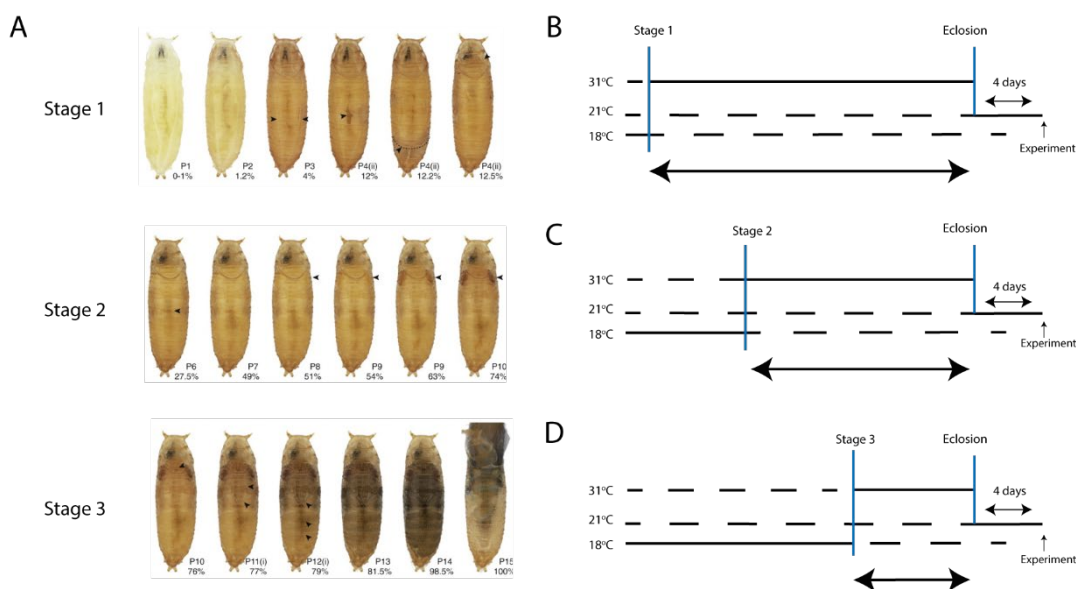


Figure 17 Pupal stages and heat scheme for Figure 18 and Figure 19.

(A) Images of pupae stages and their equivalent labelled stages for when they were extracted from their vial and placed in 31°C in Figure 18 and Figure 19. Image taken from Atlas of Drosophila, 2013. (B-D) Diagrams of the temperature the *Drosophila* were housed at and for how long for each stage.

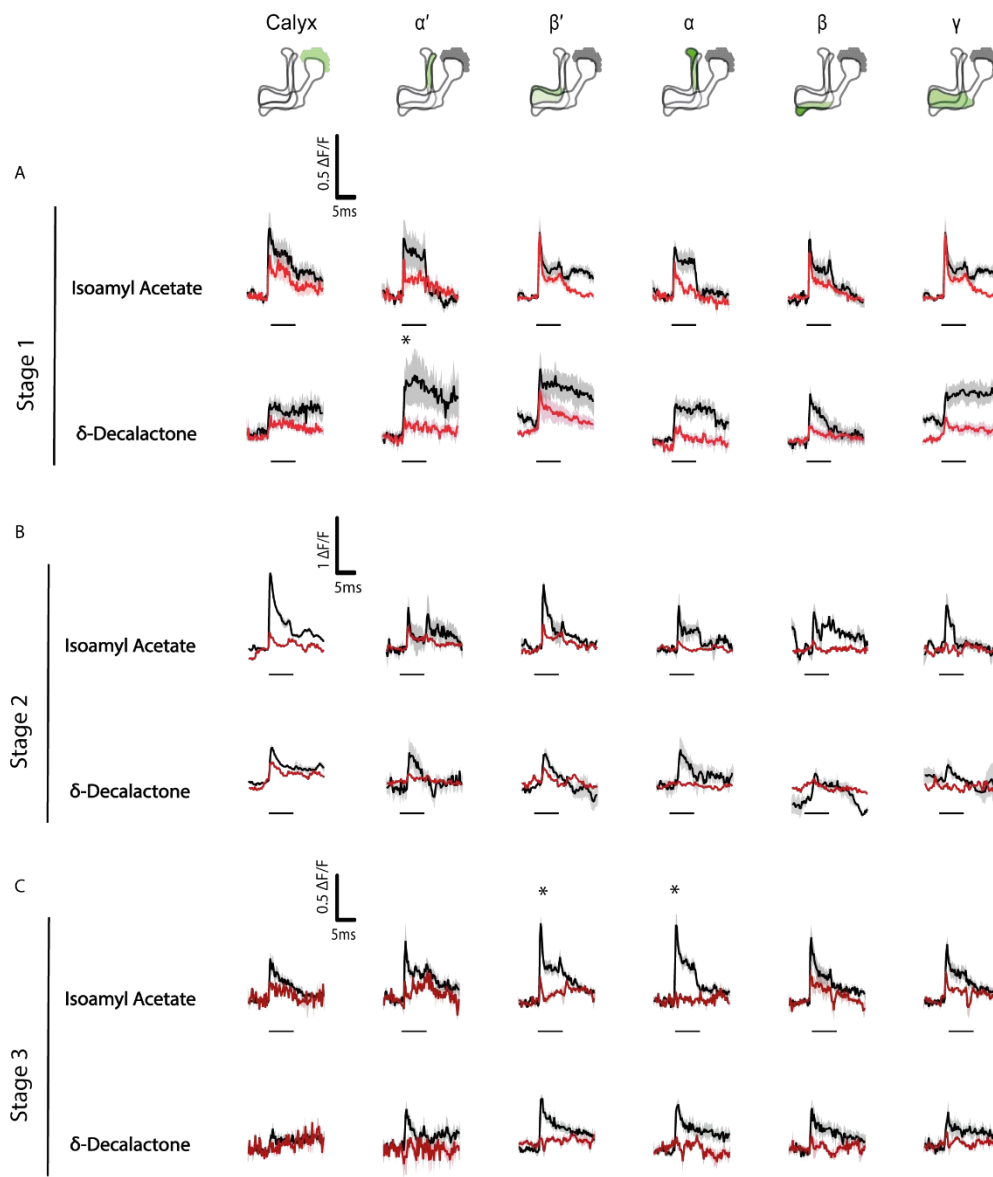


Figure 18 NaChBac expression in all three pupae stages weakens the odour responses of KCs.

Fly genotypes: Control = R13F02GAL4>GCaMP6F, GAL80^{ts}. NaChBac = R13F02GAL4>GCaMP6F, GAL80^{ts}, NaChBac.

Diagrams show mushroom body lobes. (A) Odour response traces of *Drosophila* that expressed NaChBac, GAL80^{ts} from pupae Stage 1 in all subtypes of KCs. (B) Odour response traces of *Drosophila* that expressed NaChBac, GAL80^{ts} from pupae Stage 2 in all subtypes of KCs. (C) Odour response traces of *Drosophila* that expressed NaChBac, GAL80^{ts} from pupae Stage 3 in all subtypes of KCs. (A-C) Black = Control. Red = NaChBac. Black bars = 5 seconds of odour presentation. * = peak odour response is $p < 0.05$, two-way ANOVA with Šidák multiple comparisons test. Age past eclosion = 4 days.

Average odour responses can be found in Figure 19. For detailed statistics, please see the table in Appendix A.

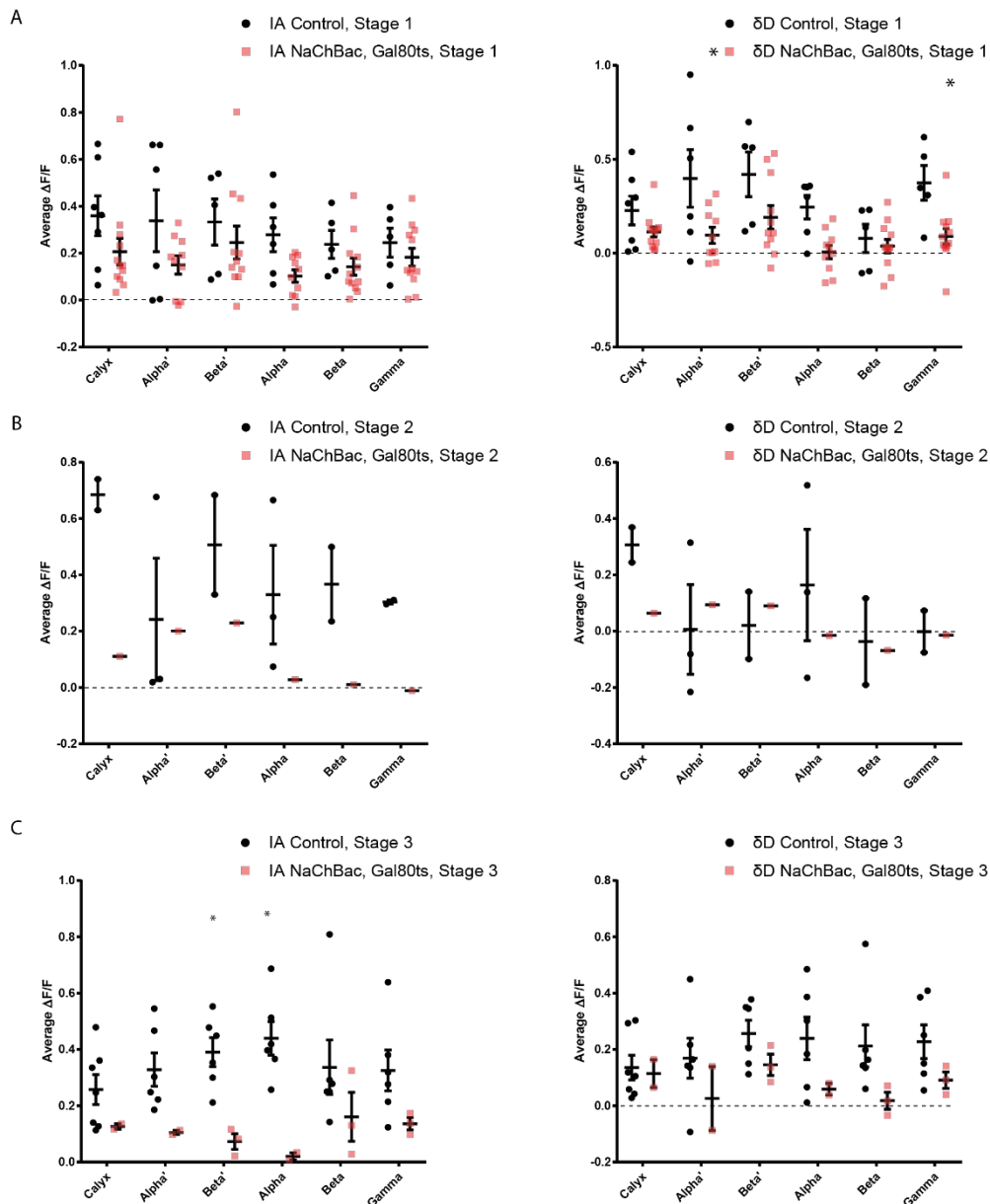


Figure 19 Quantification of the average odour responses of Figure 18.

Quantification of Figure 18. Fly genotypes: Control = R13F02GAL4>GCaMP6F, GAL80^{ts}. NaChBac = R13F02GAL4>GCaMP6F, GAL80^{ts}, NaChBac.

(A) Average odour response of *Drosophila* that expressed NaChBac, GAL80^{ts} from pupae Stage 1 in all subtypes of KCs. Left side: Response to IA. Right side: Response to δD. (B) Average odour response of *Drosophila* that expressed NaChBac, GAL80^{ts} from pupae Stage 2 in all subtypes of KCs. Left side: Response to IA. Right side: Response to δD. (C) Average odour response of *Drosophila* that expressed NaChBac, GAL80^{ts} from pupae Stage 3 in all subtypes of KCs. Left side: Response to IA. Right side: Response to δD. (A-C) Black = Control. Red = NaChBac. * = average odour response is p<0.05, two-way ANOVA with Šidák multiple comparisons test. Age past eclosion = 4 days

For detailed statistics, please see the table in Appendix A.

3.2.4 Summary of NaChBac expression in Kenyon cells

Figure 20 presents a summary of all the NaChBac conditions, displaying the mean difference between experimental and control conditions for the average odour response to isoamyl acetate (refer to see Appendix A for statistics). The summary reveals that constitutive expression of NaChBac, irrespective of the temperature at which the flies were housed, significantly weakens the odour responses of KCs. Moreover, when NaChBac was acutely expressed in pupae and for a duration of 2 days in adult flies, it resulted in a significant reduction in odour responses of Kenyon cells. In contrast, experiments involving 4 and 8 days of acute adult expression of NaChBac showed no significant difference between control and experimental flies.

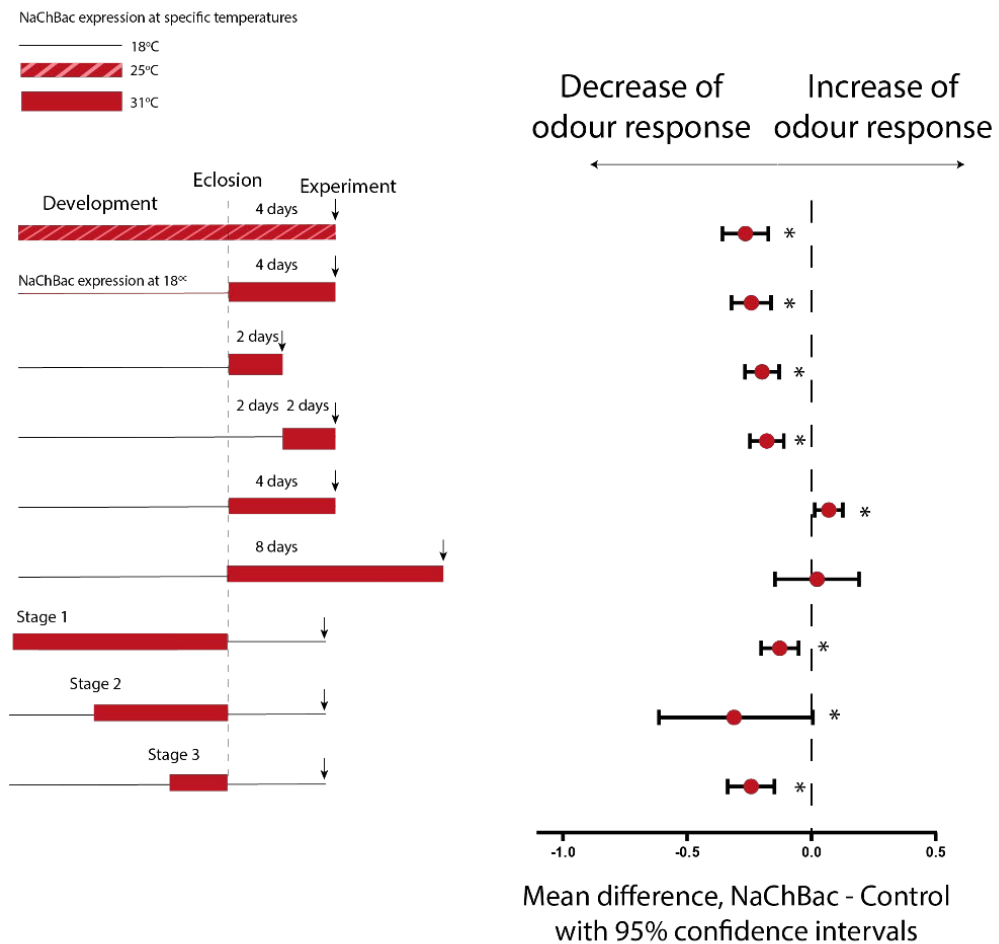


Figure 20 Summary of all NaChBac conditions.

The left panel includes a diagram of the temperature the *Drosophila* were housed at and for how long. The right panel shows the difference between predicted means of control and experimental for the average odour response for each condition shown in the panel on the left. The data is from the combination of average odour responses from all lobes in response to isoamyl acetate only. * = $p < 0.05$, main effect of genotype in two-way ANOVA. Mean difference \pm 95% confidence interval.

For detailed statistics, please see the table in Appendix A.

3.2.5 Constitutive expression of NaChBac reduces expression of Para sodium channels in KC distal axon initial segments

As described in Chapter 1, Para is the only endogenous voltage-gated sodium channel in *Drosophila* that is vital for neuronal functioning. Therefore, I wanted to investigate what effects the expression of NaChBac had on the expression levels of Para and whether Para levels contributes to the odour response results seen with NaChBac expression.

Due to the difficulties associated with obtaining specific protein antibodies for *Drosophila* and the inability to precisely determine the expression levels of Para in the KCs, I decided to use a genetic approach for cell-type-specific labelling of ion channels using GFP Flp tagging (green fluorescent protein; Fendl, Vieira, and Borst 2020; Figure 21). This method enables me to accurately determine the expression levels of Para specifically within KCs.

Past literature has shown that Para sodium channel is concentrated to the distal axon initial segment (DAIS; Ravenscroft et al., 2020), thus, ParaFlpTag was used to visualise Para in the DAIS while expressing mCherry to label the mushroom body (red fluorescent protein; Figure 22). I expressed NaChBac in the KCs and measured the fluorescence levels from ParaFlpTag and mCherry, normalising the ParaFlpTag to the mCherry fluorescence. I found that NaChBac significantly reduced the Para expression levels. This suggests that the expression of NaChBac causes the Kenyon cells to express less Para in the DAIS (Figure 22). Therefore, the reduced odour responses seen in KCs that constitutively express NaChBac could be due to a reduced level of Para because there is a reduced number of sodium channels to trigger action potentials.

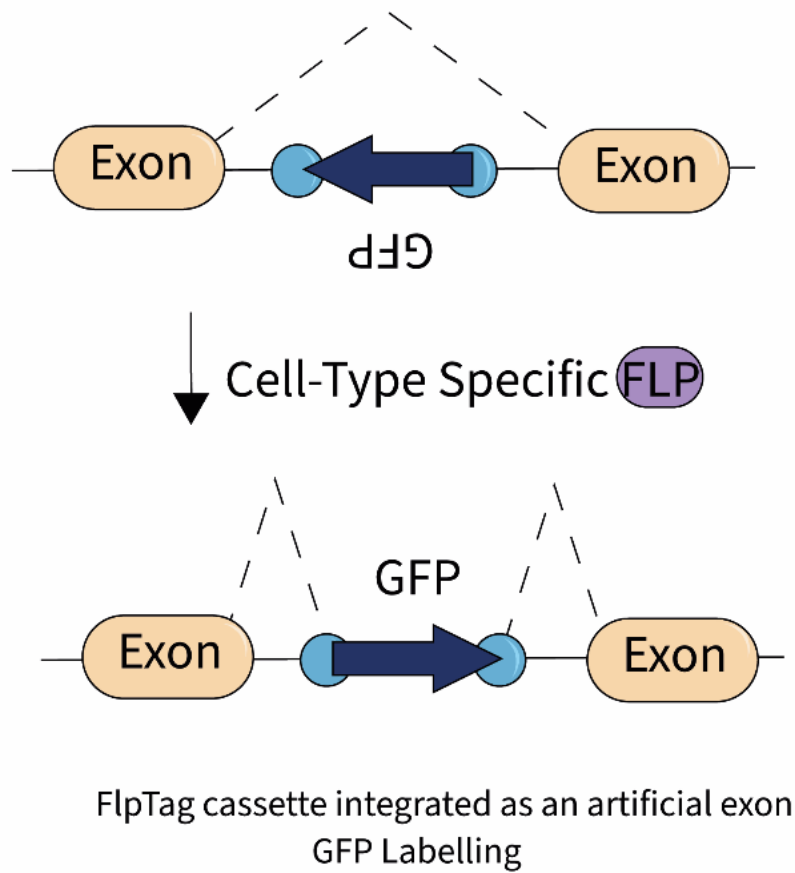


Figure 21 Diagram of the FlpTag mechanism.

GFP gene is expressed in all cells. FLP is then expressed in specific cells. This converts the GFP to become transcribed and so GFP only labels the cell specific cells.

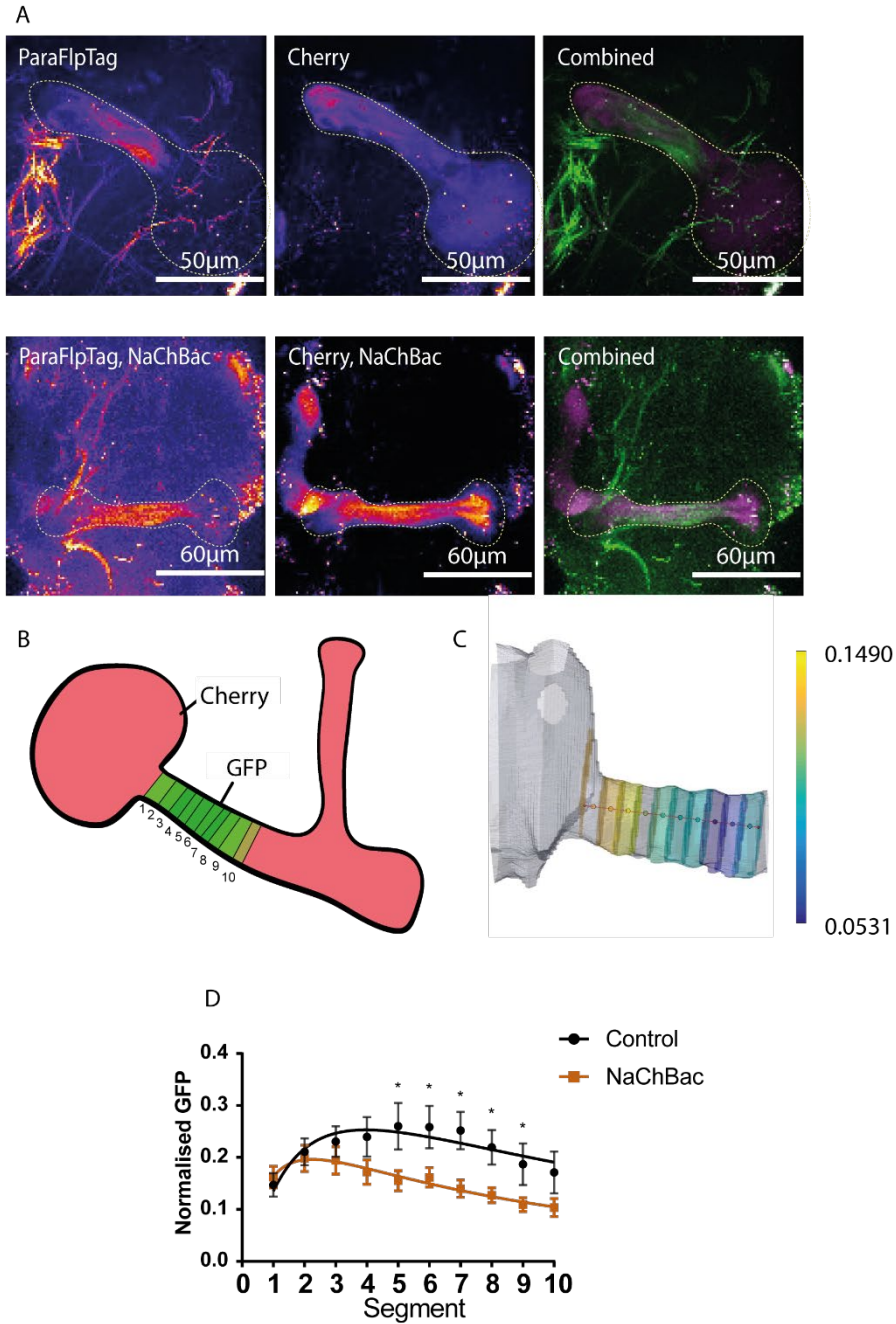


Figure 22 NaChBac lowers the number of Para sodium channels in the distal axon initial segment.

Fly Genotypes: Control = R13F02GAL4>Flp, Cherry, ParaFlpTag. NaChBac = R13F02GAL4>Flp, Cherry, ParaFlpTag, NaChBac.

(A) The top panels show ParaFlpTag, Cherry and their combined images in the peduncle of the mushroom body. The bottom panels show ParaFlpTag, Cherry and their combined images with the expression of NaChBac in the peduncle of the mushroom body. (B) A diagram of the mushroom body and how the peduncle was segmented for analysis. (C) Example of mask and skeleton used in MatLab for the analysis of the two channels. (D) Graph of the quantification of the normalised GFP in each segment of the peduncle. Black = Control, Orange = NaChBac. * = average fluorescence is $p < 0.05$, two-way ANOVA with Šidák multiple comparisons test and multiple student t tests. Age past eclosion = 4 days

For detailed statistics, please see the table in Appendix A.

3.2.6 Changing the length of the distal axon initial segment may slightly weaken odour responses of KCs

As observed, NaChBac expression decreased expression levels of Para sodium channels, known to be primarily localised in the distal axon initial segment (DAIS) (Ravenscroft et al., 2020). It is known that altering the location or length of the DAIS can impact neuron excitability (discussed in Chapter 1). Therefore, the length of the DAIS was investigated in relation to its potential effect on KC excitability.

CDK5 (Cyclin-dependent kinase 5) is an enzyme that is involved in regulating important biological processes such as development, synaptic plasticity, and cell survival. In neurons, CDK5 regulates the length and stability of the axon initial segment (Trunova et al., 2011) through the phosphorylation of various proteins, such as ankyrin-G. Dysregulation of CDK5 activity has been linked to decreasing the length of axon initial segments. Furthermore, decreasing the length of an axon initial segment been hypothesised to decrease neuronal excitability. CDK5DN (CDK5 dominant negative) expression in KCs has been shown to shorten the DAIS (Trunova et al., 2011). Thus, the expression of CDK5DN was predicted to decrease the efficiency of action potential initiation and propagation. Constitutive expression of CDK5DN significantly lowered the overall peak odour responses in KCs to both IA and δ D (Figure 23 and see Appendix A).

Another component linked to changes in length of the axon initial segment is p35. P35 is a protein that is encoded by the CDK5R1 gene (Trunova et al., 2011). It is primarily expressed in the nervous system and studies have shown that p35 expression can lead to an increase in the length and density of the DIAS (Trunova et al., 2011), but the mechanisms underlying this modulation is not fully understood and requires further research. Constitutive expression of p35, which increases the length of the DAIS, and thus, is expected to enhance excitability, resulted in weakened odour responses (Figure 23) The expression of p35 significantly weakened the overall average odour responses to IA, shown by the main effect of genotype (see Appendix A). This suggests that increasing the length of the DAIS does not increase the excitability of KCs. However, because these were preliminary experiments which did not reveal strong effects, and other experiments were considered higher priority, I did not verify whether CDK5DN or

p35 affected the length of the DAIS. Thus, these results should be considered as preliminary results only.

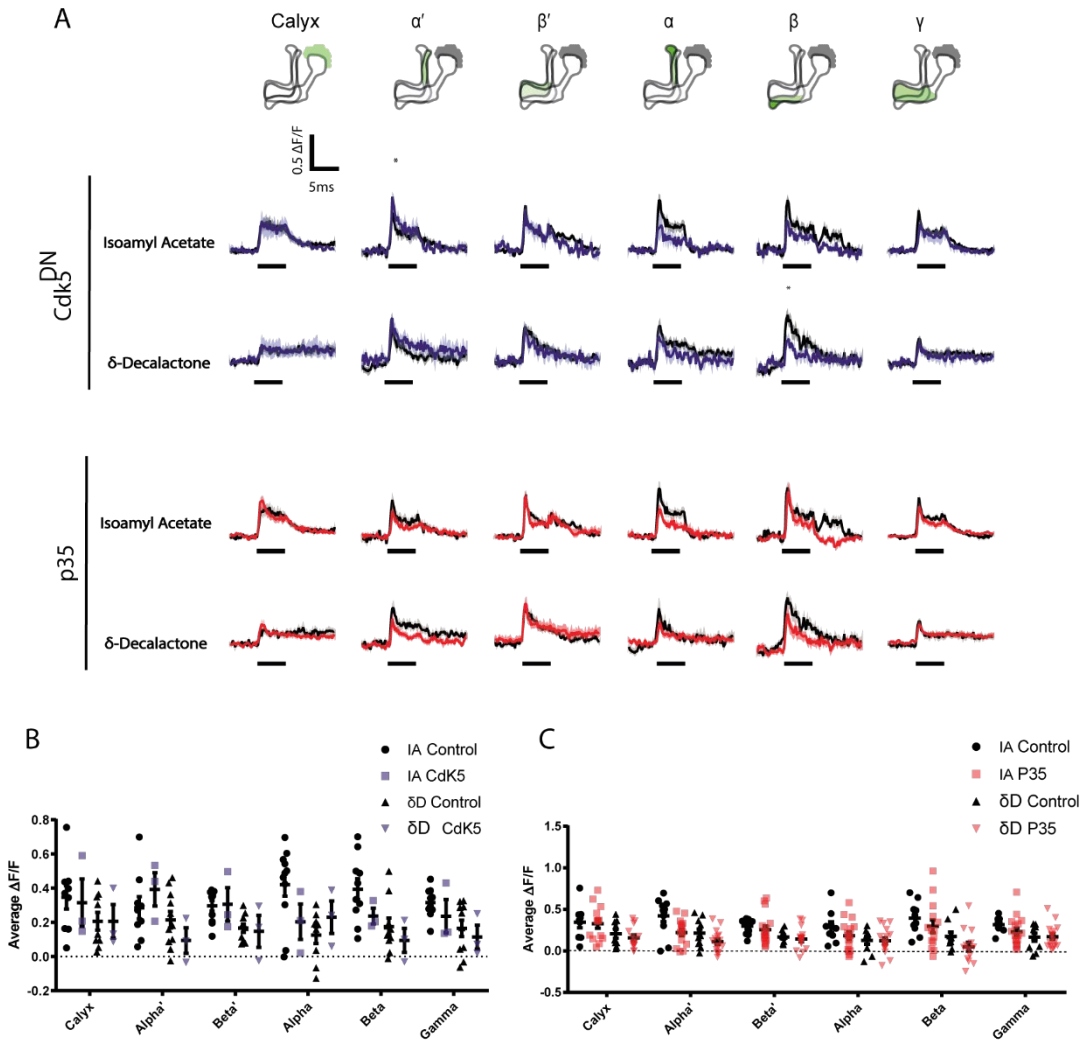


Figure 23 Expression of CDK5DN and p35 lowers odour responses in alpha and beta lobes.

Fly genotypes: Control = R13F02GAL4>GCaMP6f. CDK5DN = R13F02GAL4>GCaMP6f, CDK5DN. p35 = R13F02GAL4>GCaMP6f, p35. (A) For both Cdk5DN and p35 the top panel are odour responses to Isoamyl acetate. The bottom panel are odour responses to δ -Decalactone. Black bar = 5 s odour presentation. * = peak odour response is $p < 0.05$, two-way ANOVA with Šidák multiple comparisons test. (B) Graph of the average odour responses to isoamyl acetate and δ -Decalactone for Cdk5DN. * = average odour response is $p < 0.05$, two-way ANOVA with Šidák multiple comparisons test. (C) Graph of the average odour responses to isoamyl acetate and δ -Decalactone for P35. * = average odour response is $p < 0.05$, two-way ANOVA with Šidák multiple comparisons test. (A-C) Black = Control. Purple = CDK5DN. Red = p35. Age past eclosion = 3-4 days

For detailed statistics, please see the table in Appendix A.

3.2.7 The expression of paraRNAi reduces the odour responses in KCs but paraFlpStop increases the odour responses in the calyx

To determine whether NaChBac's effects can be solely attributed to the reduction of para, I used paraRNAi to directly lower the production of endogenous Para and observe its effects on the KCs' odour responses. The results show that the expression of paraRNAi reduced odour responses. ParaRNAi significantly reduced the peak odour responses in the α' , α and β lobes to IA and had a significant overall effect to IA and δ D (Figure 24) and significantly reduces the average odour responses, specifically in the β lobes, to IA (Figure 24). However, reducing Para via this method did not produce the same striking pattern of reduced odour responses in all lobes as seen with NaChBac expression. In particular, the odour responses in the calyx is not reduced like they were in NaChBac-expressing flies. This result is consistent with the lack of Para expression in the calyx; as para's main role is in propagating action potentials in the axon, it is unsurprising that removing Para does not reduce calcium influx levels in the calyx. Therefore, NaChBac's effects must involve additional changes within the cells, not just reducing para.

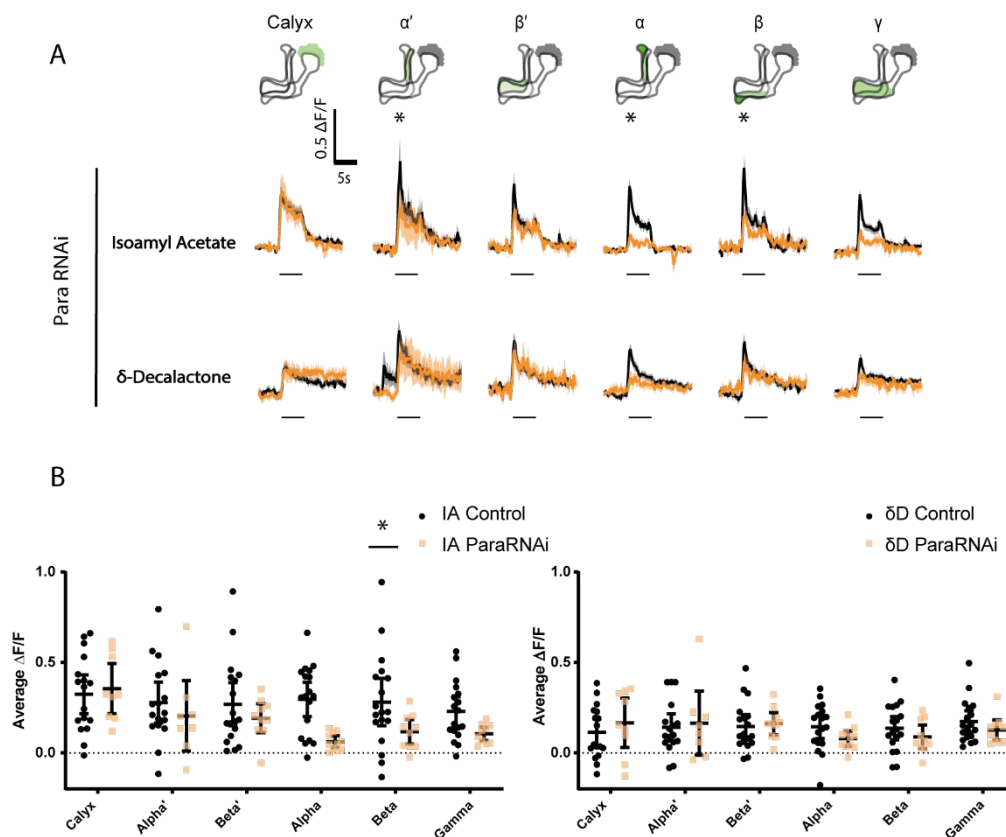


Figure 24 The expression of paraRNAi in Kenyon cells reduces their odour responses.

Fly genotypes: Control = R13F02GAL4>GCaMP6F. ParaRNAi = R13F02GAL4>GCaMP6F, ParaRNAi.

(A) Diagram of the subtypes of KCs. Odour response traces of Kenyon cells that express ParaRNAi in response to IA and δ D compared to controls. * = peak odour response is $p < 0.05$, two-way ANOVA with Šidák multiple comparisons test. (B) Quantification of the average responses in panel A. * = average odour response is $p < 0.05$, two-way ANOVA with Šidák multiple comparisons test. Black = Control, $n = 5$. Orange = ParaRNAi. Age past eclosion = 4 days

For detailed statistics, please see the table in Appendix A.

To investigate other methods of reducing Para to consolidate the results with paraRNAi, I used ParaFlpStop, in which a FlpStop cassette is inserted in an intron in Para (Figure 25). This insertion stops the production of Para specifically in cells expressing Flp recombinase. To selectively disrupt genes in specific cell populations of interest, conditional gene disruption using FlpStop can be achieved through the expression of Flp recombinase and the UAS/GAL4 system (Figure 24). I found that ParaFlpStop increases average odour responses in the calyx (Figure 26) but has no significant effect on the other lobes (Figure 26). These results also support the theory that NaChBac's effects on odour responses in KCs is not solely due to a reduction of para. These results

are surprising because paraFlpStop did not yield the same effects as paraRNAi. This finding may emphasise that RNAi does not always fully block the targeted proteins.

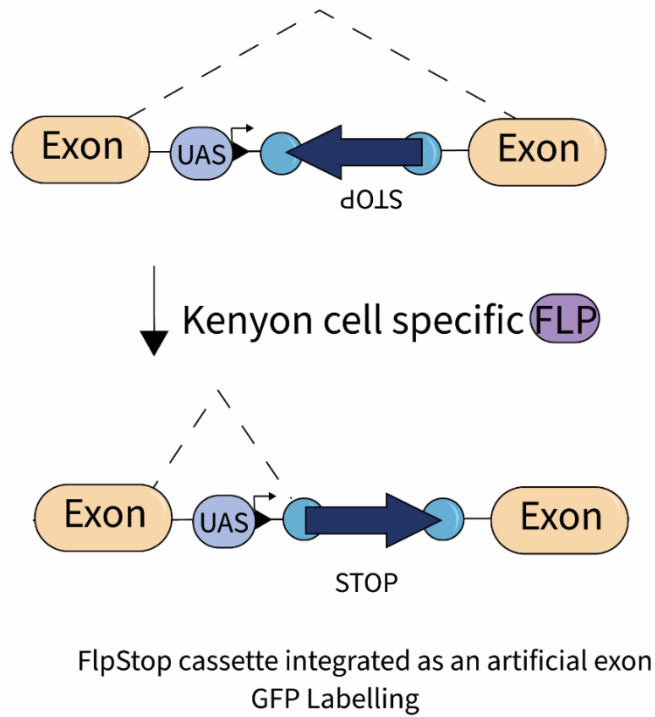


Figure 25 Diagram of ParaFlpStop mechanism.

Without the expression of FLP the cassette is backwards and so the STOP codon is not read. When the STOP cassette is flipped around by the FLP recombinase, then the STOP codons are spliced into the gene so that exon (Para) is prematurely terminated.

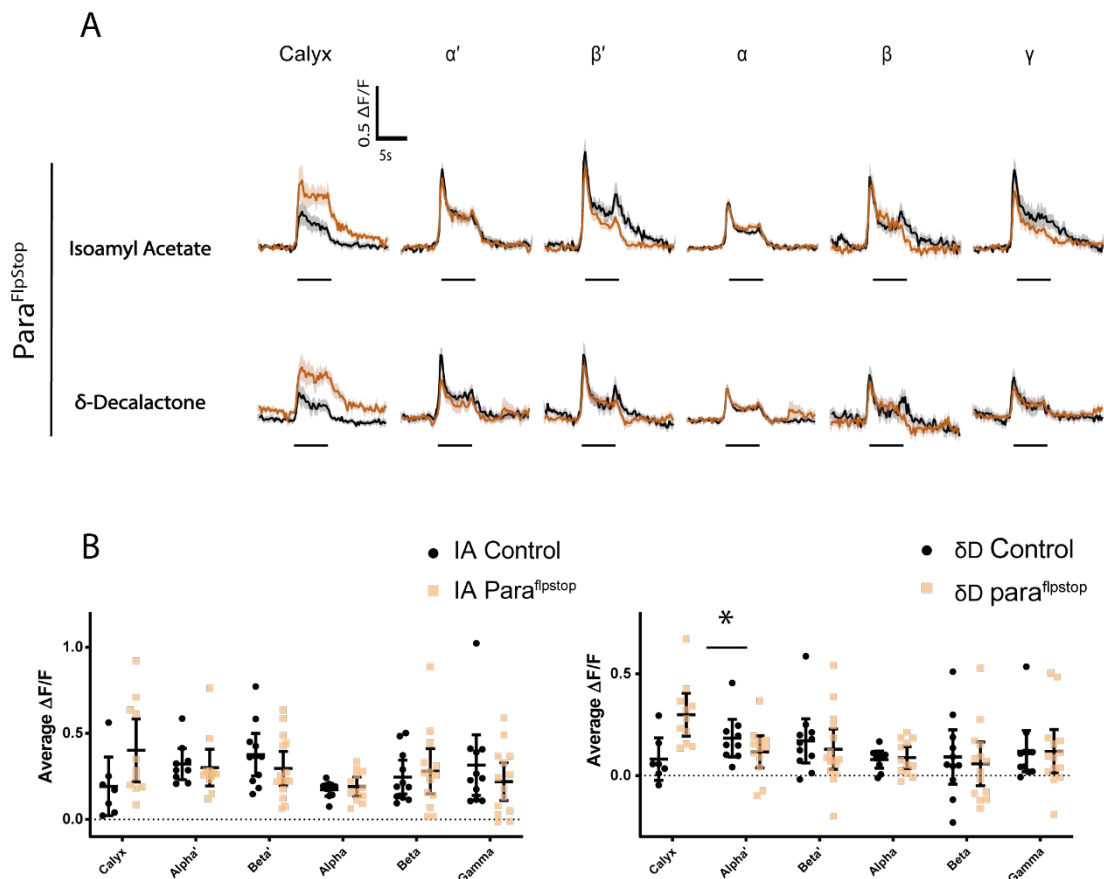


Figure 26 ParaFlpStop increases average odour responses in the calyx.

Fly genotypes: Control = *mbLexA>GCaMP6F*, Flp. ParaFlpStop = *mbLexA>GCaMP6F*, Flp, *paraFlpStop*

(A) Odour response traces of *paraFlpStop* in Kenyon cells in response to isoamyl acetate and δ -Decalactone. Two-way ANOVA with Šidák multiple comparisons test. (B) Quantification of the average response to IA and δ D from panel A. * = average odour response is $p < 0.05$, two-way ANOVA with Šidák multiple comparisons test. (A-B) Black = Control. Orange = ParaFlpStop. Age past eclosion = 4 days.

For detailed statistics, please see the table in Appendix A.

3.2.8 Preliminary results show that constitutive NaChBac expression in KCs increases the expression levels of Shaker potassium channels

As shown earlier NaChBac reduces the expression levels of *para*, but lowering the expression levels of *Para* alone does not replicate the effect of NaChBac expression. Therefore, I asked whether NaChBac expression also changes the expression levels of potassium channels. As described in Chapter 1, potassium channels contribute to the repolarisation of the membrane. Therefore, potassium channels contribute to the excitability of Kenyon cells. Thus, NaChBac expression may increase their levels, thus leading to lower odour responses. Using variations of GFP tagged channels, I

investigated the expression levels of potassium and cation channels with NaChBac expression. ShFlpTag was used to visualise the Shaker potassium channels (a major potassium channel in KC functioning) in the mushroom body while expressing mCherry to label the whole mushroom body (Figure 27). Normalising the ShFlpTag to the cherry fluorescence showed that NaChBac significantly increased the ShFlpTag fluorescence (Figure 27). These results suggest that the expression of NaChBac causes the Kenyon cells to express more Shaker. This is consistent with our hypothesis as the more potassium efflux there is then the more negative the membrane potential becomes and so this leads to a weakening in odour responses.

Next, IhFlpTag was used to visualise the I_h cation channels in the mushroom body while expressing mCherry to label the whole mushroom body and NaChBac (Figure 28). I_h is hyperpolarisation-activated current: when the membrane is hyperpolarised, I_h tends to push the membrane potential back toward resting potential. It is produced by hyperpolarization-activated cyclic nucleotide-gated (HCN) cation channels. I_h plays a vital role in regulating neuronal properties, synaptic integration and plasticity (Gonzalo-Gomez et al., 2012). Normalising the IhFlpTag to the mCherry fluorescence found that NaChBac significantly reduced the IhFlpTag fluorescence (Figure 28). These results suggest that the expression of NaChBac causes the Kenyon cells to produce less I_h channels in the KCs, thus, contributing to lower excitability in the cells.

Lastly, EagFlpTag was used to visualise the Eag potassium channels. The Eag channels were found when a different mutant, other than Shaker (described in Chapter 4), was found with leg-shaking behaviour when undergoing etherisation (ether-a-go-go; Kaplan and trout, 1969; Ganetzky and Wu, 1983; Wu et al., 1983; Drysdale et al., 1991). The Eag channel is a member of a large family of voltage-gated K^+ channels in *Drosophila*. Eag channels are localised in the presynaptic terminals in both mammals and flies, and they participate in repolarising the membrane potential. The channel is controlled not only by voltage but also by calcium dependent inhibition. Calcium dependent inhibition of EAG is used to locally amplify the effects of depolarisation at the active zone by decreasing the repolarising current in that domain (Bronk et al., 2018). Therefore, investigating Eag will provide insight into whether NaChBac modifies the excitation through this method. However, I found that NaChBac expression did not affect the expression levels of EagFlpTag (Figure 29).

These results show that constitutive NaChBac expression in KCs likely increases the endogenous Shaker potassium channels and lowers the I_h cation channels which contribute to the low activity seen in the cells.

This occurs because the presence of Shaker potassium channels contributes to membrane hyperpolarisation. Consequently, an increased expression of Shaker channels hyperpolarises the cells, reducing the likelihood of generating an action potential. Furthermore, I_h channels are permeable to both potassium and sodium ions, but they predominantly conduct a mixed cation current known as the I_h current. The channels open in response to hyperpolarisation and by conducting a depolarising current they can counteract the effects of membrane hyperpolarisation, promoting the generation of action potentials. Hence, reduced expression of I_h channels leads to a diminished counteraction against neuronal hyperpolarisation, resulting in a decreased likelihood of generating action potentials.

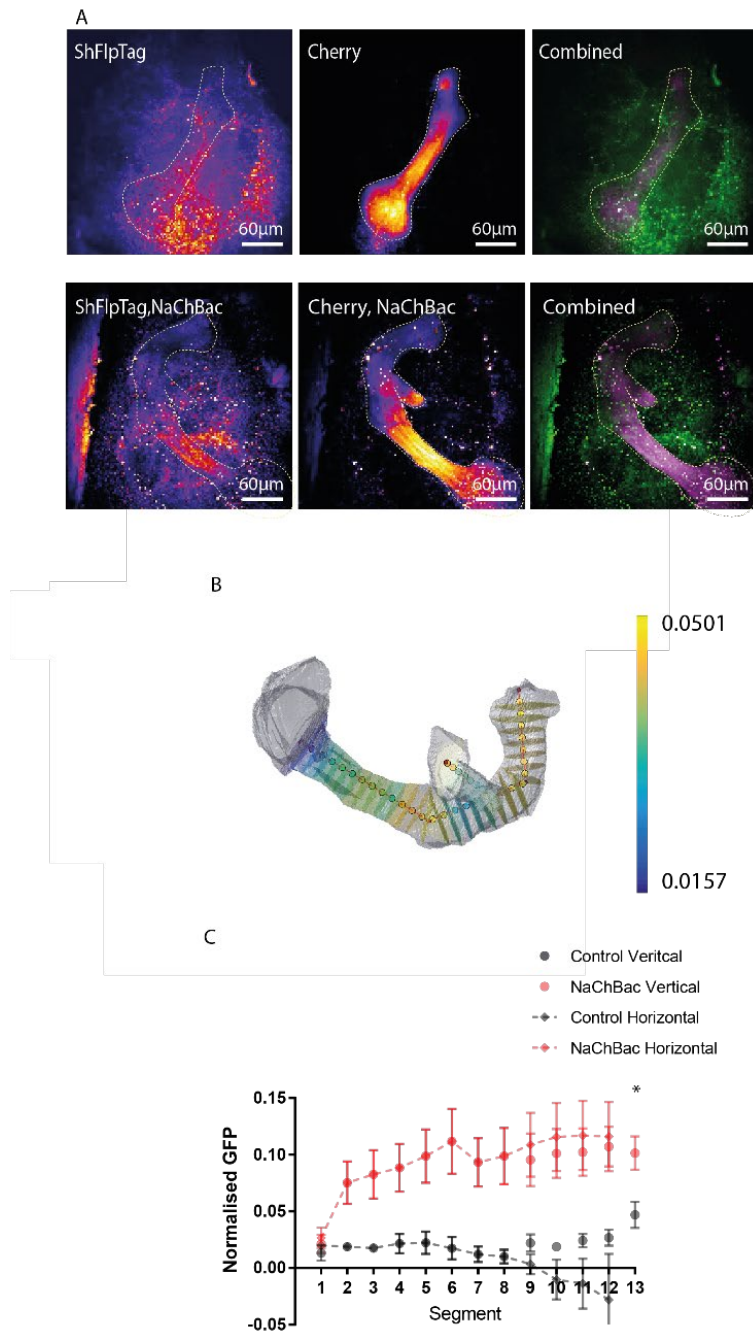


Figure 27 NaChBac increases the expression levels of ShFlpTag in Kenyon cells.

Fly Genotypes: Control = R13F02GAL4>Flp, Cherry, ShFlpTag. NaChBac = R13F02GAL4>Flp, Cherry, ShFlpTag, NaChBac. (A) The top panels are of GFP tagged ShFlpTag, Cherry and their combined images in the mushroom body. The bottom panels are of GFP tagged ShFlpTag, Cherry and their combined images with the expression of NaChBac in the mushroom body. The values for the horizontal lobes (β' , and β , γ) and vertical lobes (α' and α) are separated. The colour coded bar shows relative fluorescence between GFP and mCherry. (B) An example of the mask and skeleton used in MatLab for the analysis of the two channels. (C) Quantification of the normalised GFP in each segment. Black = Control. Red = NaChBac. * = average fluorescence is $p < 0.05$, two-way ANOVA with Šidák multiple comparisons test. Age past eclosion = 4 days.

For detailed statistics, please see the table in Appendix A.

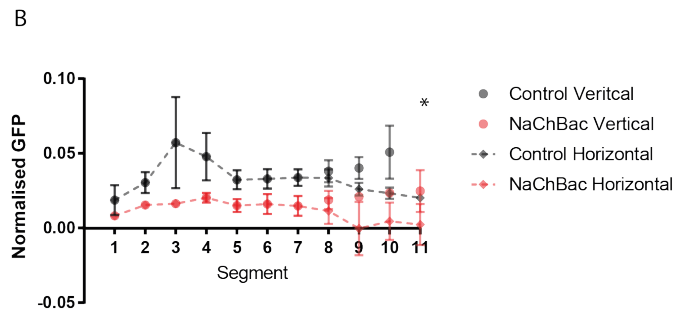
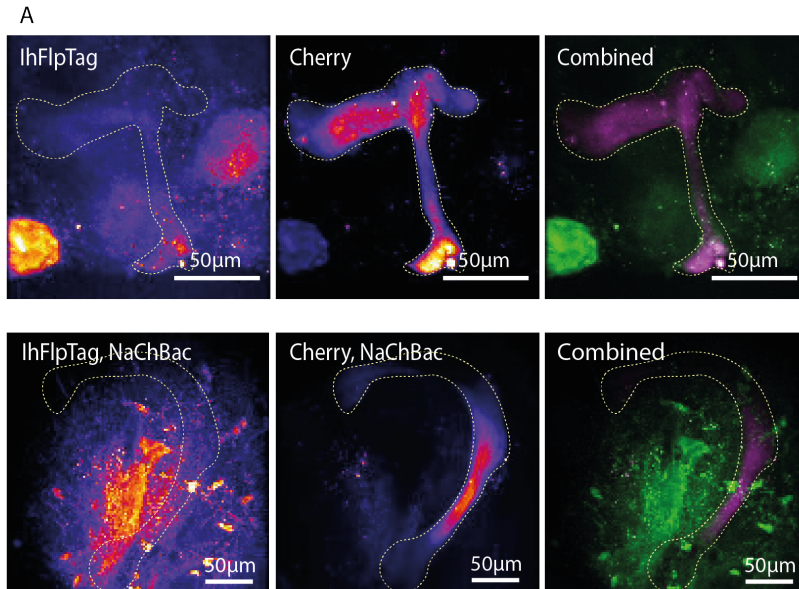


Figure 28 NaChBac expression in KCs reduces the expression levels of IhFlpTag.

Fly Genotypes: Control = R13F02GAL4>Flp, Cherry, IhFlpTag. NaChBac = R13F02GAL4>Flp, Cherry, IhFlpTag, NaChBac.

(A) The top panels are of IhFlpTag, Cherry and their combined images in the mushroom body. The bottom panels are of IhFlpTag, Cherry and their combined images with the expression of NaChBac in the mushroom body. (B) Graph of quantification of the normalised GFP in each segment. The values for the horizontal lobes (β' , and β , γ) and vertical lobes (α' and α) are separated. The colour coded bar shows relative fluorescence between GFP and mCherry. Black = Control Red = NaChBac. * = average fluorescence is $p < 0.05$, two-way ANOVA with Šidák multiple comparisons test. Age past eclosion = 4 days

For detailed statistics, please see the table in Appendix A.

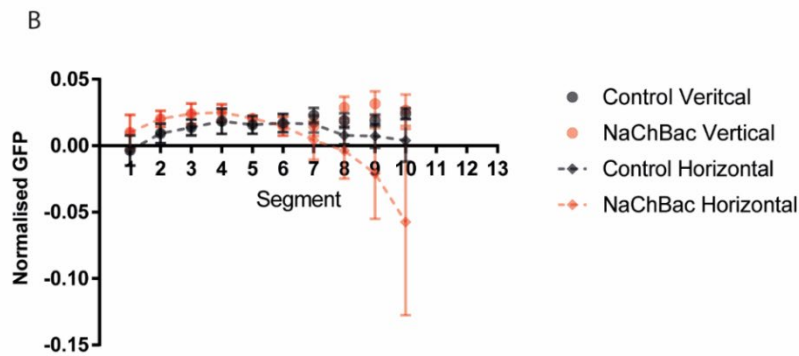
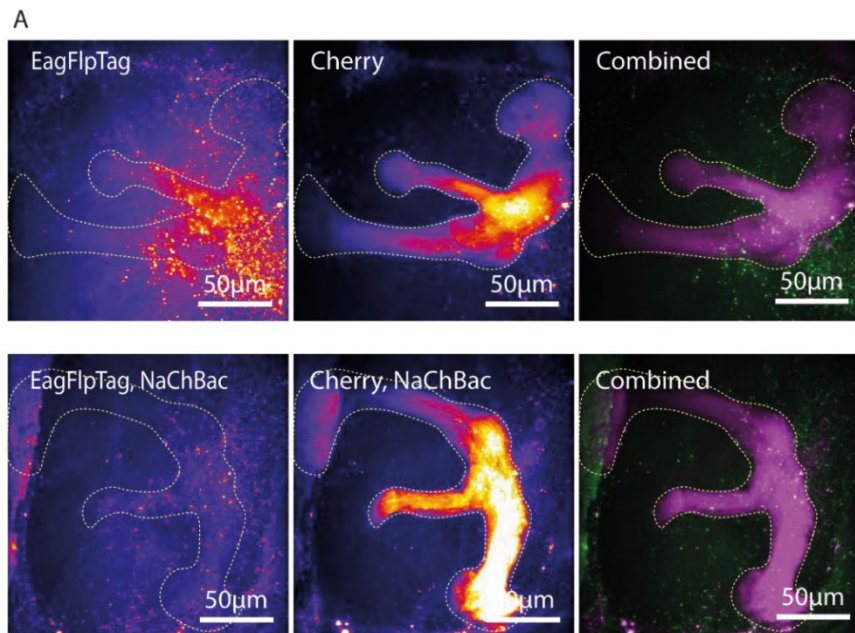


Figure 29 NaChBac expression in Kenyon cells does not change the expression of EagFlpTag.

Fly Genotypes: Control = R13F02GAL4>Flp, Cherry, EagFlpTag. NaChBac = R13F02GAL4>Flp, Cherry, EagFlpTag, NaChBac.

(A) The top panels are of EagFlpTag, Cherry and their combined images in the mushroom body. The bottom panels are of EagFlpTag, Cherry and their combined images with the expression of NaChBac in the mushroom body. (B) Graph of quantification of the normalised GFP in each segment. The values for the horizontal lobes (β' , and β , γ) and vertical lobes (α' and α) are separated. The colour coded bar shows relative fluorescence between GFP and mCherry. Black = Control. Red = NaChBac. Two-way ANOVA with Šidák multiple comparisons test was used for statistical analysis. Age past eclosion = 4 days.

For detailed statistics, please see the table in Appendix A.

3.2.9 No changes were observed in the expression levels of $\alpha 6$ and $\alpha 7$ subunit-containing nicotinic receptors with constitutive NaChBac expression

As discussed in Chapter 1, acetylcholine is responsible for KC input. Nicotinic acetylcholine receptors mediate the synaptic transmission of the Kenyon cells. Thus, NaChBac may also decrease the levels of nAChR to lower odour responses. GFP tagging of various nAChR was used to investigate what happens to nAChR levels when NaChBac is expressed (Pribbenow et al., 2022). The GFP was tagged to the α subunits using CRISPR technology. This method of tagging is endogenous, but it is not cell specific like the FlpTag method. This project focuses on nAChR6-GFP and nAChR7-GFP because they have high expression levels in Kenyon cells, and due to time constraints, other variations were not examined. The results show that there was no significant difference in GFP fluorescence between control and NaChBac-expressing KCs in either nAChR6-GFP or nAChR7-GFP (Figure 30). Note that the GFP signal in the lobes is likely from other cells such as MBONs, DANs and the APL (Figure 30) as KCs do not have nAChRs in their axons. Together with the ion channel FlpTag results, these results suggest that NaChBac may primarily affect membrane excitability rather than synaptic input. However, due to the small sample size of this experiment, these results are considered preliminary, and no definitive conclusions can be drawn at this early stage.

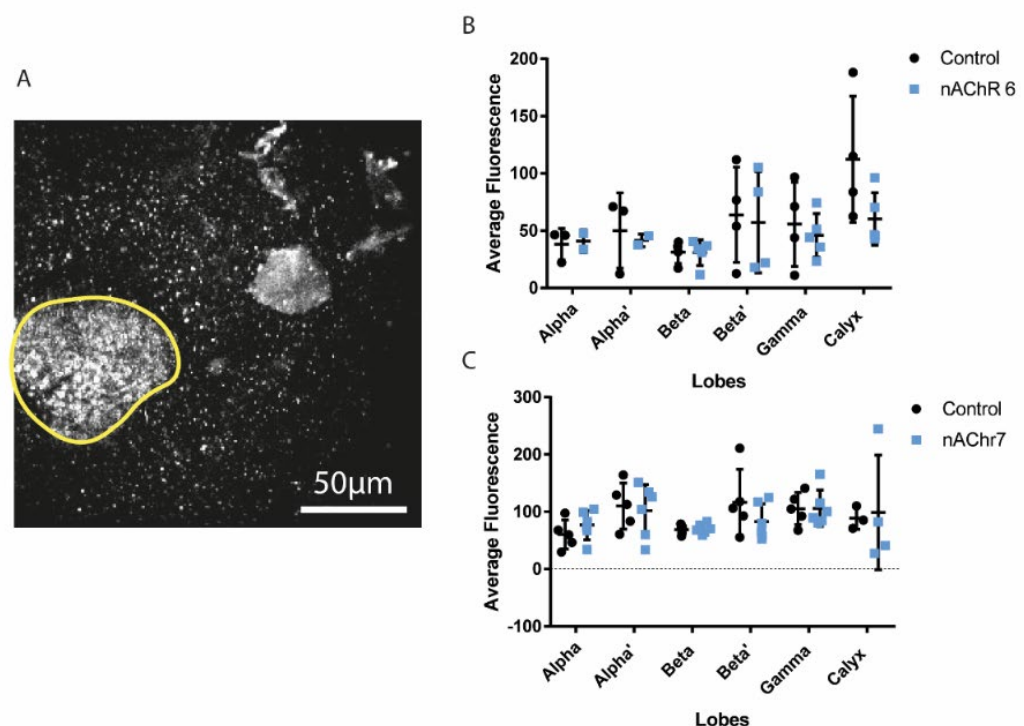


Figure 30 Levels of nicotinic receptors do not change with the expression of NaChBac.

Fly genotypes: Control = R13f02GAL4>nAChR α 6.GFP or nAChR α 6.GFP. nAChR6 = R13f02GAL4>nAChR α 6.GFP, NaChBac. nAChR7 = R13f02-GAL4>NaChR α 7.GFP, NaChBac.

(A) Example region of interest for analysis of average fluorescence. (B) Quantification of average fluorescence of nAChR6 in the different lobes. Black = Control. Blue = nAChR6. (C) Quantification of average fluorescence of nAChR7 in the different lobes. Black = Control. Blue = nAChR7. Two-way ANOVA with Šidák multiple comparisons test was used for statistical analysis. Age past eclosion = 3-4 days.

For detailed statistics, please see the table in Appendix A.

3.2.10 Constitutive NaChBac expression weakens peak odour responses of projection neurons

In the olfactory system, KCs are unique as they use sparse coding. The projection neurons, which provide the input to the KCs, do not use sparse coding. Given this disparity, I wanted to investigate whether NaChBac expression produces the same results as when it is expressed in PNs. Therefore, I constitutively expressed NaChBac

in the projection neurons and recorded their odour responses (Figure 31). The results demonstrate a significant main effect of NaChBac, which significantly weakened the average odour responses to IA and peak responses to IA and δ D (see Appendix A). Conducting multiple comparisons showed a significant decrease in response in response in the lateral horn (Figure 31 and see Appendix A). But, overall, the projection neurons do not have the same striking effect as when KCs express NaChBac.

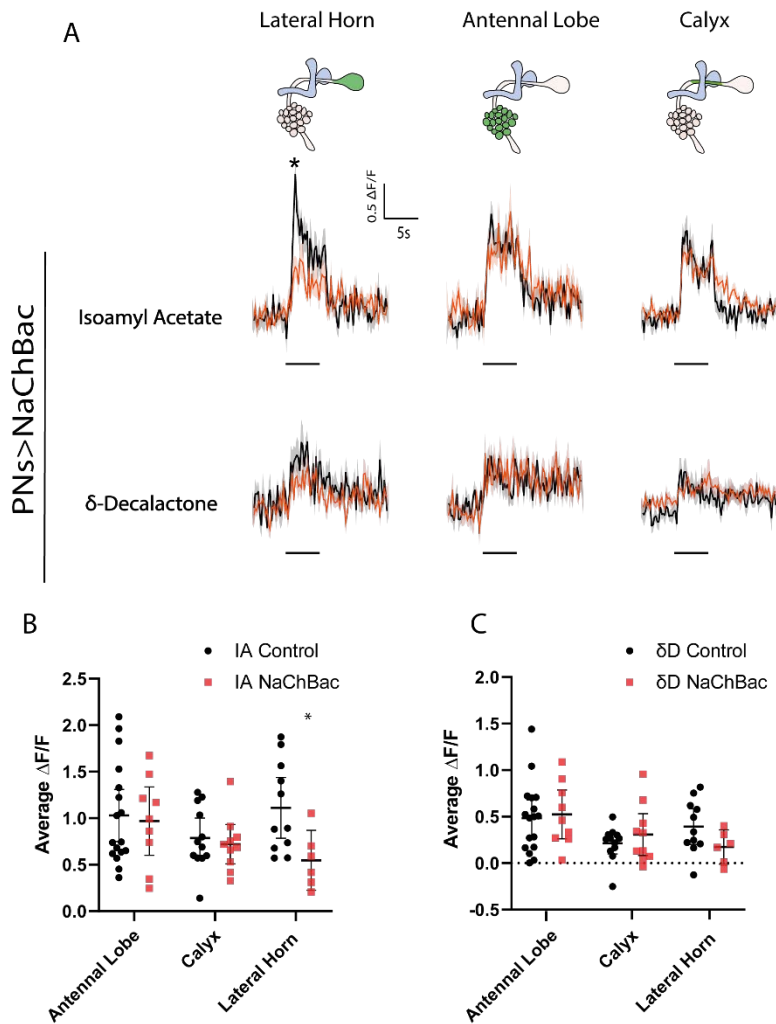


Figure 31 NaChBac weakens the odour responses in the projection when they express NaChBac.

Fly genotypes: Control = GH146-GAL4>GCaMP6f. NaChBac = GH146-GAL4>GCaMP6f, NaChBac.

(A) Diagrams of the various areas of the projection neurons. Odour response traces of projection neurons with NaChBac expression in response to IA and δ D. (B-C) Quantification of the average odour responses from panel A. Two-way ANOVA with Šidák multiple comparisons test was used for statistical analysis. Black = Control. Orange = NaChBac. Black bar = 5s odour presentation. Age past eclosion = 4 days

For detailed statistics, please see the table in Appendix A.

3.3 Discussion

My findings show that most NaChBac expression conditions result in decreased odour responses in KCs. One possible explanation for this is that the KCs homeostatically downregulate the expression levels of endogenous Para sodium channels and upregulate Shaker potassium channels. However, these alone does not fully account for the observed reduction in odour responses compared to the extent seen with NaChBac overexpression.

3.3.1 NaChBac has a paradoxical effect in KCs

Contrary to previous studies that have also constitutively expressed NaChBac, my findings with KCs do not align with their results (e.g. Nitabach et al., 2006). My results show that odour responses in KCs were significantly lower when NaChBac was expressed throughout development, whether they were kept at 25°C or 31°C (Figure 20). Although not exactly comparable, odour responses seen with GCaMP6f can be related to activity levels of the cell. Thus, the lower odour responses seen are likely showing a lower activity in the KCs with the expression of NaChBac. Therefore these results are in disagreement with past studies which express NaChBac in excitable cells and find increases activity from the larger influxes of sodium ions (Sheeba et al., 2008; Kelsch et al., 2009; Lin et al., 2010; Sim et al., 2013). These results suggest that multiple factors may be contributing to the observed effects. The Kenyon cells may have sensed an increase in sodium channels and attempted to reduce excitation, but overcompensated, leading to significant weakening of the odour responses. Alternatively, NaChBac may not be causing overexcitation in the Kenyon cells and instead may primarily weaken their responses.

I first investigated whether the odour responses were smaller because NaChBac decreases activity or because NaChBac increases baseline activity making odour responses relatively smaller. The results found that the baseline signal of GCaMP6f was lower than the control flies (Figure 10). This suggests that the odour responses are even weaker than originally thought with NaChBac expression. This could be that the baseline activity is lower in KCs or that NaChBac expression lowers the expression of GCaMP6f. NaChBac has an activation threshold of approximately 15 mV more negative

than that of native sodium channels in granule neurons (Kelsch et al., 2007). Therefore, NaChBac may be creating an unnatural environment for GCaMP6f in the KCs. In contrast, Sheeba *et al.*, (2008) found that NaChBac expression reduced the resting membrane potential from -41.5 mV (in wild type) to -103 mV. This would explain significantly reduced odour responses and possibly the lower baseline expression of GCaMP6f (seen in Figure 10). If the RMP is lower, then the Kenyon cells may not be able to depolarise to their firing threshold and the KCs may not have adjusted to accommodate this change.

Two-day expression of NaChBac in adult flies still produced significantly weaker odour responses and thus weaker activity in KCs (Figure 20). This suggests that a short period of NaChBac expression is sufficient to affect KCs and perturb their maintenance of activity. One possibility is that KCs respond to the increase in sodium channels by regulating other parameters, but an overcompensation of regulation leads to significant weakening of activity. Alternatively, it is possible that the decrease in KC activity observed does not reflect homeostatic compensation. Instead, it is possible that the primary effect of NaChBac is to decrease KC activity as the homeostatic mechanisms are unlikely to occur within the span of 2 days.

When NaChBac is acutely expressed for 4 days in adults there was an overall significant increase in odour responses in the KCs (Figure 20). This suggests that in mature *Drosophila*, KCs can overcome the weakening from NaChBac expression and 4 days of NaChBac expression is enough to create overexcitation in the β' lobe. The absence of overexcitation in KCs after 2 days acute NaChBac expression, 2 days following eclosion, indicates that the compensation seen in 4 days NaChBac expression is not attributed to the age of the *Drosophila* (Figure 20). Therefore, 4 days of NaChBac expression in adults is required to produce overexcitation of KCs and this is not reliant on the age of the *Drosophila*.

Interestingly, after 8 days of NaChBac expression in adult *Drosophila*, KCs had normal responses to odours (Figure 20). This suggests that the KCs have a mechanism to counteract the effects of NaChBac expression, overcoming both the extreme weakening of odour responses and slight overexcitation seen. However, further investigation is required to understand the dynamics of KCs activity. Does NaChBac cause KC activity to first be lower than normal, then higher than normal, then stabilise? Alternatively, does

activity start high, decrease immediately to a low level, rise again and then stabilise? Clarifying the dynamics of NaChBac-induced changes in KC activity will require further research.

To understand whether NaChBac makes KCs more excitable when expressed in the developmental stages of *Drosophila*, NaChBac was expressed in various stages of pupae development. Preliminary results also showed significant weakening of odour responses, no matter what stage NaChBac began being expressed (Figure 20). This suggests that KCs in development are not able to overcome the overexpression of NaChBac and NaChBac produces the same effects as when it is expressed constitutively. It is possible that at these stages, KCs do not have the mechanisms to compensate for the expression of NaChBac.

The results found from expressing NaChBac in KCs disagree with past literature which use NaChBac in *Drosophila* cells. For example, in cells that control feeding behaviour, an innate and learnt behaviour, NaChBac expression triggered the same behavioural effects as TRPA expression and the opposite effect of increasing the potassium channel Kir2.1, suggesting that NaChBac increases activity of the cells (Hergarden et al., 2012). Also, NaChBac expression in *Drosophila* photoreceptors causes large, slowly activating and inactivating depolarisations, thus the channel still produces the same electrophysiological effects seen in eukaryotes (Luan et al., 2006). Other studies using electrophysiological methods have shown the distinct gating and large sodium currents of NaChBac which contribute to neuronal overactivity (Ren et al., 2001; Kuzmenkin et al., 2004) Furthermore, Zimmerman et al. (2017) states that acute expression using GAL80^{ts} and NaChBac also increases activity in glutamatergic neurons. However, they never actually tested whether this was an actual increase in activity, they assumed that the change in behaviour (increase in wakefulness of *Drosophila*) was because of an increase in activity. Furthermore, Zimmerman et al. (2017), results suggest that it is unlikely that GAL80^{ts} contributes to the paradoxical results found in this project results as they used GAL80^{ts} but still found an increase in activity. These examples of literature, in addition to what has been found and discussed in the introduction, suggest that NaChBac has surprisingly distinct effects in KCs compared to other excitable cells. This may be due to several factors such as electrical parameters, ion channel concentrations or protein expression which should be investigated in future research.

Future work could establish the behavioural effects of each condition to investigate whether adult *Drosophila* that have had 8 days of NaChBac expression have better, more solidified, odour associative memories than that of 2 or 4 days of NaChBac expression. As shown in the results of this project, NaChBac expression weakens the odour responses in the KCs. This may lead to the *Drosophila* being unable to form odour associative memories due to a lack of response. In contrast, this may not affect the memories at all due to sparse coding favouring a lack of excitability through the population. However, expressing NaChBac for 4 days overexcited a subset of KCs, which may lead to poor development of odour associative memories as some KCs may be more active than others and disrupt the sparse coding of the population. KCs that have had 8 days of NaChBac expression may have better odour associative memories as the KCs have returned to control level odour responses and have overcome the disruption caused by NaChBac expression.

3.3.2 NaChBac weakens Para expression in KC distal axon initial segments and alters potassium channels

As shown above, constitutive expression of NaChBac weakens odour responses in KCs and thus likely reduces excitability. To weaken excitability in neurons, neurons can lessen their expression of sodium and calcium channels or upregulate potassium channels. My findings show that when NaChBac is constitutively expressed throughout development and some of adult life, the endogenous sodium channel, para, is significantly downregulated in the distal axon initial segment (DAIS; Figure 23). As Para is the only endogenous sodium channel that is vital for neuronal excitation in *Drosophila* (Feng et al., 1995; Miyazaki *et al.*, 1996; Mee *et al.*, 2004) it is likely that the KCs downregulate Para significantly to overcome the overactivity (or expected overactivity) caused by NaChBac. Para is highly concentrated in the DAIS (Ravenscroft et al., 2020) which has been predicted to be the site of action potential propagation. The DAIS is also distal to the dendrites of other *Drosophila* neurons (Gouwens and Wilson, 2009; Günay et al., 2015). Therefore, a reduction of Para in the DAIS, likely means that an action potential is less likely to fire, thus weakening the odour responses of KCs.

In future experiments, it would be interesting to examine the length of the KC DAIS as it has been found that in *Drosophila*, neurons with a more distal DAIS have longer DAIS (Ravenscroft et al., 2020). This differs from observations in vertebrates, where a more distal axon initial segment typically results in a shorter length of the axon initial segment (Adachi, Yamada, and Kuba, 2015).

Para has been shown to have homeostatic regulatory tendencies. Past literature using Para has increased the known methods of homeostatic regulation to include activity-dependent regulation of an ion channels through mRNA. It has been shown that artificially increasing activity (through synaptic excitation) is sufficient to significantly reduce mRNA abundance for Para to counteract membrane excitation (Mee et al., 2004). In contrast, Para is significantly increased when synaptic vesicle release is blocked (Mee et al., 2004). Additionally, feeding picrotoxin to wild type flies or GABA to *sda* ("bang-sensitive") *Drosophila* is enough to promote or reduce the splicing of Para that increases excitation (Lin et al., 2012). It is possible that expressing NaChBac caused para to splice differently to reduce excitation.

However, reducing Para using paraRNAi and paraFlpStop alone does not have the same effect on reducing odour responses as NaChBac overexpression (Figure 24 and 26). Reducing Para through RNAis did not have the same significant reduction of odour responses as NaChBac expression (Figure 24). Therefore, it is likely that there is more to NaChBac's effect than just a reduction in endogenous para. However, due to how they form and how large they are, it has been said that sodium and calcium channels are not suitable for dominant negative strategies (Hodge, 2009). Thus, RNAis or toxins are used to inhibit Para channels instead. RNAis are not perfect and do not get rid of all the targeted proteins. Therefore, another future method to investigate overexcitation in KCs may be to use toxins such as delta-ACTX-Hc1a to inhibit Para (Wu et al., 2008).

As Para cannot be the only homeostatic response to NaChBac, I therefore investigated how NaChBac expression affects potassium channel expression levels. Constitutive NaChBac expression caused a significant increase in the levels of Shaker potassium channels (Figure 27). As potassium channels are responsible for the repolarisation and hyperpolarisation of the membrane, increasing the number of potassium channels makes neurons less excitable. To explore this concept further, NaChBac induces "plateau-like" action potentials because of the kinetics of the channel. Therefore,

NaChBac makes action potentials longer and possibly the KCs can sense this and may strengthen the repolarisation potential of the membrane. Therefore, increasing the levels of Shaker would increase the repolarising currents and cutting short the longer APs. Moreover, it appears that KCs have over expressed Shaker and under expressed Para too much so that their odour responses are significantly lower than control.

My findings show that using CDK5DN to reduce CDK5 activity, which shortens the DAIS proximally, weakened the odour responses in KCs. These results would agree with previous theoretical studies that state that excitability should decrease when the DAIS moves away from the soma as depolarisation of the membrane diminishes over time and length (Baranauskas et al., 2013; Brette, 2013; Telenczuk et al., 2017; Raghuram et al., 2019; Goethals and Brette, 2020). Expressing p35, which should elongate the DAIS, significantly weakens overall odour responses. This is another surprising result as, theoretically, if the DAIS is longer then there could be an increased chance of firing an action potential. In contrast, increasing the length of the DAIS alone does not necessarily indicate a higher level of Para within it, which are required for triggering action potentials. Furthermore, it is possible that the constructs didn't work and did not affect the length of the DAIS. This could be due to multiple factors, such as, the wrong flies were sent, or they weren't being expressed properly. As there was significant weakening of odour responses with both CDK5DN and p35 expression it may be possible that the constructs are affecting factors other than the DAIS which could have a side effect on KC activity. Therefore, future experiments should include assessing the length of the DAIS in the KCs.

The results suggest that both shortening and lengthening the DAIS weakens the odour responses of KCs. It is surprising that increasing the length of the DAIS, which should theoretically increase activity, adds to the continuing list of conditions that weaken odour responses in KCs.

3.2.3 NaChBac expression doesn't alter the expression levels of acetylcholine receptors

As discussed earlier, affecting the parameters of action potentials is not the only way to alter excitability. KCs have nicotinic receptors that contribute to excitatory input (Lee

and O'Dowd 1999; Restifo and White 1990; Salvaterra and McCaman, 1985; Yasuyama, Kitamoto, and Salvaterra, 1995). Preliminary results show that constitutive NaChBac expression had no significant effect on the expression levels of nicotinic receptors (Figure 30). The n number for these results are very small and so I cannot be truly confident in these results. However, the initial results show that NaChBac is unlikely to affect the inputs of KCs.

Lastly, NaChBac expression in the second order olfactory neurons, PNs, does not have the same effect as expressing NaChBac in KCs (Figure 31). PNs do not use sparse coding to process information. Therefore, they do not require highly specific tuning like KCs. As PNs and KCs have distinct roles from one another this could be a reason as to why they are not affected by NaChBac in the same way. However, it does not explain why they are not overactive from the increase in sodium channel. This may be due to NaChBac being exogenous and the PNs may not be affected by them. It could also be that NaChBac is not forming a functional channel. Or this may be because NaChBac only increases the excitability of specific neurons within *Drosophila* and cells that contribute to olfaction are not prone to NaChBac's overexcitation.

3.2.4 Future work

It may be interesting to examine the baseline GCaMP6f fluorescence throughout the experiments involving NaChBac expression. As baseline GCaMP6f fluorescence was significantly lower in the γ KCs, it may be insightful to know whether baseline fluorescence changes with the various conditions with acute NaChBac expression. These experiments may help us understand the mechanisms involved when NaChBac is expressed in KCs.

As *Drosophila* odour associative memories rely heavily on the sparse coding in KCs, behavioural experiments could lead to insights on whether the conditions shown above affect the production and storage of associative memories. Re-creating the experimental conditions mentioned above and testing the *Drosophila*'s odour associative memories through behavioural studies could show whether this system has been disrupted by the acute and constitutive expression of NaChBac.

Another interesting experiment would be to express NaChBac for 4 days, thus increasing odour response, and investigating the levels of Para channel expression with ParaFlpTag. As ParaFlpTag was only investigated with constitutive NaChBac expression, future experiments could express NaChBac only in development and compare Para channel levels to when NaChBac is expressed only in adult life.

Potential experiments could investigate ParaFlpTag levels with CDK5DN and p35. This could answer the question of whether the expression levels of Para changes in response to the lengthening and shortening of the DAIS. For example, based on the results above, when the DAIS is lengthened with p35, the weakening of the odour responses could be due to the Para channels being more spread out across the DAIS. This would lower the possibility of firing and thus lowering the excitation. Therefore, DAIS markers such as ParaFlpTag, could be used to verify the length of the DAIS and also the localisation of Para.

The Lin lab now have collaborators working with us to patch-clamp KCs constitutively and acutely expressing NaChBac. Hopefully, we can get stimulating results that can help towards understanding the underlying mechanisms within the KCs that are contributing to the excitatory changes in the KCs. Patch clamping can help determine electrical parameters that have been changed to accommodate for an increase or decrease in excitation. Thus, electrophysiological results will help towards our understanding of what is happening in the KCs odour responses in response to constitutive and acute expression to NaChBac, respectively.

4 Decreasing endogenous potassium channel expression levels reduces odour responses in Kenyon cells

4.1 Introduction

In Chapter 3, my research revealed that the expression of NaChBac increased the expression levels of endogenous Shaker channels and decreased the expression levels of Para within the distal axon initial segment. Potassium channels, such as Shaker, are responsible for membrane repolarisation and the increase in Shaker expression likely contributes to the reduced activity observed with NaChBac expression. Therefore, it appears that changes in KCs' activity can alter the expression of potassium channels and Chapter 5 investigates the activity levels of KCs when the expression of potassium channels are altered.

As discussed in Chapter 1, potassium channels are ubiquitous in cells and play a critical role in regulating neuronal excitability. Potassium channels can be categorised into three major families based on their structure and function, all of which comprise of a pore-forming domain and a regulatory domain responsible for sensing stimuli (Hille, 2001; Reviewed by Kuang, 2015; Figure 4). The roles of potassium channels within a cell vary due to regulation by their auxiliary subunits (Jiang et al., 2002). In neurons, potassium channels play a critical role in regulating membrane potential. They facilitate potassium ion efflux, contributing to cell hyperpolarisation and repolarisation (Goldman, 1943; Hodgkin and Katz, 1949; Hodgkin and Huxley, 1945; Hodgkin and Huxley, 1952; Carrillo et al., 2015).

Kenyon cells possess multiple types of potassium channels, including Shaker, Shal, Shab, and Shaw (Amin et al., 2020). Shaker and Shal channels conduct A-type potassium currents and contribute to firing rate and action potential duration as they are crucial to facilitating membrane repolarisation (Salkoff and Wyman, 1981; Tanouye and Ferrus, 1985; Butler et al., 1989; Covarrubias et al., 1991; Singh et al., 2006). Shab channels maintain the membrane potential and contribute to spiking rate (Misonou et al., 2004; Park et al., 2006). Shaw potassium channels are slow-activating and conduct non-inactivating K⁺ currents, and they remain open at rest and drive the membrane towards a negative potential (Tsunoda and Salkoff, 1995a). Given this, inhibiting

endogenous potassium channel formation, or overexpressing non-functional versions of potassium channels should result in increased KC activity.

Past literature has provided evidence that modifying the genes of Shaker, Shal, Shab and Shaw can affect the respective currents. The overexpression of mutated Shaker has been demonstrated to elevate activity by increasing the delay in repolarisation (Tanouye et al., 1981). Furthermore, voltage clamp recordings of muscle cells show reduced A-type current with the expression of Shaker mutants (Tanouye and Ferrus, 1985). Manipulating the Shab gene to disrupt Shab currents results in significant impairments in motor-pattern generation (Ueda and Wu, 2006). Additionally, electrophysiological findings indicate that the absence of Shab can enhance both membrane excitability and synaptic transmission, as expected (Ueda and Wu, 2006). Modifying the Shal gene results in the complete elimination of the current from cell bodies, without affecting other currents, which results in a shortened latency to firing and a lower threshold for repetitive firing (Ping et al, 2011). Lastly, the absence of Shaw, through knockdown, increases resting membrane potential and firing rate response shown in whole-cell current-clamp recordings (Parisky et al., 2008) due to a lack of repolarisation current. Hence, the manipulation of Shaker, Shal, Shab, and Shaw genes produces observable outcomes, highlighting their vital roles in modulating cellular currents and, in turn, influencing neuronal excitability and behaviour.

In this chapter, I will be using specific transgenes to lower targeted potassium channel conductance's, such as expressing dysfunctional channel variants. The expression of a Shaker dominant negative transgene (ShakerDN) increases electrical excitability when expressed in *Drosophila* neurons (Mosca et al., 2005; Koon et al., 2010; Imlach et al., 2012). Furthermore, ShakerDN effectively suppresses the type A current and increases spontaneous synaptic release events when expressed (Mosca et al. 2005). A similar increase in excitability (seen with ShakerDN) was observed with the expression of ShakerRNAi, which reduces Shaker expression (Buhl et al., 2016; Smith et al., 2019). Thus, the expression of both dysfunctional and knockdown versions of Shaker increases neuronal excitability in *Drosophila*. Additionally, the expression of Shaw-truncated (an impaired version of Shaw) and ShawRNAi enhances somatic excitability in *Drosophila* making them useful tools for investigating neuronal activity (Hodge et al., 2005; Hodge and Stanewsky, 2008; Smith 2019). Furthermore, the expression of Shal dominant negative (ShalDN) significantly reduces type A current which creates defects

in repetitive firing (Ping et al., 2011; Smith et al., 2019). When expressed in KCs, this reduction impairs a *Drosophila*'s ability to differentiate between similar odours, indicating increased excitability (Groschner et al., 2018). Lastly, the expression of ShabRNAi eliminates the Shab current and increases spontaneous firing rates in some clock neurons, similar to the effects observed when Shab-specific toxins are applied (Smith et al., 2019). Therefore, the research discussed above suggests that reducing potassium channels should increase excitability in Kenyon cells.

In this chapter, I hypothesised that reducing the expression levels or function of potassium channels (using the transgenes outlined above) would increase Kenyon cell excitability. It was anticipated that the increase of activity in KCs would trigger homeostatic responses aimed at restoring the activity back to baseline levels to maintain sparse coding. Furthermore, these homeostatic mechanisms responsible for adjusting the activity levels could potentially involve other ion channels.

4.2 Results

4.2.1 Weakening the expression levels or expressing non-functional potassium channels weaken odour responses of KCs

In Chapter 1, it was discussed that past literature has shown that reducing potassium efflux can increase cell excitability. To investigate this, specific mechanisms to disrupt the endogenous potassium channels were utilised to potentially increase the activity of KCs.

As Shaker was seen to significantly increase its expression levels when NaChBac was constitutively expressed, I started by disrupting the Shaker channels. Shaker potassium channels contribute to the cells rate of firing and the duration of action potentials as they play a crucial role in facilitating membrane repolarisation (Tanouye and Ferrus, 1985; Salkoff and Wyman, 1981). Thus, when expressing ShakerDN (dominant negative, Mosca et al., 2005), a non-functional form of potassium channel, the excitability of the Kenyon cells was expected to increase. Here, jRGECO1a was used, instead of GCaMP6f, to record KC responses, because ShakerDN is tagged with GFP. Additionally, the odours 4-Methylcyclohexanol and 3-Octanol were used to trigger higher odour responses as jRGECO1a has a weaker signal than GCaMP6f. The odour response traces appeared to show that KCs that constitutively express ShakerDN exhibit higher odour responses. A two-way ANOVA showed a significant genotype main effect, i.e. increased average odour responses to both IA and δ D, as well as increased peak odour response to δ D, indicating an overall enhancement in odour responses (Figure 32, 33, 39 and see Appendix B). However, this effect was not as significant as expected, so GAL80^{ts} was used to investigate acute, 4-day adult expression of ShakerDN. This was to see if short expression of ShakerDN had a larger effect. Surprisingly, the results found a significant weakening in average and peak odour responses revealed by the main effect of genotype to both IA and δ D (Figure 32, 33 and see Appendix B). Furthermore, multiple comparisons tests showed that acute ShakerDN expression significantly weakened peak odour responses to IA and δ D in the calyx, and average responses to δ D in the calyx and β lobe (Figure 32, 33 and see Appendix B). Thus, constitutive expression of ShakerDN increases overall odour responses in KCs but acute 4-day adult expression reduces responses.

To verify this effect, another method was used to disrupt Shaker currents, ShakerRNAi, which knockdowns the expression of Shaker (Smith et al., 2019). Constitutive ShakerRNAi expression significantly weakened overall peak odour responses to δ D and average odour responses to both IA and δ D, shown in the main effect of genotype using a two-way ANOVA (Figure 32, 33, 39 and see Appendix B). Additionally, the multiple comparison test indicated significant weakening of the average odour response in the β lobe (Figure 33, 39 and see Appendix B). Acute expression of ShakerRNAi found no significant difference from control (Figure 32, 33, 39 and see Appendix B). Therefore, the results from ShakerDN and ShakerRNAi contradict each other and so I wanted to explore the effects of disrupting other potassium channels too.

Shal potassium channels, which are known to contribute to the membrane potential, postsynaptic potentials, and firing properties of neurons (Diao et al., 2010) were disrupted to examine their role. Shal poreDN (dominant negative), which blocks the pore in Shal channels, was used to disrupt the Shal currents (Smith et al., 2019). Constitutive expression of Shal poreDN did not affect the average odour responses of the KCs revealed by the main effect of genotype from a two-way ANOVA (Figure 34, 35, 39 and see Appendix B). However, multiple comparison tests revealed that the α' lobe peak odour response was significantly weakened (Figure 34 and see Appendix B). Additionally, acute expression of Shal poreDN only significantly increased the overall peak odour responses to IA (see Appendix B). Thus, disrupting Shal channels with constitutive and acute expression of Shal poreDN does not change the average odour response of KCs, but acute expression can increase the peak odour responses to IA.

The effects of disrupting Shab channels with ShabRNAi (Smith et al., 2019) were then investigated. Shab currents are involved in the regulation of action potentials and synaptic transmission through repolarising the membrane (Park et al., 2006). Constitutive ShabRNAi expression significantly weakens the overall peak and average odour responses shown by the main effect of genotype from a two-way ANOVA (Figure 34, 35, 39 and see Appendix B), but 4-day adult expression does not significantly change odour responses (Figure 34, 35, 39 and see Appendix B). Multiple comparisons tests show that ShabRNAi significantly weakens the peak odour responses in the α' and β lobes (Figure 34 and see Appendix B). Thus, it appears that the loss of Shab with constitutive expression of ShabRNAi weakens the odour responses of KCs, but acute ShabRNAi has no significant effect.

Lastly, Shaw potassium channels were disrupted. As described earlier, Shaw helps regulate the resting membrane potential because during rest Shaw potassium channels stay open, driving the potential towards negative voltages to potassium's equilibrium potential (Hodge et al., 2005; Parisky et al., 2008), and so disrupting these channels should increase the activity in the neurons. Shaw-truncated, which has insufficient potassium transport due to the loss of C-terminal targeting signals and mis-folding (Hodge et al., 2005), was used to disrupt Shaw currents in KCs. Constitutive expression of Shaw-Truncated significantly increased the peak odour response in the β lobe to δ D (shown by a multiple comparison test; Figure 36 and see Appendix B) but did not have a significant main effect of genotype. Additionally, 4-day acute adult expression of Shaw-truncated significantly weakened average (but not peak) overall odour responses to IA (but not δ D) (Figure 36, 37, 39 and see Appendix B). Unusually, the multiple comparison test shows that the calyx significantly decreased average odour response to IA but the α' significantly increased its average odour response to δ D. The results show that constitutive expression of Shaw-truncated has no overall significant effect on KC odour response but acute expression of Shaw-truncated overall decreases the odour responses of KCs.

Another method to reduce Shaw currents is through the expression of ShawRNAi (Hodge and Stanewsky, 2008). When ShawRNAi was constitutively expressed in KCs, their peak and average odour responses were significantly weakened, shown by the main effect of genotype (Figure 36, 37, 39 and see Appendix B). Furthermore, multiple comparison tests showed that the β' lobes had significantly weaker peak and average odour responses to IA and DD. However, acute expression of ShawRNAi did not significantly affect the overall peak or average odour responses of the KCs (Figure 36, 37, 39 and see Appendix B). Thus, constitutive expression of ShawRNAi weakens odour responses but acute expression does not alter odour responses.

Overall, only constitutive expression of ShakerDN significantly increased odour responses, thus suggesting an increase of activity (Figure 39 and see Appendix B). The other conditions showed weakening of odour responses and thus weakened activity (Figure 39 and see Appendix B). Therefore, the results suggest that disrupting most potassium channels individually, both acutely and constitutively, decreases the activity of KCs. Figure 39 shows that disrupting the potassium constitutively had a greater effect on the average odour responses to IA than acute expression. Further studies are

needed to elucidate the precise mechanisms by which potassium channels influence KC activity and to explore their potential homeostatic applications.

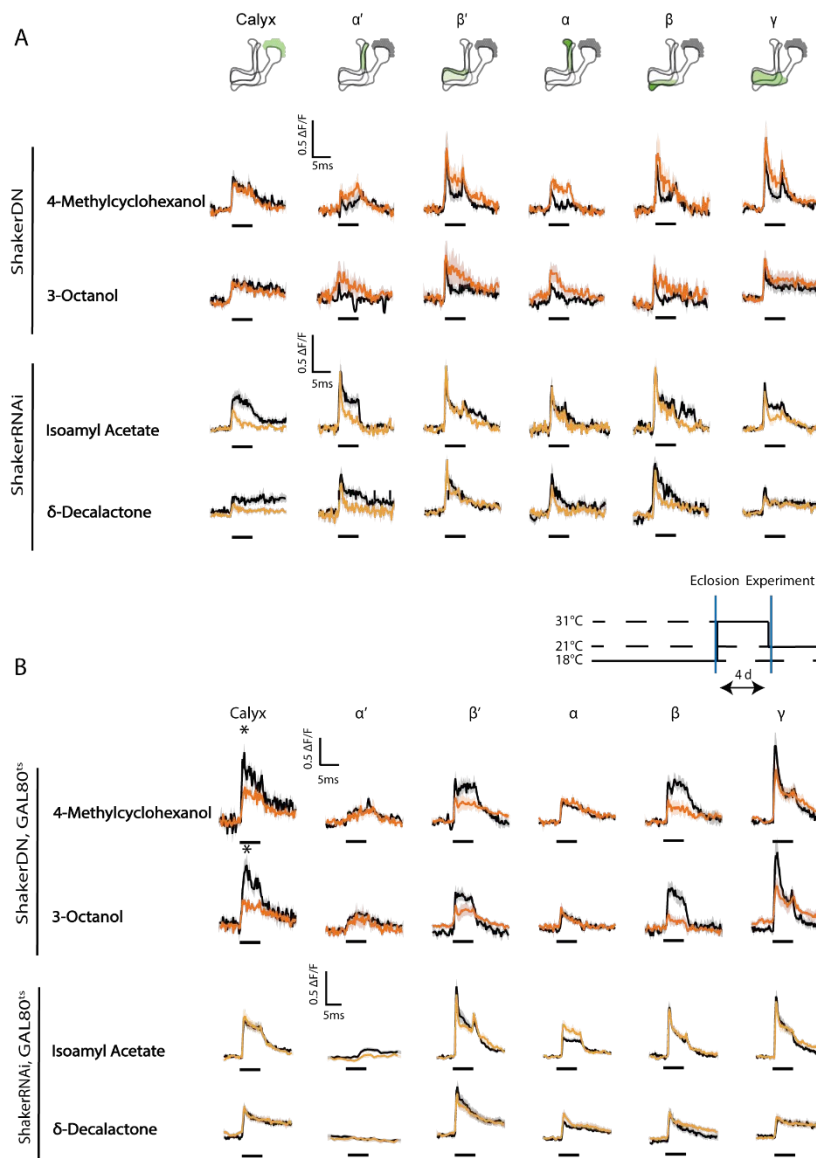


Figure 32 ShakerDN and ShakerRNAi expression appear to have opposing effects on KC odour responses.

(A) Fly genotypes: Control = R13F02GAL4>GCaMP6f. ShakerDN= R13F02GAL4>GCaMP6f, ShakerDN. ShakerRNAi = R13F02GAL4>GCaMP6f, ShakerRNAi. For ShakerDN the top panel are odour responses to 4-methylcyclohexanol. The bottom panel of ShakerDN are odour responses to 3-octanol. For ShakerRNAi the top panel are odour responses to isoamyl acetate. The bottom panel of ShakerRNAi are odour responses to delta decalactone. Black line = Control. Dark orange = ShakerDN. Light Orange = ShakerRNAi.

(B) Fly genotypes: Control = R13F02GAL4>GCaMP6f, GAL80^{ts}. ShakerDN= R13F02GAL4>GCaMP6f, GAL80^{ts}, ShakerDN. ShakerRNAi = R13F02GAL4>GCaMP6f, GAL80^{ts}, ShakerRNAi. Diagram shows temperature procedure to activate GAL80^{ts}. ShakerDN and ShakerRNAi have no impact on odour responses. For ShakerDN the top panel are odour responses to 4-methylcyclohexanol. The bottom panel of ShakerDN are odour responses to 3-octanol. For ShakerRNAi the top panel are odour responses to isoamyl acetate. The bottom panel of ShakerRNAi are odour responses to delta decalactone. Black line = Control. Dark orange = ShakerDN, GAL80^{ts}. Light Orange = ShakerRNAi, GAL80^{ts}.

(A-B) Black bar = odour presentation. * = peak odour response is $p < 0.05$, two-way ANOVA with Šidák multiple comparisons test. Age past eclosion = 3-4 days.

Average odour responses can be found in Figure 33. For detailed statistics, please see the table in Appendix B.

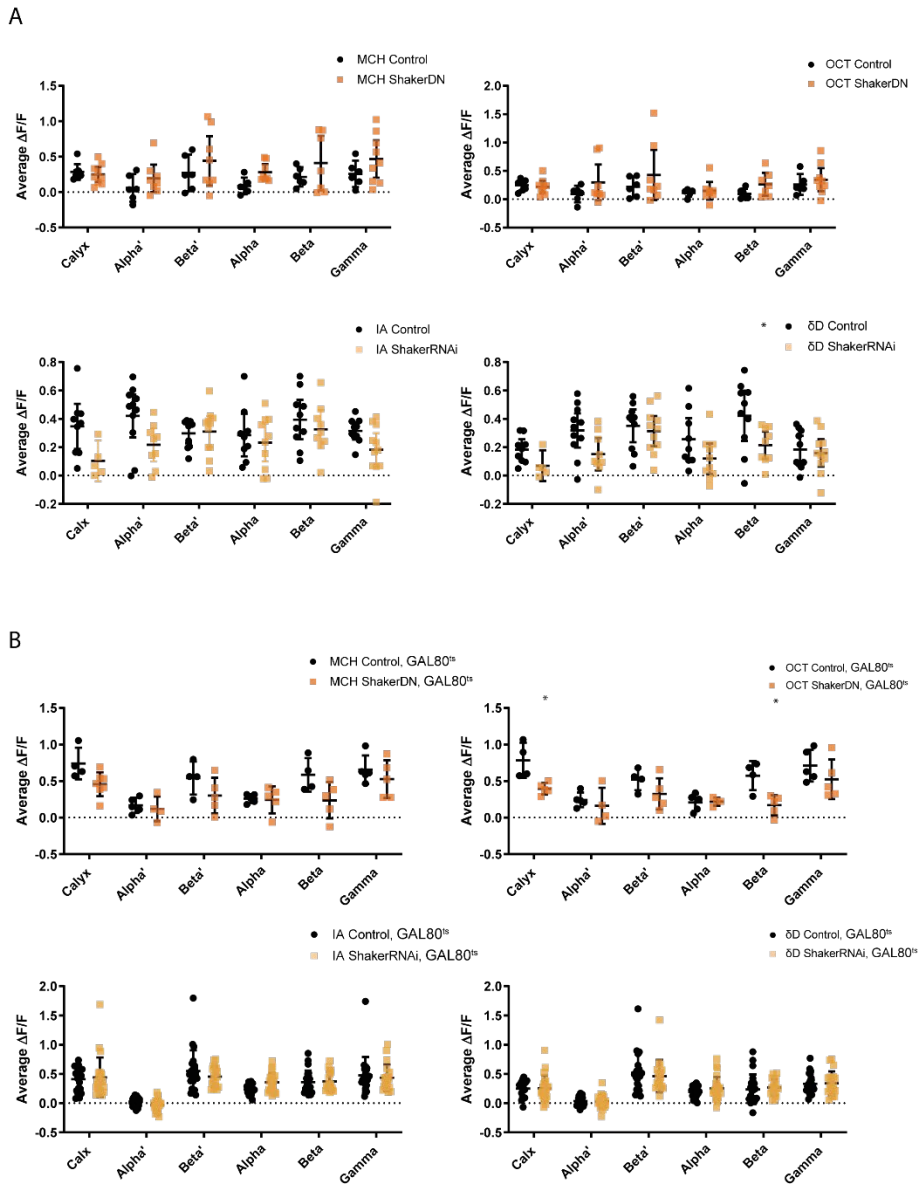


Figure 33 Quantification of the average odour responses from Figure 32.

(A) Top panels: Graphs of the average odour responses in each lobe with 4-methylcyohexanol and 3-octanol for ShakerDN flies compared to controls. Bottom panels: Graphs of the average odour responses in each lobe with isoamyl acetate and δ -Decalactone for ShakerRNAi flies compared to controls. (B) Graph of the average odour responses in each lobe with 4-methylcyohexanol and 3-octanol for ShakerDN, GAL80ts flies compared to controls. Bottom panels: Graph of the average odour responses in each lobe with isoamyl acetate and δ -Decalactone for ShakerRNAi, GAL80ts flies compared to controls.

(A-B) Black = Control. Coloured = Experimental condition labelled in keys. * = peak odour response is $p < 0.05$, two-way ANOVA with Šidák multiple comparisons test. 95% confidence interval error bars. Age past eclosion = 3-4 days.

For detailed statistics, please see the table in Appendix B.

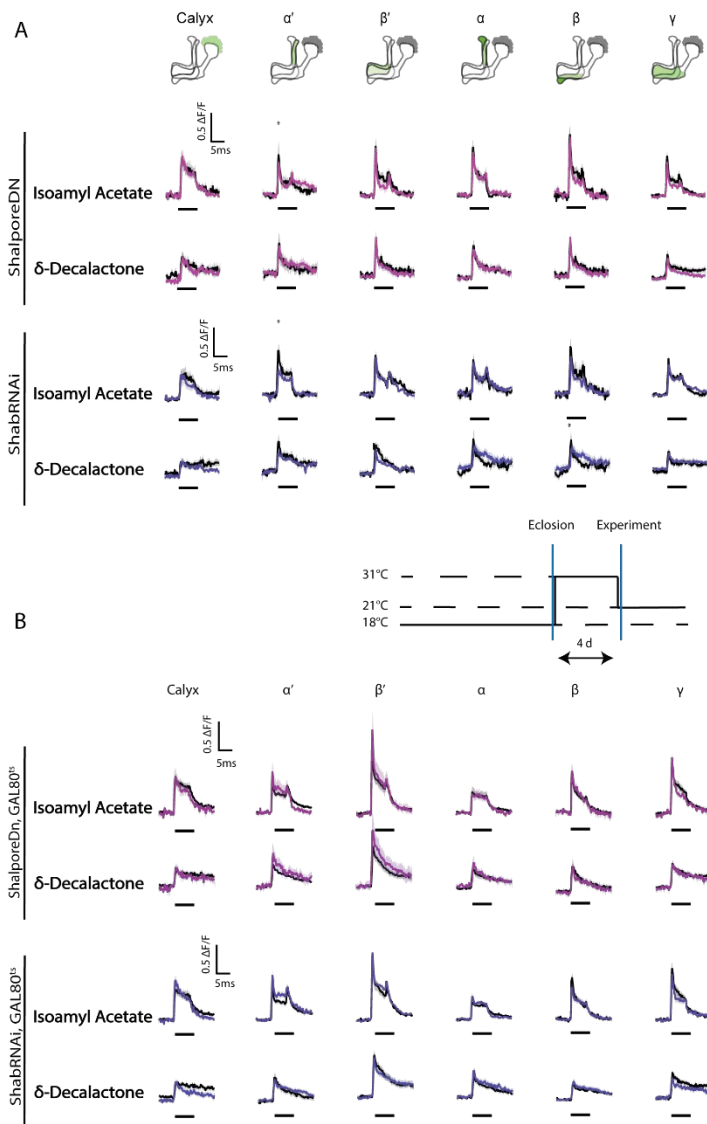


Figure 34 ShalPoreDN and ShabRNAi expression in KCs appears to weaken odour responses.

(A) Fly genotypes: Control = R13F02GAL4>GCaMP6f. ShalPoreDN= R13F02GAL4>GCaMP6f, ShalPoreDN. ShabRNAi = R13F02GAL4>GCaMP6f, ShabRNAi. Diagram highlights the area for each lobe. For both ShalPoreDN and ShabRNAi the top panel are odour responses to isoamyl acetate. The bottom panel of each fly line are odour responses to δ-Decalactone. Black = Control. Magenta = ShalPoreDN. Purple = ShabRNAi.

(B) Fly genotypes: Control = R13F02GAL4>GCaMP6f, GAL80^{ts}. ShalPoreDN= R13F02GAL4>GCaMP6f, GAL80^{ts}, ShalPoreDN. ShabRNAi = R13F02GAL4>GCaMP6f, GAL80^{ts}, ShabRNAi. Diagram shows temperature procedure to activate GAL80^{ts}. For both ShalPoreDN, GAL80^{ts} and ShabRNAi, GAL80^{ts} the top panel are odour responses to isoamyl acetate. The bottom panel of each fly line are odour responses to δ-Decalactone Black = Control. Magenta = ShalPoreDN, GAL80^{ts}. Purple = ShabRNAi, GAL80^{ts}.

(A-B) Black bar = odour presentation. * = peak odour response is $p < 0.05$, two-way ANOVA with Šidák multiple comparisons test. Age past eclosion = 3-4 days.

Average odour responses can be found in Figure 35. For detailed statistics, please see the table in Appendix B.

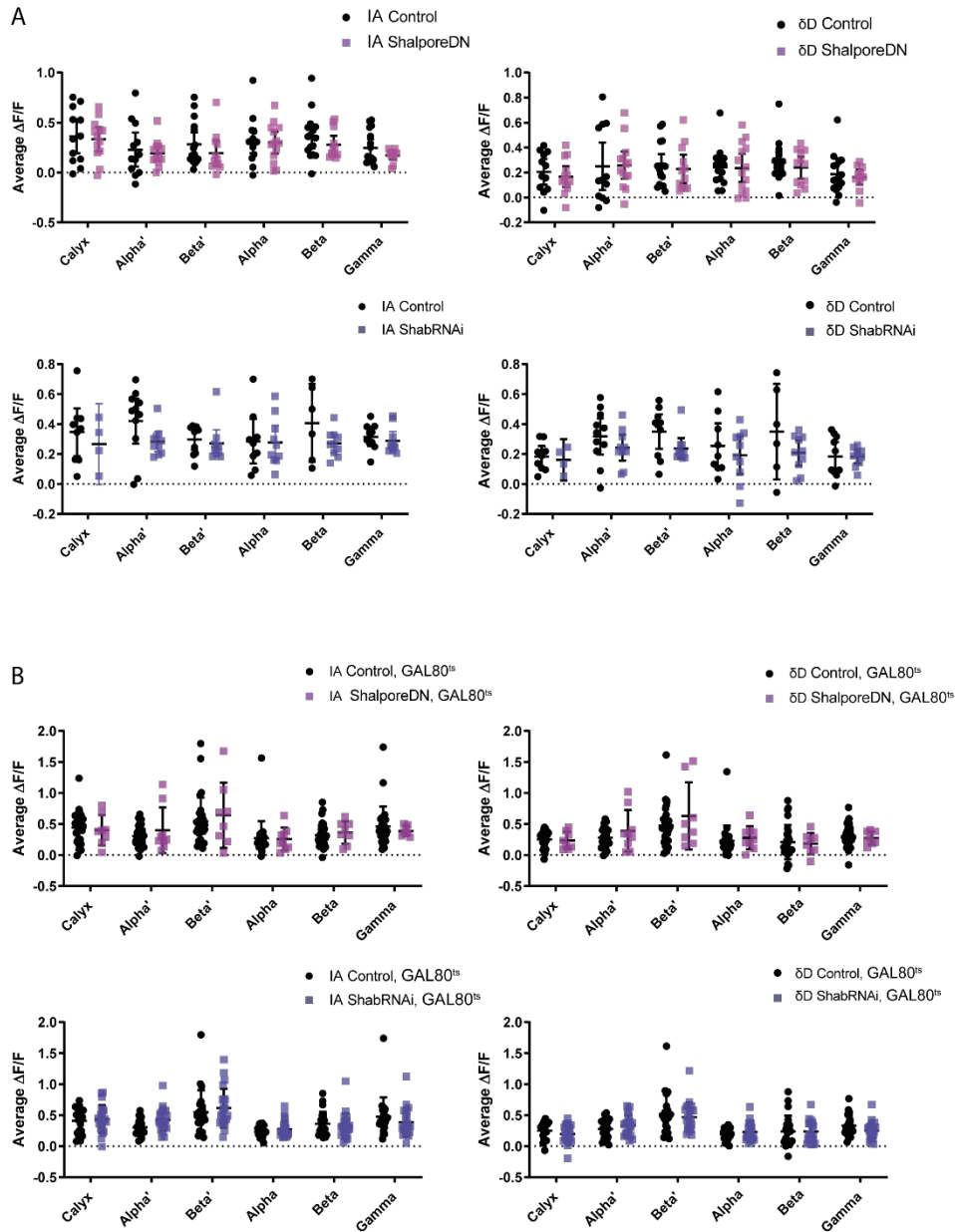


Figure 35 Quantification of the average odour responses from Figure 34.

(A) Top panels: Graphs of the average odour responses in each lobe with isoamyl acetate and δ -Decalactone for ShalpoleDN flies compared to controls. Bottom panels: Graphs of the average odour responses in each lobe with isoamyl acetate and δ -Decalactone for ShabRNAi flies compared to controls. (B) Graph of the average odour responses in each lobe with isoamyl acetate and δ -Decalactone for ShalpoleDN, GAL80ts flies compared to controls. Bottom panels: Graph of the average odour responses in each lobe with isoamyl acetate and δ -Decalactone for ShabRNAi, GAL80ts flies compared to controls.

(A-B) Black = Control. Coloured = Experimental condition labelled in keys. * = peak odour response is $p < 0.05$, two-way ANOVA with Šidák multiple comparisons test. 95% confidence interval error bars. Age past eclosion = 3-4 days.

For detailed statistics, please see the table in Appendix B.

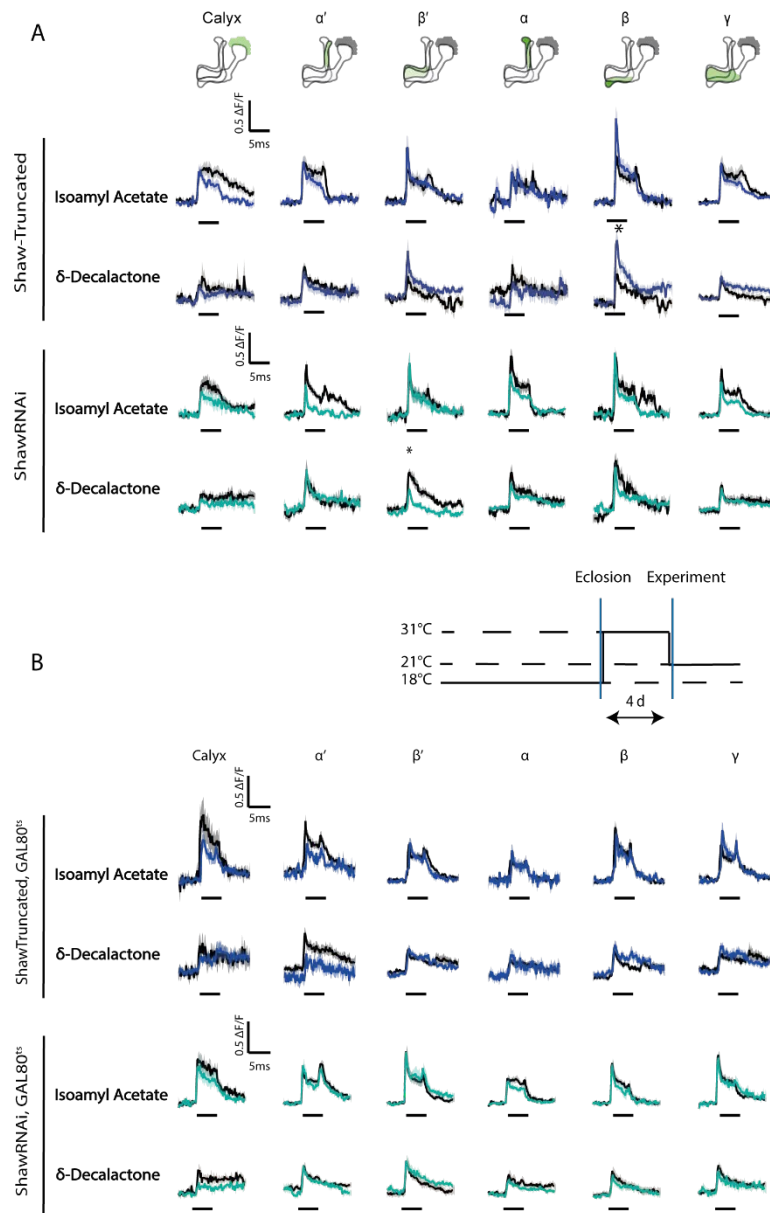


Figure 36 Expression of Shaw-Truncated and Shaw-RNAi mostly weaken odour responses in KCs.

(A) Fly genotypes: Control = R13F02GAL4>GCaMP6f. ShawTruncated = R13F02GAL4>GCaMP6f, ShawTruncated. Shaw-RNAi = R13F02GAL4>GCaMP6f, Shaw-RNAi. Diagram represents each lobe ROI. For both Shaw-Truncated and Shaw-RNAi the top panel are odour responses to isoamyl acetate. The bottom panel of each fly line are odour responses to δ -Decalactone. Black = control. Dark blue = ShawTruncated. Light blue = Shaw-RNAi.

(B) Fly genotypes: Control = R13F02 GAL4>GCaMP6f, GAL80^{ts}. ShawTruncated, GAL80^{ts} = R13F02GAL4>GCaMP6f, GAL80^{ts}, ShawTruncated. Shaw-RNAi, GAL80^{ts} = R13F02GAL4>GCaMP6f, GAL80^{ts}, Shaw-RNAi. Diagram shows temperature procedure to activate GAL80ts. For both conditions the top panel are odour responses to isoamyl acetate and the bottom panels of each condition are odour responses to δ -Decalactone. Black = Control. Dark blue = ShawTruncated, GAL80^{ts}. Light blue = Shaw-RNAi, GAL80^{ts}.

(A-B) Black = control. Black bar = odour presentation. * = peak odour response is $p < 0.05$, two-way ANOVA with Šidák multiple comparisons test. Age past eclosion = 3-4 days.

Average odour responses can be found in Figure 37. For detailed statistics, please see the table in Appendix B.

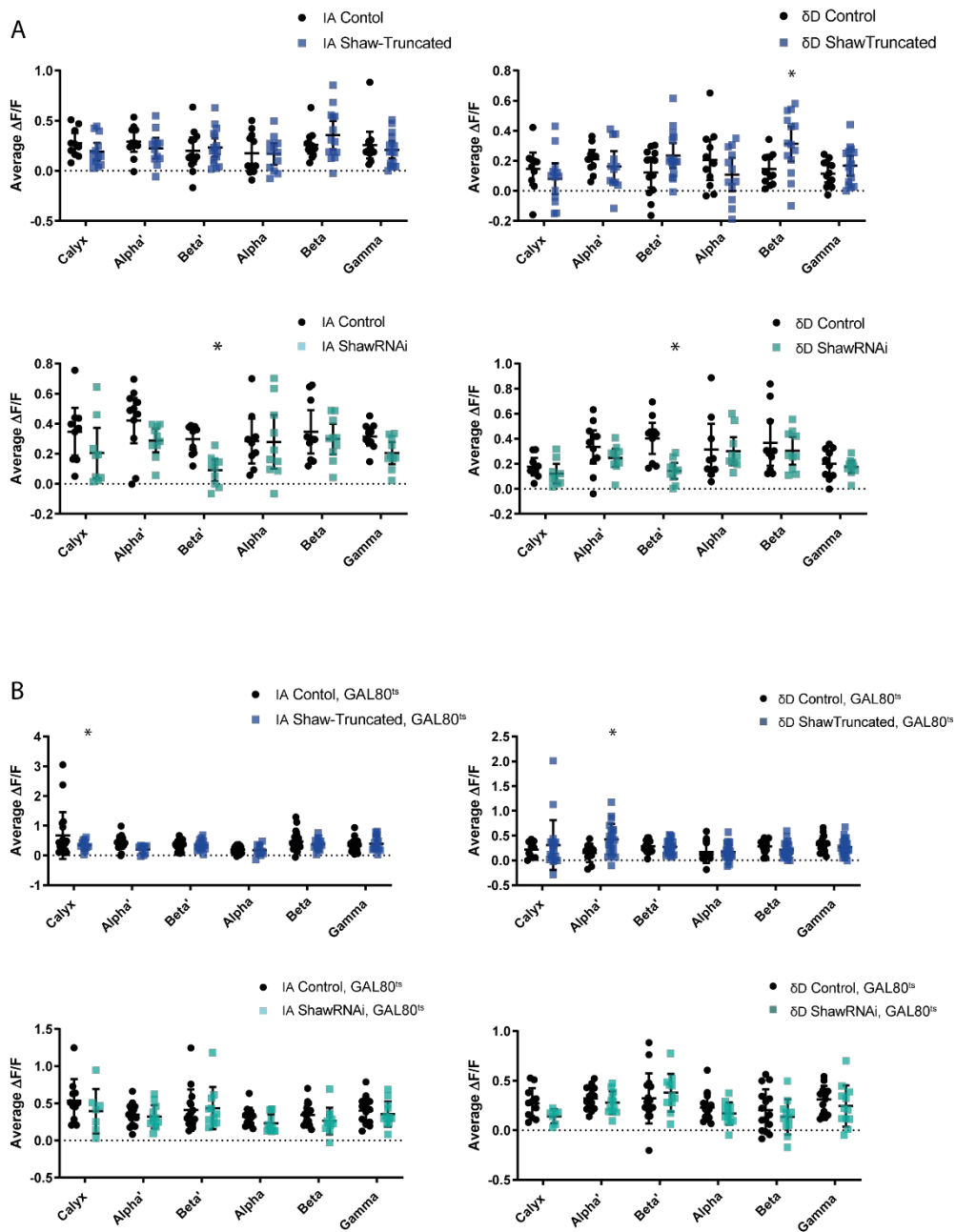


Figure 37 Quantification of the average odour responses from Figure 36.

(A) Top panels: Graphs of the average odour responses in each lobe with isoamyl acetate and δ -Decalactone for Shaw-Truncated flies compared to controls. Bottom panels: Graphs of the average odour responses in each lobe with isoamyl acetate and δ -Decalactone for ShawRNAi flies compared to controls. (B) Graph of the average odour responses in each lobe with isoamyl acetate and δ -Decalactone for Shaw-Truncated, GAL80^{ts} flies compared to controls. Bottom panels: Graph of the average odour responses in each lobe with isoamyl acetate and δ -Decalactone for ShawRNAi, GAL80^{ts} flies compared to controls.

Black = Control. Coloured = Experimental condition labelled in keys. * = peak odour response is p < 0.05, two-way ANOVA with Sidák multiple comparisons test. 95% confidence interval error bars. Age past eclosion = 3-4 days.

For detailed statistics, please see the table in Appendix B.

4.2.2 Increasing Shaw channel expression weakens odour responses in KCs

Disrupting KC potassium channels produced unexpected odour responses which led to investigating the odour responses when increasing potassium channels. Would increasing the potassium channels result in paradoxical or predictable outcomes? Experiments using Shaw-Truncated and ShawRNAi both weakened odour responses so ShawWT (wild type; Hodge et al., 2005) was overexpressed to investigate increasing Shaw potassium channels. Expectedly, the main effect of genotype from the 2-way ANOVA showed that overexpression of ShawWT significantly lowered both peak and average odour responses to IA and δ D (Figure 38, 39 and see Appendix B). Furthermore, multiple comparison tests showed that the α' and β' lobes had significantly lower odour responses to IA and the α' lobe showed significantly weaker odour responses to δ D (Figure 38, 39 and see Appendix B). These results along with Shaw-truncated and ShawRNAi expression suggests that both increasing and decreasing Shaw channel expression leads to a decrease in KC odour responses.

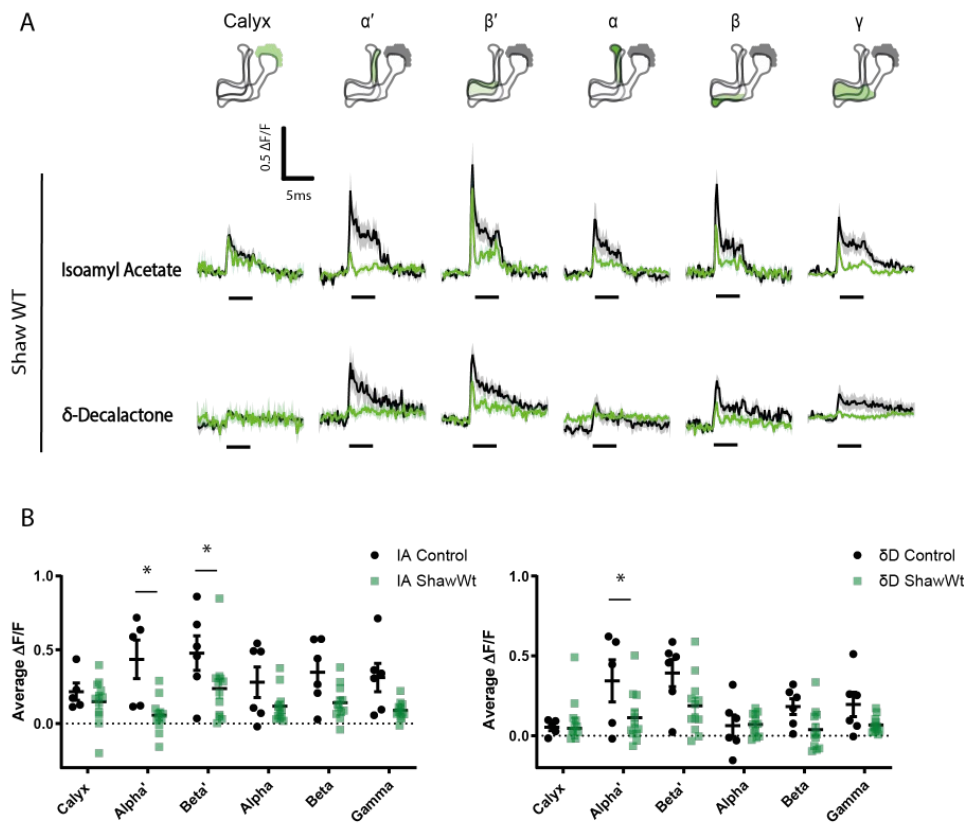


Figure 38 ShawWT expression in KCs weakens their odour responses.

Fly genotypes: Control = R13F02Gal4>GCaMP6f. ShawWT= R13F02Gal4>GCaMP6f, ShawWT. (A) The top panel are odour responses to isoamyl acetate. The bottom panel is odour responses to δ -Decalactone. Black = Control. Green= ShawWT. Black bar = 5 s odour presentation. * = peak odour response is $p < 0.05$, two-way ANOVA with Šidák multiple comparisons test. (B) Graph of the average odour response in each lobe with isoamyl acetate and δ -Decalactone for ShawWT. * = average odour response is $p < 0.05$, two-way ANOVA with Šidák multiple comparisons test. Black = Control. Green= ShawWT. (A-B) Age past eclosion = 3-4 days.

For detailed statistics, please see the table in Appendix B.

4.2.3 Summary of Chapter 4 results in Kenyon cells

Figure 39 presents a summary of all the conditions in Chapter 4, displaying the mean difference between experimental and control conditions for the average odour response to isoamyl acetate. The summary reveals that ShakerDN is the only condition that significantly increases the average odour response to IA and that other potassium channel disruptors weaken odour responses. These results suggest that potassium channel disruptors in KCs weaken activity. This is a surprising result as past literature (discussed in Chapter 1) usually shows potassium channel disruptors to increase activity and excitability in neurons.

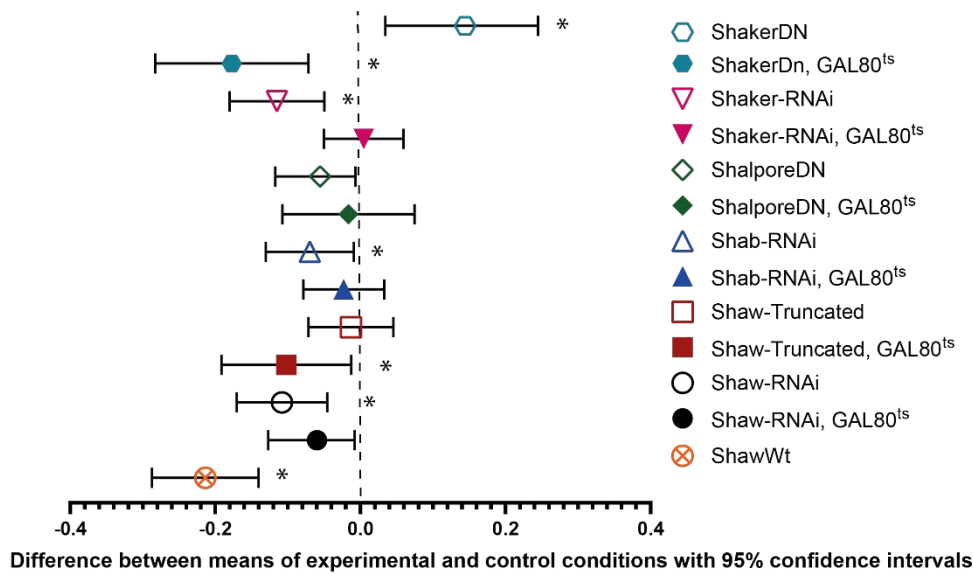


Figure 39 Summary of Chapter 4 results using average odour responses to Isoamyl Acetate

The figure shows the difference between predicted means of control and experimental for the average of odour response for each condition. The data is from the combination of odour responses from all lobes in response to isoamyl acetate only. * = $p < 0.05$, main effect of genotype in two-way ANOVA. Mean difference \pm 95% confidence interval.

For detailed statistics, please see the table in Appendix B.

4.3 Discussion

4.3.1 Potassium channel disruption weakens the excitation of KCs

Paradoxically results from Chapter 3 showed that the constitutive expression of NaChBac decrease KC activity. To investigate if reducing or disrupting specific potassium channels could increase KC activity, I utilised genetic techniques to disrupt the endogenous potassium channels. Surprisingly, most conditions decreased the overall odour responses of the KCs (Figure 39), suggesting that KC activity was lowered. Theoretically, the disruption of potassium channels should lead to a reduction in potassium currents and thus a lack of hyperpolarising currents. Past literature has shown that combining potassium channel disruptors, such as RNAis or dominant negative strategies, with GAL4/UAS allows for temporal and spatial control of disrupted channels and creates hyperexcitability in neurons and neural circuits (Peabody et al., 2008; Peabody et al., 2009; Gordon and Scott, 2009). Despite testing both constitutive and acute expression of various potassium disruptors and reducers, this project found that they did not lead to a significant increase in KCs activity.

Disrupting Shaw channels, using constitutive expression of ShawRNAi and 4-day acute expression of Shaw-truncated significantly weakened odour responses. Shaw channels are slow activating and conduct non-inactivating K⁺ current (Tsunoda and Salkoff, 1995a); they stay open during resting membrane potential and thus, in past literature, the disruption of the Shaw channels in *Drosophila* has been shown to cause hyperexcitability (Hodge et al, 2005). The general weakening of odour responses seen when Shaw RNAi was expressed constitutively (Figure 39) stands in contrast to previous findings that expressing Shaw RNAi in lateral ventral neurons of *Drosophila* made the cells hyperexcitable (Hodge and Stanewsky, 2008). There may be multiple reasons why these results were seen. Possibly, the RNAi does not work on the correct channel, or the Shaw-truncated fly line produces channels that are not altered. Alternatively, the disruption of the Shaw channels has triggered mechanisms to overcompensate for the loss of potassium current causing hypoactivity.

The expression of ShalDn did not significantly alter the odour responses of KCs. Shal channels are localised in both cell bodies and dendrites of neurons in *Drosophila* and are the main determinants of dendritic excitability by repolarising the membrane

potential (Diao et al., 2010). Shal channels activate at significantly more negative voltages than other potassium channels and their inactivation is mostly independent of voltage. They activate at these voltages to control frequency of firing through negative potentials (Ping et al., 2011). Thus, disrupting Shal channels should increase excitation, but both constitutive and acute expression of ShalPoreDN had no overall effect on odour response (Figure 39). This suggests that KC excitability is not affected by the expression of ShalPoreDN. Shal is more concentrated in the dendrites of neurons and so should have a major role in the excitability, however, the levels of ShalPoreDN may be too low for this dominant negative strategy to have an effect. Alternatively, other potassium channels may have a greater role in regulation than Shal. MacLean *et al.*, (2003) artificially elevated the transient A current with Shal (lobster version of Shal) overexpression in lobsters and found that there is a compensatory upregulation of I_h (hyperpolarization-activated inward current). Therefore, different versions of Shal are able to trigger activation of other currents to compensate for their change. This could be a possible reason as to why there is no significant difference in odour responses with ShalPoreDN expression. The expression of ShalPoreDN may trigger the increase of expression from other channels to compensate for its effects. However, as that study overexpressed Shal and in my project I overexpressed a non-function version of Shal, it might be that dysregulation of Shal may not produce the same effect. Additionally, MacLean et al., (2003) used the lobster version of Shal which may trigger different mechanisms to a *Drosophila* specific version.

Constitutive or acute expression of ShabRNAi did not change the overall odour responses (Figure 39) but did trigger significant reductions in the γ and β' lobes. Shab channels are involved in the regulation of action potentials and synaptic transmission of neurons by repolarising the membrane (Singh and Singh, 1999; Tsunoda and Salkoff, 1995b; Ueda and Wu, 2006). Thus, my findings again contradict the literature, as blocking these currents should logically increase excitability (Peng and Wu, 2007; Vähäsöyrinki et al., 2006). Possibly, ShabRNAi expression is not as potent as expected and so isn't strong enough to create an effect. However, it has been verified that ShabRNAi abolishes the effect of an anti-Shab toxin (guangxitoxin-1E) on K^+ currents (Smith and Hodge, 2019).

Among the potassium channel disruptors tested, only ShakerDN exhibited overexcitation when expressed constitutively. However, the opposite was seen when

expressed acutely (Figure 39). In past literature, Shaker expression in *Drosophila* has been shown to not induce homeostatic effects as Shaker EKO, expressed to increase the K⁺ current, hyperpolarised the resting membrane potential and reduced firing. These changes were partially reversed by the Shaker channel blocker 4-AP, but no homeostatic changes were seen (White et al., 2001). As Shaker was the first potassium channel to be discovered, it has been used in for studies for many years for investigating over and under expression of potassium currents. In mammals there are 8 types of Shaker, in mice, loss of function of Kv1.1 channels severely affects neuronal communication and creates hyperexcitation in the nociceptive neurons leading to seizures (Clark and Tempel, 1998; Rho et al., 1999). In humans, the malfunction of KV1.1 can cause episodic ataxia type 1, which causes uncoordinated movements for varying durations of time (Browne et al., 1994; Lee et al., 2004). Thus, ShakerDN does have the expected results. However, as the other potassium channel disruptors decreased activity, this result does not reflect what normally happens when potassium channels are disrupted or reduced. In contrary to ShakerDN's results, when investigating ShakerRNAi, the results showed a significant overall weakening of the odour responses. Past literature has shown that the inhibition of ShakerRNAi in dorsal fan-shaped body neurons (*in Drosophila*) resulted in reduced activity. This decrease in activity occurred because Shaker plays a critical role in repetitive firing by facilitating membrane repolarization, which is necessary to remove the inactivation block on Na⁺ channels (Pimentel et al., 2016). Using electrophysiological results, Pimentel et al., (2016) suggest that other potassium channels are expressed to replace the principle hyperpolarising force due to slow inactivation kinetics replacing the fast-inactivating Shaker kinetics. Thus, reducing Shaker through RNAi methods may promote the expression of other potassium channels, but ShakerDN methods does not.

Although potassium channel disruptors are useful for determining basic functioning, they can be limited in terms of their spatial and temporal control as the channels are typically broadly expressed. When disruption happens in development this could induce compensatory changes in other channels to equalise the excitability change. For example, HCN1 knock-out mice (channels that underlie *I_h* currents) have a reduction in *I_h* channels which leads to a decrease in synaptic summation (Chen et al., 2010). But there was an unexpected observation, as the decrease in *I_h* channels triggered an increase in GABA_A currents, thought to be due to an increase in $\alpha 5$ subunit.

Furthermore, when tonic GABAA currents were blocked with bicuculline, synaptic summation was enhanced to a greater extent in the knock-out mice compared to the wild-type mice. This suggests that the compensatory upregulation of $\alpha 5$ subunit-mediated GABAA receptor tonic current quantitatively compensates for the loss of dendritic Ih, maintaining normal synaptic summation in the knock-out mice (Chen et al., 2010). Another example of how potassium channels can counterbalance alterations in activity levels is demonstrated when mouse GABAA subunits, responsible for mediating Cl⁻ currents essential for tonic inhibition of granule cells, are knocked out. This event triggers an up-regulation of TASK-1 K⁺ channels, ultimately preserving the excitability properties of the cells (Brickley et al., 2001). Thus, overexcitation may not have been seen in the results of this project because another potassium channel may have been upregulated to lower the excitation in the KCs to maintain the delicate excitability for sparse coding. Thus, future experiments could investigate the developmental expression of other channels when expressing these potassium channel disruptors to assess whether they produce homeostatic compensation.

KCs may have mechanisms that bias their activity towards hypoactivity rather than hyperactivity. As mentioned before, hypoactivity is better for sparse coding than hyperactivity. Thus, for the cells to remain as active as one another and that one subset is not more active than another, hypoactivity is favoured to maintain sparse coding. Thus, KCs may have fast mechanisms, which cannot be seen here, that ensure that they always achieve under excitation, like the loss of Para seen with NaChBac expression.

However, we must consider the more straightforward possibilities for why there was no change with some of the potassium channel disruptors. Possibly, the RNAi and DN variants don't work, but the studies they originated from had shown significant effects on potassium conductance. The results seen could be due to the driver being weak and so doesn't produce the expected expression levels, however, the same driver was used with NaChBac and produced effects. Or the genes themselves do not fully disrupt the functioning or expression. Therefore, other drivers could be used in the future to validate the effects of these channel disruptors or assess protein levels of the channels. Possibly the reason there was no significant change is due to the KCs not being affected by the loss of these channels.

4.3.2 Future work

To gain a better understanding of the puzzling results obtained from this chapter, further research should be conducted. One potential approach is to utilise GAL80^{ts} and create shorter acute expression, as this could provide insight into the short-term disruption of potassium channels and their roles.

Also, previous literature has demonstrated that ion channels can change expression levels to compensate for disruptions in other channels. Thus, using ShFlpTag, EagFlpTag and IhFlpTag from Chapter 3 could determine whether the levels of these channel change in response to the potassium channel disruptors mentioned above.

Chapter 5: General Discussion

5.1 Summary of findings

This project aimed to investigate whether KCs have homeostatic plasticity mechanisms that can help maintain their sparse coding for odour associative memories. I have found one method of homeostatic regulation within the KCs via changing the levels of the ion channels that contribute to the excitability of the cell.

Constitutive expression of ion channels and ion channel disruptors, that in theory should excite KCs, either weakened or had no effect on KC odour responses. My findings showed that when NaChBac, an exogenous sodium channel, was expressed in all KC subtypes (no matter the temperature) it significantly weakened the odour responses. KC odour responses were also significantly weakened when NaChBac was expressed in pupal at varying stages and for 2 days in adults. However, acutely expressing NaChBac for 4 days after eclosion lead to significantly higher odour responses in the β' lobe but the responses returned to control levels after 8 days of adult NaChBac expression.

Using GFP to tag Para channels, I found that constitutive expression of NaChBac decreased the endogenous levels of Para sodium channel in the peduncle. A reduction of para in the peduncle, where the distal axon initial segment is located, is likely a contributing factor to why the KCs have significantly weaker odour responses. A lower level of sodium channel expression likely means that there is a lower chance of action potential firing. However, altering the levels of Para channel (using paraRNAi and paraFlpStop) did not replicate the outcomes observed with NaChBac. Thus, changes in the excitability of KCs could not solely be attributed to modifications in Para channel expression.

GFP-tagged Shaker channel expression was significantly higher in KCs when NaChBac was simultaneous and constitutively expressed. As Shaker is responsible for the repolarisation of the membrane, a higher level of Shaker means that the membrane is closer to the potassium equilibrium and thus harder to depolarise for action potentials. Thus, constitutive expression of NaChBac likely elicits homeostatic changes in Shaker to maintain stability of KC activity.

Surprisingly, disrupting potassium channels, acutely or constitutively, had very little effect on increasing the odour responses in KCs. This suggests that the loss of potassium channels in KCs has very little effect on excitation. This may be due to other potassium channels counteracting the loss of the disrupted potassium channel.

The following sections will discuss the implications of these findings, how the methodology could be improved and what future work could be conducted to expand on the findings.

5.2 Contributions to neuronal excitability and homeostasis

Our cerebral cortex is composed of highly unstable networks, yet disorders related to hyperexcitability are rare, such as epilepsy that only affects ~1-2% of the population. Tiny changes can affect the balance in these networks, disrupting the fragile balance between excitation and inhibition. Our brains can maintain a stable functioning despite all the daily influences that can perturb the balance, such as changes in synapse numbers or strength which is induced by learning and development. To maintain stability, networks as well as individual neurons employ an array of feedback mechanisms to adjust their excitability (Turrigiano and Nelson, 2004; Marder and Goaillard, 2006; Liu and Davis, 2009).

To trigger homeostatic plasticity, the network or neurons need to sense changes in activity levels. Typically, the activity causes the system to deviate from a set range and activate adjustments to alter neuronal excitability back towards this target range. When comparing individual cells and networks, in theory, if an individual neuron stabilises their own excitability, this contributes to the overall network stability. However, this depends heavily on network architecture and function. As described in the main introduction there are many possible methods for neurons to attain homeostasis regarding activity levels and maintenance of neuronal stability happens throughout species. For example, even in Zebrafish weakening electrical activity when the CNS is developing is sufficient enough to evoke homeostatic changes in glutamatergic and GABAergic neurons (Borodinsky et al., 2004). In this project I chose *Drosophila* as they make a good experimental model due to their size, genetics, and fewer interconnected networks.

The results from Chapter 3 show that KCs are able to significantly alter the level of Para and Shaker channels in response to exogenous NaChBac expression. NaChBac channels allow the influx of positive sodium ions. As discussed earlier, overexpressing NaChBac in neurons typically increases the excitability of neurons because the channels open at a more negative potential and high levels of sodium channels means that depolarisation of the membrane can occur faster (Lin et al. 2010; Kelsch *et al.*, 2009; Sheeba *et al.*, 2008). However, the results showed significant weakening in the odour responses in KCs. These results show that KCs are unlikely to have the same electrical components that other *Drosophila* neurons have. Furthermore, KCs also do not have the same mechanisms of compensation as other neurons within the animal. This is also shown with dysregulation of potassium channels as they fail to excite KCs too. Future investigation of KCs mechanisms should be done to understand how KCs differ from the typical neuron, both in *Drosophila* and in other experimental models.

However, similar to other neurons in past literature, discussed above, my results show that KCs use ion channels to regulate their activity. Constitutive NaChBac expression either directly or indirectly triggers Shaker upregulation and Para downregulation. But this leads to significant weakening of the odour responses, thus overexpressing and under-expressing Para and Shaker does not regulate the KCs back to baseline activity. In mice, cerebellar Purkinje neurons have a robust all-or-nothing burst firing (Swensen and Bean, 2005). When given tetrodotoxin (which blocks sodium currents contributing to firing), burst firing continued due to a feedback mechanism which changed the waveform. There was a reduced spike height and a hyperpolarizing shift in postspike voltage from decreased voltage-dependent potassium current and calcium-activated potassium current which allowed normal firing to be maintained (Swensen and Bean, 2005). Thus, the change in sodium channels triggered a response in the potassium channels which was also seen in this project. Furthermore, genetic methods of constitutively reducing sodium currents with Nav1.6^{-/-} mice saw an upregulation of both T-type and P-type calcium current (Swensen and Bean, 2005). Thus, they have shown that there are both acute and long-term feedback mechanisms to maintain functioning after a reduction of sodium currents. Therefore, similar to KCs, those cells use other ion channels to maintain neuronal stability.

One important concept to establish is whether the KCs are reacting to NaChBac because of the protein levels or changes in activity, i.e. whether the compensation is

activity-dependent or activity-independent. In lobsters, when the lobster variant of Shal RNA is injected into neurons they react by increasing the transient IA current (MacClean et al., 2003). This increase is also accompanied by a compensatory increase in hyperpolarisation activated Ih cation current to maintain neuronal firing. Non-conducting Shal also induced the same behaviour. Thus, suggesting the compensation is based on protein levels, not the current change. However, there was no compensatory effect when Ih was increased first (MacClean et al., 2003). Therefore, KCs may be reacting the protein levels of NaChBac rather than their electrical properties. NaChBac may not result in larger sodium currents in KCs, the KCs appear to overexpress Shaker and under express Para based on NaChBac's protein levels. Thus, the KCs have possibly incorrectly adjusted to protein levels of NaChBac rather than the current that NaChBac produces. But why would the KCs have a mechanism for an exogenous sodium channel? As NaChBac has sections similar to eukaryotic sodium channels, 17-23% (Ito et al., 2004; Koishi et al., 2004; Irie et al., 2010; Charalambous and Wallace, 2011), maybe these sections are what trigger KCs to respond homeostatically. This is another reason why it is important to use electrophysiology to investigate underlying mechanisms to support calcium imaging work. Electrophysiological work would be able to determine whether the NaChBac is functioning correctly and facilitating sodium currents.

However, KCs may react to current levels but as NaChBac is exogenous its expression in KCs may mean that they don't have a specific method of regulating their excitability correctly. Past literature has shown that larval *Drosophila* motor neurons can stabilise hyperactivity induced by the loss of Shab by upregulating the slowpoke gene which is a Ca²⁺-dependent potassium channel (SLO; Kim et al., 2017). However, this compensation is not reciprocal when there is a loss of SLO as it does not trigger an upregulation of Shab. Their argument was that homeostatic signalling pathways use compensatory pathways unique to the channel that was mutated, and the compensations are influenced by the identity of the lost conductance. Thus, not only can *Drosophila* cells increase in excitability through ion channel levels, but they can compensate for the changes by altering other ion channels. Thus, NaChBac's unusual weakening effects on KCs may be due to a lack of specific compensatory pathways as it is exogenous. This hypothesis might also explain why disrupting endogenous potassium channels doesn't lead to any significant differences, as they might have

specific compensatory pathways to maintain activity stability. This is another reason why the potassium channel disruptors should be investigated alongside ShFlpTag, EagFlpTag and IhFlpTag.

Furthering that concept, in eukaryotes, sodium channels have a higher sodium influx, 15-50 times faster than potassium or calcium currents (Ovchinnikov, 1981). Eukaryotes have a sodium influx rate of $>10^7$ ions/s and favour sodium over other cations by factors of $>100:1$ (Marban et al., 1998; Catterall, 2000). As shown in Chapter 1, NaChBac's structure is different from eukaryotic channels and so we could theorise that the KCs cannot properly sense the change NaChBac's expression, given the currents are not native to the KC. Thus, the feedback mechanism may not be appropriate for NaChBac's expression.

Regardless of whether KCs are reacting to the protein levels or current levels, it is probable that the weakening of odour responses was primarily due to genetic changes in the cells. As demonstrated in *Drosophila*, single point mutations can result in a cascade of transcriptional changes in genes that are responsible for excitability (van Swinderen and Greenspan, 2005). *Drosophila* likely possess genetic networks that exhibit compensatory mechanisms, wherein the loss of a gene or genetic component can be offset through rearrangements of the remaining genes, thereby preserving overall functionality. This could be the reason why the RNAis of the potassium channels had very little effect on the odour responses. The KCs may have methods for stabilising excitability by compensating their gene expression disruption with the remaining genes.

Of the papers where NaChBac was reported to increase excitability of *Drosophila* neurons, most studied peptidergic neurons, such as the ILN-vs (Nitahbach et al., 2006). As KCs are not peptidergic, this may be a significant reason why KCs do not become overexcited when NaChBac is produced. Peptidergic neurons are cells that secrete peptide hormones as their neurotransmitters. Neuropeptides are large molecules in comparison to other types of neurotransmitters which are relatively smaller (Davison, 1989; Russo, 2017). The main difference between neuropeptides and other neurotransmitters is that neuropeptides are slow-acting and produce a prolonged action (Russo, 2017). In contrast, neurotransmitters are fast-acting and produce a short-term response. They are also produced and stored in different locations of the neuron (Russo, 2017). Of course, this is only speculation and may not be the reason behind

why KCs do not respond in the same way; however, it is striking that both the PNs and the KCs (both cholinergic neurons) don't increase their odour responses when NaChBac is expressed.

5.3 Improving the experimental approach

5.3.1 Calcium imaging for neuronal activity

Throughout the project, I was investigating the levels of GCaMP6f fluorescence and relating it to the activity of the cell. Whilst this is not a perfect measure of neuronal activity, the use of GCaMP6f was sufficient for characterising the excitation levels of KCs in this study. However, the drawbacks of using GCaMP6f should be discussed.

When comparing calcium imaging data between different cells or animals, it's important to consider a variety of factors that can affect the reliability of the comparison. For example, there could be variations in the expression levels of GCaMP6f across cells or animals. In order to minimise these variations, the physiological state of the animals during development and time of imaging are highly controlled. These controls include but are not limited to temperature, pH, and oxygen levels. But whilst these controls are necessary and useful, they have limitations and cannot account for every possible variation. Furthermore, the way we measure GCaMP signal changes, i.e., $\Delta F/F$, automatically normalises for baseline GCaMP signal. Consequently, the $\Delta F/F$ values should remain consistent for the same change in calcium levels, even if there are variations in GCaMP expression levels. Although fluctuations in GCaMP expression might influence the measured $\Delta F/F$ (e.g. to buffering effects), any inter-fly variability would be random and only introduce noise into our data. It would not lead to false effects, unless there are systematic differences in GCaMP expression levels between the conditions being compared.

In these experiments, it was not the aim to determine the exact levels of calcium that were reached. Instead, the objective was to monitor the changes in the calcium levels over time between conditions. However, it may have been useful to verify that each condition had a similar level of calcium within its KCs to deepen our understanding of what is happening in each condition. Therefore, this could be a future experiment.

GCaMP6f is one of the fastest of the GCaMP sensors but can only resolve individual spikes if they are more than 50-75 ms apart (Chen et al., 2013). Thus, this method of sensing activity is unreliable for higher rates of spiking and there can be large disparities between voltage fluctuations and the activity reported by genetically encoded calcium indicators (Chen et al., 2013; Yang et al., 2016). However, this project focused on looking at how a whole population responds and, thus, I didn't need a high resolution method. However, this could be necessary for future experiments.

Another limitation is the nonlinearity between cytoplasmic calcium levels to the spike frequency and the fluorescence intensity of the fluorophore (Akerboom et al., 2012; Chen et al., 2013). This is another reason why we can only approximate activity with GCaMP6f.

Could the use of genetically encoded voltage sensors, such as ASAP2f, have been a more suitable option than GgCaMP6f? Voltage sensors like ASAP2f have faster kinetics than GCaMP6f and its variants. Compared to GCaMP6f, ASAP2f exhibits a peak response five times faster and returns to baseline ten times faster (Yang et al., 2016). Although this is a benefit over genetically encoded calcium sensors, the main issue with voltage sensors is the relatively low peak $\Delta F/F$. The peak can be as much as 20-fold lower in ASAP2f compared to GCaMP6f (Yang et al., 2016). Furthermore, speed is not always an advantage as it means that the experimenter must scan at a high enough frame rate to capture the event which sometimes may not be possible (Sjulson and Miesenböck, 2007). As voltage sensors are more comparable to the activity of the cell it would have been better to use this when discussing activity of KCs. However, when I had used ASAP2f for an experiment, the response fluorescent levels were so low that ASAP2f was considered less effective than GCaMP6f.

Another possible problem of using calcium sensors is that past literature has found that their expression can possibly perturb cell physiology. Calcium dynamics can be affected by certain variants of GCaMP which have a high affinity for calcium. This can lead to them acting as potentially strong buffers. This was shown when GCaMP6f expression in mouse cortical neurons altered the calcium dynamics and calmodulin-dependent gene expression (Yang et al., 2018). Additionally, expressing GCaMP6m, a variant of GCaMP6f, has been shown to change the release probability of synapses in the giant axosomatic synapse in the auditory brainstem of mice (Singh et al., 2018). Furthermore,

the cells that expressed NaChBac may have had a lower expression of GCaMP because the GAL4 splits between the two UAS constructs (UAS-GCaMP and UAS-NaChBac). This is compared to the control that has only has one UAS construct, UAS-GCaMP6f. This speculation seems unlikely as the experiments which expressed other UAS- constructs had no effect. Unfortunately, there wasn't any experiments done to determine if GCaMP6f affected the physiology of KCs, but as I recorded odour responses from the KCs this suggests that the neurons were functional enough to respond. Furthering that, both the control and experimental flies expressed GCaMP and so this is unlikely to explain the effects I observed. However, future experiments could be done to investigate the possible physiological effects.

The fluorescence levels of GCaMP6f were only investigated in the experiment where NaChBac was solely expressed in γ KCs (Figure 10). Therefore, it is unknown how baseline GCaMP6f fluorescence levels are affected between the other conditions in the project. In future experiments, it may be valuable to assess the baseline fluorescence levels of each condition to confirm that they remain consistent across conditions. Additionally, it would also be important to investigate whether the fluorescence levels reflect a change in GCaMP6f protein levels or a change in baseline calcium concentration.

Lastly, validating synaptic connectivity with these techniques is limited by a lack of spatial or temporal resolution and so it is difficult to decipher between whether cells are connected via monosynaptic or polysynaptic synapses. This is another reason why studies back up their data with electrophysiological recordings (Giachello et al., 2022), which is what I aim to do in the future with this research.

Concluding these remarks, calcium imaging has some limitations as to how much 'activity' we can gauge from these experiments, but for this project genetically encoded calcium indicators were the correct method to use.

5.3.2 Altering ion channel levels through gene expression

An issue with using NaChBac is that it is an exogenous channel to *Drosophila*. Although shown to be functionally and structurally correct when expressed in other models it remains that it has characteristics different to that of Para in *Drosophila*. For example,

NaChBac inactivates in the hundreds of milliseconds whereas sodium channels of *Drosophila* inactivate in less than 1 ms (Ren *et al.*, 2001). It may have been better to over express para, the only endogenous sodium channel, in *Drosophila*. However, Para is notorious for having multiple splice variants (Lin *et al.*, 2009) and so it would be difficult to know which variant's cDNA to choose for overexpression. In previous attempts conducted outside the laboratory, there were unsuccessful efforts to overexpress UAS-Para. Despite expressing the mRNA, no additional Para protein was produced (R. Baines, personal communication). Thus, I believe overexpressing NaChBac was the correct decision for this project. However, future experiments could focus on para.

Expressing the RNAi of a channel doesn't necessarily mean that all expression is lost (Pak *et al.*, 2012). Instead, it lowers their expression considerably but seldom eliminates all of the targeted protein. This limits what can be inferred from these results. For example, ShakerDn was able to increase odour responses whereas ShakerRNAi did not. This may be because the dominant negative version of Shaker weakens the Shaker current more than ShakerRNAi, i.e., the ShakerRNAi doesn't stop the production of Shaker channels as well as I intended.

Dominant negative mutations may also not affect all targeted proteins. DN strategies in this project usually block an aspect of the function of the target channel (Veitia, 2008). Unfortunately, during this project, due to time constraints, I did not check the expression levels of channels or measure their currents (e.g. inward currents for NaChBac or A-type outward currents for Shaker), so I could not definitively say if our manipulations had the expected effects on channel expression levels or function. Thus, this could be a reason why the potassium channel disruptors did not increase the excitability of KCs. But, disappointingly, demonstrating localisation in *Drosophila* presents challenges due to the limited availability of antibodies specifically produced for *Drosophila*, and conventional strategies for protein visualization often prove ineffective. However, in the future, for example, it may be possible to check if Shaker-RNAi reduces Shaker expression using ShakerFlpTag flies.

5.4 Insights into the role of Kenyon cells in the mushroom body based on my results

KCs with NaChBac may weaken odour responses because they rely heavily on only activating 5% of their population. Therefore, to retain the ability to encode odour associative memories for specific odours, it is better to have less cells responding than to have more cells responding. Less cells responding means that certain KCs can be reserved for specific odours, but if there was overexcitation then it would be harder to keep specificity of KCs to odours. Overexcitation of KCs would mean more Kenyon cells would spike when an odour is delivered. Further study of which population of KCs are active for each odour may help determine whether weakening odour responses is a problem for them when NaChBac is activated.

5.5 Comparisons to other systems

As described before, potassium channels were first discovered in *Drosophila*. Although this was pioneering, potassium channels would have been found eventually. However, the quick generation of *Drosophila* and ability to show significantly unique phenotypes made the discovery far faster.

The network between APL and the KCs is quite different from what is found in mammals. The APL is the exclusive neuron that provides inhibition to all the KCs in the MB. This cannot be compared to the cerebellum, an area that is usually compared to the MB of *Drosophila*. In the mammalian cerebellum there are numerous inhibitory Golgi cells connected to the granule cells to provide inhibitory feedback. Unlike the APL, which is non spiking, Golgi cells are spiking and use that to encode their information (D'Angelo et al., 2013). Furthermore, the cerebellum contains basket and stellate cells which are inhibitory interneurons that inhibit the Purkinje cells (Prestori et al., 2019). We cannot therefore make true comparisons between the MB and mammalian systems as the vertebrate system is more diverse.

An obvious difference between a vertebrate's CNS and a *Drosophila*'s is the size of the brain. A vertebrate's brain has a larger area to house neurons and their projections. The mouse brain is $\sim 415 \text{ mm}^3$ (Kovačević et al., 2005) which is 5000-fold larger than the

volume of a *Drosophila* brain, which is $\sim 8 \times 10^7 \mu\text{m}^3$ (Zheng et al., 2018). In contrast. It is understandable that the smaller brains of *Drosophila* cannot attain the complexity of a larger brain and so at first it may seem like there is no obvious comparison.

Having a smaller brain area means that they must increase their specialisation for individual cells. For example, the APL neuron synapses with all 2000 KC. But a Golgi cell can only synapse onto a few granule cells (D'Angelo et al., 2013). Thus, the APL has evolved to have contact with all, and studying this one cell may reveal more than trying to study a population of cells, like the Golgi cells. On the other hand, the APL has highly compartmentalised activity so that activity doesn't spread between the calyx and the lobes (Grimes et al., 2010; Amin et al., 2020). Therefore, it could mean that the APL has different roles for different areas, so although it is one neuron, it could functionally act as multiple distinct neurons.

The benefits of using *Drosophila*, such as easy genetics, *in vivo* imaging, and lack of interconnecting networks, made it an ideal experimental model for this project.

6 References

- Abdelrahman, N.Y., Vasilaki, E. and Lin, A.C. 2021. Compensatory variability in network parameters enhances memory performance in the *Drosophila* mushroom body. *Proceedings of the National Academy of Sciences of the United States of America*. **118**(49).
- Adachi, R., Yamada, R. and Kuba, H. 2015. Plasticity of the Axonal Trigger Zone. *The Neuroscientist*. **21**(3), pp.255–265.
- Adams, M.D., Celniker, S.E., Holt, R.A., Evans, C.A., Gocayne, J.D., Amanatides, P.G., Scherer, S.E., Li, P.W., Hoskins, R.A., Galle, R.F., George, R.A., Lewis, S.E., Richards, S., Ashburner, M., Henderson, S.N., Sutton, G.G., Wortman, J.R., Yandell, M.D., Zhang, Q., Chen, L.X., Brandon, R.C., Rogers, Y.-H.C., Blazej, R.G., Champe, M., Pfeiffer, B.D., Wan, K.H., Doyle, C., Baxter, E.G., Helt, G., Nelson, C.R., Gabor, G.L., Miklos, Abril, J.F., Agbayani, A., An, H.-J., Andrews-Pfannkoch, C., Baldwin, D., Ballew, R.M., Basu, A., Baxendale, J., Bayraktaroglu, L., Beasley, E.M., Beeson, K.Y., Benos, P. V., Berman, B.P., Bhandari, D., Bolshakov, S., Borkova, D., Botchan, M.R., Bouck, J., Brokstein, P., Brottier, P., Burtis, K.C., Busam, D.A., Butler, H., Cadieu, E., Center, A., Chandra, I., Cherry, J.M., Cawley, S., Dahlke, C., Davenport, L.B., Davies, P., Pablos, B. de, Delcher, A., Deng, Z., Mays, A.D., Dew, I., Dietz, S.M., Dodson, K., Doup, L.E., Downes, M., Dugan-Rocha, S., Dunkov, B.C., Dunn, P., Durbin, K.J., Evangelista, C.C., Ferraz, C., Ferriera, S., Fleischmann, W., Fosler, C., Gabrielian, A.E., Garg, N.S., Gelbart, W.M., Glasser, K., Glodek, A., Gong, F., Gorrell, J.H., Gu, Z., Guan, P., Harris, M., Harris, N.L., Harvey, D., Heiman, T.J., Hernandez, J.R., Houck, J., Hostin, D., Houston, K.A., Howland, T.J., Wei, M.-H., Ibegwam, C., Jalali, M., Kalush, F., Karpen, G.H., Ke, Z., Kennison, J.A., Ketchum, K.A., Kimmel, B.E., Kodira, C.D., Kraft, C., Kravitz, S., Kulp, D., Lai, Z., Lasko, P., Lei, Y., Levitsky, A.A., Li, J., Li, Z., Liang, Y., Lin, X., Liu, X., Mattei, B., McIntosh, T.C., McLeod, M.P., McPherson, D., Merkulov, G., Milshina, N. V., Mobarry, C., Morris, J., Moshrefi, A., Mount, S.M., Moy, M., Murphy, B., Murphy, L., Muzny, D.M., Nelson, D.L., Nelson, D.R., Nelson, K.A., Nixon, K., Nusskern, D.R., Pacleb, J.M., Palazzolo, M., Pittman, G.S., Pan, S., Pollard, J., Puri, V., Reese, M.G., Reinert, K., Remington, K., Saunders, R.D.C., Scheeler, F., Shen, H., Shue, B.C., Sidén-Kiamos, I., Simpson, M., Skupski, M.P., Smith, T., Spier, E., Spradling, A.C., Stapleton, M., Strong, R., Sun, E., Svirskas,

- R., Tector, C., Turner, R., Venter, E., Wang, A.H., Wang, X., Wang, Z.-Y., Wassarman, D.A., Weinstock, G.M., Weissenbach, J., Williams, S.M., Woodage, T., Worley, K.C., Wu, D., Yang, S., Yao, Q.A., Ye, J., Yeh, R.-F., Zaveri, J.S., Zhan, M., Zhang, G., Zhao, Q., Zheng, L., Zheng, X.H., Zhong, F.N., Zhong, W., Zhou, X., Zhu, S., Zhu, X., Smith, H.O., Gibbs, R.A., Myers, E.W., Rubin, G.M. and Venter, J.C. 2000. The Genome Sequence of *Drosophila melanogaster*. *Science*. **287**(5461), pp.2185–2195.
- Akerboom, J., Chen, T.-W., Wardill, T.J., Tian, L., Marvin, J.S., Mutlu, S., Calderon, N.C., Esposti, F., Borghuis, B.G., Sun, X.R., Gordus, A., Orger, M.B., Portugues, R., Engert, F., Macklin, J.J., Filosa, A., Aggarwal, A., Kerr, R.A., Takagi, R., Kracun, S., Shigetomi, E., Khakh, B.S., Baier, H., Lagnado, L., Wang, S.S.-H., Bargmann, C.I., Kimmel, B.E., Jayaraman, V., Svoboda, K., Kim, D.S., Schreiter, E.R. and Looger, L.L. 2012. Optimization of a GCaMP Calcium Indicator for Neural Activity Imaging. *Journal of Neuroscience*. **32**(40), pp.13819–13840.
- Albuquerque, E.X., Pereira, E.F.R., Alkondon, M. and Rogers, S.W. 2009. Mammalian Nicotinic Acetylcholine Receptors: From Structure to Function. *Physiological Reviews*. **89**(1), pp.73–120.
- Amichot, M., Castella, C., Bergé, J.B. and Pauron, D. 1993. Transcription analysis of the para gene by in situ hybridization and immunological characterization of its expression product in wild-type and mutant strains of *Drosophila*. *Insect Biochemistry and Molecular Biology*. **23**(3), pp.381–390.
- Amin, H., Apostolopoulou, A.A., Suárez-Grimalt, R., Vrontou, E. and Lin, A.C. 2020. Localized inhibition in the *Drosophila* mushroom body. *eLife*. **9**.
- Andrásfalvy, B.K., Makara, J.K., Johnston, D. and Magee, J.C. 2008. Altered synaptic and non-synaptic properties of CA1 pyramidal neurons in Kv4.2 knockout mice. *The Journal of Physiology*. **586**(16), pp.3881–3892.
- Apostolopoulou, A.A. and Lin, A.C. 2020. Mechanisms underlying homeostatic plasticity in the *Drosophila* mushroom body in vivo. *Proceedings of the National Academy of Sciences*. **117**(28), pp.16606–16615.
- Ashley, C.C. and Ridgway, E.B. 1968. Simultaneous Recording of Membrane Potential, Calcium Transient and Tension in Single Muscle Fibres. *Nature*. **219**(5159), pp.1168–1169.
- Aso, Y., Hattori, D., Yu, Y., Johnston, R.M., Iyer, N.A., Ngo, T.-T., Dionne, H., Abbott, L., Axel, R., Tanimoto, H. and Rubin, G.M. 2014. The neuronal architecture of the

- mushroom body provides a logic for associative learning. *eLife*. **3**.
- Baranauskas, G., David, Y. and Fleidervish, I.A. 2013. Spatial mismatch between the Na⁺ flux and spike initiation in axon initial segment. *Proceedings of the National Academy of Sciences*. **110**(10), pp.4051–4056.
- Baranauskas, G., Tkatch, T. and Surmeier, D.J. 1999. Delayed Rectifier Currents in Rat Globus Pallidus Neurons Are Attributable to Kv2.1 and Kv3.1/3.2 K⁺ Channels. *The Journal of Neuroscience*. **19**(15), pp.6394–6404.
- Barnstedt, O., Oswald, D., Felsenberg, J., Brain, R., Moszynski, J.-P., Talbot, C.B., Perrat, P.N. and Waddell, S. 2016. Memory-Relevant Mushroom Body Output Synapses Are Cholinergic. *Neuron*. **89**(6), pp.1237–1247.
- Berridge, M.J., Lipp, P. and Bootman, M.D. 2000. The versatility and universality of calcium signalling. *Nature Reviews Molecular Cell Biology*. **1**(1), pp.11–21.
- Beshel, J. and Zhong, Y. 2013. Graded Encoding of Food Odor Value in the Drosophila Brain. *Journal of Neuroscience*. **33**(40), pp.15693–15704.
- Bhandawat, V., Olsen, S.R., Gouwens, N.W., Schlieff, M.L. and Wilson, R.I. 2007. Sensory processing in the Drosophila antennal lobe increases reliability and separability of ensemble odor representations. *Nature Neuroscience*. **10**(11), pp.1474–1482.
- Bielopolski, N., Amin, H., Apostolopoulou, A.A., Rozenfeld, E., Lerner, H., Huetteroth, W., Lin, A.C. and Parnas, M. 2019. Inhibitory muscarinic acetylcholine receptors enhance aversive olfactory learning in adult Drosophila. *eLife*. **8**.
- Bier, E. 2005. Drosophila, the golden bug, emerges as a tool for human genetics. *Nature Reviews Genetics*. **6**(1), pp.9–23.
- Borodinsky, L.N., Root, C.M., Cronin, J.A., Sann, S.B., Gu, X. and Spitzer, N.C. 2004. Activity-dependent homeostatic specification of transmitter expression in embryonic neurons. *Nature*. **429**(6991), pp.523–530.
- Brand, a H. and Perrimon, N. 1993. Targeted gene expression as a means of altering cell fates and generating dominant phenotypes. *Development*. **118**(2), pp.401–15.
- Brette, R. 2013. Sharpness of Spike Initiation in Neurons Explained by Compartmentalization N. Brunel, ed. *PLoS Computational Biology*. **9**(12), p.e1003338.
- Brickley, S.G., Revilla, V., Cull-Candy, S.G., Wisden, W. and Farrant, M. 2001. Adaptive regulation of neuronal excitability by a voltage-independent potassium conductance. *Nature*. **409**(6816), pp.88–92.

- Bronk, P., Kuklin, E.A., Gorur-Shandilya, S., Liu, C., Wiggin, T.D., Reed, M.L., Marder, E. and Griffith, L.C. 2018. Regulation of Eag by Ca²⁺/calmodulin controls presynaptic excitability in *Drosophila*. *Journal of Neurophysiology*. **119**(5), pp.1665–1680.
- Browne, D., Gancher, S., Nutt, J., Brunt, E., Smith, E., Kramer, P. and Litt, M. 1994. Episodic ataxia/myokymia syndrome is associated with point mutations in the human potassium channel gene, KCNA1. *Nature Genetics*. **8**(4), pp.136–140.
- Buhl, E., Bradlaugh, A., Ogueta, M., Chen, K.-F., Stanewsky, R. and Hodge, J.J.L. 2016. Quasimodo mediates daily and acute light effects on *Drosophila* clock neuron excitability. *Proceedings of the National Academy of Sciences*. **113**(47), pp.13486–13491.
- Burrone, J., O'Byrne, M. and Murthy, V.N. 2002. Multiple forms of synaptic plasticity triggered by selective suppression of activity in individual neurons. *Nature*. **420**(6914), pp.414–418.
- Butcher, N.J., Friedrich, A.B., Lu, Z., Tanimoto, H. and Meinertzhagen, I.A. 2012. Different classes of input and output neurons reveal new features in microglomeruli of the adult *Drosophila* mushroom body calyx. *The Journal of Comparative Neurology*. **520**(10), pp.2185–2201.
- Butler, A., Wei, A., Baker, K. and Salkoff, L. 1989. A family of putative potassium channel genes in *Drosophila*. *Science*.
- Campusano, J.M., Su, H., Jiang, S.A., Sicaeros, B. and O'Dowd, D.K. 2007. nAChR-mediated calcium responses and plasticity in *Drosophila* Kenyon cells. *Developmental Neurobiology*. **67**(11), pp.1520–1532.
- Cannon, J. and Miller, P. 2016. Synaptic and intrinsic homeostasis cooperate to optimize single neuron response properties and tune integrator circuits. *Journal of Neurophysiology*. **116**(5), pp.2004–2022.
- Caron, S.J.C., Ruta, V., Abbott, L.F. and Axel, R. 2013. Random convergence of olfactory inputs in the *Drosophila* mushroom body. *Nature*. **497**(7447), pp.113–117.
- Carrillo, E., Pacheco, L., Balleza, D. and Gomez-Lagunas, F. 2015. K⁺-Dependent Selectivity and External Ca²⁺ Block of Shab K⁺ Channels. *PLOS ONE*. **10**(3), p.e0120431.
- Catterall, W.A. 2000. From ionic currents to molecular mechanisms: The structure and function of voltage-gated sodium channels. *Neuron*. **26**(1), pp.13–25.
- Cavaliere, S. and Hodge, J.J.L. 2011. *Drosophila* KCNQ Channel Displays

- Evolutionarily Conserved Electrophysiology and Pharmacology with Mammalian KCNQ Channels M. N. Nitabach, ed. *PLoS ONE*. **6**(9), p.e23898.
- Chahine, M., Pilote, S., Pouliot, V., Takami, H. and Sato, C. 2004. Role of arginine residues on the S4 segment of the *Bacillus halodurans* Na⁺ channel in voltage-sensing. *Journal of Membrane Biology*. **201**(1), pp.9–24.
- Charalambous, K. and Wallace, B.A. 2011. NaChBac: The long lost sodium channel ancestor. *Biochemistry*. **50**(32), pp.6742–6752.
- Chen, T., Wardill, T.J., Sun, Y., Pulver, S.R., Renninger, S.L., Baohan, A., Schreiter, E.R., Kerr, R.A., Orger, M.B., Jayaraman, V., Looger, L.L., Svoboda, K. and Kim, D.S. 2013. Ultrasensitive fluorescent proteins for imaging neuronal activity. *Nature*. **499**(7458), pp.295–300.
- Chen, X., Shu, S., Schwartz, L.C., Sun, C., Kapur, J. and Bayliss, D.A. 2010. Homeostatic Regulation of Synaptic Excitability: Tonic GABAA Receptor Currents Replace Ih in Cortical Pyramidal Neurons of HCN1 Knock-Out Mice. *Journal of Neuroscience*. **30**(7), pp.2611–2622.
- Cirelli, C., Bushey, D., Hill, S., Huber, R., Kreber, R., Ganetzky, B. and Tononi, G. 2005. Reduced sleep in *Drosophila* Shaker mutants. *Nature*. **434**(7037), pp.1087–1092.
- Claes, L., Del-Favero, J., Ceulemans, B., Lagae, L., Van Broeckhoven, C. and De Jonghe, P. 2001. De Novo Mutations in the Sodium-Channel Gene SCN1A Cause Severe Myoclonic Epilepsy of Infancy. *The American Journal of Human Genetics*. **68**(6), pp.1327–1332.
- Claridge-Chang, A., Roorda, R.D., Vrontou, E., Sjulson, L., Li, H., Hirsh, J. and Miesenböck, G. 2009. Writing Memories with Light-Addressable Reinforcement Circuitry. *Cell*. **139**(2), pp.405–415.
- Clark, J.D. and Tempel, B.L. 1998. Hyperalgesia in mice lacking the Kv1.1 potassium channel gene. *Neuroscience Letters*. **251**(2), pp.121–124.
- Clyne, P.J., Warr, C.G., Freeman, M.R., Lessing, D., Kim, J. and Carlson, J.R. 1999. A novel family of divergent seven-transmembrane proteins: Candidate odorant receptors in *Drosophila*. *Neuron*. **22**(2), pp.327–338.
- Cohn, R., Morantte, I. and Ruta, V. 2015. Coordinated and Compartmentalized Neuromodulation Shapes Sensory Processing in *Drosophila*. *Cell*. **163**(7), pp.1742–1755.
- Connolly, J.B., Roberts, I.J.H., Armstrong, J.D., Kaiser, K., Forte, M., Tully, T. and O’Kane, C.J. 1996. Associative Learning Disrupted by Impaired G s Signaling in

- Drosophila Mushroom Bodies. *Science*. **274**(5295), pp.2104–2107.
- Covarrubias, M., Wei, A. and Salkoff, L. 1991. Shaker, Shal, Shab, and Shaw express independent K⁺ current systems. *Neuron*. **7**(5), pp.763–773.
- D'Angelo, E., Solinas, S., Mapelli, J., Gandolfi, D., Mapelli, L. and Prestori, F. 2013. The cerebellar Golgi cell and spatiotemporal organization of granular layer activity. *Frontiers in Neural Circuits*. **7**.
- Davis, G.W. 2006. Homeostatic control of neural activity: From phenomenology to molecular design. *Annual Review of Neuroscience*. **29**, pp.307–323.
- Davis, R.L. 1993. Mushroom bodies and drosophila learning. *Neuron*. **11**(1), pp.1–14.
- Davison, A. 1989. Basic Neurochemistry: Molecular, Cellular, and Medical Aspects. *Journal of Neurology, Neurosurgery & Psychiatry*. **52**(8), pp.1021–1021.
- Demmer, H. and Kloppenburg, P. 2009. Intrinsic membrane properties and inhibitory synaptic input of kenyon cells as mechanisms for sparse coding? *Journal of Neurophysiology*. **102**(3), pp.1538–1550.
- Denk, W., Strickler, J.H. and Webb, W.W. 1990. Two-Photon Laser Scanning Fluorescence Microscopy. *Science*. **248**(4951), pp.73–76.
- Diao, F., Chaufty, J., Waro, G. and Tsunoda, S. 2010. SIDL interacts with the dendritic targeting motif of Shal (Kv4) K⁺ channels in Drosophila. *Molecular and Cellular Neuroscience*. **45**(1), pp.75–83.
- Donlea, J.M., Thimgan, M.S., Suzuki, Y., Gottschalk, L. and Shaw, P.J. 2011. Inducing Sleep by Remote Control Facilitates Memory Consolidation in Drosophila. *Science*. **332**(6037), pp.1571–1576.
- Dowd, H.S. and D.K. 2003. Fast Synaptic Currents in Drosophila Mushroom body kenyon Cells. *The Journal of neuroscience : the official journal of the Society for Neuroscience*. **23**(27), pp.9246–9253.
- Driscoll, C.T., Mason, R.P., Chan, H.M., Jacob, D.J. and Pirrone, N. 2013. Mercury as a Global Pollutant: Sources, Pathways, and Effects. *Environmental Science & Technology*. **47**(10), pp.4967–4983.
- Drysdale, R., Warmke, J., Kreber, R. and Ganetzky, B. 1991. Molecular characterization of eag: a gene affecting potassium channels in Drosophila melanogaster. *Genetics*. **127**(3), pp.497–505.
- Dubnau, J., Grady, L., Kitamoto, T. and Tully, T. 2001. Disruption of neurotransmission in Drosophila mushroom body blocks retrieval but not acquisition of memory. *Nature*. **411**(6836), pp.476–480.

- Duch, C., Vonhoff, F. and Ryglewski, S. 2008. Dendrite Elongation and Dendritic Branching Are Affected Separately by Different Forms of Intrinsic Motoneuron Excitability. *Journal of Neurophysiology*. **100**(5), pp.2525–2536.
- Dulhunty, A. 2006. Excitation-contraction coupling from the 1950s into the new millennium. *Clinical and Experimental Pharmacology and Physiology*. **33**(9), pp.763–772.
- Dupuis, J., Louis, T., Gauthier, M. and Raymond, V. 2012. Insights from honeybee (*Apis mellifera*) and fly (*Drosophila melanogaster*) nicotinic acetylcholine receptors: From genes to behavioral functions. *Neuroscience & Biobehavioral Reviews*. **36**(6), pp.1553–1564.
- Eilers, J., Augustine, G.J. and Konnerth, A. 1995. Subthreshold synaptic Ca²⁺ signalling in fine dendrites and spines of cerebellar Purkinje neurons. *Nature*. **373**(6510), pp.155–158.
- Evans, M.D., Dumitrescu, A.S., Kruijssen, D.L.H., Taylor, S.E. and Grubb, M.S. 2015. Rapid Modulation of Axon Initial Segment Length Influences Repetitive Spike Firing. *Cell Reports*. **13**(6), pp.1233–1245.
- Farris, S.M. 2011. Are mushroom bodies cerebellum-like structures? *Arthropod Structure and Development*. **40**(4), pp.368–379.
- Fékété, A., Ankri, N., Brette, R. and Debanne, D. 2021. Neural excitability increases with axonal resistance between soma and axon initial segment. *Proceedings of the National Academy of Sciences*. **118**(33).
- Fendl, S., Vieira, R.M. and Borst, A. 2020. Conditional protein tagging methods reveal highly specific subcellular distribution of ion channels in motion-sensing neurons. *eLife*. **9**, pp.1–48.
- Fernandes, D. and Carvalho, A.L. 2016. Mechanisms of homeostatic plasticity in the excitatory synapse. *Journal of Neurochemistry*. **139**(6), pp.973–996.
- Ganetzky, B. and Wu, C.-F. 1983. Neurogenetic Analysis of Potassium Currents in *Drosophila*: Synergistic Effects on Neuromuscular Transmission in Double Mutants. *Journal of Neurogenetics*. **1**(1), pp.17–28.
- Giachello, C.N.G., Fan, Y.N., Landgraf, M. and Baines, R.A. 2021. Nitric oxide mediates activity-dependent change to synaptic excitation during a critical period in *Drosophila*. *Scientific Reports*. **11**(1), p.20286.
- Giachello, C.N.G., Hunter, I., Pettini, T., Coulson, B., Knüfer, A., Cachero, S., Winding, M., Arzan Zarin, A., Kohsaka, H., Fan, Y.N., Nose, A., Landgraf, M. and Baines,

- R.A. 2022. Electrophysiological Validation of Monosynaptic Connectivity between Premotor Interneurons and the aCC Motoneuron in the *Drosophila* Larval CNS. *The Journal of Neuroscience*. **42**(35), pp.6724–6738.
- Gilchrist, J., Olivera, B.M. and Bosmans, F. 2014. Animal toxins influence voltage-gated sodium channel function. *Handbook of Experimental Pharmacology*. **221**, pp.203–229.
- Goethals, S. and Brette, R. 2020. Theoretical relation between axon initial segment geometry and excitability. *eLife*. **9**.
- Goldin, A., Barchi, R., Caldwell, J., Hofmann, F., Howe, J., Hunter, J., Kallen, R., Mandel, G., Meisler, M., Netter, Y., Noda, M., Tumkun, M., Waxman, S., Wood, J. and Catterall, W.A. 2000. Nomenclature of Voltage-Gated Sodium Channels. *Neuron*. **28**, pp.365–368.
- Goldman, D.E. 1943. Potential, impedance, and rectification in membranes. *Journal of General Physiology*. **27**(1), pp.37–60.
- Gonzalo-Gomez, A., Turiegano, E., León, Y., Molina, I., Torroja, L. and Canal, I. 2012. Ih Current Is Necessary to Maintain Normal Dopamine Fluctuations and Sleep Consolidation in *Drosophila*. X. Zhuang, ed. *PLoS ONE*. **7**(5), p.e36477.
- Gordon, M.D. and Scott, K. 2009. Motor Control in a *Drosophila* Taste Circuit. *Neuron*. **61**(3), pp.373–384.
- Gouwens, N.W. and Wilson, R.I. 2009. Signal propagation in *Drosophila* central neurons. *Journal of Neuroscience*. **29**(19), pp.6239–6249.
- Gray, I.C. 2000. Single nucleotide polymorphisms as tools in human genetics. *Human Molecular Genetics*. **9**(16), pp.2403–2408.
- Grimes, W.N., Zhang, J., Graydon, C.W., Kachar, B. and Diamond, J.S. 2010. Retinal Parallel Processors: More than 100 Independent Microcircuits Operate within a Single Interneuron. *Neuron*. **65**(6), pp.873–885.
- Groschner, L.N., Chan Wah Hak, L., Bogacz, R., DasGupta, S. and Miesenböck, G. 2018. Dendritic Integration of Sensory Evidence in Perceptual Decision-Making. *Cell*. **173**(4), pp.894-905.e13.
- Grubb, Matthew S and Burrone, J. 2010. Activity-dependent relocation of the axon initial segment fine-tunes neuronal excitability. *Nature*. **465**(7301), pp.1070–1074.
- Grubb, Matthew S. and Burrone, J. 2010. Activity-dependent relocation of the axon initial segment fine-tunes neuronal excitability. *Nature*. **465**(7301), pp.1070–1074.
- Gruntman, E. and Turner, G.C. 2013. Integration of the olfactory code across dendritic

- claws of single mushroom body neurons. *Nature Neuroscience*. **16**(12), pp.1821–1829.
- Gu, H. and O’Dowd, D.K. 2006. Cholinergic Synaptic Transmission in Adult *Drosophila* Kenyon Cells In Situ. *The Journal of Neuroscience*. **26**(1), pp.265–272.
- Guan, Z., Buhl, L.K., Quinn, W.G. and Littleton, J.T. 2011. Altered gene regulation and synaptic morphology in *Drosophila* learning and memory mutants. *Learning & Memory*. **18**(4), pp.191–206.
- Guardiani, C., Rodger, P.M., Fedorenko, O.A., Roberts, S.K. and Khovanov, I.A. 2017. Sodium Binding Sites and Permeation Mechanism in the NaChBac Channel: A Molecular Dynamics Study. *Journal of Chemical Theory and Computation*. **13**(3), pp.1389–1400.
- Günay, C., Sieling, F.H., Dharmar, L., Lin, W.H., Wolfram, V., Marley, R., Baines, R.A. and Prinz, A.A. 2015. Distal Spike Initiation Zone Location Estimation by Morphological Simulation of Ionic Current Filtering Demonstrated in a Novel Model of an Identified *Drosophila* Motoneuron. *PLoS Computational Biology*. **11**(5), pp.1–26.
- Hall, J.C. 1994. The Mating of a Fly. *Science*. **264**(5166), pp.1702–1714.
- Hamada, F.N., Rosenzweig, M., Kang, K., Pulver, S.R., Ghezzi, A., Jegla, T.J. and Garrity, P.A. 2008. An internal thermal sensor controlling temperature preference in *Drosophila*. *Nature*. **454**(7201), pp.217–220.
- Hamada, M.S., Goethals, S., de Vries, S.I., Brette, R. and Kole, M.H.P. 2016. Covariation of axon initial segment location and dendritic tree normalizes the somatic action potential. *Proceedings of the National Academy of Sciences*. **113**(51), pp.14841–14846.
- Handler, A., Graham, T.G.W., Cohn, R., Morante, I., Siliciano, A.F., Zeng, J., Li, Y. and Ruta, V. 2019. Distinct Dopamine Receptor Pathways Underlie the Temporal Sensitivity of Associative Learning. *Cell*. **178**(1), pp.60-75.e19.
- Hatch, R.J., Wei, Y., Xia, D. and Götz, J. 2017. Hyperphosphorylated tau causes reduced hippocampal CA1 excitability by relocating the axon initial segment. *Acta Neuropathologica*. **133**(5), pp.717–730.
- Haugland, F. and Wu, C. 1990. A voltage-clamp analysis of gene-dosage effects of the Shaker locus on larval muscle potassium currents in *Drosophila*. *The Journal of Neuroscience*. **10**(4), pp.1357–1371.
- Hergarden, A.C., Tayler, T.D. and Anderson, D.J. 2012. Allatostatin-A neurons inhibit

- feeding behavior in adult *Drosophila*. *Proceedings of the National Academy of Sciences*. **109**(10), pp.3967–3972.
- Higley, M.J. and Sabatini, B.L. 2008. Calcium Signaling in Dendrites and Spines: Practical and Functional Considerations. *Neuron*. **59**(6), pp.902–913.
- Hodge, J.J. and Stanewsky, R. 2008. Function of the Shaw Potassium Channel within the *Drosophila* Circadian Clock. *PLoS ONE*. **3**(5), p.e2274.
- Hodge, J.J.L. 2009. Ion channels to inactivate neurons in *Drosophila*. *Frontiers in Molecular Neuroscience*. **2**.
- Hodge, J.J.L., Choi, J.C., O’Kane, C.J. and Griffith, L.C. 2005. Shaw potassium channel genes in *Drosophila*. *Journal of Neurobiology*. **63**(3), pp.235–254.
- Hodgkin, A.L. and Huxley, A.F. 1952. A quantitative description of membrane current and its application to conduction and excitation in nerve. *The Journal of Physiology*. **117**(4), pp.500–544.
- Hodgkin, A.L. and Huxley, A.F. 1945. Resting and action potentials in single nerve fibres. *The Journal of Physiology*. **104**(2), pp.176–195.
- Hodgkin, A.L. and Katz, B. 1949. The effect of sodium ions on the electrical activity of the giant axon of the squid. *The Journal of Physiology*. **108**(1), pp.37–77.
- Höfflin, F., Jack, A., Riedel, C., Mack-Bucher, J., Roos, J., Corcelli, C., Schultz, C., Wahle, P. and Engelhardt, M. 2017. Heterogeneity of the Axon Initial Segment in Interneurons and Pyramidal Cells of Rodent Visual Cortex. *Frontiers in Cellular Neuroscience*. **11**.
- Honegger, K.S., Campbell, R.A.A. and Turner, G.C. 2011. Cellular-Resolution Population Imaging Reveals Robust Sparse Coding in the *Drosophila* Mushroom Body. *The Journal of Neuroscience*. **31**(33), pp.11772–11785.
- Hong, C.S. and Ganetzky, B. 1994. Spatial and temporal expression patterns of two sodium channel genes in *Drosophila*. *Journal of Neuroscience*. **14**(9), pp.5160–5169.
- Huang, W., Liu, M., Yan, S.F. and Yan, N. 2017. Structure-based assessment of disease-related mutations in human voltage-gated sodium channels. *Protein and Cell*. **8**(6), pp.401–438.
- Hughes, T.T., Allen, A.L., Bardin, J.E., Christian, M.N., Daimon, K., Dozier, K.D., Hansen, C.L., Holcomb, L.M. and Ahlander, J. 2012. *Drosophila* as a genetic model for studying pathogenic human viruses. *Virology*. **423**(1), pp.1–5.
- Imlach, W.L., Beck, E.S., Choi, B.J., Lotti, F., Pellizzoni, L. and McCabe, B.D. 2012.

- SMN Is Required for Sensory-Motor Circuit Function in *Drosophila*. *Cell*. **151**(2), pp.427–439.
- Inada, K., Tsuchimoto, Y. and Kazama, H. 2017. Origins of Cell-Type-Specific Olfactory Processing in the *Drosophila* Mushroom Body Circuit. *Neuron*. **95**(2), pp.357-367.e4.
- Irie, K., Kitagawa, K., Nagura, H., Imai, T., Shimomura, T. and Fujiyoshi, Y. 2010. Comparative study of the gating motif and C-type inactivation in prokaryotic voltage-gated sodium channels. *Journal of Biological Chemistry*. **285**(6), pp.3685–3694.
- Ito, I., Ong, R.C.Y., Raman, B. and Stopfer, M. 2008. Sparse odor representation and olfactory learning. *Nature Neuroscience*. **11**(10), pp.1177–1184.
- Ito, M., Xu, H., Guffanti, A.A., Wei, Y., Zvi, L., Clapham, D.E. and Krulwich, T.A. 2004. The voltage-gated Na⁺ channel NavBP has a role in motility, chemotaxis, and pH homeostasis of an alkaliphilic *Bacillus*. *Proceedings of the National Academy of Sciences of the United States of America*. **101**(29), pp.10566–10571.
- Jamann, N., Jordan, M. and Engelhardt, M. 2018. Activity-Dependent Axonal Plasticity in Sensory Systems. *Neuroscience*. **368**, pp.268–282.
- Jefferis, G.S.X.E., Potter, C.J., Chan, A.M., Marin, E.C., Rohlffing, T., Maurer, C.R. and Luo, L. 2007. Comprehensive Maps of *Drosophila* Higher Olfactory Centers: Spatially Segregated Fruit and Pheromone Representation. *Cell*. **128**(6), pp.1187–1203.
- Jefferis, G.S.X.E., Vyas, R.M., Berdnik, D., Ramaekers, A., Stocker, R.F., Tanaka, N.K., Ito, K. and Luo, L. 2004. Developmental origin of wiring specificity in the olfactory system of *Drosophila*. *Development*. **131**(1), pp.117–130.
- Jenett, A., Rubin, G.M., Ngo, T.-T.B., Shepherd, D., Murphy, C., Dionne, H., Pfeiffer, B.D., Cavallaro, A., Hall, D., Jeter, J., Iyer, N., Fetter, D., Hausenfluck, J.H., Peng, H., Trautman, E.T., Svirskas, R.R., Myers, E.W., Iwinski, Z.R., Aso, Y., DePasquale, G.M., Enos, A., Hulamm, P., Lam, S.C.B., Li, H.-H., Lavery, T.R., Long, F., Qu, L., Murphy, S.D., Rokicki, K., Safford, T., Shaw, K., Simpson, J.H., Sowell, A., Tae, S., Yu, Y. and Zugates, C.T. 2012. A GAL4-Driver Line Resource for *Drosophila* Neurobiology. *Cell Reports*. **2**(4), pp.991–1001.
- Jiang, Y., Lee, A., Chen, J., Cadene, M., Chait, B.T. and MacKinnon, R. 2002. The open pore conformation of potassium channels. *Nature*. **417**(6888), pp.523–526.
- Jiang, Y., Lee, A., Chen, J., Ruta, V., Cadene, M., Chait, B.T. and MacKinnon, R. 2003.

- X-ray structure of a voltage-dependent K⁺ channel. *Nature*. **423**(6935), pp.33–41.
- Jinek, M., Chylinski, K., Fonfara, I., Hauer, M., Doudna, J.A. and Charpentier, E. 2012. A Programmable Dual-RNA–Guided DNA Endonuclease in Adaptive Bacterial Immunity. *Science*. **337**(6096), pp.816–821.
- Jurkat-Rott, K., Lehmann-Horn, F., Elbaz, A., Heine, R., Gregg, R.G., Hogan, K., Powers, P.A., Laple, P., Vale-Santos, J.E., Weissenbach, J. and Fontaine, B. 1994. A calcium channel mutation causing hypokalemic periodic paralysis. *Human Molecular Genetics*. **3**(8), pp.1415–1419.
- Kamb, A., Iverson, L.E. and Tanouye, M.A. 1987. Molecular characterization of Shaker, a *Drosophila* gene that encodes a potassium channel. *Cell*. **50**(3), pp.405–413.
- Kanerva, P. 1988. *Sparse distributed memory*. MIT Press, Cambridge, MA.
- Kaplan, D.I., Isom, L.L. and Petrou, S. 2016. Role of sodium channels in epilepsy. *Cold Spring Harbor Perspectives in Medicine*. **6**(6), pp.1–17.
- Kaplan, W.D. and Trout, W.E. 1969. The behavior of four neurological mutants of *Drosophila*. *Genetics*. **61**(2), pp.399–409.
- Kazama, H. and Wilson, R.I. 2008. Homeostatic Matching and Nonlinear Amplification at Identified Central Synapses. *Neuron*. **58**(3), pp.401–413.
- Keck, T., Hübener, M. and Bonhoeffer, T. 2017. Interactions between synaptic homeostatic mechanisms: an attempt to reconcile BCM theory, synaptic scaling, and changing excitation/inhibition balance. *Current Opinion in Neurobiology*. **43**, pp.87–93.
- Keck, T., Toyozumi, T., Chen, L., Doiron, B., Feldman, D.E., Fox, K., Gerstner, W., Haydon, P.G., Hübener, M., Lee, H.-K., Lisman, J.E., Rose, T., Sengpiel, F., Stellwagen, D., Stryker, M.P., Turrigiano, G.G. and van Rossum, M.C. 2017. Integrating Hebbian and homeostatic plasticity: the current state of the field and future research directions. *Philosophical Transactions of the Royal Society B: Biological Sciences*. **372**(1715), p.20160158.
- Keene, A.C. and Waddell, S. 2007. *Drosophila* olfactory memory: single genes to complex neural circuits. *Nature Reviews Neuroscience*. **8**(5), pp.341–354.
- Kelsch, W., Lin, C.-W., Mosley, C.P. and Lois, C. 2009. A Critical Period for Activity-Dependent Synaptic Development during Olfactory Bulb Adult Neurogenesis. *The Journal of Neuroscience*. **29**(38), pp.11852–11858.
- Kelsch, W., Mosley, C.P., Lin, C.-W. and Lois, C. 2007. Distinct Mammalian Precursors Are Committed to Generate Neurons with Defined Dendritic Projection Patterns J.

- Macklis, ed. *PLoS Biology*. **5**(11), p.e300.
- Kim, E.Z., Vienne, J., Rosbash, M. and Griffith, L.C. 2017. Nonreciprocal homeostatic compensation in *Drosophila* potassium channel mutants. *Journal of Neurophysiology*. **117**(6), pp.2125–2136.
- Kise, Y., Kasuya, G., Okamoto, H.H., Yamanouchi, D., Kobayashi, K., Kusakizako, T., Nishizawa, T., Nakajo, K. and Nureki, O. 2021. Structural basis of gating modulation of Kv4 channel complexes. *Nature*. **599**(7883), pp.158–164.
- Koishi, R., Xu, H., Ren, D., Navarro, B., Spiller, B.W., Shi, Q. and Clapham, D.E. 2004. A Superfamily of Voltage-gated Sodium Channels in Bacteria. *Journal of Biological Chemistry*. **279**(10), pp.9532–9538.
- Koon, A.C., Ashley, J., Barria, R., DasGupta, S., Brain, R., Waddell, S., Alkema, M.J. and Budnik, V. 2010. Autoregulatory and paracrine control of synaptic and behavioral plasticity by octopaminergic signaling. *Nature Neuroscience*. **14**(2), pp.190–199.
- Kovačević, N., Henderson, J.T., Chan, E., Lifshitz, N., Bishop, J., Evans, A.C., Henkelman, R.M. and Chen, X.J. 2005. A Three-dimensional MRI Atlas of the Mouse Brain with Estimates of the Average and Variability. *Cerebral Cortex*. **15**(5), pp.639–645.
- Kuang, Q., Purhonen, P. and Hebert, H. 2015. Structure of potassium channels. *Cellular and Molecular Life Sciences*. **72**(19), pp.3677–3693.
- Kuba, H., Adachi, R. and Ohmori, H. 2014. Activity-dependent and activity-independent development of the axon initial segment. *Journal of Neuroscience*. **34**(9), pp.3443–3453.
- Kuba, H., Yamada, R., Ishiguro, G. and Adachi, R. 2015. Redistribution of Kv1 and Kv7 enhances neuronal excitability during structural axon initial segment plasticity. *Nature Communications*. **6**(May).
- Kurtovic, A., Widmer, A. and Dickson, B.J. 2007. A single class of olfactory neurons mediates behavioural responses to a *Drosophila* sex pheromone. *Nature*. **446**(7135), pp.542–546.
- Kuzmenkin, A., Bezanilla, F. and Correa, A.M. 2004. Gating of the bacterial sodium channel, NaChBac: Voltage-dependent charge movement and gating currents. *Journal of General Physiology*. **124**(4), pp.349–356.
- Lai, S.-L. and Lee, T. 2006. Genetic mosaic with dual binary transcriptional systems in *Drosophila*. *Nature Neuroscience*. **9**(5), pp.703–709.

- Lee, D. and O'Dowd, D.K. 1999. Fast excitatory synaptic transmission mediated by nicotinic acetylcholine receptors in *Drosophila* neurons. *Journal of Neuroscience*. **19**(13), pp.5311–5321.
- Lee, H., Wang, H., Jen, J.C., Sabatti, C., Baloh, R.W. and Nelson, S.F. 2004. A novel mutation in KCNA1 causes episodic ataxia without myokymia. *Human Mutation*. **24**(6), pp.536–536.
- Lee, T., Lee, A. and Luo, L. 1999. Development of the *Drosophila* mushroom bodies: Sequential generation of three distinct types of neurons from a neuroblast. *Development*. **126**(18), pp.4065–4076.
- Lezmy, J., Lipinsky, M., Khrapunsky, Y., Patrich, E., Shalom, L., Peretz, A., Fleidervish, I.A. and Attali, B. 2017. M-current inhibition rapidly induces a unique CK2-dependent plasticity of the axon initial segment. *Proceedings of the National Academy of Sciences of the United States of America*. **114**(47), pp.E10234–E10243.
- Lin, A.C., Bygrave, A.M., de Calignon, A., Lee, T. and Miesenböck, G. 2014. Sparse, decorrelated odor coding in the mushroom body enhances learned odor discrimination. *Nature Neuroscience*. **17**(4), pp.559–568.
- Lin, C.-W., Sim, S., Ainsworth, A., Okada, M., Kelsch, W. and Lois, C. 2010. Genetically Increased Cell-Intrinsic Excitability Enhances Neuronal Integration into Adult Brain Circuits. *Neuron*. **65**(1), pp.32–39.
- Lin, W.H., Günay, C., Marley, R., Prinz, A.A. and Baines, R.A. 2012. Activity-dependent alternative splicing increases persistent Sodium current and promotes seizure. *Journal of Neuroscience*. **32**(21), pp.7267–7277.
- Lin, W.H., Wright, D.E., Muraro, N.I. and Baines, R.A. 2009. Alternative splicing in the voltage-gated sodium channel DmNav regulates activation, inactivation, and persistent current. *Journal of Neurophysiology*. **102**(3), pp.1994–2006.
- Liu, X. and Davis, R.L. 2009. The GABAergic anterior paired lateral neuron suppresses and is suppressed by olfactory learning. *Nature Neuroscience*. **12**(1), pp.53–59.
- Luan, H. 2006. Functional Dissection of a Neuronal Network Required for Cuticle Tanning and Wing Expansion in *Drosophila*. *Journal of Neuroscience*. **26**(2), pp.573–584.
- Luan, H., Lemon, W.C., Peabody, N.C., Pohl, J.B., Zelensky, P.K., Wang, D., Nitabach, M.N., Holmes, T.C. and White, B.H. 2006. Functional Dissection of a Neuronal Network Required for Cuticle Tanning and Wing Expansion in *Drosophila*. *The*

- Journal of Neuroscience*. **26**(2), pp.573–584.
- Lyons, M.R. and West, A.E. 2011. Mechanisms of specificity in neuronal activity-regulated gene transcription. *Progress in Neurobiology*. **94**(3), pp.259–295.
- MacKinnon, R. 2003. Potassium channels. *FEBS Letters*. **555**(1), pp.62–65.
- MacLean, J.N., Zhang, Y., Johnson, B.R. and Harris-Warrick, R.M. 2003. Activity-independent homeostasis in rhythmically active neurons. *Neuron*. **37**(1), pp.109–120.
- Maffei, A. and Turrigiano, G.G. 2008. Multiple Modes of Network Homeostasis in Visual Cortical Layer 2/3. *Journal of Neuroscience*. **28**(17), pp.4377–4384.
- Malin, S.A. and Nerbonne, J.M. 2002. Delayed Rectifier K⁺ Currents, I_K , Are Encoded by Kv2 α -Subunits and Regulate Tonic Firing in Mammalian Sympathetic Neurons. *The Journal of Neuroscience*. **22**(23), pp.10094–10105.
- Marban, E., Yamagishi, T. and Tomaselli, G.F. 1998. Structure and function of voltage-gated sodium channels. *Journal of Physiology*. **508**(3), pp.647–657.
- Marder, E. 2011. Variability, compensation, and modulation in neurons and circuits. *Proceedings of the National Academy of Sciences*. **108**, pp.15542–15548.
- Marder, E. and Goaillard, J.-M. 2006. Variability, compensation and homeostasis in neuron and network function. *Nature Reviews Neuroscience*. **7**(7), pp.563–574.
- Marder, E. and Prinz, A.A. 2002. Modeling stability in neuron and network function: The role of activity in homeostasis. *BioEssays*. **24**(12), pp.1145–1154.
- Matthews, K.A., Kaufman, T.C. and Gelbart, W.M. 2005. Research resources for *Drosophila*: the expanding universe. *Nature Reviews Genetics*. **6**(3), pp.179–193.
- Mattila, J., Bremer, A., Ahonen, L., Kostianen, R. and Puig, O. 2009. *Drosophila* FoxO Regulates Organism Size and Stress Resistance through an Adenylate Cyclase. *Molecular and Cellular Biology*. **29**(19), pp.5357–5365.
- McGuire, S.E., Le, P.T., Osborn, A.J., Matsumoto, K. and Davis, R.L. 2003. Spatiotemporal Rescue of Memory Dysfunction in *Drosophila*. *Science*. **302**(5651), pp.1765–1768.
- McGuire, S.E., Mao, Z. and Davis, R.L. 2004. Spatiotemporal Gene Expression Targeting with the TARGET and Gene-Switch Systems in *Drosophila*. *Science's STKE*. **2004**(220).
- Mee, C.J., Pym, E.C.G., Moffat, K.G. and Baines, R.A. 2004. Regulation of neuronal excitability through pumilio-dependent control of a sodium channel gene. *Journal of Neuroscience*. **24**(40), pp.8695–8703.

- Min, S., Ai, M., Shin, S.A. and Suh, G.S.B. 2013. Dedicated olfactory neurons mediating attraction behavior to ammonia and amines in *Drosophila*. *Proceedings of the National Academy of Sciences*. **110**(14).
- Misonou, H., Mohapatra, D.P., Park, E.W., Leung, V., Zhen, D., Misonou, K., Anderson, A.E. and Trimmer, J.S. 2004. Regulation of ion channel localization and phosphorylation by neuronal activity. *Nature Neuroscience*. **7**(7), pp.711–718.
- Miyawaki, A., Llopis, J., Heim, R., McCaffery, J.M., Adams, J.A., Ikura, M. and Tsien, R.Y. 1997. Fluorescent indicators for Ca²⁺ based on green fluorescent proteins and calmodulin. *Nature*. **388**(6645), pp.882–887.
- Miyazaki, M., Ohyama, K., Dunlap, D.Y. and Matsumura, F. 1996. Cloning and sequencing of the para-type sodium channel gene from susceptible and kdr-resistant German cockroaches (*Blattella germanica*) and house fly (*Musca domestica*). *Molecular and General Genetics*. **252**(1–2), pp.61–68.
- Mombaerts, P., Wang, F., Dulac, C., Chao, S.K., Nemes, A., Mendelsohn, M., Edmondson, J. and Axel, R. 1996. Visualizing an olfactory sensory map. *Cell*. **87**(4), pp.675–686.
- Moreaux, L. and Laurent, G. 2007. Estimating firing rates from calcium signals in locust projection neurons in vivo. *Frontiers in neural circuits*. **1**, p.2.
- Mosca, T.J., Carrillo, R.A., White, B.H. and Keshishian, H. 2005. Dissection of synaptic excitability phenotypes by using a dominant-negative Shaker K⁺ channel subunit. *Proceedings of the National Academy of Sciences*. **102**(9), pp.3477–3482.
- Murakoshi, H. and Trimmer, J.S. 1999. Identification of the Kv2.1 K⁺ Channel as a Major Component of the Delayed Rectifier K⁺ Current in Rat Hippocampal Neurons. *The Journal of Neuroscience*. **19**(5), pp.1728–1735.
- Murthy, M., Fiete, I. and Laurent, G. 2008. Testing Odor Response Stereotypy in the *Drosophila* Mushroom Body. *Neuron*. **59**(6), pp.1009–1023.
- Nakai, J., Ohkura, M. and Imoto, K. 2001. A high signal-to-noise Ca²⁺ probe composed of a single green fluorescent protein. *Nature Biotechnology*. **19**(2), pp.137–141.
- Neher, E. 1995. The use of fura-2 for estimating Ca buffers and Ca fluxes. *Neuropharmacology*. **34**(11), pp.1423–1442.
- Neher, E. and Sakaba, T. 2008. Multiple Roles of Calcium Ions in the Regulation of Neurotransmitter Release. *Neuron*. **59**(6), pp.861–872.
- Nitabach, M.N., Wu, Y., Sheeba, V., Lemon, W.C., Strumbos, J., Zelensky, P.K., White, B.H. and Holmes, T.C. 2006. Electrical Hyperexcitation of Lateral Ventral

- Pacemaker Neurons Desynchronizes Downstream Circadian Oscillators in the Fly Circadian Circuit and Induces Multiple Behavioral Periods. *The Journal of Neuroscience*. **26**(2), pp.479–489.
- Nurani, G., Radford, M., Charalambous, K., O'Reilly, A.O., Cronin, N.B., Haque, S. and Wallace, B.A. 2008. Tetrameric bacterial sodium channels: Characterization of structure, stability, and drug binding. *Biochemistry*. **47**(31), pp.8114–8121.
- Oleskevich, S. 1999. Cholinergic synaptic transmission in insect mushroom bodies in vitro. *Journal of Neurophysiology*. **82**(2), pp.1091–1096.
- Olson, R.O.D., Liu, Z., Nomura, Y., Song, W. and Dong, K. 2008. Molecular and functional characterization of voltage-gated sodium channel variants from *Drosophila melanogaster*. *Insect Biochemistry and Molecular Biology*. **38**(5), pp.604–610.
- Ophoff, R.A., Terwindt, G.M., Vergouwe, M.N., van Eijk, R., Oefner, P.J., Hoffman, S.M., Lamerdin, J.E., Mhrenweiser, H.W., Bulman, D.E., Ferrari, M., Haan, J., Lindhout, D., van Ommen, G.-J.B., Hofker, M.H., Ferrari, M.D. and Frants, R.R. 1996. Familial Hemiplegic Migraine and Episodic Ataxia Type-2 Are Caused by Mutations in the Ca²⁺ Channel Gene CACNL1A4. *Cell*. **87**(3), pp.543–552.
- Orrenius, S., Zhivotovsky, B. and Nicotera, P. 2003. Regulation of cell death: the calcium–apoptosis link. *Nature Reviews Molecular Cell Biology*. **4**(7), pp.552–565.
- Ovchinnikov, Y.A. 1981. Ion Channels of Excitable Membranes *In: Science and Scientists*. Sunderland: Sinauer Associates Inc., pp.235–241.
- Pak, J., Maniar, J.M., Mello, C.C. and Fire, A. 2012. Protection from Feed-Forward Amplification in an Amplified RNAi Mechanism. *Cell*. **151**(4), pp.885–899.
- Pak, M.D., Baker, K., Covarrubias, M., Butler, A., Ratcliffe, A. and Salkoff, L. 1991. mShal, a subfamily of A-type K⁺ channel cloned from mammalian brain. *Proceedings of the National Academy of Sciences*. **88**(10), pp.4386–4390.
- Parisky, K.M., Agosto, J., Pulver, S.R., Shang, Y., Kuklin, E., Hodge, J.J.L., Kang, K., Liu, X., Garrity, P.A., Rosbash, M. and Griffith, L.C. 2008. PDF Cells Are a GABA-Responsive Wake-Promoting Component of the *Drosophila* Sleep Circuit. *Neuron*. **60**(4), pp.672–682.
- Park, K.-S., Mohapatra, D.P., Misonou, H. and Trimmer, J.S. 2006. Graded Regulation of the Kv2.1 Potassium Channel by Variable Phosphorylation. *Science*. **313**(5789), pp.976–979.
- Peabody, N.C., Diao, F., Luan, H., Wang, H., Dewey, E.M., Honegger, H.W. and White,

- B.H. 2008. Bursicon functions within the *Drosophila* CNS to modulate wing expansion behavior, hormone secretion, and cell death. *Journal of Neuroscience*. **28**(53), pp.14379–14391.
- Peabody, N.C., Pohl, J.B., Diao, F., Vreede, A.P., Sandstrom, D.J., Wang, H., Zelensky, P.K. and White, B.H. 2009. Characterization of the decision network for wing expansion in *drosophila* using targeted expression of the TRPM8 channel. *Journal of Neuroscience*. **29**(11), pp.3343–3353.
- Peng, I.F. and Wu, C.F. 2007. Differential contributions of Shaker and Shab K⁺ currents to neuronal firing patterns in *Drosophila*. *Journal of Neurophysiology*. **97**(1), pp.780–794.
- Perez-Orive, J., Mazor, O., Turner, G.C., Cassenaer, S., Wilson, R.I. and Laurent, G. 2002. Oscillations and Sparsening of Odor Representations in the Mushroom Body. *Science*. **297**(5580), pp.359–365.
- Perkins, L.A., Holderbaum, L., Tao, R., Hu, Y., Sopko, R., McCall, K., Yang-Zhou, D., Flockhart, I., Binari, R., Shim, H.S., Miller, A., Housden, A., Foos, M., Randkelv, S., Kelley, C., Namgyal, P., Villalta, C., Liu, L.P., Jiang, X., Huan-Huan, Q., Wang, X., Fujiyama, A., Toyoda, A., Ayers, K., Blum, A., Czech, B., Neumuller, R., Yan, D., Cavallaro, A., Hibbard, K., Hall, D., Cooley, L., Hannon, G.J., Lehmann, R., Parks, A., Mohr, S.E., Ueda, R., Kondo, S., Ni, J.Q. and Perrimon, N. 2015. The transgenic RNAi project at Harvard medical school: Resources and validation. *Genetics*. **201**(3), pp.843–852.
- Pilauri, V., Bewley, M., Diep, C. and Hopper, J. 2005. Gal80 dimerization and the yeast GAL gene switch. *Genetics*. **169**(4), pp.1903–1914.
- Pimentel, D., Donlea, J.M., Talbot, C.B., Song, S.M., Thurston, A.J.F. and Miesenböck, G. 2016. Operation of a homeostatic sleep switch. *Nature*. **536**(7616), pp.333–337.
- Ping, Y., Waro, G., Licursi, A., Smith, S., Vo-Ba, D.-A. and Tsunoda, S. 2011. Shal/Kv4 Channels Are Required for Maintaining Excitability during Repetitive Firing and Normal Locomotion in *Drosophila*. B. D. McCabe, ed. *PLoS ONE*. **6**(1), p.e16043.
- Pongs, O., Kecskemethy, N., Müller, R., Krah-Jentgens, I., Baumann, A., Kiltz, H.H., Canal, I., Llamazares, S. and Ferrus, A. 1988. Shaker encodes a family of putative potassium channel proteins in the nervous system of *Drosophila*. *The EMBO Journal*. **7**(4), pp.1087–1096.
- Poo, C. and Isaacson, J.S. 2009. Odor Representations in Olfactory Cortex: ‘Sparse’ Coding, Global Inhibition, and Oscillations. *Neuron*. **62**(6), pp.850–861.

- Porter, J.T. and Sepulveda-Orengo, M.T. 2020. Learning-induced intrinsic and synaptic plasticity in the rodent medial prefrontal cortex. *Neurobiology of Learning and Memory*. **169**, p.107117.
- Potter, C.J. and Luo, L. 2011. Using the Q system in *Drosophila melanogaster*. *Nature Protocols*. **6**(8), pp.1105–1120.
- Powl, A.M., O'Reilly, A.O., Miles, A.J. and Wallace, B.A. 2010. Synchrotron radiation circular dichroism spectroscopy-defined structure of the C-terminal domain of NaChBac and its role in channel assembly. *Proceedings of the National Academy of Sciences of the United States of America*. **107**(32), pp.14064–14069.
- Prestori, F., Mapelli, L. and D'Angelo, E. 2019. Diverse Neuron Properties and Complex Network Dynamics in the Cerebellar Cortical Inhibitory Circuit. *Frontiers in Molecular Neuroscience*. **12**.
- Pribbenow, C., Chen, Y.-C., Heim, M.-M., Laber, D., Reubold, S., Reynolds, E., Balles, I., Fernández-d V Alquicira, T., Suárez-Grimalt, R., Scheunemann, L., Rauch, C., Matkovic, T., Rösner, J., Lichtner, G., Jagannathan, S.R. and Oswald, D. 2022. Postsynaptic plasticity of cholinergic synapses underlies the induction and expression of appetitive and familiarity memories in *Drosophila*. *eLife*. **11**.
- Prinz, A.A., Bucher, D. and Marder, E. 2004. Similar network activity from disparate circuit parameters. *Nature Neuroscience*. **7**(12), pp.1345–1352.
- Raghuram, V., Werginz, P. and Fried, S.I. 2019. Scaling of the AIS and Somatodendritic Compartments in α S RGCs. *Frontiers in Cellular Neuroscience*. **13**.
- Ravenscroft, T.A., Janssens, J., Lee, P.-T., Tepe, B., Marcogliese, P.C., Makhzami, S., Holmes, T.C., Aerts, S. and Bellen, H.J. 2020. *Drosophila* Voltage-Gated Sodium Channels Are Only Expressed in Active Neurons and Are Localized to Distal Axonal Initial Segment-like Domains. *The Journal of Neuroscience*. **40**(42), pp.7999–8024.
- Reiter, L.T., Potocki, L., Chien, S., Gribskov, M. and Bier, E. 2001. A Systematic Analysis of Human Disease-Associated Gene Sequences In *Drosophila melanogaster*. *Genome Research*. **11**(6), pp.1114–1125.
- Remme, C.A. and Bezzina, C.R. 2010. Sodium channel (Dys)function and cardiac arrhythmias. *Cardiovascular Therapeutics*. **28**(5), pp.287–294.
- Ren, D., Navarro, B., Xu, H., Yue, L., Shi, Q. and Clapham, D.E. 2001. A Prokaryotic Voltage-Gated Sodium Channel. *Science*. **294**(5550), pp.2372–2375.
- Restifo, L. and White, K. 1990. Molecular and Genetic Approaches to Neurotransmitter and Neuromodulator Systems in *Drosophila*. *Advances in Insect Physiology*. **22**,

pp.115–219.

- Rho, J.M., Szot, P., Tempel, B.L. and Schwartzkroin, P.A. 1999. Developmental Seizure Susceptibility of Kv1.1 Potassium Channel Knockout Mice. *Developmental Neuroscience*. **21**(3–5), pp.320–327.
- Richardson, J., Blunck, R., Ge, P., Selvin, P.R., Bezanilla, F., Papazian, D.M. and Correa, A.M. 2006. Distance measurements reveal a common topology of prokaryotic voltage-gated ion channels in the lipid bilayer. *Proceedings of the National Academy of Sciences of the United States of America*. **103**(43), pp.15865–15870.
- Robertson, H.M., Warr, C.G. and Carlson, J.R. 2003. Molecular evolution of the insect chemoreceptor gene superfamily in *Drosophila melanogaster*. *Proceedings of the National Academy of Sciences*. **100**(suppl_2), pp.14537–14542.
- Rogero, O., Hämmerle, B. and Tejedor, F.J. 1997. Diverse expression and distribution of Shaker potassium channels during the development of the *Drosophila* nervous system. *Journal of Neuroscience*. **17**(13), pp.5108–5118.
- Rosenthal, J.S. and Yuan, Q. 2021. Constructing and Tuning Excitatory Cholinergic Synapses: The Multifaceted Functions of Nicotinic Acetylcholine Receptors in *Drosophila* Neural Development and Physiology. *Frontiers in Cellular Neuroscience*. **15**.
- Russell, J.T. 2011. Imaging calcium signals in vivo : a powerful tool in physiology and pharmacology. *British Journal of Pharmacology*. **163**(8), pp.1605–1625.
- Russo, A.F. 2017. Overview of Neuropeptides: Awakening the Senses? *Headache: The Journal of Head and Face Pain*. **57**, pp.37–46.
- Salkoff, L., Baker, K., Butler, A., Covarrubias, M., Pak, M.D. and Wei, A. 1992. An essential 'set' of K⁺ channels conserved in flies, mice and humans. *Trends in Neurosciences*. **15**(5), pp.161–166.
- Salkoff, L. and Wyman, R. 1981. Genetic modification of potassium channels in *Drosophila* Shaker mutants. *Nature*. **293**(5829), pp.228–230.
- Salvaterra, P.M. and McCaman, R.E. 1985. Choline acetyltransferase and acetylcholine levels in *Drosophila melanogaster*: A study using two temperature-sensitive mutants. *Journal of Neuroscience*. **5**(4), pp.903–910.
- Schulz, D.J., Goillard, J.-M. and Marder, E. 2006. Variable channel expression in identified single and electrically coupled neurons in different animals. *Nature Neuroscience*. **9**(3), pp.356–362.

- Sheeba, V., Gu, H., Sharma, V.K., O'Dowd, D.K. and Holmes, T.C. 2008. Circadian- and Light-Dependent Regulation of Resting Membrane Potential and Spontaneous Action Potential Firing of *Drosophila* Circadian Pacemaker Neurons. *Journal of Neurophysiology*. **99**(2), pp.976–988.
- Shimomura, T., Irie, K., Nagura, H., Imai, T. and Fujiyoshi, Y. 2011. Arrangement and mobility of the voltage sensor domain in prokaryotic voltage-gated sodium channels. *Journal of Biological Chemistry*. **286**(9), pp.7409–7417.
- Sim, S., Antolin, S., Lin, C.-W., Lin, Y. and Lois, C. 2013. Increased Cell-Intrinsic Excitability Induces Synaptic Changes in New Neurons in the Adult Dentate Gyrus That Require *Npas4*. *The Journal of Neuroscience*. **33**(18), pp.7928–7940.
- Singh, A. and Singh, S. 1999. Unmasking of a novel potassium current in *Drosophila* by a mutation and drugs. *Journal of Neuroscience*. **19**(16), pp.6838–6843.
- Singh, B., Ogiwara, I., Kaneda, M., Tokonami, N., Mazaki, E., Baba, K., Matsuda, K., Inoue, Y. and Yamakawa, K. 2006. A Kv4.2 truncation mutation in a patient with temporal lobe epilepsy. *Neurobiology of Disease*. **24**(2), pp.245–253.
- Singh, M., Miura, P. and Renden, R. 2018. Age-related defects in short-term plasticity are reversed by acetyl-L-carnitine at the mouse calyx of Held. *Neurobiology of Aging*. **67**, pp.108–119.
- Sjulson, L. and Miesenböck, G. 2007. Optical Recording of Action Potentials and Other Discrete Physiological Events: A Perspective from Signal Detection Theory. *Physiology*. **22**(1), pp.47–55.
- Skou, J.C. 1998. The identification of the sodium pump. *Chem.Int.Ed.* **24**(4–5), pp.436–451.
- Smith, P., Buhl, E., Tsaneva-Atanasova, K. and Hodge, J. 2019. Shaw and Shal voltage-gated potassium channels mediate circadian changes in *Drosophila* clock neuron excitability. *Journal of Physiology*. **597**(23), pp.5707–5722.
- Smith, S.J. and Augustine, G.J. 1988. Calcium ions, active zones and synaptic transmitter release. *Trends in Neurosciences*. **11**(10), pp.458–464.
- Spillane, J., Kullmann, D.M. and Hanna, M.G. 2016. Genetic neurological channelopathies: Molecular genetics and clinical phenotypes. *Journal of Neurology, Neurosurgery and Psychiatry*. **87**(1), pp.37–48.
- Stafstrom, C.E. and Carmant, L. 2015. Seizures and epilepsy: An overview for neuroscientists. *Cold Spring Harbor Perspectives in Biology*. **7**(5), pp.1–19.
- Stettler, D.D. and Axel, R. 2009. Representations of Odor in the Piriform Cortex. *Neuron*.

63(6), pp.854–864.

- Steuber, V., Mittmann, W., Hoebeek, F.E., Silver, R.A., De Zeeuw, C.I., Häusser, M. and De Schutter, E. 2007. Cerebellar LTD and Pattern Recognition by Purkinje Cells. *Neuron*. **54**(1), pp.121–136.
- Stocker, M., Stuhmer, W., Wittka, R., Wang, X., Muller, R., Ferrus, A. and Pongs, O. 1990. Alternative shaker transcripts express either rapidly inactivating or noninactivating K⁺ channels. *Proceedings of the National Academy of Sciences of the United States of America*. **87**(22), pp.8903–8907.
- Stocker, R.F. 2001. Drosophila as a focus in olfactory research: Mapping of olfactory sensilla by fine structure, odor specificity, odorant receptor expression, and central connectivity. *Microscopy Research and Technique*. **55**(5), pp.284–296.
- Stocker, R.F., Heimbeck, G., Gendre, N. and De Belle, J.S. 1997. Neuroblast ablation in Drosophila P[GAL4] lines reveals origins of olfactory interneurons. *Journal of Neurobiology*. **32**(5), pp.443–456.
- Stosiek, C., Garaschuk, O., Holthoff, K. and Konnerth, A. 2003. In vivo two-photon calcium imaging of neuronal networks. *Proceedings of the National Academy of Sciences of the United States of America*. **100**(12), pp.7319–7324.
- Strong, M., Chandy, K.G. and Gutman, G.A. 1993. Molecular evolution of voltage-sensitive ion channel genes: On the origins of electrical excitability. *Molecular Biology and Evolution*. **10**(1), pp.221–242.
- Stühmer, W., Conti, F., Suzuki, H., Wang, X. D., Noda, M., Yahagi, N., Kubo, H. and Numa, S. 1989. Structural parts involved in activation and inactivation of the sodium channel. *Nature*. **339**, p.597603.
- Suh, G.S.B., Wong, A.M., Hergarden, A.C., Wang, J.W., Simon, A.F., Benzer, S., Axel, R. and Anderson, D.J. 2004. A single population of olfactory sensory neurons mediates an innate avoidance behaviour in Drosophila. *Nature*. **431**(7010), pp.854–859.
- Swensen, A.M. and Bean, B. 2005. Robustness of Burst Firing in Dissociated Purkinje Neurons with Acute or Long-Term Reductions in Sodium Conductance. *Journal of Neuroscience*. **25**(14), pp.3509–3520.
- van Swinderen, B. and Greenspan, R.J. 2005. Flexibility in a Gene Network Affecting a Simple Behavior in Drosophila melanogaster. *Genetics*. **169**(4), pp.2151–2163.
- Tanaka, N.K., Tanimoto, H. and Ito, K. 2008. Neuronal assemblies of the Drosophila mushroom body. *The Journal of Comparative Neurology*. **508**(5), pp.711–755.

- Tanouye, M.A. and Ferrus, A. 1985. Action Potentials in Normal and Shaker Mutant *Drosophila*. *Journal of Neurogenetics*. **2**(4), pp.253–271.
- Tanouye, M.A., Ferrus, A. and Fujita, S.C. 1981. Abnormal action potentials associated with the *Shaker* complex locus of *Drosophila*. *Proceedings of the National Academy of Sciences*. **78**(10), pp.6548–6552.
- Telenczuk, M., Fontaine, B. and Brette, R. 2017. The basis of sharp spike onset in standard biophysical models M. J. Chacron, ed. *PLOS ONE*. **12**(4), p.e0175362.
- Tempel, B.L., Papazian, D.M., Schwarz, T.L., Jan, Y.N. and Jan, L.Y. 1987. Sequence of a Probable Potassium Channel Component Encoded at *Shaker* Locus of *Drosophila*. *Science*. **237**(4816), pp.770–775.
- Tickoo, S. 2002. *Drosophila melanogaster* as a model system for drug discovery and pathway screening. *Current Opinion in Pharmacology*. **2**(5), pp.555–560.
- Troy Littleton and Barry Ganetzky 2000. Ion Channels and Synaptic Organization: Analysis of the *Drosophila* Genome. *Neuron*. **26**, pp.35–43.
- Trunova, S., Baek, B. and Giniger, E. 2011. Cdk5 Regulates the Size of an Axon Initial Segment-Like Compartment in Mushroom Body Neurons of the *Drosophila* Central Brain. *Journal of Neuroscience*. **31**(29), pp.10451–10462.
- Tsunoda, S and Salkoff, L. 1995. Genetic analysis of *Drosophila* neurons: *Shal*, *Shaw*, and *Shab* encode most embryonic potassium currents. *The Journal of Neuroscience*. **15**(3), pp.1741–1754.
- Tsunoda, S. and Salkoff, L. 1995. The major delayed rectifier in both *Drosophila* neurons and muscle is encoded by *Shab*. *Journal of Neuroscience*. **15**(7 II), pp.5209–5221.
- Turner, G.C., Bazhenov, M. and Laurent, G. 2008a. Olfactory representations by *Drosophila* mushroom body neurons. *Journal of Neurophysiology*. **99**(2), pp.734–746.
- Turner, G.C., Bazhenov, M. and Laurent, G. 2008b. Olfactory Representations by *Drosophila* Mushroom Body Neurons. *Journal of Neurophysiology*. **99**(2), pp.734–746.
- Turrigiano, G. 2011. Too Many Cooks? Intrinsic and Synaptic Homeostatic Mechanisms in Cortical Circuit Refinement. *Annual Review of Neuroscience*. **34**(1), pp.89–103.
- Turrigiano, G., Abbott, L.F. and Marder, E. 1994. Activity-Dependent Changes in the Intrinsic Properties of Cultured Neurons. *Science*. **264**(5161), pp.974–977.
- Turrigiano, G.G. 2008. The Self-Tuning Neuron: Synaptic Scaling of Excitatory Synapses. *Cell*. **135**(3), pp.422–435.

- Turrigiano, G.G., Leslie, K.R., Desai, N.S., Rutherford, L.C. and Nelson, S.B. 1998. Activity-dependent scaling of quantal amplitude in neocortical neurons. *Nature*. **391**(6670), pp.892–896.
- Turrigiano, G.G. and Nelson, S.B. 2004. Homeostatic plasticity in the developing nervous system. *Nature Reviews Neuroscience*. **5**(2), pp.97–107.
- Ueda, A. and Wu, C.F. 2006. Distinct frequency-dependent regulation of nerve terminal excitability and synaptic transmission by IA and IK potassium channels revealed by *Drosophila* Shaker and Shab mutations. *The Journal of neuroscience : the official journal of the Society for Neuroscience*. **26**(23), pp.6238–6248.
- Vähäsöyrinki, M., Niven, J.E., Hardie, R.C., Weckström, M. and Juusola, M. 2006. Robustness of neural coding in *Drosophila* photoreceptors in the absence of slow delayed rectifier K⁺ channels. *Journal of Neuroscience*. **26**(10), pp.2652–2660.
- Vosshall, L.B., Amrein, H., Morozov, P.S., Rzhetsky, A. and Axel, R. 1999. A Spatial Map of Olfactory Receptor Expression in the *Drosophila* Antenna. *Cell*. **96**(5), pp.725–736.
- Vosshall, L.B. and Stocker, R.F. 2007. Molecular Architecture of Smell and Taste in *Drosophila*. *Annual Review of Neuroscience*. **30**(1), pp.505–533.
- Wang, Y., Chiang, A.-S., Xia, S., Kitamoto, T., Tully, T. and Zhong, Y. 2003. Blockade of Neurotransmission in *Drosophila* Mushroom Bodies Impairs Odor Attraction, but Not Repulsion. *Current Biology*. **13**(21), pp.1900–1904.
- Wang, Y., Guo, H.-F., Pologruto, T.A., Hannan, F., Hakker, I., Svoboda, K. and Zhong, Y. 2004. Stereotyped Odor-Evoked Activity in the Mushroom Body of *Drosophila* Revealed by Green Fluorescent Protein-Based Ca²⁺ Imaging. *The Journal of Neuroscience*. **24**(29), pp.6507–6514.
- Wefelmeyer, W., Cattaert, D. and Burrone, J. 2015. Activity-dependent mismatch between axo-axonic synapses and the axon initial segment controls neuronal output. *Proceedings of the National Academy of Sciences of the United States of America*. **112**(31), pp.9757–9762.
- Wei, A., Covarrubias, M., Butler, A., Baker, K., Pak, M. and Salkoff, L. 1990. K⁺ Current Diversity Is Produced by an Extended Gene Family Conserved in *Drosophila* and Mouse. *Science*. **248**(4955), pp.599–603.
- Werner, J., Arian, J., Bernhardt, I., Ryglewski, S. and Duch, C. 2020. Differential localization of voltage-gated potassium channels during *Drosophila* metamorphosis. *Journal of Neurogenetics*. **34**(1), pp.133–150.

- West, J.W., Pattont, D.E., Scheuer, T., Wang, Y., Goldint, A.L. and Catterall, W.A. 1992. *A cluster of hydrophobic amino acid residues required for fast Na⁺-channel inactivation.*
- White, B.H., Osterwalder, T.P., Yoon, K.S., Joiner, W.J., Whim, M.D., Kaczmarek, L.K. and Keshishian, H. 2001. Neurotechnique Targeted Attenuation of Electrical Activity in Drosophila Using a Genetically Modified K Channel The intrinsic properties of some channel types clearly limit their effectiveness in suppressing activity. Ca²⁺-activated K channels, for examp. *Neuron*. **31**, pp.699–711.
- Wicher, D., Walther, C. and Wicher, C. 2001. Non-synaptic ion channels in insects - Basic properties of currents and their modulation in neurons and skeletal muscles. *Progress in Neurobiology*. **64**(5), pp.431–525.
- Wilson, R.I., Turner, G.C. and Laurent, G. 2004. Transformation of Olfactory Representations in the Drosophila Antennal Lobe. *Science*. **303**(5656), pp.366–370.
- Wu, C.-F., Ganetzky, B., Haugland, F.N. and Liu, A.-X. 1983. Potassium Currents in Drosophila: Different Components Affected by Mutations of Two Genes. *Science*. **220**(4601), pp.1076–1078.
- Wu, Y., Cao, G., Pavlicek, B., Luo, X. and Nitabach, M.N. 2008. Phase Coupling of a Circadian Neuropeptide With Rest/Activity Rhythms Detected Using a Membrane-Tethered Spider Toxin U. Schibler, ed. *PLoS Biology*. **6**(11), p.e273.
- Wulff, P. and Wisden, W. 2005. Dissecting neural circuitry by combining genetics and pharmacology. *Trends in Neurosciences*. **28**(1), pp.44–50.
- Xiao, L. and Scheiffele, P. 2018. Local and long-range circuit elements for cerebellar function. *Current Opinion in Neurobiology*. **48**, pp.146–152.
- Yang, H.H., St-Pierre, F., Sun, X., Ding, X., Lin, M.Z. and Clandinin, T.R. 2016. Subcellular Imaging of Voltage and Calcium Signals Reveals Neural Processing In Vivo. *Cell*. **166**(1), pp.245–257.
- Yang, Y., Liu, N., He, Y., Liu, Y., Ge, L., Zou, L., Song, S., Xiong, W. and Liu, X. 2018. Improved calcium sensor GCaMP-X overcomes the calcium channel perturbations induced by the calmodulin in GCaMP. *Nature Communications*. **9**(1), p.1504.
- Yasuyama, K., Kitamoto, T. and Salvaterra, P.M. 1995. Localization of choline acetyltransferase-expressing neurons in the larval visual system of *Drosophila melanogaster*. *Cell & Tissue Research*. **282**(2), pp.193–202.
- Yu, F.H. and Catterall, W.A. 2003. Overview of the voltage-gated sodium channel

- family. *Genome Biology*. **4**(3).
- Yusuyama, K., Meinertzhagen, I.A. and Schürmann, F.W. 2002. Synaptic organization of the mushroom body calyx in *Drosophila melanogaster*. *Journal of Comparative Neurology*. **445**(3), pp.211–226.
- Zelle, K.M., Lu, B., Pyfrom, S.C. and Ben-Shahar, Y. 2013. The Genetic Architecture of Degenerin/Epithelial Sodium Channels in *Drosophila*. *G3 Genes|Genomes|Genetics*. **3**(3), pp.441–450.
- Zheng, Z., Lauritzen, J.S., Perlman, E., Robinson, C.G., Nichols, M., Milkie, D., Torrens, O., Price, J., Fisher, C.B., Sharifi, N., Calle-Schuler, S.A., Kmecova, L., Ali, I.J., Karsh, B., Trautman, E.T., Bogovic, J.A., Hanslovsky, P., Jefferis, G.S.X.E., Kazhdan, M., Khairy, K., Saalfeld, S., Fetter, R.D. and Bock, D.D. 2018. A Complete Electron Microscopy Volume of the Brain of Adult *Drosophila melanogaster*. *Cell*. **174**(3), pp.730-743.e22.
- Zheng, Z., Li, F., Fisher, C., Ali, I.J., Sharifi, N., Calle-Schuler, S., Hsu, J., Masoodpanah, N., Kmecova, L., Kazimiers, T., Perlman, E., Nichols, M., Li, P.H., Jain, V. and Bock, D.D. 2022. Structured sampling of olfactory input by the fly mushroom body. *Current Biology*. **32**(15), pp.3334-3349.e6.
- Zhou, M., Chen, N., Tian, J., Zeng, J., Zhang, Y., Zhang, X., Guo, J., Sun, J., Li, Yulong, Guo, A. and Li, Yan 2019. Suppression of GABAergic neurons through D2-like receptor secures efficient conditioning in *Drosophila* aversive olfactory learning. *Proceedings of the National Academy of Sciences*. **116**(11), pp.5118–5125.
- Zhu, W., Li, T., Silva, J.R. and Chen, J. 2020. Conservation and divergence in NaChBac and NaV1.7 pharmacology reveals novel drug interaction mechanisms. *Scientific Reports*. **10**(1), p.10730.
- Zimmerman, J.E., Chan, M.T., Lenz, O.T., Keenan, B.T., Maislin, G. and Pack, A.I. 2017. Glutamate Is a Wake-Active Neurotransmitter in *Drosophila melanogaster*. *Sleep*. **40**(2).
- Zucker, R.S. 1999. Calcium- and activity-dependent synaptic plasticity. *Current Opinion in Neurobiology*. **9**(3), pp.305–313.

Figure	Data	Breakdown of conditions	Statistical Test	Comparison (c = con, e = exp)	Age of the flies	Control n	Exp. n	Con. hemis. n	Exp hemis. n	P-value	Significance	Predicted mean	95%	Interaction DF	Interaction F	Interaction P Value	Main effect of obse DF	Main effect of obse F	Main effect of obse P Value	Main effect of genotype DF	Main effect of genotype F	Main effect of genotype P Value						
10	YKCs - Odour responses	IA - Calyx - Odour Resonances	Two-Way ANOVA Sidak multiple comparison	c vs e	Imaged 4 days after eclosion	5	6	8	8	<0.0001	****	IA = 0.7852 DD = 0.2251	0.4507 to 0.6695	1	21.89	P<0.0001	1	13.99	0.0008	1	51.3	P<0.0001						
		IA - Lobe - Odour Resonances	c vs e	9				11	0.0002	***	1		5.722	0.0279	1	0.161	0.0003	1	13.94	0.0015								
		δD - Calyx - Odour Resonances	c vs e	8				8	0.1718	ns																		
		δD - Lobe - Odour Resonances	c vs e	9				11	0.1973	ns																		
		Calyx - Baseline Fluorescence	Unpaired t test - Two-tailed	c vs e				10	10	20	20		0.0017	**	c = 3205 n = 2421	-1253 to -314.6	19	4.88	0.003									
	YKCs - Baseline Responses	Lobes - Baseline Fluorescence	c vs e	20		20	0.0043	**	c = 2105 n = 1191	-1524 to -303.9	19	1.552	0.3467															
		Panel C - Peak odour responses R13F02GAL4>NaChBac	IA - Calyx - Peak Odour Resonances	Two way Anova - Sidak multiple comparison test		c vs e	Imaged 4 days after eclosion	7	7	9	11	0.8666	ns															
			IA - Alpha' - Peak Odour Resonances			c vs e				10	9	0.0833	ns															
			IA - Beta' - Peak Odour Resonances			c vs e				5	9	0.0013	**															
			IA - Alpha - Peak Odour Resonances			c vs e				10	10	0.359	ns															
IA - Beta - Peak Odour Resonances	c vs e		6		9	0.0072				**																		
IA - Gamma - Peak Odour Resonances	c vs e		7		12	0.3595				ns																		
Predicted mean of IA - Control	c vs e								0.8933	0.3401 to 0.6477	5	1.474	0.2047	5	4.076	0.0021	1	36.07	P<0.0001									
Predicted mean of IA - NaChBac	c vs e								0.4115																			
11	Panel D - R13F02GAL4>NaChBac	IA - Calyx - Average Odour Resonances	Two way Anova - Sidak multiple comparison test	c vs e	Imaged 4 days after eclosion	7	7	9	11	0.0918	ns																	
		IA - Alpha' - Average Odour Resonances		c vs e				12	9	0.8999	ns																	
		IA - Beta' - Average Odour Resonances		c vs e				5	9	0.0123	*																	
		IA - Alpha - Average Odour Resonances		c vs e				12	10	0.4237	ns																	
		IA - Beta - Average Odour Resonances		c vs e				6	9	0.0482	*																	
		IA - Gamma - Average Odour Resonances		c vs e				7	12	0.0416	*																	
		Predicted mean of IA - Control		c vs e											0.4297													
		Predicted mean of IA - NaChBac		c vs e											0.1643	0.1734 to 0.3575	5	0.919	0.4719	5	2.752	0.0225	1	32.74	P<0.0001			
		δD - Calyx - Average Odour Resonances		c vs e				9	11	0.8898	ns																	
		δD - Alpha' - Average Odour Resonances		c vs e				12	9	0.1583	ns																	
δD - Beta' - Average Odour Resonances	c vs e	5	9	0.0828	ns																							
δD - Alpha - Average Odour Resonances	c vs e	12	10	0.5912	ns																							
δD - Beta - Average Odour Resonances	c vs e	6	9	>0.9999	ns																							
δD - Gamma - Average Odour Resonances	c vs e	7	12	0.0091	**																							
Predicted mean of δD - Control	c vs e									0.1838																		
Predicted mean of δD - NaChBac	c vs e									0.07811	0.05687 to 0.1545	5	1.241	0.2956	5	1.012	0.4143	1	18.45	P<0.0001								

Figure	Data	Breakdown of conditions	Statistical Test	Comparison (c = con, e = exp)	Age of the flies	Control n	Exp. n	Con. hemis. n	Exp hemis. n	P-value	Significance	Predicted mean	95%	Interaction DF	Interaction F	Interaction P Value	Main effect of obse DF	Main effect of obse F	Main effect of obse P Value	Main effect of genotype DF	Main effect of genotype F	Main effect of genotype P Value						
13	2 Days R13F02GAL4>NaChBac.Gal80ts	IA - Calyx - Peak Odour Resonances	Two way Anova - Šidák multiple comparison test	c vs e	Imaged 2 days after eclosion	13	11	13	8	0.4873	ns																	
		IA - Alpha' - Peak Odour Resonances		c vs e				16	8	0.9877	ns																	
		IA - Beta' - Peak Odour Resonances		c vs e				22	16	<0.0001	****																	
		IA - Alpha - Peak Odour Resonances		c vs e				16	8	0.691	ns																	
		IA - Beta - Peak Odour Resonances		c vs e				22	16	0.0114	*																	
		IA - Gamma - Peak Odour Resonances		c vs e				22	16	0.8243	ns																	
		Predicted mean of IA - Control		c vs e													0.7573											
		Predicted mean of IA - NaChBac		c vs e													0.459	0.1750 to 0.4215	5	1.742	0.1275	5	5.834	P<0.0001	1	22.82	P<0.0001	
		δD - Calyx - Peak Odour Resonances		c vs e				13	8	0.9998	ns																	
		δD - Alpha' - Peak Odour Resonances		c vs e				16	8	>0.9999	ns																	
		δD - Beta' - Peak Odour Resonances		c vs e				22	16	0.0248	*																	
		δD - Alpha - Peak Odour Resonances		c vs e				16	8	0.9733	ns																	
		δD - Beta - Peak Odour Resonances		c vs e				22	16	0.9027	ns																	
		δD - Gamma - Peak Odour Resonances		c vs e				22	16	0.003	**																	
	Predicted mean of δD- Control	c vs e										0.3667																
	Predicted mean of δD - NaChBac	c vs e										0.2626	0.02829 to 0.1800	5	2.023	0.778	5	5.912	P<0.0001	1	7.345	0.0074						
	4 Days R13F02GAL4>NaChBac.Gal80ts	Two way Anova - Šidák multiple comparison test	IA - Calyx - Peak Odour Resonances	Imaged 4 days after eclosion	13	9	21	16	0.9661	ns																		
			IA - Alpha' - Peak Odour Resonances				c vs e	20	15	0.9559	ns																	
			IA - Beta' - Peak Odour Resonances				c vs e	22	17	0.0004	***																	
			IA - Alpha - Peak Odour Resonances				c vs e	20	16	>0.9999	ns																	
			IA - Beta - Peak Odour Resonances				c vs e	23	17	0.9841	ns																	
			IA - Gamma - Peak Odour Resonances				c vs e	23	17	0.9988	ns																	
			Predicted mean of IA - Control				c vs e									0.5441												
			Predicted mean of IA - NaChBac				c vs e									0.6409	-0.1874 to -0.006040	5	2.78	0.0198	5	6.812	P<0.0001	1	4.2	0.0367		
			δD - Calyx - Peak Odour Resonances				c vs e	21	16	0.4502	ns																	
			δD - Alpha' - Peak Odour Resonances				c vs e	20	15	>0.9999	ns																	
δD - Beta' - Peak Odour Resonances			c vs e				22	17	0.1911	ns																		
δD - Alpha - Peak Odour Resonances			c vs e				20	16	0.8455	ns																		
δD - Beta - Peak Odour Resonances			c vs e				23	17	0.275	ns																		
δD - Gamma - Peak Odour Resonances			c vs e				23	17	0.9968	ns																		
Predicted mean of δD- Control	c vs e									-	-	0.3121																
Predicted mean of δD - NaChBac	c vs e									-	-	0.2815	-0.01431 to 0.07557	5	2.177	0.0578	5	2790	0.0183	1	1.805	0.1805						
8 Days R13F02GAL4>NaChBac.Gal80ts	Two way Anova - Šidák multiple comparison test	IA - Calyx - Peak Odour Resonances	Imaged 8 days after eclosion	4	6	3	12	0.6623	ns																			
		IA - Alpha' - Peak Odour Resonances				c vs e	6	12	>0.9999	ns																		
		IA - Beta' - Peak Odour Resonances				c vs e	6	12	0.9849	ns																		
		IA - Alpha - Peak Odour Resonances				c vs e	6	12	0.9994	ns																		
		IA - Beta - Peak Odour Resonances				c vs e	6	12	>0.9999	ns																		
		IA - Gamma - Peak Odour Resonances				c vs e	6	12	0.9969	ns																		
		Predicted mean of IA - Control				c vs e									0.9043													
		Predicted mean of IA - NaChBac				c vs e									0.9087	-0.3577 to 0.3488	5	0.548	0.7396	5	2513	0.0352	1	6E-04	0.98			
		δD - Calyx - Peak Odour Resonances				c vs e	3	12	0.9946	ns																		
		δD - Alpha' - Peak Odour Resonances				c vs e	6	12	0.9691	ns																		
		δD - Beta' - Peak Odour Resonances				c vs e	6	12	0.9775	ns																		
		δD - Alpha - Peak Odour Resonances				c vs e	6	12	>0.9999	ns																		
		δD - Beta - Peak Odour Resonances				c vs e	6	12	0.9881	ns																		
		δD - Gamma - Peak Odour Resonances				c vs e	6	12	0.0008	***																		
Predicted mean of δD- Control	c vs e									0.3762																		
Predicted mean of δD - NaChBac	c vs e									0.303	-0.02257 to 0.1691	5	2.896	0.0178	5	3.762	0.0038	1	2.304	0.1324								

Figure	Data	Breakdown of conditions	Statistical Test	Comparison (c = con, e = exp)	Age of the flies	Control n	Exp. n	Con. hemis. n	Exp hemis. n	P-value	Significance	Predicted mean	95%	Interaction DF	Interaction F	Interaction P Value	Main effect of obse DF	Main effect of obse F	Main effect of obse P Value	Main effect of genotype DF	Main effect of genotype F	Main effect of genotype P Value					
14	2 Days R13F02GAL4>NaChBac.Gal80ts	IA - Calyx - Average Odour Resonances	Two way Anova - Šidák multiple comparison test	c vs e	Imaged 2 days after eclosion	13	11	13	8	0.1516	ns																
		IA - Alpha' - Average Odour Resonances		c vs e				16	8	0.9996	ns																
		IA - Beta' - Average Odour Resonances		c vs e				22	16	<0.0001	****																
		IA - Alpha - Average Odour Resonances		c vs e				16	8	0.7267	ns																
		IA - Beta - Average Odour Resonances		c vs e				22	16	0.0049	**																
		IA - Gamma - Average Odour Resonances		c vs e				22	16	0.0537	ns																
		Predicted mean of IA - Control		c vs e												0.3487											
		Predicted mean of IA - NaChBac		c vs e												0.1502	0.1299 to 0.2671		5	1.977	0.0843	5	2.867	0.0164	1	32.8	P<0.0001
		δD - Calyx - Average Odour Resonances		c vs e				13	8	0.9948	ns																
		δD - Alpha' - Average Odour Resonances		c vs e				16	8	0.9999	ns																
		δD - Beta' - Average Odour Resonances		c vs e				22	16	0.0028	**																
		δD - Alpha - Average Odour Resonances		c vs e				16	8	0.9255	ns																
	δD - Beta - Average Odour Resonances	c vs e	22	16	0.9866	ns																					
	δD - Gamma - Average Odour Resonances	c vs e	22	16	0.3821	ns																					
	Predicted mean of δD- Control	c vs e									0.1741																
	Predicted mean of δD - NaChBac	c vs e									0.09684	0.02445 to 0.1301		5	1.255	0.2995	5	8.115	P<0.0001	1	8.341	0.0044					
	4 Days R13F02GAL4>NaChBac.Gal80ts	Two way Anova - Šidák multiple comparison test	IA - Calyx - Average Odour Resonances	Imaged 4 days after eclosion	13	9	21	16	>0.9999	ns																	
			IA - Alpha' - Average Odour Resonances				c vs e	20	15	0.8299	ns																
			IA - Beta' - Average Odour Resonances				c vs e	22	17	0.0011	**																
			IA - Alpha - Average Odour Resonances				c vs e	20	16	>0.9999	ns																
			IA - Beta - Average Odour Resonances				c vs e	23	17	0.999	ns																
			IA - Gamma - Average Odour Resonances				c vs e	23	17	0.9981	ns																
			Predicted mean of IA - Control				c vs e									0.2608											
			Predicted mean of IA - NaChBac				c vs e									0.3306	-0.1258 to -0.01375		5	1.979	0.083	5	5.249	0.0001	1	6.028	0.0149
δD - Calyx - Average Odour Resonances			c vs e				21	16	>0.9999	ns																	
δD - Alpha' - Average Odour Resonances			c vs e				20	15	0.8788	ns																	
δD - Beta' - Average Odour Resonances			c vs e				22	17	0.0152	*																	
δD - Alpha - Average Odour Resonances			c vs e				20	16	>0.9999	ns																	
δD - Beta - Average Odour Resonances	c vs e	23	17	0.8233	ns																						
δD - Gamma - Average Odour Resonances	c vs e	23	17	0.9697	ns																						
Predicted mean of δD- Control	c vs e									0.1563																	
Predicted mean of δD - NaChBac	c vs e									0.1841	-0.06475 to 0.009145		5	2.036	0.0749	5	3.524	0.0044	1	2.2	0.1395						
8 Days R13F02GAL4>NaChBac.Gal80ts	Two way Anova - Šidák multiple comparison test	IA - Calyx - Average Odour Resonances	Imaged 8 days after eclosion	4	6	3	12	0.8874	ns																		
		IA - Alpha' - Average Odour Resonances				c vs e	6	12	>0.9999	ns																	
		IA - Beta' - Average Odour Resonances				c vs e	6	12	>0.9999	ns																	
		IA - Alpha - Average Odour Resonances				c vs e	6	12	0.9988	ns																	
		IA - Beta - Average Odour Resonances				c vs e	6	12	>0.9999	ns																	
		IA - Gamma - Average Odour Resonances				c vs e	6	12	0.4918	ns																	
		Predicted mean of IA - Control				c vs e									0.4864												
		Predicted mean of IA - NaChBac				c vs e									0.4636	-0.1464 to 0.1920		5	0.746	0.591	5	2.441	0.0399	1	0.072	0.7894	
		δD - Calyx - Average Odour Resonances				c vs e	3	12	0.9761	ns																	
		δD - Alpha' - Average Odour Resonances				c vs e	6	12	0.6996	ns																	
		δD - Beta' - Average Odour Resonances				c vs e	6	12	0.9985	ns																	
		δD - Alpha - Average Odour Resonances				c vs e	6	12	>0.9999	ns																	
δD - Beta - Average Odour Resonances	c vs e	6	12	0.9971	ns																						
δD - Gamma - Average Odour Resonances	c vs e	6	12	0.0188	*																						
Predicted mean of δD- Control	c vs e									0.205																	
Predicted mean of δD - NaChBac	c vs e									0.1816	-0.04855 to 0.09520		5	2.246	0.0562	5	4.745	0.0007	1	0.415	0.5209						

Figure	Data	Breakdown of conditions	Statistical Test	Comparison (c = con, e = exp)	Age of the flies	Control n	Exp. n	Con. hemis. n	Exp hemis. n	P-value	Significance	Predicted mean	95%	Interaction DF	Interaction F	Interaction P Value	Main effect of obse DF	Main effect of obse F	Main effect of obse P Value	Main effect of genotype DF	Main effect of genotype F	Main effect of genotype P Value						
15	Panel A - Peak responses for 4 days temperature control R13f02GAL4>NaChBac	IA - Calyx - Peak Odour Resonances	Two way Anova - Šidák multiple comparison test	c vs e	Imaged 4 days after eclosion	5	3	4	5	0.0063	**																	
		IA - Alpha' - Peak Odour Resonances		c vs e				7	4	0.7632	ns																	
		IA - Beta' - Peak Odour Resonances		c vs e				8	6	0.2037	ns																	
		IA - Alpha - Peak Odour Resonances		c vs e				7	5	0.7869	ns																	
		IA - Beta - Peak Odour Resonances		c vs e				9	6	0.0141	*																	
		IA - Gamma - Peak Odour Resonances		c vs e				8	6	0.9365	ns																	
		Predicted mean of IA - Control		c vs e												0.68												
		Predicted mean of IA - NaChBac		c vs e												0.3493	0.1979 to 0.4637		5	1.265	0.2904	5	5.254	0.0004	1	24.74	0.0001	
		δD - Calyx - Peak Odour Resonances		c vs e				4	5	<0.0001	****																	
		δD - Alpha' - Peak Odour Resonances		c vs e				7	4	0.2193	ns																	
		δD - Beta' - Peak Odour Resonances		c vs e				8	6	0.9905	ns																	
		δD - Alpha - Peak Odour Resonances		c vs e				7	5	0.9969	ns																	
	δD - Beta - Peak Odour Resonances	c vs e	9	6	0.2951	ns																						
	δD - Gamma - Peak Odour Resonances	c vs e	8	6	0.0415	*																						
	Predicted mean of δD- Control	c vs e									0.437																	
	Predicted mean of δD - NaChBac	c vs e									0.1812	0.1633 to 0.3484		5	3.321	0.0102	5	1.978	0.0947	1	30.55	0.0001						
	Panel B and C - Average responses for 4 days temperature control R13f02GAL4>NaChBac	Two way Anova - Šidák multiple comparison test	IA - Calyx - Average Odour Resonances	Imaged 4 days after eclosion	5	3	4	5	0.0006	***																		
			IA - Alpha' - Average Odour Resonances				c vs e	7	4	0.7452	ns																	
			IA - Beta' - Average Odour Resonances				c vs e	8	6	0.1725	ns																	
			IA - Alpha - Average Odour Resonances				c vs e	7	5	0.5064	ns																	
			IA - Beta - Average Odour Resonances				c vs e	9	6	0.0135	*																	
			IA - Gamma - Average Odour Resonances				c vs e	8	6	0.1125	ns																	
			Predicted mean of IA - Control				c vs e									0.3631												
			Predicted mean of IA - NaChBac				c vs e									0.1212	0.1624 to 0.3215		5	1.241	0.3008	5	2.443	0.0436	1	36.93	0.0001	
δD - Calyx - Average Odour Resonances			c vs e				4	5	<0.0001	****																		
δD - Alpha' - Average Odour Resonances			c vs e				7	4	0.5497	ns																		
δD - Beta' - Average Odour Resonances			c vs e				8	6	0.9131	ns																		
δD - Alpha - Average Odour Resonances			c vs e				7	5	0.9979	ns																		
δD - Beta - Average Odour Resonances	c vs e	9	6	0.8276	ns																							
δD - Gamma - Average Odour Resonances	c vs e	8	6	0.0638	ns																							
Predicted mean of δD- Control	c vs e									0.2651																		
Predicted mean of δD - NaChBac	c vs e									0.07928	0.1116 to 0.2600		5	3.148	0.0134	5	2.155	0.0703	1	25.03	0.0001							

Figure	Data	Breakdown of conditions	Statistical Test	Comparison (c = con, e = exp)	Age of the flies	Control n	Exp. n	Con. hemis. n	Exp hemis. n	P-value	Significance	Predicted mean	95%	Interaction DF	Interaction F	Interaction P Value	Main effect of obse DF	Main effect of obse F	Main effect of obse P Value	Main effect of genotype DF	Main effect of genotype F	Main effect of genotype P Value					
16	Panel A - 2 Days 18 - 2 Days 31 - Age Control R13F02GAL4>NaChBac, Gal80ts	IA - Calyx - Peak Odour Resonances	Two way Anova - Šidák multiple comparison test	c vs e	Imaged 4 days after eclosion	7	6	7	8	0.011	*																
		IA - Alpha' - Peak Odour Resonances		c vs e				8	8	0.2824	ns																
		IA - Beta' - Peak Odour Resonances		c vs e				13	10	0.017	*																
		IA - Alpha - Peak Odour Resonances		c vs e				9	5	0.4594	ns																
		IA - Beta - Peak Odour Resonances		c vs e				12	10	0.5125	ns																
		IA - Gamma - Peak Odour Resonances		c vs e				11	9	0.4042	ns																
		Predicted mean of IA - Control		c vs e												0.7401											
		Predicted mean of IA - NaChBac		c vs e												0.3825	0.2247 to 0.4904		5	0.586	0.711	5	0.427	0.0015	1	4.27	0.0001
		δD - Calyx - Peak Odour Resonances		c vs e				7	8	0.0221	*																
		δD - Alpha' - Peak Odour Resonances		c vs e				8	8	0.9979	ns																
		δD - Beta' - Peak Odour Resonances		c vs e				13	10	>0.9999	ns																
		δD - Alpha - Peak Odour Resonances		c vs e				9	5	0.9519	ns																
	δD - Beta - Peak Odour Resonances	c vs e	12	10	0.9748	ns																					
	δD - Gamma - Peak Odour Resonances	c vs e	11	9	0.8437	ns																					
	Predicted mean of δD- Control	c vs e									0.3167																
	Predicted mean of δD - NaChBac	c vs e									0.1994	0.02788 to 0.2068		5	1.051	0.3926	5	2.027	0.0817	1	6.781	0.0107					
	Panel B and C - 2 Days 18 - 2 Days 31 - Age Control R13F02GAL4>NaChBac, Gal80ts	Two way Anova - Šidák multiple comparison test	IA - Calyx - Average Odour Resonances	Imaged 4 days after eclosion	7	6	7	8	0.0154	*																	
			IA - Alpha' - Average Odour Resonances				c vs e	8	8	0.613	ns																
			IA - Beta' - Average Odour Resonances				c vs e	13	10	0.0678	ns																
			IA - Alpha - Average Odour Resonances				c vs e	9	5	0.3194	ns																
			IA - Beta - Average Odour Resonances				c vs e	12	10	0.3315	ns																
			IA - Gamma - Average Odour Resonances				c vs e	11	9	0.1912	ns																
			Predicted mean of IA - Control				c vs e									0.342											
			Predicted mean of IA - NaChBac				c vs e									0.1626	0.1113 to 0.2475		5	0.333	0.8922	5	2.223	0.0582	1	27.36	0.0001
δD - Calyx - Average Odour Resonances			c vs e				7	8	0.9685	ns																	
δD - Alpha' - Average Odour Resonances			c vs e				8	8	0.9993	ns																	
δD - Beta' - Average Odour Resonances			c vs e				13	10	>0.9999	ns																	
δD - Alpha - Average Odour Resonances			c vs e				9	5	0.9748	ns																	
δD - Beta - Average Odour Resonances	c vs e	12	10	>0.9999	ns																						
δD - Gamma - Average Odour Resonances	c vs e	11	9	0.9864	ns																						
Predicted mean of δD- Control	c vs e									0.1005																	
Predicted mean of δD - NaChBac	c vs e									0.06888	-0.02390 to 0.08710		5	0.151	0.9793	5	0.965	0.4435	1	1.278	0.2612						

Figure	Data	Breakdown of conditions	Statistical Test	Comparison (c = con, e = exp)	Age of the flies	Control n	Exp. n	Con. hemis. n	Exp hemis. n	P-value	Significance	Predicted mean	95%	Interaction DF	Interaction F	Interaction P Value	Main effect of obse DF	Main effect of obse F	Main effect of obse P Value	Main effect of genotype DF	Main effect of genotype F	Main effect of genotype P Value								
18	Panel A - Stage 1	IA - Calyx - Peak Odour Resonances	Two way Anova - Šidák multiple comparison test	c vs e	Imaged 4 days after eclosion	4	7	7	12	0.6987	ns																			
		IA - Alpha' - Peak Odour Resonances		c vs e				6	10	0.9457	ns																			
		IA - Beta' - Peak Odour Resonances		c vs e				5	6	>0.9999	ns																			
		IA - Alpha - Peak Odour Resonances		c vs e				6	10	0.9678	ns																			
		IA - Beta - Peak Odour Resonances		c vs e				5	12	0.9958	ns																			
		IA - Gamma - Peak Odour Resonances		c vs e				5	12	>0.9999	ns																			
		Predicted mean of IA - Control		c vs e													0.5385													
		Predicted mean of IA - NaChBac		c vs e													0.4508	-0.05475 to 0.2302	5	0.362	0.8731	5	0.814	0.5429	1	1.497	0.2244			
		δD - Calyx - Peak Odour Resonances		c vs e				7	12	0.9609	ns																			
		δD - Alpha' - Peak Odour Resonances		c vs e				6	10	0.0415	*																			
		δD - Beta' - Peak Odour Resonances		c vs e				5	6	0.4087	ns																			
		δD - Alpha - Peak Odour Resonances		c vs e				6	10	0.2637	ns																			
		δD - Beta - Peak Odour Resonances		c vs e				5	12	0.9969	ns																			
		δD - Gamma - Peak Odour Resonances		c vs e				5	12	0.9609	ns																			
	Predicted mean of δD- Control	c vs e										0.3988																		
	Predicted mean of δD - NaChBac	c vs e										0.2216	0.07806 to 0.2763	5	0.817	0.5404	5	2.217	0.0592	1	12.61	0.0006								
	Panel B - Stage 2	IA - Calyx - Peak Odour Resonances	Two way Anova - Šidák multiple comparison test	Imaged 4 days after eclosion	2	1	2	1	0.2266	ns																				
		IA - Alpha' - Peak Odour Resonances					c vs e	3	1	0.9707	ns																			
		IA - Beta' - Peak Odour Resonances					c vs e	2	1	0.5942	ns																			
		IA - Alpha - Peak Odour Resonances					c vs e	3	1	0.6647	ns																			
		IA - Beta - Peak Odour Resonances					c vs e	2	1	0.7956	ns																			
		IA - Gamma - Peak Odour Resonances					c vs e	2	1	0.6552	ns																			
		Predicted mean of IA - Control					c vs e										0.9252													
		Predicted mean of IA - NaChBac					c vs e										0.2679	0.2561 to 1.059	5	0.307	0.8957	5	0.653	0.6684	1	14.28	0.0054			
		δD - Calyx - Peak Odour Resonances					c vs e	2	1	0.8407	ns																			
		δD - Alpha' - Peak Odour Resonances					c vs e	3	1	>0.9999	ns																			
		δD - Beta' - Peak Odour Resonances					c vs e	2	1	>0.9999	ns																			
		δD - Alpha - Peak Odour Resonances					c vs e	3	1	0.8095	ns																			
δD - Beta - Peak Odour Resonances		c vs e					2	1	0.9992	ns																				
δD - Gamma - Peak Odour Resonances		c vs e					2	1	>0.9999	ns																				
Predicted mean of δD- Control	c vs e										0.2426																			
Predicted mean of δD - NaChBac	c vs e										0.1035	-0.09188 to 0.3701	5	0.272	0.9162	5	0.433	0.8143	1	1.929	0.2023									
Panel C - Stage 3	IA - Calyx - Peak Odour Resonances	Two way Anova - Šidák multiple comparison test	Imaged 4 days after eclosion	4	2	7	2	0.8402	ns																					
	IA - Alpha' - Peak Odour Resonances					c vs e	6	2	0.2106	ns																				
	IA - Beta' - Peak Odour Resonances					c vs e	6	3	0.0258	*																				
	IA - Alpha - Peak Odour Resonances					c vs e	6	2	0.0163	*																				
	IA - Beta - Peak Odour Resonances					c vs e	6	3	0.2583	ns																				
	IA - Gamma - Peak Odour Resonances					c vs e	6	3	0.5974	ns																				
	Predicted mean of IA - Control					c vs e										0.72														
	Predicted mean of IA - NaChBac					c vs e										0.2673	0.2805 to 0.6250	5	0.699	0.6273	5	0.357	0.8749	1	28.21	0.0001				
	δD - Calyx - Peak Odour Resonances					c vs e	7	2	>0.9999	ns																				
	δD - Alpha' - Peak Odour Resonances					c vs e	6	2	0.7659	ns																				
	δD - Beta' - Peak Odour Resonances					c vs e	6	3	0.752	ns																				
	δD - Alpha - Peak Odour Resonances					c vs e	6	2	0.8451	ns																				
	δD - Beta - Peak Odour Resonances					c vs e	6	3	0.5821	ns																				
	δD - Gamma - Peak Odour Resonances					c vs e	6	3	0.6117	ns																				
Predicted mean of δD- Control	c vs e										0.3457																			
Predicted mean of δD - NaChBac	c vs e										0.2054	0.03458 to 0.2461	5	0.263	0.9304	5	0.152	0.9781	1	7.132	0.0106									

Figure	Data	Breakdown of conditions	Statistical Test	Comparison (c = con, e = exp)	Age of the flies	Control n	Exp. n	Con. hemis. n	Exp hemis. n	P-value	Significance	Predicted mean	95%	Interaction DF	Interaction F	Interaction P Value	Main effect of obse DF	Main effect of obse F	Main effect of obse P Value	Main effect of genotype DF	Main effect of genotype F	Main effect of genotype P Value			
Panel A - Stage 1	Two way Anova - Šidák multiple comparison test	IA - Calyx - Average Odour Resonances	c vs e	7	12	0.3768	ns																		
		IA - Alpha' - Average Odour Resonances	c vs e	6	10	0.2421	ns																		
		IA - Beta' - Average Odour Resonances	c vs e	5	6	0.9364	ns																		
		IA - Alpha - Average Odour Resonances	c vs e	6	10	0.3114	ns																		
		IA - Beta - Average Odour Resonances	c vs e	5	12	0.9014	ns																		
		IA - Gamma - Average Odour Resonances	c vs e	5	12	0.9874	ns																		
		Predicted mean of IA - Control	c vs e									0.2984													
		Predicted mean of IA - NaChBac	c vs e									0.1715	0.05148 to 0.2023	5	0.31	0.9058	5	0.918	0.4733	1	11.18	0.0012			
		δD - Calyx - Average Odour Resonances	c vs e	7	12	0.703	ns																		
		δD - Alpha' - Average Odour Resonances	c vs e	6	10	0.0087	**																		
		δD - Beta' - Average Odour Resonances	c vs e	5	6	0.1123	ns																		
		δD - Alpha - Average Odour Resonances	c vs e	6	10	0.0642	ns																		
		δD - Beta - Average Odour Resonances	c vs e	5	12	0.9986	ns																		
		δD - Gamma - Average Odour Resonances	c vs e	5	12	0.0206	*																		
		Predicted mean of δD- Control	c vs e									0.2905													
		Predicted mean of δD - NaChBac	c vs e									0.08861	0.1267 to 0.2770	5	1.229	0.3023	5	3.58	0.0054	1	28.49	0.0001			
Panel B - Stage 2	Two way Anova - Šidák multiple comparison test	IA - Calyx - Average Odour Resonances	c vs e	2	1	0.5276	ns																		
		IA - Alpha' - Average Odour Resonances	c vs e	3	1	>0.9999	ns																		
		IA - Beta' - Average Odour Resonances	c vs e	2	1	0.9627	ns																		
		IA - Alpha - Average Odour Resonances	c vs e	3	1	0.929	ns																		
		IA - Beta - Average Odour Resonances	c vs e	2	1	0.8898	ns																		
		IA - Gamma - Average Odour Resonances	c vs e	2	1	0.9344	ns																		
		Predicted mean of IA - Control	c vs e									0.4058													
		Predicted mean of IA - NaChBac	c vs e									0.09473	0.008576 to 0.6135	5	0.288	0.907	5	0.424	0.82	1	5.623	0.0451			
		δD - Calyx - Average Odour Resonances	c vs e	2	1	0.9701	ns																		
		δD - Alpha' - Average Odour Resonances	c vs e	3	1	0.9998	ns																		
		δD - Beta' - Average Odour Resonances	c vs e	2	1	>0.9999	ns																		
		δD - Alpha - Average Odour Resonances	c vs e	3	1	0.9913	ns																		
		δD - Beta - Average Odour Resonances	c vs e	2	1	>0.9999	ns																		
		δD - Gamma - Average Odour Resonances	c vs e	2	1	>0.9999	ns																		
		Predicted mean of δD- Control	c vs e									0.07663													
		Predicted mean of δD - NaChBac	c vs e									0.02524	-0.2262 to 0.3289	5	0.206	0.9507	5	0.292	0.9046	1	0.182	0.6807			
Panel C - Stage 3	Two way Anova - Šidák multiple comparison test	IA - Calyx - Average Odour Resonances	c vs e	7	2	0.8637	ns																		
		IA - Alpha' - Average Odour Resonances	c vs e	6	2	0.3775	ns																		
		IA - Beta' - Average Odour Resonances	c vs e	6	3	0.028	*																		
		IA - Alpha - Average Odour Resonances	c vs e	6	2	0.0085	**																		
		IA - Beta - Average Odour Resonances	c vs e	6	3	0.485	ns																		
		IA - Gamma - Average Odour Resonances	c vs e	6	3	0.4	ns																		
		Predicted mean of IA - Control	c vs e									0.3464													
		Predicted mean of IA - NaChBac	c vs e									0.1037	0.1486 to 0.3369	5	0.824	0.5403	5	0.11	0.9895	1	27.14	0.0001			
		δD - Calyx - Average Odour Resonances	c vs e	7	2	>0.9999	ns																		
		δD - Alpha' - Average Odour Resonances	c vs e	6	2	0.7758	ns																		
		δD - Beta' - Average Odour Resonances	c vs e	6	3	0.8502	ns																		
		δD - Alpha - Average Odour Resonances	c vs e	6	2	0.5507	ns																		
		δD - Beta - Average Odour Resonances	c vs e	6	3	0.3017	ns																		
		δD - Gamma - Average Odour Resonances	c vs e	6	3	0.6918	ns																		
		Predicted mean of δD- Control	c vs e									0.2068													
		Predicted mean of δD - NaChBac	c vs e									0.07565	0.04267 to 0.2197	5	0.317	0.8999	5	0.502	0.7729	1	8.972	0.0047			

Figure	Data	Breakdown of conditions	Statistical Test	Comparison (c = con, e = exp)	Age of the flies	Control n	Exp. n	Con. hemis. n	Exp hemis. n	P-value	Significance	Predicted mean	95%	Interaction DF	Interaction F	Interaction P Value	Main effect of obse DF	Main effect of obse F	Main effect of obse P Value	Main effect of genotype DF	Main effect of genotype F	Main effect of genotype P Value							
23	Panel A - CDK5DN	IA - Calyx - Peak Odour Resonances	Two-way ANOVA, Sidak's multiple comparison test	c vs e	Imaged at 4 days after eclosion	6	3	9	3	0.9749	ns																		
		9		3				0.0153	*																				
		10		3				0.999	ns																				
		11		3				0.9831	ns																				
		10		3				0.199	ns																				
		10		3				0.9897	ns																				
		Predicted mean - Control		c vs e										0.7252															
		Predicted mean - Experimental		c vs e										0.5689		0.05393 to 0.2586	5	1.093	0.3692	5	1.662	0.1509	1	9.18	0.0031				
		δD - Calyx - Peak Odour Resonances		c vs e				6	3	9	3	0.9128	ns																
		δD - Alpha' - Peak Odour Resonances		c vs e						9	3	0.3163	ns																
		δD - Beta' - Peak Odour Resonances		c vs e						10	3	0.7364	ns																
		δD - Alpha - Peak Odour Resonances		c vs e						11	3	>0.9999	ns																
	δD - Beta - Peak Odour Resonances	c vs e			10	3	0.0353			*																			
	δD - Gamma - Peak Odour Resonances	c vs e			10	3	>0.9999			ns																			
	Predicted mean - Control	c vs e									0.4037																		
	Predicted mean - Experimental	c vs e									0.3057		0.02959 to 0.1665	5	1.141	0.3437	5	1.739	0.1325	1	8.071	0.0054							
	Panel A - p35	Two-way ANOVA, Sidak's multiple comparison test	IA - Calyx - Peak Odour Resonances	c vs e	Imaged at 4 days after eclosion	6	9	9	14	0.9901	ns																		
			11	16				0.1773	ns																				
			10	17				0.8649	ns																				
			9	17				0.9686	ns																				
			10	14				0.9948	ns																				
			10	14				0.9967	ns																				
			Predicted mean - Control	c vs e										0.6619															
			Predicted mean - Experimental	c vs e									0.6141		-0.05989 to 0.1554	5	1.278	0.277	5	10.56	0.0001	1	0.77	0.3818					
δD - Calyx - Peak Odour Resonances			c vs e			6	9	9	14	0.9763	ns																		
δD - Alpha' - Peak Odour Resonances			c vs e						11	16	0.2988	ns																	
δD - Beta' - Peak Odour Resonances			c vs e						10	17	0.9193	ns																	
δD - Alpha - Peak Odour Resonances			c vs e						9	17	0.9241	ns																	
δD - Beta - Peak Odour Resonances	c vs e			10	14			0.9974	ns																				
δD - Gamma - Peak Odour Resonances	c vs e			10	14			0.9966	ns																				
Predicted mean - Control	c vs e									0.7267																			
Predicted mean - Experimental	c vs e								0.6761		-0.07412 to 0.1754	5	1.115	0.3556	5	1.608	0.1627	1	0.646	0.4232									
Panel B - CDK5DN	Two-way ANOVA, Sidak's multiple comparison test	IA - Calyx - Average Odour Resonances	c vs e	Imaged at 4 days after eclosion	6	3	9	3	>0.9999	ns																			
		9	3				0.9338	ns																					
		10	3				>0.9999	ns																					
		11	3				0.324	ns																					
		10	3				0.692	ns																					
		10	3				0.9838	ns																					
		Predicted mean - Control	c vs e										0.3431																
		Predicted mean - Experimental	c vs e									0.2816		-0.03289 to 0.1559	5	1.007	0.4208	5	0.151	0.979	1	1.694	0.1977						
		δD - Calyx - Average Odour Resonances	c vs e			6	3	9	3	>0.9999	ns																		
		δD - Alpha' - Average Odour Resonances	c vs e						9	3	0.7437	ns																	
		δD - Beta' - Average Odour Resonances	c vs e						10	3	>0.9999	ns																	
		δD - Alpha - Average Odour Resonances	c vs e						11	3	0.8654	ns																	
δD - Beta - Average Odour Resonances	c vs e			10	3			0.9523	ns																				
δD - Gamma - Average Odour Resonances	c vs e			10	3			0.9955	ns																				
Predicted mean - Control	c vs e									0.1755																			
Predicted mean - Experimental	c vs e								0.1474		-0.04988 to 0.1060	5	0.664	0.6524	5	0.308	0.9066	1	0.518	0.47475									

Figure	Data	Breakdown of conditions	Statistical Test	Comparison (c = con, e = exp)	Age of the flies	Control n	Exp. n	Con. hemis. n	Exp hemis. n	P-value	Significance	Predicted mean	95%	Interaction DF	Interaction F	Interaction P Value	Main effect of obe DF	Main effect of obe F	Main effect of obe P Value	Main effect of genotype DF	Main effect of genotype F	Main effect of genotype P Value						
Panel C - p35		IA - Calyx - Average Odour Responses	Two-way ANOVA, Sidak's multiple comparison test.	c vs e	Imaged at 4 days after eclosion	6	9	9	14	>0.9999	ns																	
		11		16				0.0511	ns																			
		IA - Alpha' - Average Odour Responses		c vs e																								
		IA - Beta' - Average Odour Responses		c vs e																								
		IA - Alpha - Average Odour Responses		c vs e																								
		IA - Beta - Average Odour Responses		c vs e																								
		IA - Gamma - Average Odour Responses		c vs e																								
		Predicted mean - Control		c vs e												0.3431												
		Predicted mean - Experimental		c vs e											0.252		0.02839 to 0.1538		5	0.661	0.6536	5	1.224	0.3008	1	8.246	0.0047	
		δD - Calyx - Average Odour Responses		c vs e							6	9	9	14	0.9699	ns												
		δD - Alpha' - Average Odour Responses		c vs e																								
		δD - Beta' - Average Odour Responses		c vs e																								
		δD - Alpha - Average Odour Responses		c vs e																								
		δD - Beta - Average Odour Responses		c vs e																								
		δD - Gamma - Average Odour Responses		c vs e																								
		Predicted mean - Control		c vs e												0.1755												
		Predicted mean - Experimental		c vs e												0.1255		0.001755 to 0.09838		5	0.825	0.5337	5	0.791	0.5582	1	4.197	0.0423

Figure	Data	Breakdown of conditions	Statistical Test	Comparison (c = con, e = exp)	Age of the flies	Control n	Exp. n	Con. hemis. n	Exp hemis. n	P-value	Significance	Predicted mean	95%	Interaction DF	Interaction F	Interaction P Value	Main effect of obse DF	Main effect of obse F	Main effect of obse P Value	Main effect of genotype DF	Main effect of genotype F	Main effect of genotype P Value					
24	Panel A - paraRNAi	IA - Calyx - Peak Odour Responses	Two way Anova - Sidak multiple comparison test	c vs e	Imaged 4 days after eclosion	11	6	22	11	0.0231	*																
		IA - Alpha' - Peak Odour Responses		c vs e				22	10	0.0443	*																
		IA - Beta' - Peak Odour Responses		c vs e				21	8	0.0219	*																
		IA - Alpha - Peak Odour Responses		c vs e				22	10	0.5337	ns																
		IA - Beta - Peak Odour Responses		c vs e				22	10	0.3216	ns																
		IA - Gamma - Peak Odour Responses		c vs e				21	9	>0.9999	ns																
		Predicted mean of IA - Control		c vs e											0.7257												
		Predicted mean of IA - NaChBac		c vs e											0.3645		0.2173 to 0.5050		5	1.143	0.3397	5	1.556	0.175	1	25.55	0.0001
		δD - Calyx - Peak Odour Responses		c vs e				22	11	0.5156	ns																
		δD - Alpha' - Peak Odour Responses		c vs e				22	10	0.6712	ns																
		δD - Beta' - Peak Odour Responses		c vs e				21	8	0.8121	ns																
		δD - Alpha - Peak Odour Responses		c vs e				22	10	0.9969	ns																
	δD - Beta - Peak Odour Responses	c vs e	22	10	0.9084	ns																					
	δD - Gamma - Peak Odour Responses	c vs e	21	9	0.9971	ns																					
	Predicted mean of δD - Control	c vs e									0.332																
	Predicted mean of δD - NaChBac	c vs e									0.2686		0.004004 to 0.1229		5	0.588	0.7093	5	1.876	0.1007	1	4.437	0.0366				
	Panel B - paraRNAi	IA - Calyx - Average Odour Responses	Two way Anova - Sidak multiple comparison test	c vs e	Imaged 4 days after eclosion	11	6	22	11	-0.03154	ns																
		IA - Alpha' - Average Odour Responses		c vs e				22	10	0.07405	ns																
		IA - Beta' - Average Odour Responses		c vs e				21	8	0.0774	ns																
		IA - Alpha - Average Odour Responses		c vs e				22	10	0.2335	*																
		IA - Beta - Average Odour Responses		c vs e				22	10	0.1645	ns																
		IA - Gamma - Average Odour Responses		c vs e				21	9	0.1242	ns																
		Predicted mean of IA - Control		c vs e												0.2794											
		Predicted mean of IA - NaChBac		c vs e												0.1724		-0.04504 to 0.1690		5	1.398	0.2281	5	2.6	0.0275	1	11.64
δD - Calyx - Average Odour Responses		c vs e		22				11	-0.0528	ns																	
δD - Alpha' - Average Odour Responses		c vs e		22				10	-0.02353	ns																	
δD - Beta' - Average Odour Responses		c vs e		21				8	-0.01512	ns																	
δD - Alpha - Average Odour Responses		c vs e		22				10	0.06536	ns																	
δD - Beta - Average Odour Responses	c vs e	22	10	0.04797	ns																						
δD - Gamma - Average Odour Responses	c vs e	21	9	0.04747	ns																						
Predicted mean of δD - Control	c vs e										0.1423																
Predicted mean of δD - NaChBac	c vs e										0.1308		-0.03074 to 0.05385		5	0.844	0.5206	5	0.58	0.7152	1	0.292	0.5901				

Figure	Data	Breakdown of conditions	Statistical Test	Comparison (c = con, e = exp)	Age of the flies	Control n	Exp. n	Con. hemis. n	Exp hemis. n	P-value	Significance	Predicted mean	95%	Interaction DF	Interaction F	Interaction P Value	Main effect of obse DF	Main effect of obse F	Main effect of obse P Value	Main effect of genotype DF	Main effect of genotype F	Main effect of genotype P Value								
26	Panel A - paraFlpStop	IA - Calyx - Peak Odour Resonances	Two way Anova - Šidák multiple comparison test	c vs e	Imaged 4 days after eclosion	6	8	9	12	>0.9999	ns																			
		IA - Alpha' - Peak Odour Resonances		c vs e				11	14	>0.9999	ns																			
		IA - Beta' - Peak Odour Resonances		c vs e				9	12	>0.9999	ns																			
		IA - Alpha - Peak Odour Resonances		c vs e				11	15	0.9545	ns																			
		IA - Beta - Peak Odour Resonances		c vs e				11	14	0.5462	ns																			
		IA - Gamma - Peak Odour Resonances		c vs e				7	11	0.2525	ns																			
		Predicted mean of IA - Control		c vs e												0.6523														
		Predicted mean of IA - NaChBac		c vs e												0.6427	-0.1060 to 0.1253		5	1.4	0.2287	5	3.595	0.0045	1	0.027	0.8695			
		δD - Calyx - Peak Odour Resonances		c vs e																										
		δD - Alpha' - Peak Odour Resonances		c vs e																										
	δD - Beta' - Peak Odour Resonances	c vs e																												
	δD - Alpha - Peak Odour Resonances	c vs e																												
	δD - Beta - Peak Odour Resonances	c vs e																												
	δD - Gamma - Peak Odour Resonances	c vs e																												
	Predicted mean of δD- Control	c vs e									0.4665																			
	Predicted mean of δD - NaChBac	c vs e									0.4593	-0.09104 to 0.1053		5	1.888	0.101	5	2.573	0.0298	1	0.021	0.886								
	Panel B - paraFlpStop	IA - Calyx - Average Odour Resonances	Two way Anova - Šidák multiple comparison test	Imaged 4 days after eclosion	6	8	9	12	0.1225	ns																				
		IA - Alpha' - Average Odour Resonances					c vs e	11	14	>0.9999	ns																			
		IA - Beta' - Average Odour Resonances					c vs e	9	12	0.8605	ns																			
		IA - Alpha - Average Odour Resonances					c vs e	11	15	>0.9999	ns																			
IA - Beta - Average Odour Resonances		c vs e					11	14	0.9981	ns																				
IA - Gamma - Average Odour Resonances		c vs e					7	11	0.7477	ns																				
Predicted mean of IA - Control		c vs e													0.2706															
Predicted mean of IA - NaChBac		c vs e													0.2815	-0.07547 to 0.05366		5	1.17	0.1372	5	1.89	0.1158	1	0.112	0.7388				
δD - Calyx - Average Odour Resonances		c vs e																												
δD - Alpha' - Average Odour Resonances		c vs e																												
δD - Beta' - Average Odour Resonances	c vs e																													
δD - Alpha - Average Odour Resonances	c vs e																													
δD - Beta - Average Odour Resonances	c vs e																													
δD - Gamma - Average Odour Resonances	c vs e																													
Predicted mean of δD- Control	c vs e									0.1209																				
Predicted mean of δD - NaChBac	c vs e									0.135	-0.06751 to 0.03920		5	2.063	0.0745	5	1.694	0.141	1	0.276	0.6005									

Figure	Data	Breakdown of conditions	Statistical Test	Comparison (c = con, e = exp)	Age of the flies	Control n	Exp. n	Con. hemis. n	Exp hemis. n	P-value	Significance	Predicted mean	95%	Interaction DF	Interaction F	Interaction P Value	Main effect of obe DF	Main effect of obe F	Main effect of obe P Value	Main effect of genotype DF	Main effect of genotype F	Main effect of genotype P Value
27	ShFlpTag - NaChBac	Segment - 1 Average fluorescence	Two way Anova - Sidak multiple comparison test	c vs e	Imaged 4 days after eclosion	2	5	3	10	>0.9999	ns	Control = 0.0131 NaChBac = 0.09615	-0.1744 to 0.008380	16	3.738	P<0.0001	Segment = 16	2.181	0.0072	1	3.997	0.0709
		Segment - 2 Average fluorescence		c vs e						0.9806	ns											
		Segment - 3 Average fluorescence		c vs e						0.9322	ns											
		Segment - 4 Average fluorescence		c vs e						0.915	ns											
		Segment - 5 Average fluorescence		c vs e						0.7887	ns											
		Segment - 6 Average fluorescence		c vs e						0.4583	ns											
		Segment - 7 Average fluorescence		c vs e						0.707	ns											
		Segment - 8 Average fluorescence		c vs e						0.5667	ns											
		Segment - 9 Average fluorescence		c vs e						0.8373	ns											
		Segment - 10 Average fluorescence		c vs e						0.6872	ns											
		Segment - 11 Average fluorescence		c vs e						0.7645	ns											
		Segment - 12 Average fluorescence		c vs e						0.7237	ns											
		Segment - 13 Average fluorescence		c vs e						0.9861	ns											
		Segment - 14 Average fluorescence		c vs e						0.2796	ns											
		Segment - 15 Average fluorescence		c vs e						0.0845	ns											
		Segment - 16 Average fluorescence		c vs e						0.0619	ns											
		Segment - 17 Average fluorescence		c vs e						0.0241	*											
28	InFlpTag - NaChBac	Segment - 1 Average fluorescence	Two way Anova - Sidak multiple comparison test	c vs e	Imaged 4 days after eclosion	2	2	4	4	>0.9999	ns	Control = 0.04287 NaChBac = 0.01416	0.01385 to 0.04356	14	0.939	0.5221	Segment = 14	1.587	0.0997	1	22.35	0.0032
		Segment - 2 Average fluorescence		c vs e						>0.9999	ns											
		Segment - 3 Average fluorescence		c vs e						0.9482	ns											
		Segment - 4 Average fluorescence		c vs e						0.9989	ns											
		Segment - 5 Average fluorescence		c vs e						>0.9999	ns											
		Segment - 6 Average fluorescence		c vs e						>0.9999	ns											
		Segment - 7 Average fluorescence		c vs e						>0.9999	ns											
		Segment - 8 Average fluorescence		c vs e						>0.9999	ns											
		Segment - 9 Average fluorescence		c vs e						>0.9999	ns											
		Segment - 10 Average fluorescence		c vs e						0.999	ns											
		Segment - 11 Average fluorescence		c vs e						0.0004	***											
		Segment - 12 Average fluorescence		c vs e						>0.9999	ns											
		Segment - 13 Average fluorescence		c vs e						0.9993	ns											
		Segment - 14 Average fluorescence		c vs e						>0.9999	ns											
		Segment - 15 Average fluorescence		c vs e						>0.9999	ns											

Figure	Data	Breakdown of conditions	Statistical Test	Comparison (c = con, e = exp)	Age of the flies	Control n	Exp. n	Con. hemis. n	Exp hemis. n	P-value	Significance	Predicted mean	95%	Interaction DF	Interaction F	Interaction P Value	Main effect of obse DF	Main effect of obse F	Main effect of obse P Value	Main effect of genotype DF	Main effect of genotype F	Main effect of genotype P Value										
31	Panel A - Projection Neurons with NaChBac	IA - LH - Peak Odour Resonances	Two-way ANOVA, Sidak's multiple comparisons test	c vs e	4 days after eclosion	9	6	11	6	0.0628	no	Control = 2.526 NaChBac= 1.804	0.2174 to 1.227	2	0.706	0.4975	2	2.025	0.1411	1	0.203	0.0058										
		IA - AL - Peak Odour Resonances		c vs e				17	9	0.6329	no																					
		IA - Calyx - Peak Odour Resonances		c vs e				11	10	0.433	no																					
		δD - LH - Peak Odour Resonances		c vs e				11	6	0.0697	no																					
		δD - AL - Peak Odour Resonances		c vs e				17	8	0.2042	no																					
		δD - Calyx - Peak Odour Resonances		c vs e				12	10	0.8037	no												Control = 1.556 NaChBac= 0.9885	0.1787 to 0.9616	2	0.785	0.4607	2	0.785	0.4607	1	8.494
	IA - LH - Average Odour Resonances	c vs e		11				6	0.0424	*	Control = 0.9762 NaChBac= 0.7456	0.0009620 to 0.4604	2	0.187	0.1636	2	0.184	0.1682	1	4.038	0.0491											
	IA - AL - Average Odour Resonances	c vs e		17				9	0.9824	no																						
	IA - Calyx - Average Odour Resonances	c vs e		11				10	0.9789	no																						
	δD - LH - Average Odour Resonances	c vs e		11				6	0.4082	no																						
	δD - AL - Average Odour Resonances	c vs e		17				9	0.9853	no												Control = 0.3636 NaChBac= 0.3351										
	δD - Calyx - Average Odour Resonances	c vs e		12				10	0.8532	no																						

Figure	Data	Breakdown of conditions	Statistical Test	Comparison (c = con, e = exp)	Age of the flies	Control n	Exp. n	Con. hemis. n	Exp hemis. n	P-value	Significance	Predicted mean	95% CI of difference	Interaction DF	Interaction F	Interaction P Value	Main effect of lobe DF	Main effect of lobe F	Main effect of lobe P Value	Main effect of genotype DF	Main effect of genotype F	Main effect of genotype P Value								
33	Panel A ShakerDN	MCH - Calyx - Average Odour Responses	Two-way ANOVA, Sidak's multiple comparison test	c vs e	Imaged at 4 days after eclosion	4	5	7	9	>0.9999	ns																			
		MCH - Alpha' - Average Odour Responses		c vs e				6	8	0.9075	ns																			
		MCH - Beta' - Average Odour Responses		c vs e				6	8	0.7726	ns																			
		MCH - Alpha - Average Odour Responses		c vs e				6	8	0.6478	ns																			
		MCH - Beta - Average Odour Responses		c vs e				6	7	0.6735	ns																			
		MCH - Gamma - Average Odour Responses		c vs e				6	9	0.5357	ns																			
		Predicted mean - Control		c vs e												0.1959														
		Predicted mean - Experimental		c vs e												0.3403	-0.2541 to -0.03458		5	0.5008	0.7747	5	1.969	0.0933	1	6.865	0.0107			
		OCT - Calyx - Average Odour Responses		c vs e																										
		OCT - Alpha' - Average Odour Responses		c vs e																										
	OCT - Beta' - Average Odour Responses	c vs e																												
	OCT - Alpha - Average Odour Responses	c vs e																												
	OCT - Beta - Average Odour Responses	c vs e																												
	OCT - Gamma - Average Odour Responses	c vs e																												
	Predicted mean - Control	c vs e										0.1697																		
	Predicted mean - Experimental	c vs e										0.2829	-0.2230 to -0.003350		5	0.5369	0.7477	5	1.198	0.3184	1	4.216	0.0436							
	Panel A ShakerRNAi	IA - Calyx - Average Odour Responses	Two-way ANOVA, Sidak's multiple comparison test	c vs e	Imaged at 4 days after eclosion	6	6	9	5	0.0732	ns																			
		IA - Alpha' - Average Odour Responses		c vs e				11	9	0.0564	ns																			
		IA - Beta' - Average Odour Responses		c vs e				10	11	>0.9999	ns																			
		IA - Alpha - Average Odour Responses		c vs e				9	10	0.9847	ns																			
IA - Beta - Average Odour Responses		c vs e		10				9	0.9507	ns																				
IA - Gamma - Average Odour Responses		c vs e		10				11	0.3832	ns																				
Predicted mean - Control		c vs e													0.3431															
Predicted mean - Experimental		c vs e													0.2283	0.04970 to 0.1801		5	1.395	0.2325	5	1.509	0.1936	1	12.22	0.0007				
δD - Calyx - Average Odour Responses		c vs e																												
δD - Alpha' - Average Odour Responses		c vs e																												
δD - Beta' - Average Odour Responses	c vs e																													
δD - Alpha - Average Odour Responses	c vs e																													
δD - Beta - Average Odour Responses	c vs e																													
δD - Gamma - Average Odour Responses	c vs e																													
Predicted mean - Control	c vs e										0.2848																			
Predicted mean - Experimental	c vs e										0.1708	0.05300 to 0.1752		5	1.009	0.4163	5	4.678	0.007	1	13.72	0.0003								
Panel B ShakerDN Gal80's	IA - Calyx - Average Odour Responses	Two-way ANOVA, Sidak's multiple comparison test	c vs e	Imaged at 4 days after eclosion	3	3	4	5	0.149	ns																				
	IA - Alpha' - Average Odour Responses		c vs e				5	4	0.9996	ns																				
	IA - Beta' - Average Odour Responses		c vs e				4	5	0.3806	ns																				
	IA - Alpha - Average Odour Responses		c vs e				5	4	>0.9999	ns																				
	IA - Beta - Average Odour Responses		c vs e				4	5	0.0669	ns																				
	IA - Gamma - Average Odour Responses		c vs e				5	5	0.888	ns																				
	Predicted mean - Control		c vs e												0.4905															
	Predicted mean - Experimental		c vs e												0.3133	0.07165 to 0.2827		5	1.085	0.3811	5	8.073	0.0001	1	11.42	0.0015				
	δD - Calyx - Average Odour Responses		c vs e																											
	δD - Alpha' - Average Odour Responses		c vs e																											
δD - Beta' - Average Odour Responses	c vs e																													
δD - Alpha - Average Odour Responses	c vs e																													
δD - Beta - Average Odour Responses	c vs e																													
δD - Gamma - Average Odour Responses	c vs e																													
Predicted mean - Control	c vs e										0.5058																			
Predicted mean - Experimental	c vs e										0.2982	0.1085 to 0.3067		5	1.839	0.1254	5	8.907	0.0001	1	17.86	0.0001								
Panel B ShakerRNA GAL80's	IA - Calyx - Average Odour Responses	Two-way ANOVA, Sidak's multiple comparison test	c vs e	Imaged at 4 days after eclosion	12	12	19	23	0.9983	ns																				
	IA - Alpha' - Average Odour Responses		c vs e				21	22	0.9406	ns																				
	IA - Beta' - Average Odour Responses		c vs e				23	19	0.6845	ns																				
	IA - Alpha - Average Odour Responses		c vs e				21	24	0.3043	ns																				
	IA - Beta - Average Odour Responses		c vs e				22	19	>0.9999	ns																				
	IA - Gamma - Average Odour Responses		c vs e				23	20	0.9909	ns																				
	Predicted mean - Control		c vs e												0.3422															
	Predicted mean - Experimental		c vs e												0.3375	-0.05014 to 0.05946		5	1.365	0.238	5	29.08	0.0001	1	0.0281	0.8671				
	δD - Calyx - Average Odour Responses		c vs e																											
	δD - Alpha' - Average Odour Responses		c vs e																											
δD - Beta' - Average Odour Responses	c vs e																													
δD - Alpha - Average Odour Responses	c vs e																													
δD - Beta - Average Odour Responses	c vs e																													
δD - Gamma - Average Odour Responses	c vs e																													
Predicted mean - Control	c vs e										0.2596																			
Predicted mean - Experimental	c vs e										0.2667	-0.05631 to 0.04200		5	0.3985	0.8496	5	23.95	0.0001	1	0.0822	0.7746								

Figure	Data	Breakdown of conditions	Statistical Test	Comparison (c = con, e = exp)	Age of the flies	Control n	Exp. n	Con. hemis. n	Exp. hemis. n	P-value	Significance	Predicted mean	95% CI of difference	Interaction DF	Interaction F	Interaction P Value	Main effect of lobe DF	Main effect of lobe F	Main effect of lobe P Value	Main effect of genotype DF	Main effect of genotype F	Main effect of genotype P Value								
35	Panel A ShalpooreDN	IA - Calyx - Average Odour Responses	Two-way ANOVA, Sidak's multiple comparison test	c vs e	Imaged at 4 days after eclosion	8	7	12	13	0.9994	ns																			
		12		14				0.9974	ns																					
		IA - Alpha' - Average Odour Responses		c vs e																										
		IA - Beta' - Average Odour Responses		c vs e																										
		IA - Alpha - Average Odour Responses		c vs e																										
		IA - Beta - Average Odour Responses		c vs e																										
		IA - Gamma - Average Odour Responses		c vs e																										
		Predicted mean - Control		c vs e													0.2996													
		Predicted mean - Experimental		c vs e													0.2442	-0.006430 to 0.1172	5	0.1604	0.9765	5	2.458	0.0357	1	3.133	0.0787			
		δD - Calyx - Average Odour Responses		c vs e																										
		δD - Alpha' - Average Odour Responses		c vs e																										
		δD - Beta' - Average Odour Responses		c vs e																										
		δD - Alpha - Average Odour Responses		c vs e																										
		δD - Beta - Average Odour Responses		c vs e																										
		δD - Gamma - Average Odour Responses		c vs e																										
		Predicted mean - Control		c vs e													0.2366													
		Predicted mean - Experimental		c vs e													0.2153	-0.03298 to 0.07553	5	0.0817	0.995	5	1.148	0.3374	1	0.6002	0.4397			
		35		Panel A ShabRNAi				IA - Calyx - Average Odour Responses	Two-way ANOVA, Sidak's multiple comparison test	c vs e	Imaged at 4 days after eclosion	5	5	9	4	0.9471	ns													
								9		10				0.2418	ns															
								IA - Alpha' - Average Odour Responses		c vs e																				
IA - Beta' - Average Odour Responses	c vs e																													
IA - Alpha - Average Odour Responses	c vs e																													
IA - Beta - Average Odour Responses	c vs e																													
IA - Gamma - Average Odour Responses	c vs e																													
Predicted mean - Control	c vs e																0.3453													
Predicted mean - Experimental	c vs e																0.2758	0.008725 to 0.1303	5	0.638	0.6712	5	0.681	0.639	1	5.151	0.0255			
δD - Calyx - Average Odour Responses	c vs e																													
δD - Alpha' - Average Odour Responses	c vs e																													
δD - Beta' - Average Odour Responses	c vs e																													
δD - Alpha - Average Odour Responses	c vs e																													
δD - Beta - Average Odour Responses	c vs e																													
δD - Gamma - Average Odour Responses	c vs e																													
Predicted mean - Control	c vs e																0.2729													
Predicted mean - Experimental	c vs e																0.2038	0.009155 to 0.1291	5	0.5148	0.7645	5	2.044	0.0792	1	5.233	0.0243			
35	Panel B ShalpooreDN GAL80s		IA - Calyx - Average Odour Responses		Two-way ANOVA, Sidak's multiple comparison test	c vs e	Imaged at 4 days after eclosion	15		5				24	8	0.9996	ns													
			27			9								0.9594	ns															
			IA - Alpha' - Average Odour Responses			c vs e																								
		IA - Beta' - Average Odour Responses	c vs e																											
		IA - Alpha - Average Odour Responses	c vs e																											
		IA - Beta - Average Odour Responses	c vs e																											
		IA - Gamma - Average Odour Responses	c vs e																											
		Predicted mean - Control	c vs e														0.3913													
		Predicted mean - Experimental	c vs e														0.4077	-0.1074 to 0.07463	5	0.4016	0.8473	5	3.891	0.0022	1	0.1263	0.7227			
		δD - Calyx - Average Odour Responses	c vs e																											
		δD - Alpha' - Average Odour Responses	c vs e																											
		δD - Beta' - Average Odour Responses	c vs e																											
		δD - Alpha - Average Odour Responses	c vs e																											
		δD - Beta - Average Odour Responses	c vs e																											
		δD - Gamma - Average Odour Responses	c vs e																											
		Predicted mean - Control	c vs e														0.2912													
		Predicted mean - Experimental	c vs e														0.3319	-0.1191 to 0.03774	5	0.6272	0.6792	5	6.659	0.0001	1	1.047	0.3075			
		35	ShabRNAi GAL80s	IA - Calyx - Average Odour Responses		Two-way ANOVA, Sidak's multiple comparison test			c vs e		Imaged at 4 days after eclosion	12	12	19	21	0.9989	ns													
				21					23					0.3692	ns															
				IA - Alpha' - Average Odour Responses					c vs e																					
IA - Beta' - Average Odour Responses	c vs e																													
IA - Alpha - Average Odour Responses	c vs e																													
IA - Beta - Average Odour Responses	c vs e																													
IA - Gamma - Average Odour Responses	c vs e																													
Predicted mean - Control	c vs e																0.3883													
Predicted mean - Experimental	c vs e																0.4112	-0.07849 to 0.03271	5	1.209	0.3052	5	10.33	0.0001	1	0.6576	0.4182			
δD - Calyx - Average Odour Responses	c vs e																													
δD - Alpha' - Average Odour Responses	c vs e																													
δD - Beta' - Average Odour Responses	c vs e																													
δD - Alpha - Average Odour Responses	c vs e																													
δD - Beta - Average Odour Responses	c vs e																													
δD - Gamma - Average Odour Responses	c vs e																													
Predicted mean - Control	c vs e																0.3001													
Predicted mean - Experimental	c vs e																0.2856	-0.03125 to 0.06013	5	0.8954	0.4847	5	13.87	0.0001	1	0.3874	0.5343			

Figure	Data	Statistical Test	Comparison (c = con, e = exp)	Age of the flies	Control n	Exp. n	Con. hemis. n	Exp hemis. n	P-value	Significance	Predicted mean	95% CI of difference	Interaction DF	Interaction F	Interaction P Value	Main effect of lobe DF	Main effect of lobe F	Main effect of lobe P Value	Main effect of genotype DF	Main effect of genotype F	Main effect of genotype P Value							
37	Panel A Shaw-Truncated	Two-way ANOVA, Sidak's multiple comparison test	c v s e	Imaged at 4 days after eclosion	6	8	10	13	0.8464	ns																		
							11	12	0.9383	ns																		
							12	16	0.9975	ns																		
							11	12	>0.9999	ns																		
							12	14	0.6961	ns																		
							12	16	0.9819	ns																		
															0.2426													
															0.2296			-0.04567 to 0.07170		5	0.891	0.489	5	1.516	0.1888	1	0.1922	0.6617
							10	13	0.8817	ns																		
							11	12	0.9678	ns																		
	12	16	0.2736	ns																								
	11	12	0.5567	ns																								
	12	14	0.0354	*																								
	12	16	0.9297	ns																								
									0.1573																			
									0.1775			-0.06980 to 0.02939		5	3.074	0.0116	5	1.709	0.1364	1	0.6488	0.4219						
	Panel A ShawRNAi	Two-way ANOVA, Sidak's multiple comparison test	c v s e	Imaged at 4 days after eclosion	6	5	9	9	0.3958	ns																		
							11	10	0.385	ns																		
							10	10	0.047	*																		
							9	10	>0.9999	ns																		
10							10	0.988	ns																			
10							10	0.6145	ns																			
														0.3352														
														0.2273			0.04565 to 0.1702		5	0.8405	0.5239	5	2.099	0.0712	1	11.8	0.0008	
9							9	0.9766	ns																			
11							10	0.7606	ns																			
10	10	0.0029	**																									
9	10	>0.9999	ns																									
10	10	0.9493	ns																									
10	10	0.9996	ns																									
								0.2987																				
								0.2149			0.02502 to 0.1426		5	1.552	0.18	5	3.91	0.0027	1	7.989	0.0056							
Panel B Shaw-Truncated GAL80s	Two-way ANOVA, Sidak's multiple comparison test	c v s e	Imaged at 4 days after eclosion	11	9	19	11	0.0373	*																			
						22	10	0.3192	ns																			
						22	15	>0.9999	ns																			
						22	10	>0.9999	ns																			
						22	15	0.9254	ns																			
						22	15	0.9897	ns																			
														0.4078														
														0.3059			0.01252 to 0.1914		5	1.671	0.1434	5	3.362	0.0062	1	5.055	0.0257	
						19	11	0.9027	ns																			
						22	10	0.0121	*																			
22	15	>0.9999	ns																									
22	10	>0.9999	ns																									
22	15	0.92	ns																									
22	15	0.9907	ns																									
								0.2756																				
								0.2373			-0.02905 to 0.1056		5	2.285	0.0479	5	1.114	0.3541	1	1.257	0.2636							
Panel B ShawRNAi GAL80s	Two-way ANOVA, Sidak's multiple comparison test	c v s e	Imaged at 4 days after eclosion	8	6	11	7	0.6419	ns																			
						14	12	0.9996	ns																			
						16	11	0.9996	ns																			
						14	12	0.8535	ns																			
						15	11	0.89	ns																			
						15	12	0.9915	ns																			
														0.3918														
														0.3322			-0.007564 to 0.1268		5	0.4487	0.8137	5	2.835	0.0181	1	3.079	0.0815	
						11	7	0.5103	ns																			
						14	12	0.9903	ns																			
16	11	0.9476	ns																									
14	12	0.9288	ns																									
15	11	0.9023	ns																									
15	12	0.9026	ns																									
								0.2753																				
								0.2237			-0.004540 to 0.1077		5	0.7496	0.5877	5	4.208	0.0014	1	3.303	0.0713							

Figure	Data	Breakdown of conditions	Statistical Test	Comparison (c = con, e = exp)	Age of the flies	Control n	Exp. n	Con. hemis. n	Exp hemis. n	P-value	Significance	Predicted mean	95% CI of difference	Interaction DF	Interaction F	Interaction P Value	Main effect of lobe DF	Main effect of lobe F	Main effect of lobe P Value	Main effect of genotype DF	Main effect of genotype F	Main effect of genotype P Value				
																							Interaction DF	Interaction F	Interaction P Value	Main effect of lobe DF
38	Panel A - ShawWT	IA - Calyx - Peak Odour Resonances	Two-way ANOVA, Sidak's multiple comparison test	c vs e	Imaged at 4 days after eclosion	3	6	5	12	>0.9999	ns															
		IA - Alpha' - Peak Odour Resonances		c vs e				5	12	0.2626	ns															
		IA - Beta' - Peak Odour Resonances		c vs e				6	12	>0.9999	ns															
		IA - Alpha - Peak Odour Resonances		c vs e				6	12	0.9991	ns															
		IA - Beta - Peak Odour Resonances		c vs e				6	12	0.7294	ns															
		IA - Gamma - Peak Odour Resonances		c vs e				6	12	0.9879	ns															
		Predicted mean - Control		c vs e										0.7904	0.06645 to 0.4205											
		Predicted mean - Experimental		c vs e										0.5469			5	0.8648	0.5078	5	5.097	0.0004	1	7.457	0.0075	
		δD - Calyx - Peak Odour Resonances		c vs e		3	6	5	12	>0.9999	ns															
		δD - Alpha' - Peak Odour Resonances		c vs e				5	12	0.9647	ns															
		δD - Beta' - Peak Odour Resonances		c vs e				6	12	>0.9999	ns															
		δD - Alpha - Peak Odour Resonances		c vs e				6	12	>0.9999	ns															
	δD - Beta - Peak Odour Resonances	c vs e	6	12	>0.9999			ns																		
	δD - Gamma - Peak Odour Resonances	c vs e	6	12	>0.9999			ns																		
	Predicted mean - Control	c vs e									0.4558	0.02536 to 0.2470														
	Predicted mean - Experimental	c vs e									0.3196			5	0.8861	0.4937	5	6.737	0.0001	1	5.953	0.0166				
	Panel B - ShawWT	Two-way ANOVA, Sidak's multiple comparison test	IA - Calyx - Average Odour Resonances	Imaged at 4 days after eclosion	3	6	5	12	0.9787	ns																
			IA - Alpha' - Average Odour Resonances				c vs e	5	12	0.0007	***															
			IA - Beta' - Average Odour Resonances				c vs e	6	12	0.0466	*															
			IA - Alpha - Average Odour Resonances				c vs e	6	12	0.3535	ns															
			IA - Beta - Average Odour Resonances				c vs e	6	12	0.1222	ns															
			IA - Gamma - Average Odour Resonances				c vs e	6	12	0.078	ns															
			Predicted mean - Control		c vs e									0.3444	0.1401 to 0.2870											
			Predicted mean - Experimental		c vs e									0.1309			5	1.184	0.3227	5	2.041	0.0799	1	33.33	0.0001	
δD - Calyx - Average Odour Resonances			c vs e		3	6	5	12	>0.9999	ns																
δD - Alpha' - Average Odour Resonances			c vs e				5	12	0.0472	*																
δD - Beta' - Average Odour Resonances			c vs e				6	12	0.067	ns																
δD - Alpha - Average Odour Resonances			c vs e				6	12	>0.9999	ns																
δD - Beta - Average Odour Resonances	c vs e	6	12	0.3733			ns																			
δD - Gamma - Average Odour Resonances	c vs e	6	12	0.5034			ns																			
Predicted mean - Control	c vs e									0.2053																
Predicted mean - Experimental	c vs e									0.08744	0.05174 to 0.1839		5	1.455	0.212	5	5.351	0.0002	1	12.53	0.0006					
39	Condition		Difference between predicted means		95% CI of difference		Pvalue																			
					Lower limit	Upper Limit																				
	ShakerDN		0.1444		-0.03458	0.2451	0.0107																			
	ShakerDN, GAL80ts		-0.1772		-0.2827	-0.07185	0.0015																			
	Shaker-RNAi		-0.1149		-0.1801	-0.0497	0.0007																			
	Shaker-RNAi, GAL80ts		0.00466		-0.05014	0.05946	0.8671																			
	ShalPoreDN		-0.05537		-0.1172	-0.00643	0.0787																			
	ShalPoreDN, GAL80ts		-0.01641		-0.1074	0.07463	0.7227																			
	Shab-RNAi		-0.06953		-0.008725	-0.1303	0.255																			
	Shab-RNAi, GAL80ts		-0.02289		-0.07849	0.03271	0.4182																			
	Shaw-Truncated		-0.01301		0.04567	-0.0717	0.6617																			
	Shaw-Truncated, GAL80ts		-0.102		-0.1914	-0.01252	0.0257																			
	ShawRNAi		-0.1079		-0.04565	-0.1702	0.0008																			
ShawRNAi, GAL80ts		-0.05961		-0.007564	-0.1268	0.0815																				
ShawWT		-0.2136		-0.287	-0.1401	0.0001																				